



HAL
open science

Microstructural approach to evaluate the reliability of lead-free electronic assemblies in thermomechanical fatigue

Emna Ben Romdhane

► **To cite this version:**

Emna Ben Romdhane. Microstructural approach to evaluate the reliability of lead-free electronic assemblies in thermomechanical fatigue. Electronics. Université de Bordeaux, 2022. English. NNT : 2022BORD0364 . tel-04048661

HAL Id: tel-04048661

<https://theses.hal.science/tel-04048661v1>

Submitted on 28 Mar 2023

HAL is a multi-disciplinary open access archive for the deposit and dissemination of scientific research documents, whether they are published or not. The documents may come from teaching and research institutions in France or abroad, or from public or private research centers.

L'archive ouverte pluridisciplinaire **HAL**, est destinée au dépôt et à la diffusion de documents scientifiques de niveau recherche, publiés ou non, émanant des établissements d'enseignement et de recherche français ou étrangers, des laboratoires publics ou privés.

THÈSE PRÉSENTÉE
POUR OBTENIR LE GRADE DE

**DOCTEUR DE
L'UNIVERSITÉ DE BORDEAUX**

ÉCOLE DOCTORALE SCIENCES PHYSIQUES ET DE L'INGÉNIEUR
SPÉCIALITÉ ÉLECTRONIQUE

Par Emna BEN ROMDHANE

**MICROSTRUCTURAL APPROACH TO EVALUATE THE
RELIABILITY OF LEAD-FREE ELECTRONIC ASSEMBLIES
IN THERMOMECHANICAL FATIGUE**

Sous la direction de Hélène FRÉMONT
et Alexandrine GUEDON-GRACIA

Soutenue le 5 décembre 2022 à Talence

Membres du jury :

M. Jean-Yves BUFFIERE Professeur, Université de Lyon	Président du jury
M. Olivier DALVERNY Professeur, École Nationale d'Ingénieurs de Tarbes	Rapporteur
M. David DANOVTCH Professeur, Université de Sherbrooke	Rapporteur
Mme Hélène FRÉMONT Professeure, Université de Bordeaux	Directrice de thèse
Mme Alexandrine GUEDON-GRACIA Maître de conférences, Université de Bordeaux	Co-directrice de thèse
M. Pierre ROUMANILLE Docteur, IRT Saint Exupéry Toulouse	Co-encadrant
M. Wilson Carlos MAIA Docteur, Thales	Examineur
M. Manoubi Auguste BAH Docteur, Safran	Examineur
M. Fabio COCCETTI Ingénieur HDR, IRT Saint Exupéry Toulouse	Invité

Acknowledgements

I would like to express my sincere gratitude to my various thesis supervisors: Hélène FREMONT, Alexandrine GUEDON-GRACIA and Pierre ROUMANILLE for their support, excellent advice, encouragement and constructive remarks in all aspects of completing my doctorate at the University of Bordeaux. I am deeply grateful to my advisory committee members including Samuel PIN, Patrick NGUYEN and Fabio COCCETTI for their insightful discussion about this research work. Thanks should also go to the various trainees Corentin, Adrien and Hugues for their contribution to the different works presented in this dissertation.

I would like to extend my gratitude to all the members of the thesis jury. I am thankful to Jean-Yves BUFFIERE for having done me the honor of chairing the thesis jury. Thanks to Olivier DALVERNY and David DANOVITCH for having devoted their time to report my work by enlightening it with enriching remarks. Finally, I would like to acknowledge Wilson Carlos MAIA and Manoubi Auguste BAHY for agreeing to examine my work and providing her expertise during the defence.

I am also grateful to my family members especially to my parents (Noureddine and Kaouther), my brother Firas, relatives, friends and all of my well-wisher for their continuous support and prayers throughout my life. Special thanks are extended to my friend Saliha for his friendship and support. Finally, I solemnly dedicate this dissertation and all achievements in pursuit of doctoral degree to my husband Mounir and my son Tayem, for their love, support, patience and heartfelt consideration.

Abstract

With the prohibition on the use of certain hazardous substances by the European RoHS directive, such as lead in a series of electrical products, the SnPb eutectic, which was the most used solder alloy in electronic assemblies, is replaced by SnAgCu (SAC) alloys. Despite the early appearance of these materials, their insertion into the industry is hindered by the observation of early failures of solder joints under thermomechanical fatigue. These alloys have a complex and variable microstructure that significantly influences their behavior. The main objective of this work is to improve the prediction of the lifetime of SAC interconnections by developing a generic damage criterion, based on the microstructural evolution of the alloy and which can be implemented in a fatigue model. This work also involves studying the various factors that can affect the aging of SAC solders in thermomechanical fatigue. The initial microstructure of the SAC alloy and its evolution due to thermomechanical fatigue were examined based on accelerated tests and microstructural investigation by EBSD analyses. Recrystallization of β -SN grains and coarsening of Ag_3Sn intermetallics appear to be precursors to intergranular cracking of the different solders studied (BGA, R1206 and QFN). The QFN case reveals another mixed dynamic where we observe a competition between the intergranular cracking and the interfacial failure that occurs along the intermetallics layer, without microstructural evolution of the SAC alloy. The analysis of microstructural damage indicators is approached with the quantitative characterization of recrystallization and Ag_3Sn particles coarsening. The size of the recrystallized grains varies from 1 to 30 μm independently of the solder geometry. This is a characteristic of the SAC alloy. A low degree of recrystallization seems sufficient to trigger crack propagation in BGA and R1206 joints (8% and 10% respectively). A higher degree of recrystallization is required for crack propagation of QFN solder joints (27%). This may be due to the mixed cracking mode observed on this geometry. Regarding the coalescence of intermetallics, particles with a diameter greater than 2 μm seem to promote recrystallization. It would be interesting to be able to implement these damage indicators in the prediction models. The study of the different parameters influencing the thermomechanical performance of SAC solders shows that isothermal aging, the location of the solder joint and the initial microstructure have an effect on the thermomechanical behavior of SAC interconnections. They are essential factors to take into account when developing the thermomechanical fatigue model.

Keywords: Solder joint, SAC, aging, thermomechanical fatigue, thermal cycling, microstructure, reliability.

Résumé

Approche microstructurale pour l'évaluation de la fiabilité des assemblages électroniques en fatigue thermomécanique

Avec l'interdiction d'utilisation de certaines substances dangereuses par la directive européenne RoHS, comme le plomb dans une série de produits électriques, l'eutectique SnPb, qui était l'alliage de brasure le plus utilisé dans les assemblages électroniques, est remplacé par des alliages SnAgCu (SAC). Malgré l'apparition précoce de ces matériaux, leur insertion dans l'industrie est freinée par l'observation de défaillances précoces des brasures par fatigue thermomécanique. Ces alliages présentent une microstructure complexe et variable qui influence de façon importante leur comportement. Le principal objectif de ce travail est d'améliorer la prédiction de la durée de vie des interconnexions SAC en développant un critère d'endommagement générique, basé sur l'évolution microstructurale de l'alliage et pouvant être implémenté dans un modèle de fatigue. Ce travail consiste aussi à étudier les différents facteurs pouvant affecter le vieillissement des brasures SAC en fatigue thermomécanique. La microstructure initiale de l'alliage SAC et son évolution due à la fatigue thermomécanique ont été examinées en se basant sur des essais accélérés et sur l'investigation microstructurale par analyses EBSD. La recristallisation des grains β -SN et la coalescence des intermétalliques Ag_3Sn apparaissent bien comme les précurseurs à la fissuration intergranulaire des différentes brasures étudiées (BGA, R1206 et QFN). Le boîtier QFN révèle une autre dynamique mixte où l'on observe une compétition entre la fissuration intergranulaire et la rupture interfaciale qui se produit le long de la couche d'intermétalliques, sans évolution microstructurale de l'alliage SAC. L'analyse des indicateurs d'endommagement microstructural est abordée avec la caractérisation quantitative de la recristallisation et de la coalescence des particules Ag_3Sn . La taille des grains recristallisés varie de 1 à 30 μm indépendamment de la géométrie de brasure. C'est une caractéristique de l'alliage SAC. Un faible degré de recristallisation semble suffisant pour déclencher la propagation des fissures dans les joints BGA et R1206 (respectivement 8% et 10%). Un degré de recristallisation plus élevé est requis pour la propagation des fissures dans les joints QFN (27%). Cela peut être dû au mode de fissuration mixte observé sur cette géométrie. Concernant la coalescence des intermétalliques, les particules ayant un diamètre supérieur à 2 μm semblent favoriser la recristallisation. Il serait intéressant de pouvoir implémenter ces indicateurs d'endommagement dans les modèles de prédiction. L'étude des différents paramètres influençant les performances thermomécaniques des brasures SAC montre que le vieillissement isotherme, la localisation de la brasure et la microstructure initiale ont un effet sur le comportement thermomécanique des joints brasés SAC. Ils sont des facteurs primordiaux à prendre en compte lors du développement du modèle de fatigue thermomécanique.

Mots clés : Joint de brasure, SAC, vieillissement, fatigue thermomécanique, cyclage thermique, microstructure, fiabilité.

Index

ATC	Accelerated Temperature Cycling
BGA	Ball Grid Array
BT	Bismaleimide Triazine
CTE	Coefficient of Thermal Expansion
DNP	Distance to the Neutral Point
EBSD	Electron BackScatter Diffraction
EDS	Electron Dispersive Spectroscopy
FEM	Finite element Model
ENIG	Electroless Nickel Immersion Gold
FR-4	Flame Retardant
IMC	InterMetallic Compound
MUD	Multiple of Uniform Density
NSMD	Non Solder Mask Defined
OPS	Oxide Polishing Suspension
OSP	Organic Solderability Preservative
PCB	Printed Circuit Board
QFN	Quad Flat No-leads
RoHS	Restriction on Hazardous Substances
SAC	Sn-Ag-Cu
SiC	Silicon Carbide
SMD	Surface Mounted Device
SMD	Solder Mask Defined
SEM	Scanning Electron Microscopy
TMA	ThermoMechanical Analysis
TC	Thermal cycle
WEEE	Waste from Electrical and Electronic Equipment

Content

General introduction	1
Chapter I. Literature review	4
I.1 Introduction	5
I.2 Microelectronic assemblies and transition to lead-free interconnections	6
I.2.1 Architecture of an electrical assembly	6
I.2.2 Assembly processes	7
I.2.3 Lead-free electronics	8
I.2.4 Synthesis	8
I.3 SAC solder alloy	9
I.3.1 SAC Alloy composition	9
I.3.2 Tin structure in SAC solder joints	10
I.3.3 Intermetallic compounds in SAC solders	14
I.3.4 Influence of Ag and Cu mass content	15
I.3.5 Influence of the reflow profile	16
I.3.6 Influence of the surface finish layer	17
I.3.7 Influence of isothermal aging	19
I.3.8 Synthesis	21
I.4 Thermomechanical fatigue of SAC solder joint	22
I.4.1 Evolution of SAC solder joint microstructure during thermal cycling	23
I.4.2 Thermomechanical fatigue models	26
I.4.3 Factors impacting SAC solder joints thermomechanical response	28
I.4.4 Synthesis	33
I.5 SAC alloy constitutive models	34
I.5.1 Ramberg-Osgood elastoplastic model	34
I.5.2 Creep models	34
I.5.3 Anand model	37
I.5.4 Crystal plasticity Model	37
I.5.5 Synthesis	40
I.6 Context and objectives of the thesis	41
Chapter II. Research methodology	43
II.1 Introduction	44
II.2 Thesis approach	45
II.3 Experimental approach	47

II.3.1	Test vehicles and components	47
II.3.2	Test conditions and plan	49
II.3.3	In situ electrical monitoring apparatus	50
II.3.4	Microstructural characterization.....	51
II.3.5	Synthesis.....	55
II.4	Preliminary numerical simulations	56
II.4.1	Modeling at the scale of the Board.....	56
II.4.2	Impact of the tin grain anisotropy on thermomechanical behavior of Lead-Free Solder Joints.....	59
II.4.3	Synthesis.....	63
II.5	Conclusion	64
Chapter III.	Role of tin grain recrystallization and Ag ₃ Sn intermetallic coalescence in SAC305 solder cracking during thermomechanical fatigue	65
III.1	Introduction	66
III.2	As-reflowed SAC solder joint microstructure.....	68
III.2.1	SAC solder joints composition and microstructure	68
III.2.2	SAC solder joints tin grain structure.....	71
III.2.3	Isothermal pre-ageing effect on SAC305 solder joints microstructure	82
III.2.4	Synthesis	84
III.3	Thermal cycling effect on pre-aged SAC305 solder joints microstructural.....	86
III.3.1	Global recrystallization of tin grains.....	86
III.3.2	Local recrystallization of tin grains	94
III.3.3	Ag ₃ Sn particles coarsening	95
III.3.4	Synthesis	98
III.4	Role of tin grain recrystallization and Ag ₃ Sn intermetallic coalescence in SAC305 solder cracking during thermomechanical fatigue.....	99
III.4.1	Crack initiation.....	99
III.4.2	Crack propagation	101
III.4.3	Synthesis	105
III.5	Conclusion.....	106
Chapter IV.	Identification of SAC alloy microstructural damage criterion	108
IV.1	Introduction	109
IV.2	General approach for assessing the reliability of solder joints.....	110
IV.2.1	SAC solder joints lifetimes	110
IV.2.2	Measurements of crack propagation	111
IV.2.3	Definition of microstructural damage indicators	112

IV.2.4	Synthesis	114
IV.3	Lifetimes analysis results	115
IV.3.1	R1206 solder joints lifetimes	115
IV.3.2	BGA288 solder joints lifetimes	116
IV.3.3	QFN68 solder joints lifetimes	117
IV.3.4	Synthesis	118
IV.4	Crack evolution	119
IV.4.1	R1206 solder joint.....	119
IV.4.2	BGA solder joint	120
IV.4.3	QFN solder joint	122
IV.4.4	Correlation with lifetimes results.....	123
IV.4.5	Synthesis	124
IV.5	Tin grain recrystallization	125
IV.5.1	Characterization of the BGA solder joint evolution	125
IV.5.2	Comparison with the R1206 and QFN solder joints geometries	129
IV.5.3	Synthesis	132
IV.6	Ag ₃ Sn coarsening	133
IV.6.1	Characterization of the BGA solder joint evolution	133
IV.6.2	Comparison with the R1206 and QFN solder joints geometries	140
IV.6.3	Synthesis	143
IV.7	Conclusion.....	144
Chapter V.	Different factors affecting solder joint reliability under thermomechanical fatigue.....	146
V.1	Introduction.....	147
V.2	Effect of pre-aging on SAC solder joint under thermal cycling	148
V.2.1	Lifetime's analysis.....	148
V.2.2	Microstructural and failure analysis	153
V.2.3	Synthesis.....	155
V.3	SAC solder joint location effect under thermal cycling.....	156
V.3.1	Solder joint behavior under component edge	156
V.3.2	Solder joint behavior under silicon die edge	157
V.3.3	Finite element simulation	160
V.3.4	Synthesis.....	163
V.4	Effect of the as-reflowed microstructure	164

V.4.1	Impact of the crystalline orientation on thermomechanical behavior of mono-grained SAC solder joint.....	164
V.4.2	Tin grain structure influence.....	170
V.4.3	Synthesis.....	176
V.5	Conclusion	177
	General conclusion	179
	References.....	185

General introduction

The electronic packaging industry is still experiencing rapid development in the field of design and manufacturing. Thus, many main challenges arise from a reliability point of view on electronic boards. As a result of external loadings, including temperature variation and vibration, and structural effects, among the different elements that make up electronic assemblies, solder joints have been identified as potentially critical parts, which can ultimately determine the lifetime of the electronic devices in long term operation. Their material properties are a crucial factor affecting the durability of electronic boards.

With the ban on the use of certain hazardous substances by the European RoHS directive, such as lead in a series of electrical products, the SnPb eutectic, which was the most used solder alloy in electronic assemblies, is replaced by SnAgCu (SAC) alloys. Despite the early appearance of these materials, their insertion in industry is hampered by a lack of understanding of the solder failure mechanisms of certain types of package under the different use conditions. The behavior of SAC alloys is complex due to their stochastic as-reflowed microstructure coupled with the highly anisotropic properties of the tin phase. The SAC microstructure is continuously evolving under the effect of different aging conditions, which affects the mechanical strength of the solder joints. Generally, within the study of the solder joint reliability, the microstructural characteristics of the SAC solder alloys are not taken into account by the fatigue models. However, it appears that the implementation of the SAC microstructural properties is an important step to provide representative numerical models allowing the accurate prediction of electronic packaging lifetime.

In this context of the development of representative fatigue models, the FELINE project of the IRT (Technological Research Institute) Saint Exupery seeks to provide a new approach for assessing the SAC solder joints reliability. It involves the IMS (Integration: from Material to Systems) laboratory as well as industries in different fields: Continental Automotive, Elemca, Airbus Defense and Space, Safran, Thales Alenia Space, Actia and Liebherr. The aim is to better understand and characterize the lead-free microelectronic assemblies' behavior focusing on the most promising fatigue criterion: the microstructure.

The objectives of this project are the logical continuation of the work carried out within the framework of a previous project called ROBUSTESSE. This project focused on the characterization of BGA solder joints when they successively undergo isothermal aging and thermal cycling and on the development of a model with a high level of representativeness. To achieve this goal an experimental flow was performed to get solder lifetime and discriminate failure modes as a function of isothermal and thermal cycling harshness. However, the test could not be taken to complete failure of the boards due to the closure of the ROBUSTESSE project. Lifetimes data from test vehicles under thermal cycling have been useful to the FELINE project. The test boards represent a good starting point, both for setting up the sample preparation protocol for micro sections, and for first results of understanding of the aging phenomena.

The FELINE project is therefore an opportunity to extend this work on several axes:

- Study of different component geometries (BGA, QFN, passive components) to cover a large range of use cases.
- Comparison of the impact of different aging conditions on the durability of electronic assemblies
- Understanding the impact of the microstructure on the SAC solder behavior and identification of microstructural indicators that can be implemented in Finite Element models
- Development of multiscale finite element models (board, component, solder joint and tin microstructure) to master every aspect of the study: geometrical parameters, boundary conditions, microstructure properties and defects

In this context, this thesis presents a microstructural approach to evaluate the reliability of lead-free electronic assemblies in thermomechanical fatigue. It aims to contribute to the understanding of the SAC microstructural evolution under thermal aging and the impact of tin grain properties on the failure mechanism. Several parameters of the packaging (design, materials properties and solder geometry and microstructure) will be studied to identify those most critical to the reliability of SAC solder joints. The main objective is to define a common microstructural damage criterion that can be exploited in a more representative fatigue model to improve the prediction of SAC solder joint lifetimes.

This manuscript is divided into five chapters.

Chapter one provides a literature review focusing on the reliability of lead free-assemblies and the microstructure of SAC solder joints. We are first interested in the definition of electronic assemblies and developments related to the application of new legislations that prohibit lead. The microstructure knowledge on the SAC solder alloy has then been emphasized. Reliability assessment approaches are also presented along with typical conditions leading to solder joint failure. The effects of thermomechanical fatigue on the behavior of solder joints highlighted in particular in this chapter correspond to the most essential introductory stage of the work carried out during the thesis. A review of the different elastoplastic and viscoplastic behavior laws commonly used in the electronics industry is also carried to determine the most relevant behavioral model for the numerical part of the study. The context and the objectives of the thesis are finally introduced.

The research methodology is explored in the second chapter. The different electronic components as well as the test vehicles design are presented. A major accelerated test campaign is conducted on different test vehicles in order to generate enough experimental results to enable an in-depth microstructural study of the SAC solder joints as well as the analysis of their characteristic lifetime. Isothermal aging followed by thermal cycling is the test type considered in this study. The test plan was based on different isothermal storage conditions and two thermal cycles with a successive sampling of the boards at different number of thermal cycles. The different observation techniques used for the microstructural analysis of solder joints are also described in detail. In the last part of this chapter, preliminary simulations were carried out to give first clues on the influence of certain parameters such as the materials properties of the

assembly, the position of the electronic components on the board and the as-reflowed microstructure of the SAC solder joints.

Chapter three deals with the study of the microstructural evolution of lead-free interconnect joints under thermomechanical fatigue. We first investigate of the microstructure of SAC305 interconnect joints after reflow soldering. This type of assembly process gives the solder alloy specific microstructural characteristics which are analyzed to understand their implications on the thermomechanical behavior of the interconnections. A detailed description of SAC305 microstructure evolution is then presented with the associated failure mode(s) generated during thermomechanical loading. The phenomena of tin grain recrystallization and Ag_3Sn particles coalescence that are characteristic of the thermomechanical damage of SAC interconnections are in particular explained; this makes it possible to understand the intergranular cracking failure mode systematically observed during the failure analysis of different studied components (BGA, QFN and R1206). An unusual interfacial crack was observed only in the QFN solder joints and can be related to the material properties and the solder geometry that unify this type of components.

Chapter four proposes then a developed microstructural approach, allowing the assessment of the thermomechanical reliability of SAC solder joints. The measurement of the solder joints lifetimes by electrical monitoring, the study of crack development and the quantitative investigation of the microstructural evolution are the different steps considered to define a microstructural criterion representative of the fatigue of solder joints under thermal cycles. The size of recrystallized grains and the degree of recrystallization, the size of Ag_3Sn particles and their density will be defined as microstructural indicators allowing the reproduction of recrystallization of tin grain and coarsening of Ag_3Sn particles and monitoring the microstructural evolution of the SAC solder alloy. The changes of these indicators under thermal cycles are presented in order to define the microstructural state promoting the crack propagation. The link between the characteristic lifetimes, the crack development phases and the microstructural indicators evolution will make it possible to identify a microstructural damage criterion feature of the SAC alloy.

The different factors that can have an effect on the microstructural behavior of SAC solder joint under thermomechanical fatigue and consequently the reliability of the lead-free packaging are investigated in the chapter five. The isothermal aging, the location of the solder joints on the package, the initial microstructure of the SAC alloy are the influential factors studied to identify mandatory parameters to develop future reliability models. Tools used to assess these parameters are: lifetime analysis, microstructural characterization and finite element modeling.

Finally, the conclusion summarizes the main results obtained at the end of the thesis. It also proposes perspectives for future work to improve and refine models for predicting the lifetime of lead-free electronic assemblies.

Chapter I. Literature review

I.1 Introduction

SAC alloys are the most widely used materials for soldering electronic assemblies. These ternary alloys are based on tin, silver and copper. The SAC microstructure, which mainly consists of the β -Sn phase and the Ag_3Sn intermetallic compounds, is very dynamic and plays a very important role in the study of the SAC solder joints reliability. The main goal of this chapter is to furnish a state of art focusing on the effect of the SAC solder joints microstructure on the reliability of lead free-assemblies.

We will introduce first the fundamental notions for a good understanding of the developed work. The basic concepts of electronic assemblies used throughout this document will be defined. Then, the microstructure and behavior of SAC alloys will be presented in relation to the mission profiles of electronic assemblies. The thermomechanical fatigue of SAC solder joint will be presented in detail since it is considered to be the major cause of solder joint failure. Finally, different constitutive laws used in the literature for the modeling of the SAC solder joints behavior will be reviewed to identify the most appropriate law for our study. This chapter will be an opportunity to show the shortcomings in the literature and to introduce the context of the thesis and the objectives identified to respond to the problem posed.

I.2 Microelectronic assemblies and transition to lead-free interconnections

I.2.1 Architecture of an electrical assembly

Schematically, an electronic assembly consists of three main elements: a printed circuit board, an electronic component and a solder alloy. The definition of these elements is necessary for the good understanding of the work developed in this thesis.

(a) The printed circuit board

The two main roles played by the printed circuit board or PCB (Printed Circuit Board) are the mechanical support of the components and their electrical interconnection thanks to the routing defined by the electronics engineers through copper tracks and report ranges. Today, the vast majority of assembled boards are multilayered: conductive copper layers are alternated with dielectric layers. The FR-4 (Flame Retardant) material is today the most used material for the manufacture of printed circuits for its attractive price and its good mechanical properties. The constituent materials of the internal structure of the printed circuit have an influence on its mechanical and physical properties. For example, in the case of thermomechanical fatigue resistance, depending on the type of assembled component, it will be preferable to consider a PCB material with a coefficient of thermal expansion (CTE) close to that of the component in order to minimize the resulting stresses on the level of interconnecting joints.

(b) The electronic component

The component has a functional aspect of electronic assembly. Each interconnections between the various components assembled on the PCB each plays a specific role and defines the overall function of the circuit. Three functions are ensured by the interconnections: to provide a mechanical maintenance of the packages to the printed circuit, to dissipate a part of thermal energy generated by the integrated circuit inside the component and to allow the power supply of the circuit and the transmission of electrical signals. Many types of components are available on the market. They can be grouped according to their packaging, which influences the mode of interconnection between the component and the printed circuit board. Interconnect modes can be through pins, with leads for surface transfer, with balls or direct-assembly (Figure I.2–1).

(c) The solder joint

The solder joint represents the junction element between the PCB and the component. It has a dual function since it provides both a mechanical and an electrical connection by holding the case to the circuit board and allowing the signal to communicate between the components of the assembly. The solder joint is the most vulnerable part of the electronic assembly for certain

types of stresses such as thermal and vibration loads. Cracks may appear by fatigue mechanisms leading to the rupture of the interconnection and therefore to the failure of the electronic assembly. The choice of the good solder material plays an important role in the reliability of electronic equipment. There are several solder alloys, which differ in their chemical composition and according to field of application (Sn-Pb, SAC (SnAgCu) and Innotot (SnAgCuBiNiSb)).

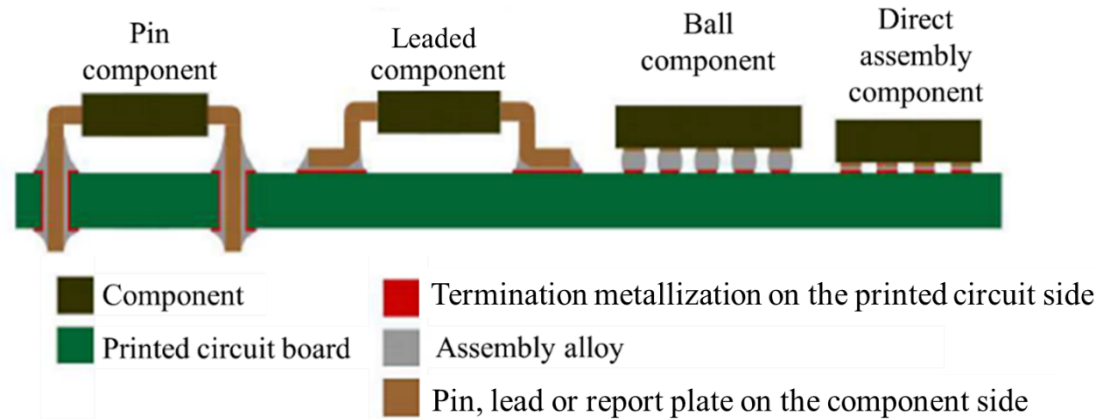


Figure I.2–1: Diagram of the different modes of interconnection between the components and the electronic board [1]

I.2.2 Assembly processes

Several assembly processes exist and allow electronic components to be soldered onto a PCB. The electronic assemblies investigated in this thesis work were exclusively made with the most prevalent process of SMD (surface mounted device) components soldered by reflow. This involves adding solder paste by screen-printing (mixture of alloy microballs and flux to activate wetting by getting rid of impurities and oxides potentially formed), the component is then placed directly on this paste which remains adhesive. The whole is then placed in a reflow furnace. The reflow profile can be divided into four distinct regions. A first preheating step consists of increasing the temperature of the PCB and the components. A stabilization phase then follows allowing homogenization of the temperature throughout the assembly in order to ensure the activation of the flux present in the solder paste. The assembly is then maintained, between 40 and 120 seconds depending on the dimensions of the board, above the melting temperature of the solder alloy to allow the complete melting of the solder paste. Finally, a solidification phase is necessary to guarantee the prevention of excessive intermetallic layers, which could cause the embrittlement of the resulting weld fillets. The temperature rise and fall steps must in particular be fast enough to respectively paste volatiles and obtain a fine microstructure, but in both cases slow enough to overcome any risk of thermal shock that could damage the constituent materials of the elements of the assembly. Differential expansion of the board and components can be also induced by the temperature variation generated during this assembly process. Residual stresses and strains can form in the solder joint which affects their reliability during their using.

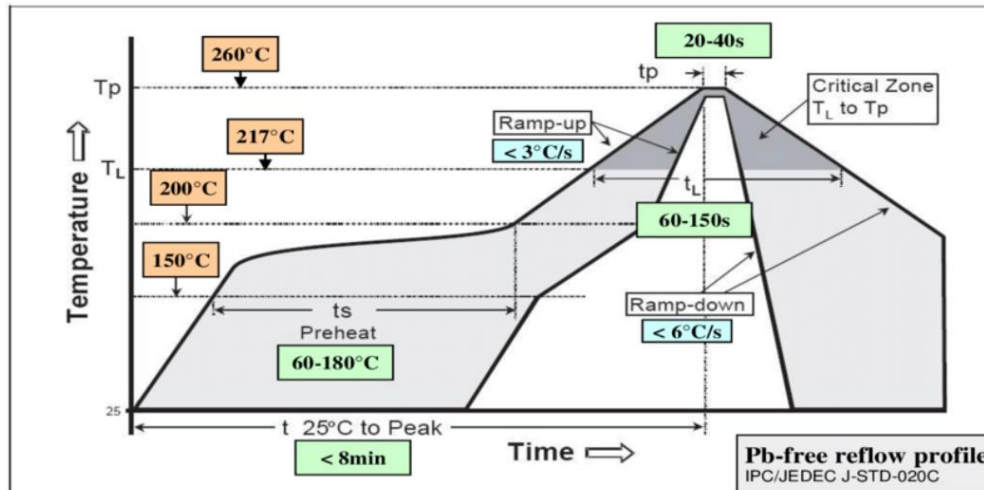


Figure I.2-2: Reflow Solder Profile [2]

I.2.3 Lead-free electronics

Eutectic Sn 63% Pb 37% has been the most widely used solder alloy since the advent of electronics due to its cost, availability, ease of use and its solder properties like low melting temperature and sustainability in reflow ovens and wave soldering processes.

However, the use of lead in our modern societies tends to be minimized because of its toxicity for humans and the environment despite all its qualities approved by the many applications developed over the centuries. In the United States, they began to consider the problem linked to the use of lead in the early 1990s, but no law was passed, mainly due to pressure exerted by manufacturers in the American electronics sector. This trend is further reinforced in Europe by the RoHS ban on harmful substances and WEEE regulations on recycling and minimizing of electronic wastes. In 2000, the EU adopted two directives, the Waste of Electrical and Electronic Equipment (WEEE) and the Directive of the Restriction of the Use of Certain Hazardous Substances (RoHS). The RoHS legislation aims to prohibit the use of lead in electronic equipment except for applications requiring a high level of reliability. So, due to the general push towards eco-efficiency and green electronics, manufacturers are motivated to switch to lead-free electronics. Therefore, the use of lead-free solder joints in the global electronics market seems imminent.

I.2.4 Synthesis

Among the three main elements that make up an electronic assembly (components, board and solder joints), we will be particularly interested in solder joints. Until 2006, they were mainly of the SnPb type, are now replaced by lead-free alloys for environmental, and health reasons. These new alloys, mainly SAC alloys, have similar mechanical properties to SnPb alloys. However, their microstructure seems to be very different, which can be critical for the reliability of electrical assemblies under severe applications.

I.3 SAC solder alloy

It is important to take into consideration that the properties of the alternative solders must be comparable or even better to Sn-Pb solders in selecting suitable substitute of SnPb soldering alloys. Compatible candidates of the Sn-Pb solders must have the following characteristic [3]:

- melting temperature similar to eutectic Sn-Pb for a similar reflow profile
- sufficient wettability for good metallization process
- good electrical properties for transmitting electrical signals
- strong mechanical properties for good fatigue resistance and reliability
- cheap and easier manufacturability

Among several alloy compositions that are considered as lead-free solder candidates, Sn-Ag-Cu alloys have been recognized as the most promising because of their relatively low melting temperature (compared with the Sn-Ag binary eutectic lead free solder), higher mechanical properties, and good compatibility with other components [4][5][6].

I.3.1 SAC Alloy composition

The SAC solder alloy is a hypo-eutectic ternary alloy characterized by a solidus temperature about 217°C and close to that of the tin lead eutectic. There are several types of SAC solder alloys, which are characterized by different mechanical properties due to their chemical composition. It is therefore important to know the order of appearance of the different phases during a reflow soldering profile.

Figure I.3–1 present the SAC alloy ternary phase diagram, which is derived from the binary phase diagrams SnAg and SnCu (Figure I.3–2). It shows the elementary phases induced for a near-eutectic composition: β -Sn and intermetallics Ag_3Sn and Cu_6Sn_5 . Based on a thermo-differential analysis and a thermodynamic model, Moon et al. determined the eutectic composition of the Sn-Ag-Cu alloy in 2000 [7]. The eutectic composition measured in this study gives a mass percentage of silver of $3.5 \pm 0.3\%$ and of $0.9 \pm 0.2\%$ of copper at $217.2 \pm 0.2^\circ C$. SAC-type alloys are made up overwhelmingly of tin (more than 95% by mass proportion). The microstructure of this type of alloy is based on a tin matrix in which the silver and copper are in solid solution.

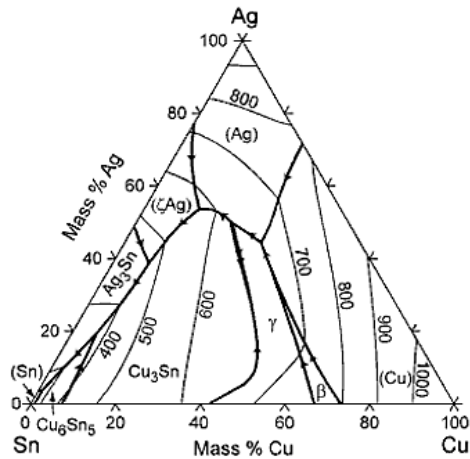


Figure I.3-1: SAC ternary phase diagram [8]

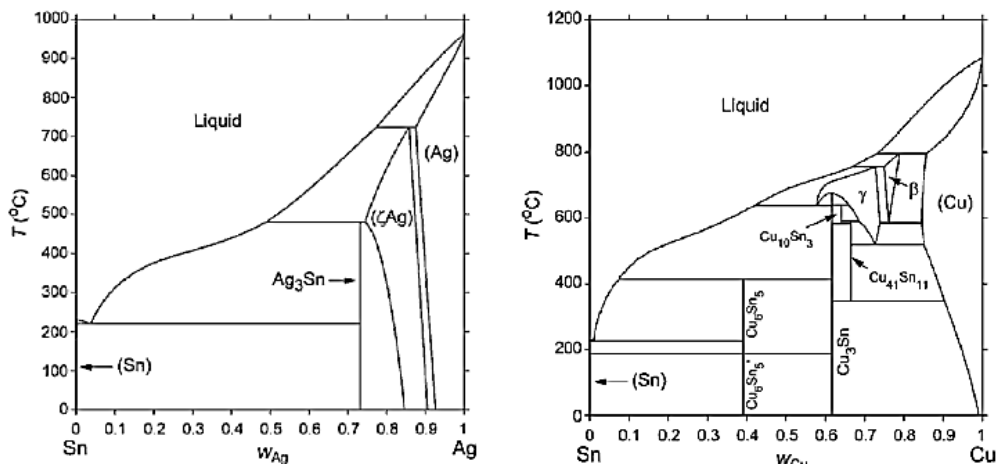


Figure I.3-2: SnAg and SnCu binary phase diagrams [7]

I.3.2 Tin structure in SAC solder joints

(a) Tin crystal structure and anisotropy

Pure tin comes in three different allotropic forms (α , β and γ) depending on the temperature range in which it is found. The structures of these phases are shown in Table I.3-1.

In solder alloys, tin is found in its β form because it exists in the temperature range in which lead-free electronic assemblies are generally used. Due to its crystal structure, there is an invariance by rotation of 90° around axis [001] which leads to equal properties of the directions [1 0 0] and [0 1 0] and clearly different of the third direction ([0 0 1]). This structure gives it anisotropic physical and mechanical properties. The Young's modulus and the Thermal Expansion Coefficient (CTE) are in fact dependent on the direction as shown in Figure I.3-3. Between the a [100] direction and the c [001] direction, the value of the CTE varies by a factor of 2 and the Young's modulus by a factor of approximately 3. From this graph, it is clear that tin in its allotropic β form exhibits the highest stiffness in the direction where its thermal expansion is greatest (direction [001]). This can generate internal stresses in the tin crystals leading to heterogeneous deformations at the grain boundaries during thermal cycling. These

deformations induced by the difference in thermal expansion between the different crystal orientations can cause a mechanism of deformation by sliding at the grain boundaries. This mechanism may make the behavior of lead-free interconnections sensitive to the SAC alloys microstructure and crystalline orientation.

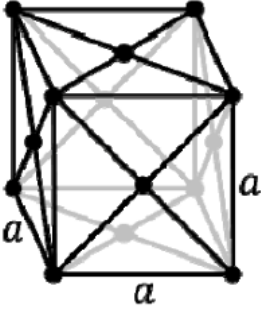
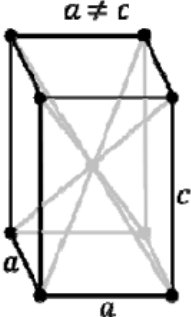
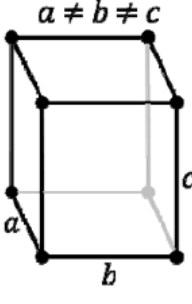
Form	α [9]	β [10]	γ [11]
Temperature	$< 13^\circ\text{C}$	$13^\circ\text{C} < T^\circ < 161^\circ\text{C}$	$161^\circ\text{C} < T^\circ < 232^\circ\text{C}$
Structure	Face-centered cubic	Tetragonal centered	Orthorhombic
Representation			

Table I.3–1: Description of tin allotropic forms [12, chap 1]

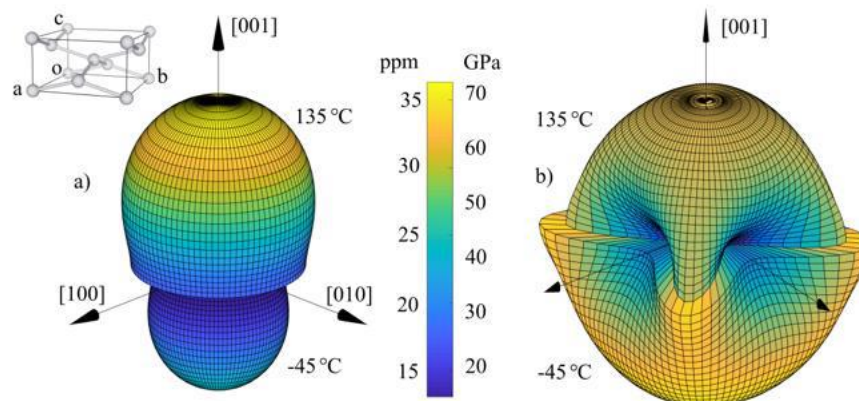


Figure I.3–3: Surface representations of the (a) coefficient of thermal expansion and (b) elastic modulus at -45°C (lower half of the surface) and 135°C (top half of the surface) for β -tin [13]

(b) *Dendritic structure*

In the cooling step, during a reflow assembly process, a phenomenon of supercooling of the SAC alloy occurs. The main consequence of this phenomenon is the dendritic structure of tin. The liquid is then in a metastable state and its temperature is lower than the temperature of the liquidus. As soon as the β -Sn phase nucleates, large ductile dendrites are quickly formed and the size of their arms increases as they move away from the nucleation site [14]. Dendrites consist of a main arm and secondary arms, the dimensions of which are in the order of a hundred and ten micrometers, respectively.

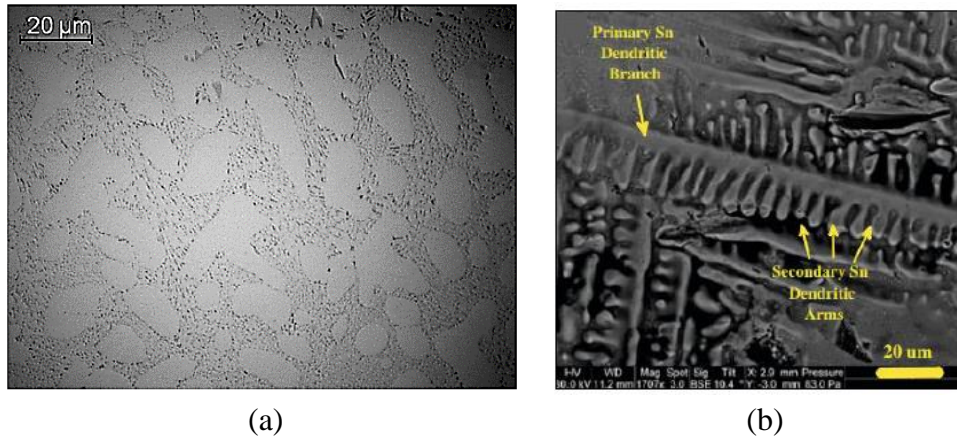


Figure I.3-4: Dendritic structure in as reflowed SAC solder joint (a) Bright light image [15], (b) SEM image of the primary and secondary arms of the tin dendrites [16]

The nucleation of tin is the key step in the solidification of SnAgCu solders. Some work [17] has suggested that the formation of dendrites can control the crystal orientation of the tin grains since the crystal lattice of these dendrites is the same as that in the tin matrix of the adjacent eutectic phase. The birefringence of tin makes it possible to observe the crystal orientations of SAC joints under an optical microscope in polarized light. Figure I.3-5 presents the dendritic structure in BGA solder joint with their different orientations observed under polarized light. They also hypothesized that the size of the tin grains was controlled by the formation of dendrites, which may explain the low number of grains possessed by SAC interconnections (Figure I.3-6).

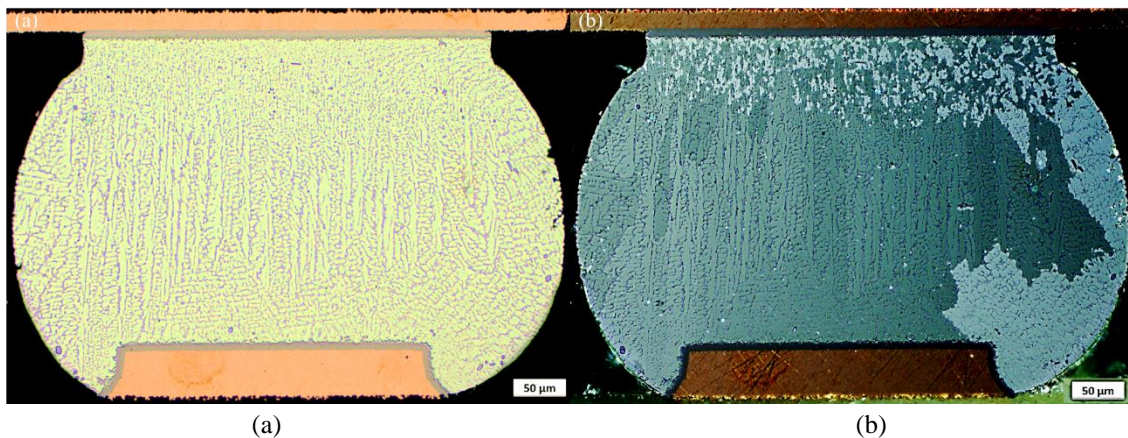


Figure I.3-5: Observation of the dendritic structure in BGA solder joint, (a) white light image, (b) polarized light image

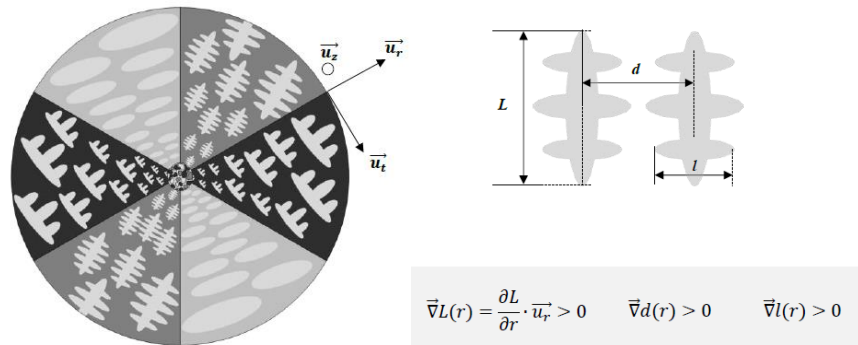


Figure I.3–6: Relationship between crystal orientation of grains and those of β -Sn dendrites. The nucleation site corresponds to a morphology of intertwined grains (the common axis of rotation [100] or [010] is collinear with the z axis) [18, chap 1]

(c) *Tin grain morphologies*

Depending on the number of nucleation sites during tin solidification and the degree of undercooling, SAC solder joints can adopt different morphologies. When solidification occurs at not too large undercooling, solder joints with only macrograined or a cyclic twin (hexacyclic) structure are normally generated [19][20][21][22]. For BGA solder joints, they usually consist of a few large Sn grains. The six-fold cyclic twinning of tin is also known to commonly occur and results in the solidification of the commonly called “beach ball” morphology in BGA components [23]. The cyclic twin phenomena is characterized by the presence of only three unique grain orientations which nominally have about 60 degrees rotations about a common axis.

SAC solder joint orientation tends to be more or less random. Adopting the colour scale of Bieler et al. [24], Lövberg et al. studied the probability of c-axis orientation if the distribution is random [13]. They determined that a red orientation should be 6 times more likely than a blue orientation by dividing the c-axis orientation into five segments with intervals of 18 degrees (Figure I.3–7).

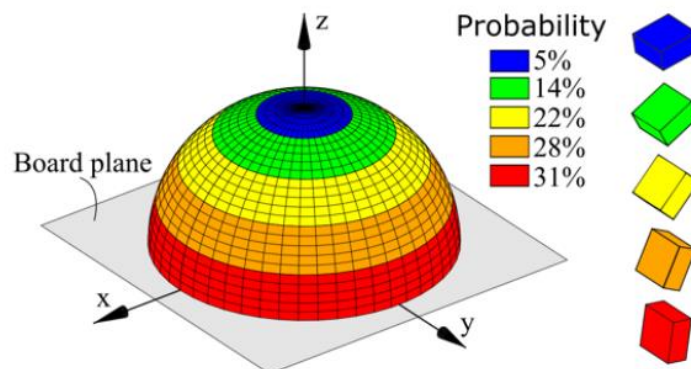


Figure I.3–7: The probability of c-axis orientation of single-grained joints if the orientation is considered stochastic [13]

At higher degrees of undercooling, an interlaced twin structure may appear in solder joints [20][21]. Although the presence of the fine grains in this structure can give the appearance of a polycrystalline structure, it is just another form of the tin twin phenomenon. As with the cyclic twin morphology, only three unique grain orientations are present with about 60 degrees rotations about a $\{100\}$ or $\{010\}$ axis.

Lehman et al. suggest that the macrograin structure is a form of hexacyclic twinning occurring at the level of the $\{101\}$ family of planes form an angle of 57.2° to each other whereas the interlaced morphology is characterized by $\{301\}$ twin planes making a 62.8° angle to each other [19].

It is also possible to observe mixed morphologies. Solder joints will have a mixture of cyclic and interlaced twin structures [25][26][27]. Normally, the interlaced structures were often localized near the interface between the solder and the copper pad on component or PCB side and at the nucleation site of the beach ball structure.

Figure I.3–8 shows the different morphologies observed in BGA SAC solder joints. The occurrence of these morphologies in BGA components depends on solder volume, alloy composition, surface finish and cooling rate. 20% to 80% of BGA solder joints are single-grained and their orientations tend to be more or less random.

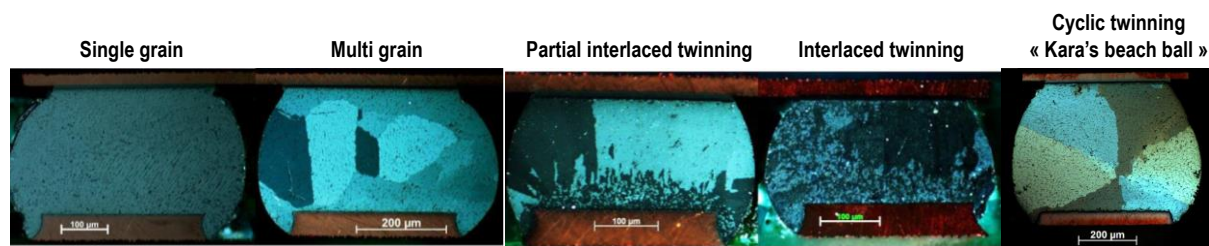


Figure I.3–8: Diversity of as-reflowed tin grain morphologies in BGA SAC solder joints [28], [29]

I.3.3 Intermetallic compounds in SAC solders

As the alloy solidifies, the silver and copper intermetallics solidify first, increasing the tin concentration in the liquid phase. Then tin begins to solidify and adopts a primary β -Sn dendritic structure which grows rapidly. The interdendritic spaces follow a binary (Sn-Ag or Sn-Cu) or ternary (Sn-Ag-Cu) eutectic structure depending on the constituents still present. In the case of SAC305 interconnection joint, due to the low copper content and its migration to interfaces during cooling, the eutectic phase is mainly composed of a fine dispersion of very small Ag_3Sn in a tin matrix. Depending on the surface finish, Cu_6Sn_5 or $(\text{Cu}, \text{Ni})_6\text{Sn}_5$ precipitates are generally dispersed in the solder joints. Intermetallic layers also form at the interfaces between the metallized transfer pads and the solder joint by reaction between the Sn in the solder alloy and the chemical elements of the solder pad and surface finish. The SAC305 solder joint microstructure is presented in Figure I.3–9.

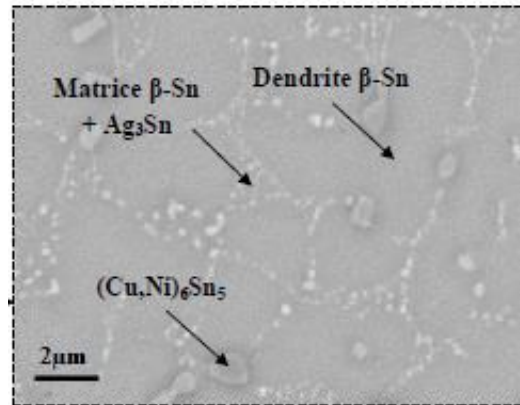


Figure I.3–9: SEM image of SAC305 alloy [18]

The dendrite size, their spacing, the tin grain size and the IMCs number and shape characterize the solder alloys microstructure. These characteristics mainly depend on the following factors:

- the alloy composition,
- the reflow profile,
- the solder joint size,
- the interface finish;

I.3.4 Influence of Ag and Cu mass content

The copper and silver contents also have a role in the order of appearance of the different phases during solidification. Thus, a very small variation in the percentage of Cu or Ag can modify the solidification process and consequently the microstructure. The dendritic growth of primary β -Sn is a very common crystal structure in binary or ternary tin-rich solder such as Sn-0.7Cu, Sn-3.5Ag, and Sn-3.8Ag-0.7Cu. It is more difficult to observe a dendritic structure in pure tin, even if the dendritic growth has already been observed there.

In these tin-rich alloys, the increase of silver content (up to 3.8%) induces a greater number of small IMCs. Figure I.3–10 clearly shows that a higher silver content also induces finer tin dendrites [30].

The Ag content can have also an impact on SAC solder morphologies. For solders with a low Ag content (1-2%), a low fraction of interlaced solder joints was obtained whereas a high fraction of interlaced solder joints was observed when the Ag content was high (3-4%) (Figure I.3–11) [31].

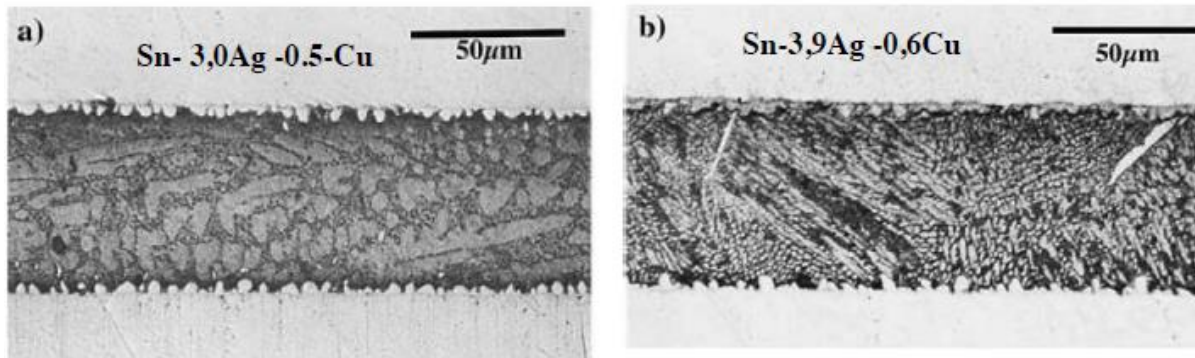


Figure I.3–10: SEM images of different compositions SAC solder joints – (a) Sn-3,0Ag-0,5Cu –(b) Sn-3,9Ag-0,6Cu [30]

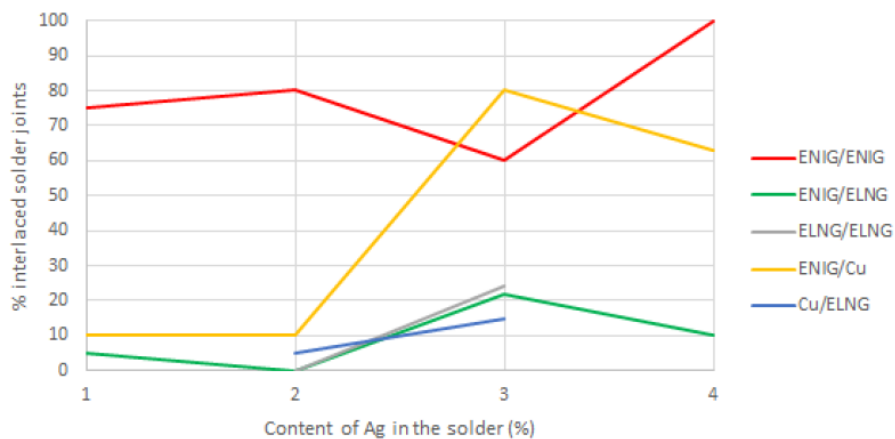


Figure I.3–11: Correlation between the content of Ag in the SAC solder balls and the fraction of interlaced solder joints for the various surfaces finishes [31]

It has been found that an increase in the proportion of Cu would produce a dendritic growth in β -Sn [32, chap 1]. The formation of the primary Ag_3Sn phase also depends on the Cu content. It allows the appearance of large Ag_3Sn plates during solidification by helping the nucleation of these plates [33].

I.3.5 Influence of the reflow profile

The initial microstructure of SAC alloys is strongly influenced by the reflow profile during the soldering process in electronic assemblies. These alloys are characterized by a low reflow temperature close to that of the tin lead eutectic. This reflow temperature represents a determining parameter in the characterization of the solder material, but is not the only important factor. Parks et al. studied the effect of the solidification temperature in the tin grain morphology. They pointed out a very high relation between this parameter and the presence of interlaced structure. Less than 15% of the solder bumps that had solidified at temperatures above 203°C had interlaced or mixed morphology, whereas more than 90% of the solder bumps that solidified below 199°C had interlaced or mixed morphology [34].

The cooling step also plays a crucial role in the final microstructure. The cooling rate has several effects on the internal structure of SAC alloys. It indeed affects the development of dendrites as well as the morphology of the IMCs formed at the interfaces. As mention in [35], several studies have been carried out in order to highlight the influence of the cooling rate on the microstructure of SAC alloys. Kim studied in particular the influence of three cooling rates on the microstructure of the SAC305 alloy. In their work, they showed that the interdendritic spacing increases as the cooling rate decreases [36]. Figure I.3–12 presents SEM pictures of cross-sections obtained on SAC305 samples obtained under different cooling rates during reflow soldering. A slow cooling can lead to the formation of large Ag_3Sn pro-eutectic plates which mechanically weaken the material. Therefore, increasing this speed can reduce the pro-eutectic phase and improve the mechanical properties. However, a high cooling rate can induce harmful effects such as thermal stress or deformation of a substrate [32, chap1].

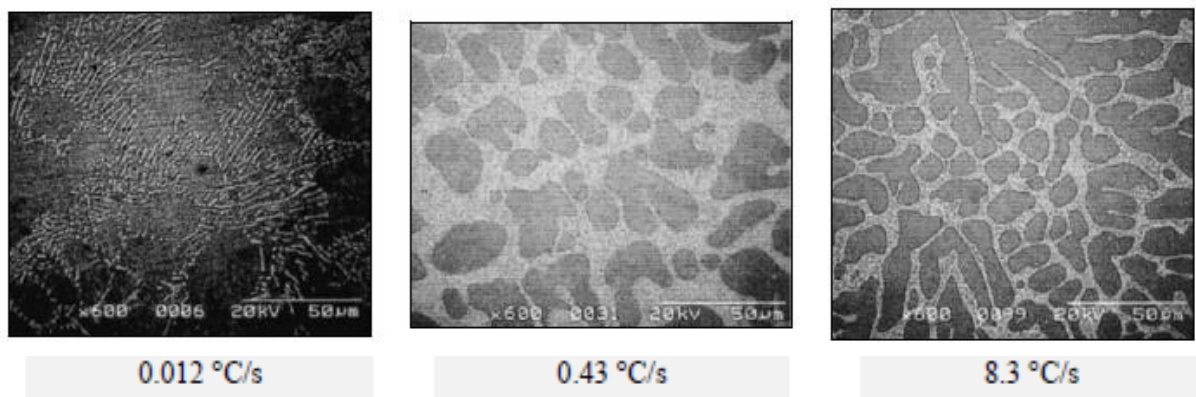


Figure I.3–12: SAC305 microstructure depending on the cooling rate [36]

I.3.6 Influence of the surface finish layer

The electronic components are soldered on copper pads of the printed circuit board. Several layers of copper are deposited during the manufacturing of the board by electrochemical and electrolytic processes. A finishing layer, either organic or metallic, is deposited on these areas whose first role is to avoid oxidation and corrosion during soldering and storage of PCBs. This allows good wetting of the alloy during assembly.

IMCs grow at the interfaces by diffusion. Some of these compounds (Cu_6Sn_5) allow a good metal bonding. Other compounds (Cu_3Sn) can weaken the interface during mechanical stresses. The Cu_3Sn compounds do not grow during the assembly process but during thermal aging. Certain metallic finishes can limit the development of weak IMCs at the interfaces. For example, a nickel-based finish is often used to avoid the diffusion of copper in the solder joint. The elements of the finishes will indeed diffuse into the more ductile solder joint and will thus be able to alter its mechanical properties. Table I.3–1 gives the main IMCs found at the interfaces depending on the finish of the board copper pads, which can be organic or metallic.

Table I.3–2: Main IMCs observed at the interface between SAC alloy and copper pads, depending on the surface finish [37]

Finish	Ag	Sn	NiAu (ENIG)	OSP (Organic Solderability Preservative)
IMCs at the interface solder/pads (Cu)	Cu_6Sn_5 Cu_3Sn (after aging)	Cu_6Sn_5 Cu_3Sn (after aging)	Ni_3Sn_4 $(\text{Cu}, \text{Ni})_3\text{Sn}_4$	Cu_6Sn_5 Cu_3Sn (after aging)

Berthou et al. also showed that surface finishes play a role in the growth dynamics of IMCs during isothermal aging [38]. The growth of IMCs is slower on ENIG finishes. Pure tin finishes give thicker IMCs layers from $t = 0$ (around $3.8 \mu\text{m}$ then 5 to $8 \mu\text{m}$ after 1000h of aging). In most cases, the Cu_6Sn_5 IMCs form a layer about $3 \mu\text{m}$ thick. In the case of Ni_3Sn_4 compounds, the layer measures from 1 to $2 \mu\text{m}$. Figure I.3–13 shows two soldered interfaces, one with copper and one with nickel.

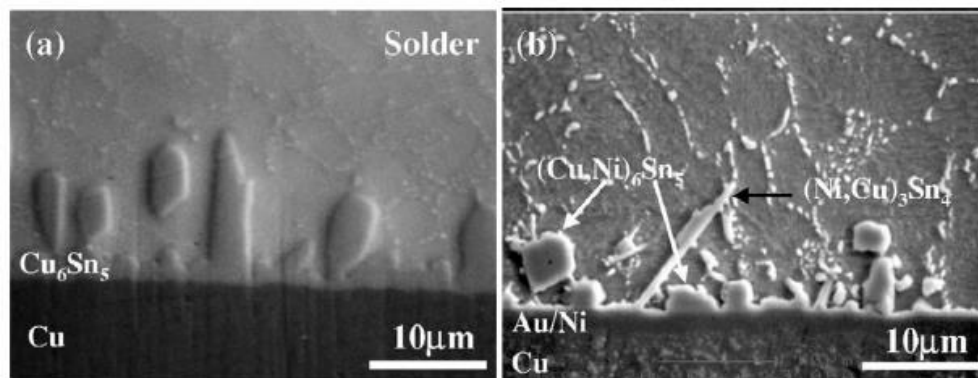


Figure I.3–13: SEM images of solder/copper interface (a) and solder/nickel interface (NiAu finish) (b) with a Sn-3,5Ag solder alloy [4]

The surface finish of solder joints can also affect tin grain morphology. Arfaei et al. clearly show that solder joints formed when both solder pads had Ni finish (ENIG/ENIG, ENIG/ELNG or ELNG/ELNG) had a low fraction of interlaced structure when at least one of the pads had ELNG as surface finish and a high fraction when both pads had ENIG as surface finish with exception for the solder joints with the smallest diameter ($250 \mu\text{m}$). For the smallest solder joints, when both pads had ELNG as surface finish, the fraction of solder joints with interlaced solder joints was still low. However, a high fraction of interlaced solder joints was observed when one of the pads had ELNG as surface finish and a low fraction when both pads had ENIG as surface finish [26].

I.3.7 Influence of isothermal aging

In certain applications, electronic boards can be subjected to a long storage period before their use. It is therefore necessary to ensure that the solder joints remain in good condition after this storage. Therefore, an understanding of the aging mechanism and its effects on the evolution of the microstructure is necessary in order to check whether a long storage period affects the reliability of the solder joint.

Several studies focused on the understanding of the evolution of the SAC solder joints microstructure under isothermal stress. Prolonged exposure to temperature causes coarsening of the bulk precipitates. They remain localized in interdendritic spaces but their average size and spacing increase. This coalescence phenomenon is illustrated by Figure I.3–14 from the literature [39]. Chauhan et al.[40] have shown that the size of the Ag_3Sn nanometric particles increased by 34% and their spacing by 67% after a thermal aging of 1000 hours at 100°C . This microstructural evolution has a direct influence on the overall mechanical properties of the solder joint. It reduces the effect of blocking dislocations by precipitates and lowering the resistance of the alloy to deformation. A drop in the yield strength and in the hardness values after a few hundred hours at more than 100°C has been observed in the work of Dompierre [12, chap 3]. Figure I.3–15 shows the evolution of Young's modulus and yield strength during isothermal aging.

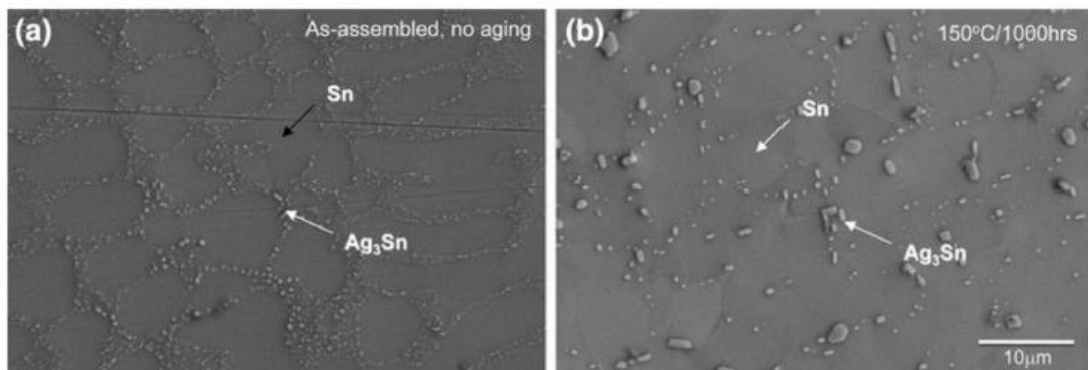


Figure I.3–14: Effect of pre-aging at 150°C (1000h) on the SAC305 microstructure [39]

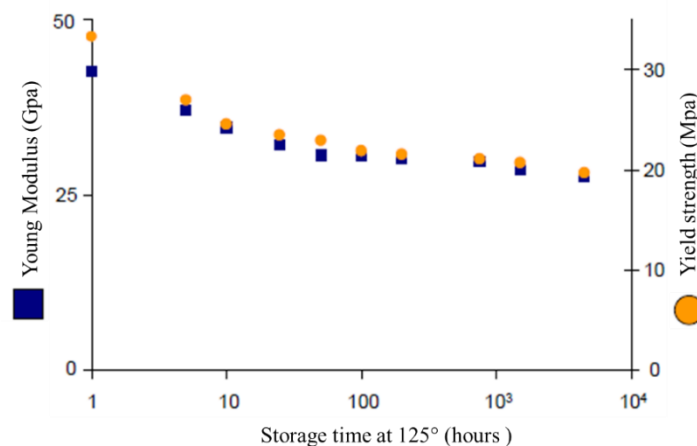


Figure I.3–15: Evolution of SAC405 Young modulus and yield strength after aging at 125°C [41]

Isothermal aging also increases the thickness of the intermetallic layers. These layers enrich with tin and copper from the SAC alloy and copper or nickel from the substrate. Figure I.3–16 presents SEM images revealing the growth of intermetallic interfaces during isothermal aging. The thickness of the intermetallic contact layers changes due to interatomic diffusion occurring during storage at constant temperature. The thermal aging conditions specific to each electronic application are therefore to be considered.

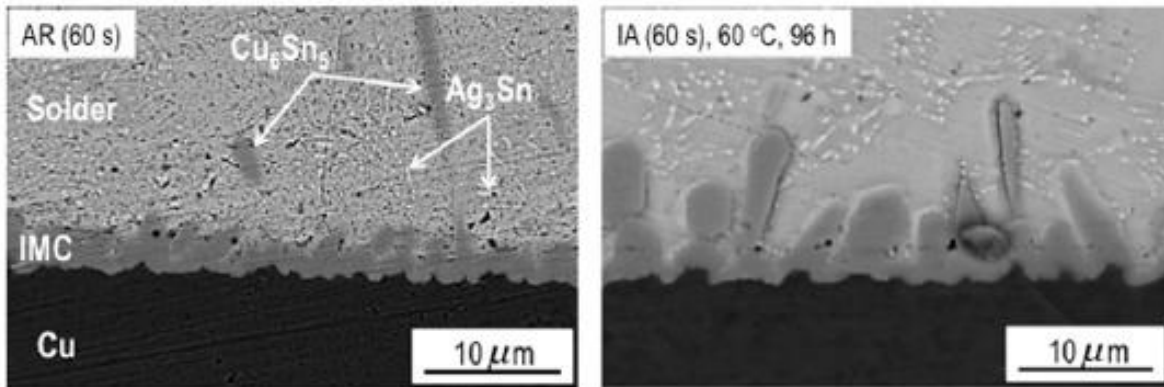


Figure I.3–16: IMCs growth at the interfaces between SAC305 and copper pads [42]

We find also in the literature several works on the evolution of visco-plasticity under different temperatures of isothermal aging [43][44]. Figure I.3–17 shows the results of a study carried out on several solder alloys and which focuses on the effects of isothermal aging at room temperature. The stress-strain curves clearly show the reduction in the strain resistance of the solder material caused by the cumulative effects of aging over time. After a certain duration, the variation of the ultimate stress reaches a slightly oblique affine asymptotic limit. This trend is present for all data series in this REF [43]. After 500 hours of aging at 25 C, the reduction in ultimate stress is approximately 24.6% and the reduction in yield stress is approximately 26.9%. This reduction is considerable, especially since, in real life, a period of several tens of days of storage between assembly and use is quite normal.

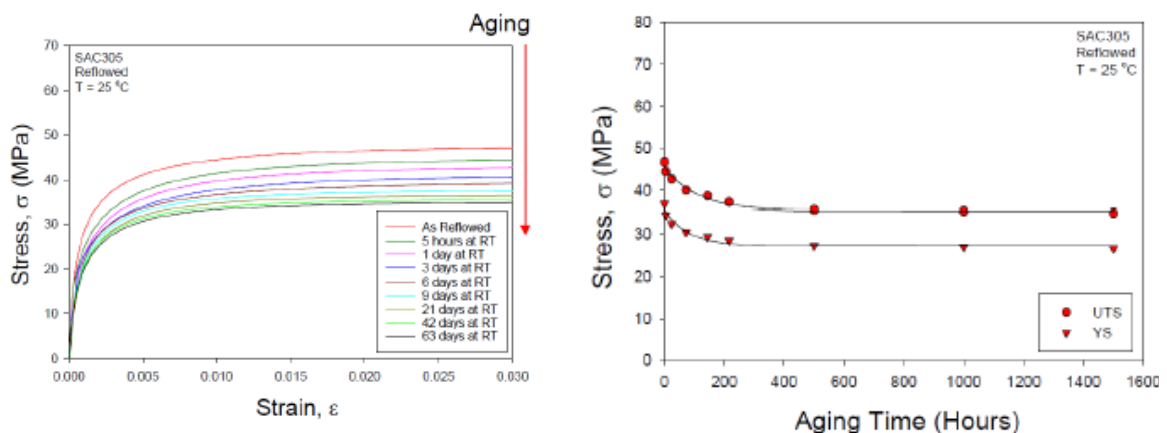


Figure I.3–17: Evolution of the SAC305 plasticity characteristic as a function of the isothermal aging time carried out at 25°C [43]

I.3.8 Synthesis

Lead-free solder joints are characterized by a complex microstructure. It often consists of only one or a few randomly oriented tin grains present in different morphologies. Several parameters influence this microstructure, in particular the cooling rate of the alloy, the composition, or even thermal aging. Due to these evolutions and coupled with the highly anisotropic properties of the tin phase, the thermomechanical response of SAC solder joints can be greatly impacted by these factors.

I.4 Thermomechanical fatigue of SAC solder joint

The solder joint of an assembly is designed to fulfill a mechanical role for a given mission profile. Therefore, it is necessary to know its behavior and performance during its operation.

The characterization of the solder joint service life takes into account various harsh stresses in operational environments: temperature, thermal and mechanical cycles, vibrations, shocks, etc. The degradation and fatigue of materials are the activated phenomena within the system. The degradation or aging of a material is the alteration of its mechanical, electrical or thermal properties. This happens both in the face of cyclic stresses and in a stationary load (eg: isothermal). Fatigue, for its part, necessarily involves cyclical stress. The repetition of this stress, although below the limiting loading conditions of the material, produces an internal change in the system leading gradually to its damage. This is in a way a special case of degradation. The Wöhler curve or S-N curve expresses the relation between the applied stress and the number of cycles to failure (Figure I.4–1).

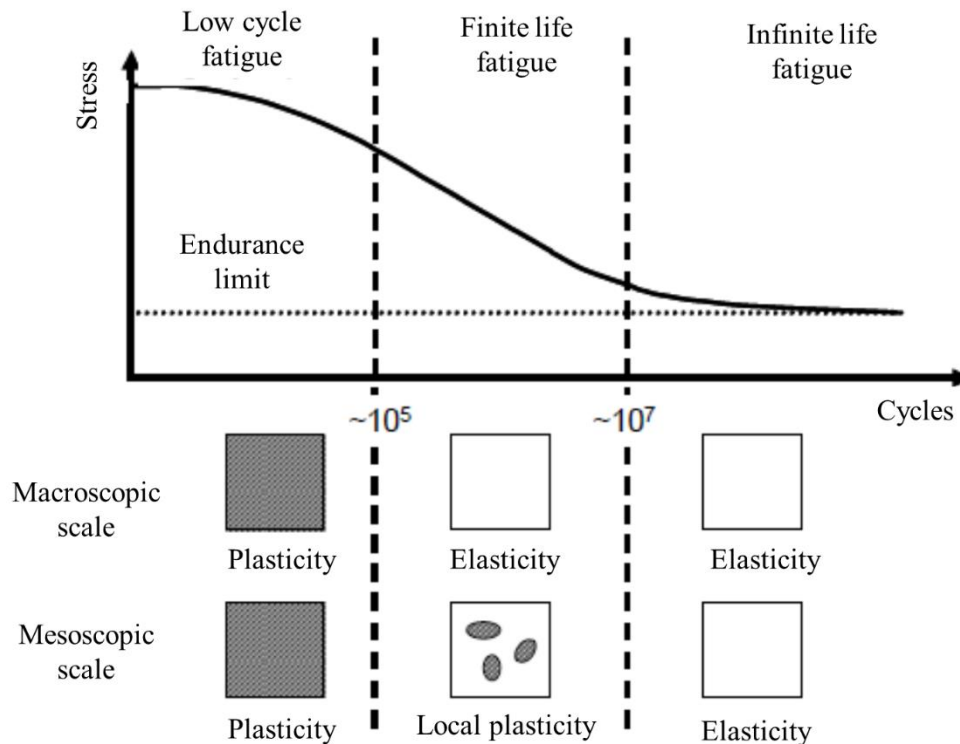


Figure I.4–1: Wöhler curve and the associated material behavior in fatigue

The fatigue characterization approach generally consists of identifying the fatigue mechanism: influencing factors, damage observation and failure mode. During their life cycle, electronic equipment will indeed undergo thermomechanical and mechanical loads during handling, storage, transport and operational phases.

Electronic boards are usually submitted to the mechanical fatigue due to the operating system and the environment. Mechanical stresses are transmitted by the system to the electronic board inducing the bending of the PCB, and especially for frequencies around the resonant frequency of the electronic board where the bending of the PCB is high. The mechanical strength of

interconnections is strongly correlated with the deformation of the PCB and the inertial forces due to the mass of the component. Mechanical shear stresses are also induced in the solder joints by this bending, conducting to the High Cycle Fatigue regime characterized by a high number of failure cycles ($> 10^4 - 10^5$ cycles).

The thermomechanical fatigue failure of solder joints induced during temperature variations is the leading cause of electronic assembly failures. Solder joints subjected to temperature fluctuations do not generally have lifetimes greater than 10^4 cycles. Therefore, solder joints thermomechanical fatigue corresponds to the domain of low number of cycles to failure (Low Cycle Fatigue). The initiation and propagation of fatigue cracks generated during thermal cycling mainly result from the very large differences in CTE between the component and the PCB. These differential expansions will indeed generate shear deformations in the interconnection joints. Tensile stress can also be observed by structural effect in particular for large package. The cyclical repetition of these sollicitations will ultimately be able to lead to the electronic assembly failure. Manufacturers use accelerated Thermal Cycling (ATC) in order to study solder joint reliability. The electronic board is submitted to a temperature profile, including dwell times at extreme temperatures. The amplitude of thermal variation is adjusted depending on the application.

I.4.1 Evolution of SAC solder joint microstructure during thermal cycling

When a lead-free solder is subjected to thermal cycling, viscoplastic strains can be generated due to the CTE mismatch between the various elements of the assembly (component, copper, board) leading to the formation of new β -Sn grains characteristic of the recrystallization phenomenon. The release of internal plastic energy accumulated in regions of high strain during thermal cycles is the main cause of tin recrystallization. The recrystallization is firstly characterized by the production of a large number of randomly orientated subgrains in the higher strain areas generated by the creation and movement of dislocations within the solder β -Sn grains. Then, a network of high angle grain boundaries along the high strain region during thermal cycling is formed by the rearrangement and / or annihilation of dislocations after a global recrystallization. This microstructural phenomenon precedes the initiation and propagation of fatigue cracks. Initially, recrystallization is slowed down due to precipitation hardening caused by Ag_3Sn intermetallic (IMC) particles but strain-enhanced coarsening will take place during the thermal cycles. This coarsening decreases the pinning effect of the secondary precipitates, allowing the formation and rotation of subgrains that will finally lead to high angle grain boundaries [45][46].

Zhou et al.[47] explained the phenomena responsible for thermomechanical damage in the SAC305 solder joints. They have shown that the local plastic stresses generated during thermal cycling create dislocations which will be able to rearrange themselves to form sub-grain boundaries. As the cycling progress, the dislocation walls mobility will increase and lead to the sub-grains rotation which will gradually become recrystallized grains without internal defects.

Arfaei et al. highlighted the damage mechanisms generated during the thermomechanical fatigue of SAC305 solder joints. They showed from EBSD analyses on BGA solder joints that

the cracks propagated by a sliding mechanism at the grain boundaries through the network of highly disoriented recrystallized grains in high strain regions. The EBSD technique reveals the crystal orientation of each grain. Observations showed that tin grains close to the fatigue crack have greater angles of misorientation than in the rest of the solder joint [29]. Figure I.4–2.c shows an EBSD orientation map obtained from a damaged SAC interconnect ball.

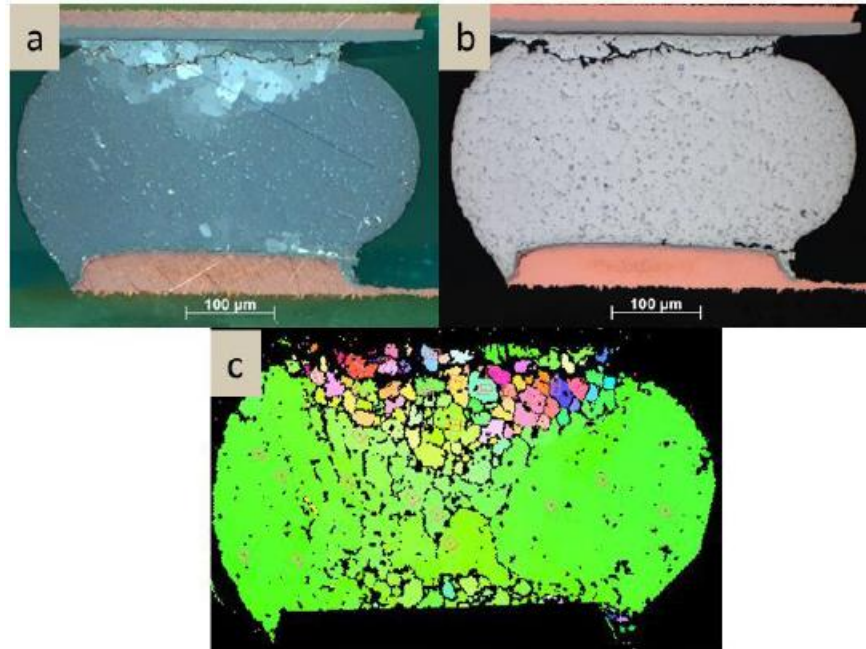


Figure I.4–2: Cross-section of a solder joint after thermal cycling : polarized light (a), optical microscope (b), EBSD orientation map [29]

Thus, two microstructural phenomena are present during thermomechanical damage. The phenomenon of recovery precedes the recrystallization and is characterized by movement, annihilation, grouping of dislocations and the formation of sub-grain boundaries with low misorientation angles. It requires less activation energy that seems to be a prerequisite for the recrystallization [48][49]. For the recrystallization phenomenon, it consists in the rotation of the sub-grain boundaries around the [001] axis allowing the nucleation and growth of new tin grains with high misorientation angles. Finally, the grains generated form a network of grain boundaries with large misorientation angles which constitutes a favorable path for the intergranular crack propagation [46].

IMCs coalescence is also a phenomenon that has an effect on solder joints damage [50][51][52]. It is very closely correlated to the recrystallization phenomenon of SAC alloys. The conditions generated during the thermal cycling tests allow the growth of these particles. The intermetallic particles in solder joints, mainly Ag_3Sn , cause precipitation hardening of the solder. The larger the number of particles and the more evenly they are distributed, the higher the precipitation hardening will be. Under thermal cycling, Ag_3Sn IMCs in the solder joints coarsen, the largest particles grow in size and smaller particles dissolve and disappear. This leads to the disappearance of the dendritic structure and will decrease the precipitation hardening and make the solder softer, which will accelerate the recrystallization. This process is called precipitation coarsening. It is also enhanced by strain that contributes to the reason

why recrystallization occurs more quickly near the package interface. At the same time, larger Ag_3Sn precipitates tend to move towards grain boundaries as coalescence takes place. This ascertainment proposes that strain-enhanced Ag_3Sn coalescence is driven by grain boundary diffusion [53]. The degree of precipitation hardening has a large influence on the number of cycles required for recrystallization. Finely dispersed IMCs of nanometric size can indeed act as barriers to the dislocations motion induced by viscoplastic strain and inhibit SAC305 solder damage by dislocation pinning process [54].

Arfaei et al. studied the microstructural evolution due to thermomechanical stresses in BGA and QFN SAC305 solder joints. Their SEM observations highlighted the Ag_3Sn IMCs coalescence in the high strain regions [54]. Yin et al. also explained the influence of thermal stresses on the size of Ag_3Sn IMCs and their spacing. They showed the increase in the size of the Ag_3Sn IMCs in the high strain regions where recrystallization occurs, leading to the disappearance of the dendritic structure (Figure I.4–3) [27]. The dwell time imposed at the maximum temperature causes isothermal aging and can participate on the coalescence of IMCs.

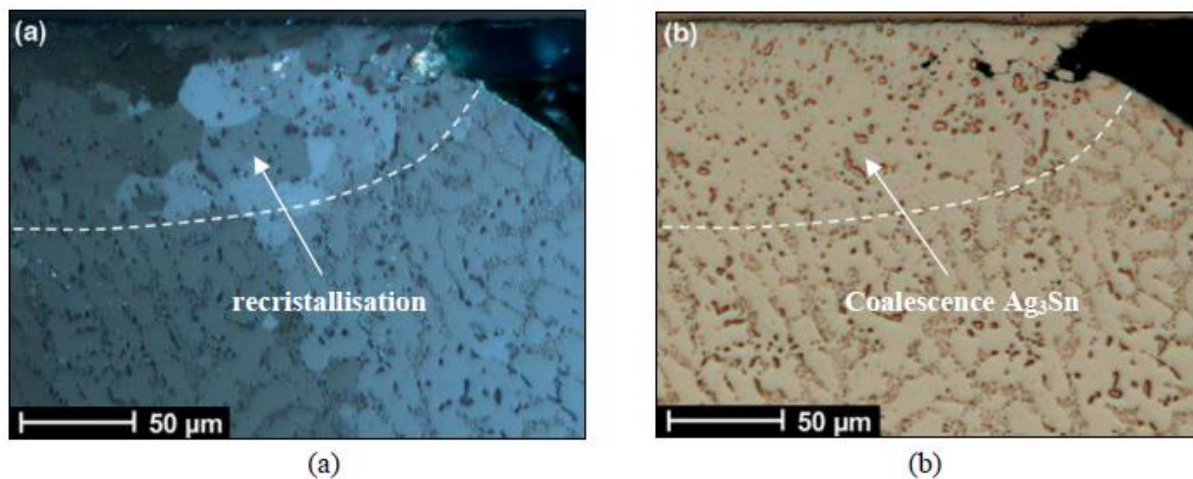


Figure I.4–3: Recrystallization (a) and Ag_3Sn phase coalescence (b) in high strain regions [27]

Yin et al. summarize thermomechanical fatigue cracking in SAC solder joints in three steps as shown in Figure I.4–4 [52]. In the first step (Figure I.4–4 (a)), IMC particles precipitation coarsening will happen primarily in the high strain regions close to the solder pads. At the same time, slowly growing transgranular cracks can also initiate at the joints corners. Secondly (Figure I.4–4 (b)), recrystallization will occur all the way through the high strain region starting in the joint corners which will facilitate intergranular crack growth between the grains. These cracks may grow considerably faster than the initial transgranular crack(s). Finally (Figure I.4–4 (c)), the intergranular cracks will propagate across the recrystallized region until a total failure.

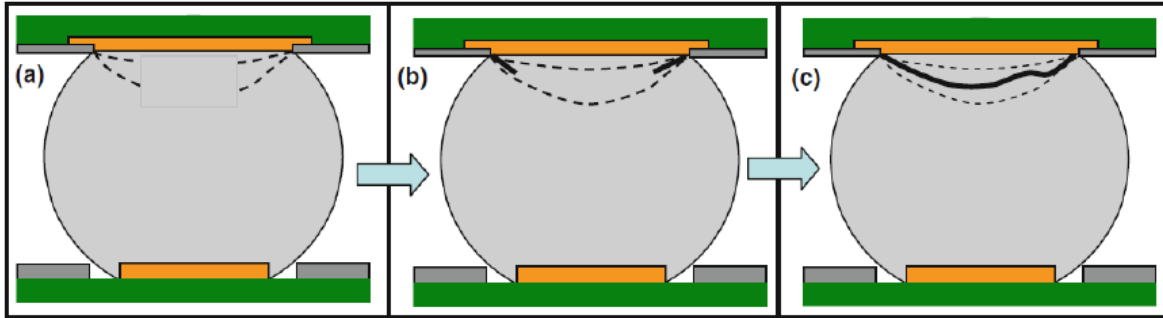


Figure I.4-4: Formation of cracks in BGA solder joints during thermomechanical fatigue [52]

I.4.2 Thermomechanical fatigue models

Once the fatigue process is known, it remains to model its behavior. A thermomechanical fatigue model correlates a certain metrics (stresses, strain, and energy) with a number of cycles to failure obtained from accelerated test results. The local assessment of the thermomechanical loads exerted on the solder joints is therefore fundamental for developing predictive lifetime models of electronic assemblies subjected to severe thermal cycles. Since the dimensions of the solder joints are too small to allow direct measurement of stresses and strains, finite element modelling is commonly used to assess the level of loading generated at the level of the interconnections during accelerated thermal cycling tests. This calculation requires the prior determination of the constitutive law of the alloy in question. The damage criterion must be chosen carefully to be representative of the solder material damage during the thermomechanical fatigue, Fatigue models are generally introduced by a power law.

$$X = k(N)^c \quad (\text{I.4-1})$$

X: Fatigue criterion
 k, c: Materials parameters
 N: number of cycles to failure

(a) Fatigue models based on plastic deformation

The most used model for the evaluation of the solder joints thermomechanical durability is the Coffin-Manson law. It involves the plastic deformations amplitude as a fatigue criterion and was initially developed to evaluate the oligocyclic fatigue of ductile metals. This constitutive equation was independently determined by L.F. Coffin and S.S. Manson in 1954 [55], hence the name it bears today.

$$\frac{\Delta \varepsilon_p}{2} = \varepsilon'_f (2N_f)^c \quad (\text{I.4-2})$$

$\Delta \varepsilon_p$: Plastic strain amplitude
 ε'_f : Ductility Coefficient
 c: Ductility exponent
 N: Number of cycles to failure

In order to account for the stress mode mainly experienced by interconnection joints during thermal cycles, Solomon developed a Coffin-Manson model modified in shear [56]. The only difference is that it is based on the plastic shear (or slip) strain. The mathematical formalism corresponding to the developed fatigue law is as follows:

$$\Delta\gamma_p N_p^\alpha = \theta \quad (\text{I.4-3})$$

$\Delta\gamma_p$: Amplitude of plastic strains in shear
 α, θ : Materials parameters
 N : Number of cycles to failure

(b) *Fatigue models based on energy*

Fatigue models commonly used today are based on an energy criterion. The determination of the inelastic strain energy density dissipated during a cycle has the advantage of taking into account both the amplitude of the strains and the stresses generated. This metric is generally calculated by finite element simulations but can also be measured by calculating the area of the stress-strain hysteresis loop obtained. The first fatigue law considering this type of criterion was developed by Morrow in 1965 [57]:

$$N^m \Delta W = C \quad (\text{I.4-4})$$

$$N = K_1 (\Delta W)^{K_2} \quad (\text{I.4-5})$$

$$K_1 = C^{\frac{1}{m}} \text{ et } K_2 = -\frac{1}{m} \quad (\text{I.4-6})$$

ΔW : Inelastic strain energy density
 m : Fatigue exponent
 C : Ductility Coefficient
 N : Number of cycles to failure

In order to improve the existing fatigue models by considerations of fracture mechanics, Darveaux set up a thermomechanical life evaluation model taking into account the initiation and propagation of fatigue cracks [58]. Its model, adapted from the law of Paris, is therefore divided into two contributions: the number of cycles necessary to initiate a fatigue crack, then the crack propagation speed. A limitation of this model lies in the assumption of a constant propagation speed which is not representative of the transient regime reached during the damage of the solder joints

$$N_i = K_1 (\Delta W)^{K_2} \quad (\text{I.4-7})$$

$$\frac{da}{dN} = K_3 (\Delta W)^{K_4} \quad (\text{I.4-8})$$

$$N = N_i + \frac{a}{\frac{da}{dN}} \quad (\text{I.4-9})$$

ΔW : Inelastic strain energy density
 N_i : Number of cycles to crack initiation
 $\frac{da}{dN}$: Crack propagation rate
 N : Number of cycles to failure
 a : Final crack length
 $K_i, i \in [1,4]$: Materials parameters

I.4.3 Factors impacting SAC solder joints thermomechanical response

(a) Influence of thermal cycling parameters

Solder failures in thermal cycling are due to the combination of two phenomena: fatigue due to plastic deformations and creep. The relative preponderance of one of the phenomena over the other depends on a large number of factors, including:

- dwell time,
- maximum temperature,
- temperature gradient.

Several studies have been conducted to understand the effects of thermal cycling conditions on the reliability of lead-free interconnections [15][18, chap 3] [38]. It has been shown that the dwell time at extreme temperatures is one of the most important parameters. The creep phenomenon is activated during the cycling, and the higher the temperature, the greater the creep. Therefore, the dwell time has an influence on the mechanical behavior of solder joints since a long holding time allows better stress relaxation than a short dwell. This time must therefore be long enough to allow stress relaxation.

The dwell times are therefore dependent on the creep / relaxation phenomenon which itself depends on the temperature ranges used during thermal cycling. Libot [18, chap 3] has shown that the durability of assemblies decreases when the dwell times increase. This therefore means that the thermomechanical damage to the joints increases with the dwell time and that the relaxation of the stress accumulated in the SAC305 solder joints requires significant time. Figure I.4–5 highlights the influence of the duration of the dwell times on the number of cycles to failure as well as the temperature range.

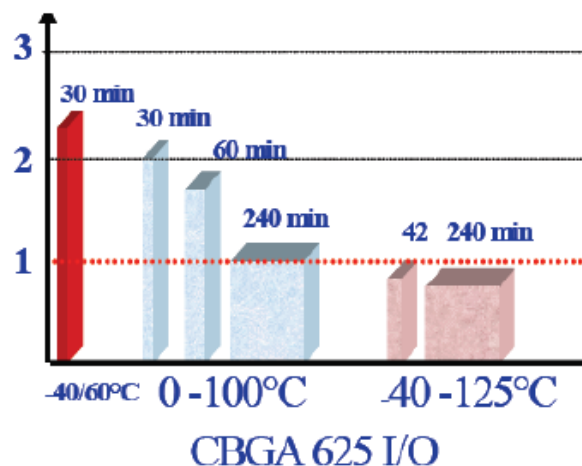


Figure I.4–5: Normalized number of cycles to failure in CBGA 625 lead-free / tin-lead solder joints, depending on temperature range and dwell time [38]

Isothermal storage, in particular at high temperature, also has an effect on the evolution of the SAC microstructure (activation of IMCs coalescence). Other studies have been conducted to better understand the effect of the maximum temperature difference on the number of cycles to failure. For example, Libot's work has shown that the maximum thermal strain generated at critical solder joints is directly proportional to the temperature range imposed during accelerated testing [18, chap 3]. The thermomechanical damage to the SAC305 interconnections is therefore greater when the thermal excursion increases and the resulting service life is therefore shorter. Figure I.4–6 shows the influence of thermal amplitudes on the number of failure cycles for LCC components.

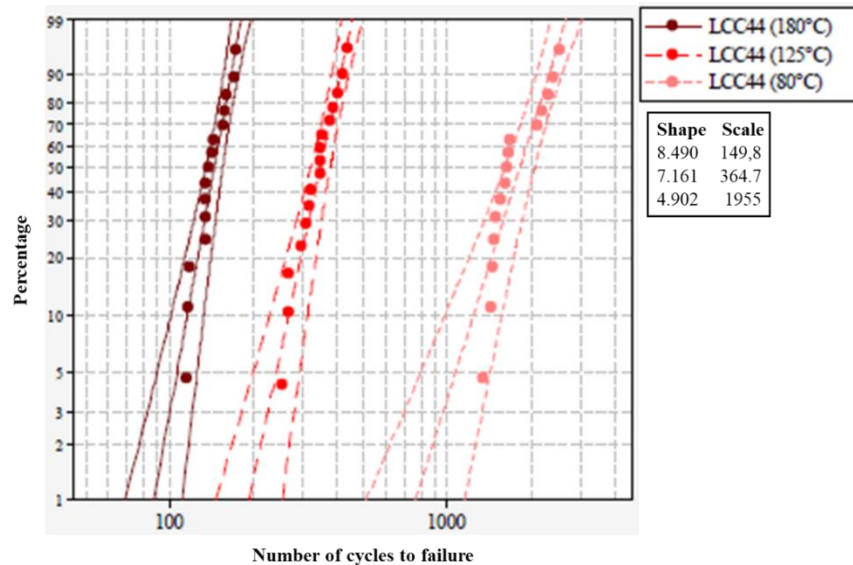


Figure I.4–6: Influence of thermal range in thermal cycling (80°C, 125°C and 180°C) : Weibull plots for LCC44 components [18, chap 3]

(b) *Effect of solder joint and package geometry*

Solder joints are designed to be submitted to different mission profiles. Consequently, their behavior depends on their geometry. However, the term geometry can imply several parameters such as the ball size, the pitch between solder joints, the die size, the molding compound size, the soldering configuration (Solder Mask Defined or not), etc.

Several works have studied the effect of the solder joint geometry of the solder joint. Arfaei et al. highlighted the effect of ball size on the durability of lead-free solder joints. The Weibull plots for BGA failures at different ball sizes show that the biggest balls have the longest lifetime in thermomechanical fatigue (Figure I.4–7) [29].

The die size is another factor that can affect the solder joints behavior during thermal cycling. Tegehall and Lovberg [59] have proven with finite element (FE) models that the die size influences the strain level in the corner joint. Figure I.4–8 shows that the accumulated creep strain value is greater in the case of a wider die.

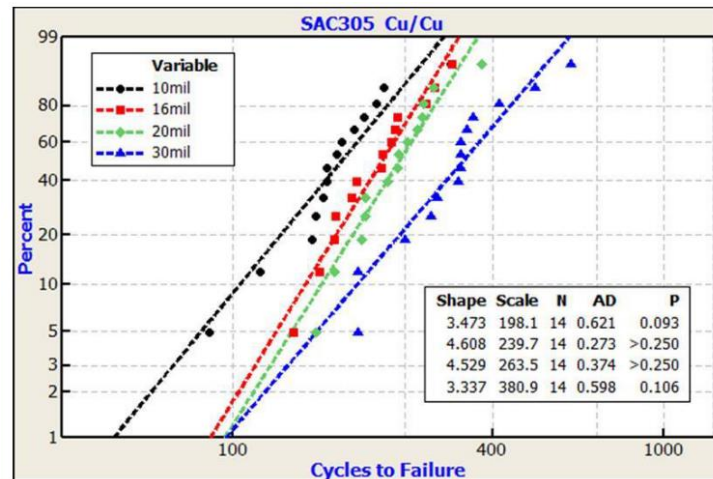


Figure I.4–7: Weibull probability for BGA failure in thermal cycling, depending on the ball size [29]

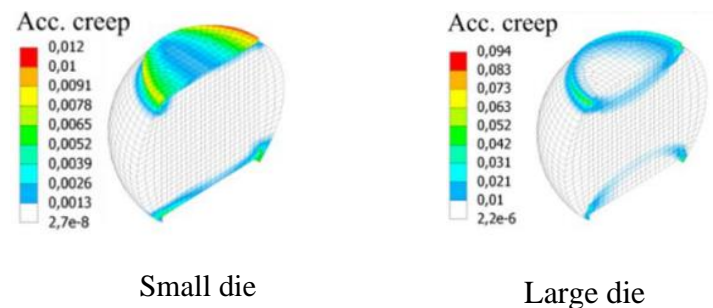


Figure I.4–8: Accumulated creep strain in the corner joint over one thermal cycle (0-100°C) [59]

(c) *Effect of as-reflowed microstructure*

Numerous studies have shown the complex microstructure observed in the initial state of SAC305 [20][60][61]. Due to this stochastic as-soldered microstructure and coupled with the highly anisotropic properties of the tin phase, the thermomechanical response of SAC solder joints greatly depends on the morphology and crystal orientation of its Sn grains [25][62]. For these reasons, early failures may occur unexpectedly and predicting the first failed joint is quite difficult [63][64]. Failures may be more or less randomly located and not always at the position of highest global strain or distance to neutral point [21][47]. The main challenge is hence to predict the position of the first cracked joints using a Finite Elements (FE) model that considers initial solder joint microstructure. Some authors already began to study the effect of anisotropy of coarse-grained joints by considering microstructure in their creep model [65].

The reliability of solder joints is affected by Sn grain morphology and orientation. In Ref. [60], single-grained solder joints with certain orientations were observed to fail unexpectedly early, as compared to multi-grained SnAgCu solder joints. The presence of an interlaced Sn grain morphology was correlated with a delay in crack initiation and the degree of interlaced tin grain morphology has an impact on the fatigue lifetime of solder joint. Arfaei et al. showed that the variation of lifetimes with changes in surface finish in LGA solder joints was directly related with these changes in Sn grain morphology for six different surface finishes (Figure I.4–9 (a)) [66]. Figure I.4–9 (b) highlights that lifetime increase with the percentage of interlacing [66]. Solder joints with mixed cyclic and interlaced twin structures may be detrimental for the

fatigue lifetime of solder joints . As the interlaced region is supposed to be stiffer, because of the larger undercooling resulting in a larger degree of precipitation hardening, it may induce a high stress level in the area that is not interlaced where the interparticle spacing is higher. If this area also has a critical orientation that maximizes the CTE mismatch to the component, very early failures may occur [67].

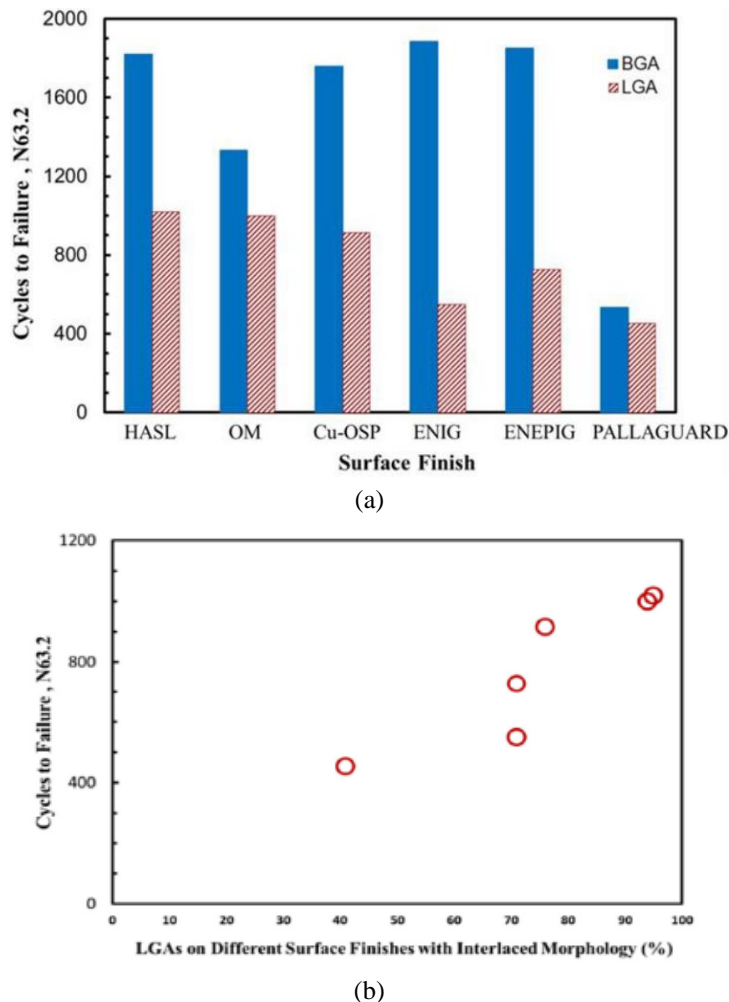


Figure I.4-9: (a) Bar charts showing the characteristic lifetimes for BGA and LGA samples assembled on six different surface finishes, (b) Plot showing the correlation between the lifetime of LGA samples and percentage of interlaced joints [66]

Several works have pointed out the importance of the c-axis orientation with respect to the board surface on the fatigue life of solder joints to area array packages. Bieler et al. observed a clear dependence of the thermomechanical response of SAC solder joints on their Sn grain orientation. They showed that Sn crystal orientations with very high CTE values (c-axis orientation parallel to the substrate) generated a maximal CTE mismatch in shear at the joint interface, and had also maximal tensile stress states in the hot part of the thermal cycle [47]. Thus, these orientations presented the worst cases and hence the best cases are characterized by orientations with low CTE values (c-axis orientation perpendicular to the substrates). Lovberg et al. investigated also the anisotropic elasticity and position of a solder joint in a package modeled at assembly level and showed the influence of the grain orientations of neighboring single grained joints on the stress/strain state on the corner joint (Figure I.4-10) [59][68][69].

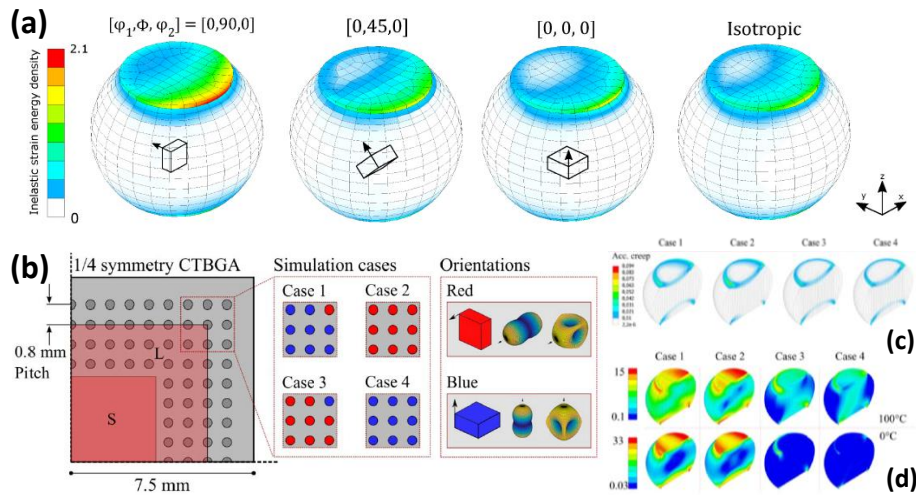


Figure I.4–10: Influence of solder grain orientation on stress-strain simulations : inelastic strain energy density as a function of c-axis orientation [68] (a), simulation cases for single-grained solder joint orientation in a BGA (b), accumulated creep strain in the corner joint over one thermal cycle (0-100°C) (c), Von Mises stress in the corner joint at 100°C and 0°C [59]

Jiang et al. have gone further in their work by developing grain-scale viscoplastic numerical model of polycrystal SAC solder joints. They studied the contribution of grain boundaries to the steady-state creep of coarse-grained SAC solder joints. The maximum creep work dissipation is located at the grain boundaries, between crystals 2 and 3 for the three cases when models take into the behavior of the grain boundaries (Figure I.4–11(a)). However, on simulations which do not reproduce this properties, we find a maximum dissipation at the interface between crystal 1 and the upper Cu pad (Figure I.4–11(b)) [48].

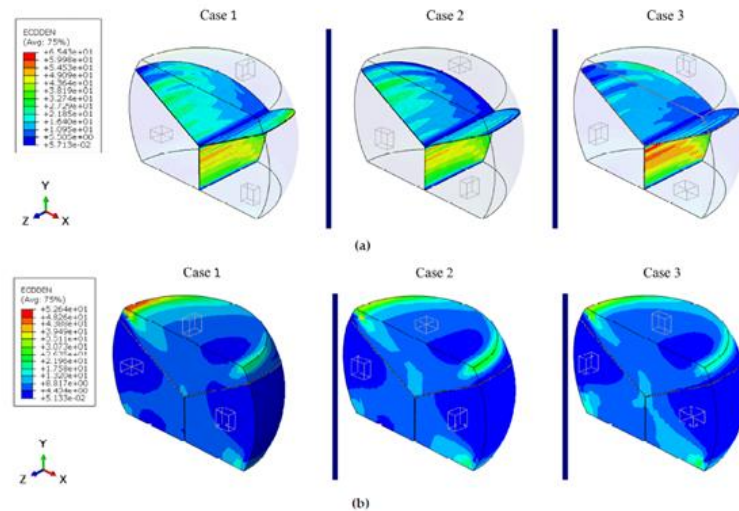


Figure I.4–11: Creep work density dissipated at the end of the fourth cycle in the (a) model with the grain boundaries behavior (b) model without the grain boundaries behavior [48]

There are indeed strong challenges in the modelling of lead-free solder joint fatigue. Other studies highlighted the interest of considering solder microstructure evolution in order to improve their lifetime prediction [70][71]. Some take into account the continuous evolution of IMCs precipitates [72][73] and others focus on the modelling of recrystallization process [74][75] (Figure I.4–12).

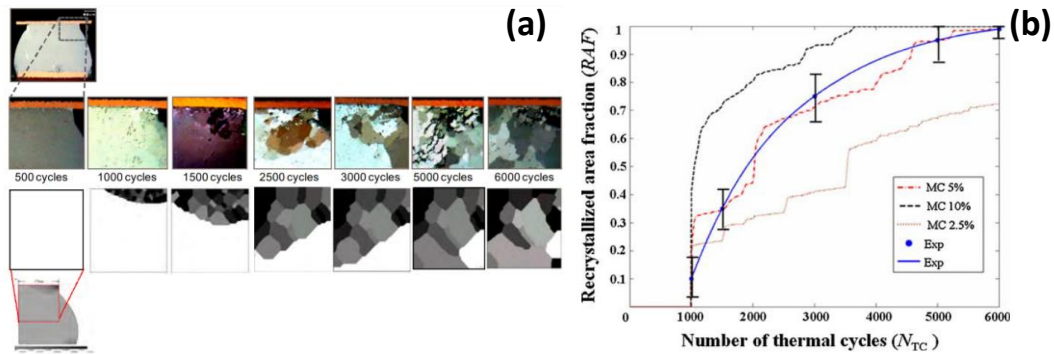


Figure I.4–12: Observed and simulated microstructural evolution (recrystallization) through thermal cycling (a) and comparison between measured and calculated recrystallized area fractions versus number of thermal cycles (b) [74][76]

I.4.4 Synthesis

SAC solder joints failure mechanism during thermomechanical fatigue is characterized by the generation of inelastic deformations in the highly stressed zone leading to the Ag_3Sn particles coalescence as well as the formation of a network of recrystallized tin grains preparing the favorable intergranular propagation cracks path. This mechanism can be impacted by several factors such as the initial microstructure of the patch joints or their geometry. For this reason, it is necessary to choose the most representative criterion of SAC solder damage in the lifetimes prediction models.

I.5 SAC alloy constitutive models

Among the various failure modes observed in electronic assemblies, solder joints cracking by fatigue mechanisms appears to be the most critical. Determining the lifetimes of an electronic assembly in harsh environments therefore requires an evaluation of the stresses and mechanical deformations undergone by the interconnection joints during loading cycles.

$$\varepsilon_t = \varepsilon_e + \varepsilon_p + \varepsilon_{vp} \quad (I.5-1)$$

ε_t : Total strain
 ε_e : Elastic strain
 ε_p : Plastic strain
 ε_{vp} : Viscoplastic strain

The solder joint materials exhibit several types of behavior, depending on the nature of applied stress. In order to fully understand the different mechanical contributions involved in stresses in solder joints, it is necessary to understand the partition of strains. The total strain is divided into an instantaneous elastic part, a plastic time-independent part and a viscoplastic contribution directly related to time. The plastic and viscoplastic contributions can be rearranged into a single part called "inelastic"

I.5.1 Ramberg-Osgood elastoplastic model

Hooke's law and the Ramberg-Osgood model are the most used to describe the non-linear elastoplastic behavior of metallic materials. The Ramberg-Osgood model makes it possible to describe work hardening during plastic deformations [77]. The stress (σ) - strain (ε) curve of the electronic solder materials is characterized by a strong dependence on the temperature (T) and the strain rate $\dot{\varepsilon}$. It is therefore necessary to use a modified model considering these parameters. This model is defined by the equation below

$$\varepsilon(T, \dot{\varepsilon}) = \frac{\sigma}{E} + \alpha \left(\frac{\sigma}{\sigma_0(T, \dot{\varepsilon})} \right)^{n(T, \dot{\varepsilon})} \quad (I.5-2)$$

E : Young's modulus (MPa)
 n : Hardening exponent
 α : Material constant
 σ_0 : hardening coefficient (MPa)

I.5.2 Creep models

In the study of solder mechanics and thermomechanical fatigue, the most used constitutive laws are based on viscoplasticity. Solder alloys used in the electronics industry, such as SAC alloys, are indeed ductile and have relatively low melting temperatures. For the SAC305 alloy subjected to temperatures between -55°C and 125°C , the thermally activated viscoplastic strain are predominant. In this case, creep allows the description of the viscoplastic behavior of the solder alloys. This phenomenon occurs mainly at high temperature and consists in the appearance of plastic strain over time under constant stress. The Figure I.5–1 shows the creep curve presented in the work of Dusek et al.[78].

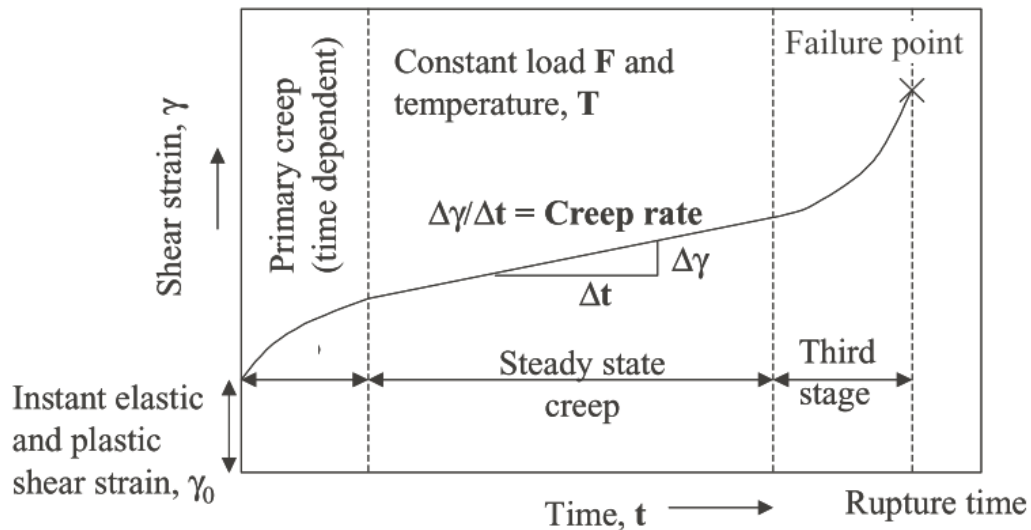


Figure I.5-1: Inelastic creep curve [78]

Creep is characterized by three different domains: primary, secondary and tertiary.

$$\varepsilon_{vp} = \varepsilon_I + \varepsilon_{II} + \varepsilon_{III} \quad (I.5-3)$$

The primary creep ε_I corresponds to a transient state where strain rate tends towards a minimum equal to the constant rate of the secondary creep ε_{II} which is characterized by a steady flow. Tertiary creep ε_{III} has a fast strain rate and terminates with the rupture of the material, hence the development of damage phenomena. When the temperature increases, secondary creep occurs more quickly and the tertiary phase will have a greater contribution. Unlike Sn-Pb alloys, the study of lead-free alloys shows that primary creep can play a significant role in the behavior of materials. Pin et al. worked on the choice of a creep law adapted to make simulations of SAC solder joints under thermal cycling. They showed that the use of a creep law taking into account the primary creep produced more accurate results [79]. Therefore, it is necessary to introduce a model describing both primary and secondary creep. In this section, we summarize the viscoplastic models developed for the solder alloys used in electronics.

(a) *Norton model*

The Norton model takes the form of a power law translating perfect viscoplasticity. It describes the secondary creep and allows the definition in a simple way of the mechanical behavior of the solder alloys. It is commonly used to model the tin-lead alloys behavior because it neglects the effect of primary creep. It is nevertheless necessary to note that the SAC solder joints are less ductile than tin-lead interconnections and primary creep may be of importance in evaluating their mechanical behavior.

$$\dot{\varepsilon}_{II} = \sum_i^2 A_i \left(\frac{\sigma}{E}\right)^{n_i} e^{-\frac{Q_i}{RT}} \quad (I.5-4)$$

$\dot{\varepsilon}_{II}$: Secondary creep strain rate (s^{-1})
 A_i : Materials constants (s^{-1})
 n_i : Viscosity exponents
 Q_i : Activation energies ($J.mol^{-1}$)
 E : Young's Modulus (MPa)
 R : Gas constant ($J.mol^{-1}.K^{-1}$)
 T : Temperature (K)

This model considers two irreversible phenomena of the microstructure that are the vacancy diffusion and the movement of dislocations. The first mechanism is activated at lower strain rates (lower than $10^{-4} s^{-1}$) than those of the second one.

(b) *Garofalo model*

The Garofalo's law is among the most used models to describe the stationary solder creep. It is based on a hyperbolic sine function [80].

$$\dot{\varepsilon}_{II} = C[\sinh(\alpha\sigma)]^n \exp\left(-\frac{Q}{RT}\right) \quad (I.5-5)$$

$\dot{\varepsilon}_{II}$: Secondary creep strain rate (s^{-1})
 A : Material constant (s^{-1})
 n : Viscosity exponent
 Q : Activation energy ($J.mol^{-1}$)
 α : Change of slope (MPa^{-1})
 R : Gas constant ($J.mol^{-1}.K^{-1}$)

The Garofalo and Norton laws are identified by monotonous tests, which does not allow considering the material hardening.

(c) *Darveaux model*

Studies of lead-free solder joints show the non-negligible effect of transient primary creep compared to stationary secondary creep. The Darveaux's model is part of the models combining both secondary and primary creep. Its simple formulation allows the decoupling of the mechanisms responsible for transient creep from the stationary part of creep [81][82]. The total creep strain is expressed as a function of time:

$$\varepsilon_c = \varepsilon_t + \frac{d\varepsilon_s}{dt}t \quad (I.5-6)$$

ε_t : Transient creep strain
 ε_s : Stationary creep strain

The transient creep strain is written as :

$$\varepsilon_t = \varepsilon_t^s [1 - \exp(-K\varepsilon_s t)] \quad (I.5-7)$$

ε_t^s, K : Material constants

The formulation of secondary creep follows the Garofalo's law (Stationary creep = steady state creep = secondary creep).

I.5.3 Anand model

The phenomenon of work hardening corresponds to the strengthening of the material and the evolution of the internal stress state after plastic deformation. The Anand model allows for creep to consider the hardening of the material by the introduction of an internal variable [83]. The creep rate is written in a form analogous to a monotonous model, such as:

$$\dot{\epsilon}_c = A \left[\sinh \left(\xi \frac{\sigma}{s} \right) \right]^{\frac{1}{m}} \exp \left(-\frac{Q}{RT} \right) \quad (\text{I.5-8})$$

$\dot{\epsilon}_c$: Creep strain rate (s^{-1})
 A: Material constant (s^{-1})
 m : Viscosity exponent
 Q: Activation energy ($J.mol^{-1}$)
 ξ : Stress multiplier
 s : Resistance to deformation (MPa)

The stress is moderated by an internal variable s representing “the resistance to plastic deformation”, i.e the hardening. The law of evolution of this variable is such that:

$$\dot{s} = h_0 \left(1 - \frac{s}{s^*} \right)^a \dot{\epsilon}_c \quad (\text{I.5-9})$$

$$s^* = \hat{s} \left(\frac{\dot{\epsilon}_c}{A} \exp \left(-\frac{Q}{RT} \right) \right)^n \quad (\text{I.5-10})$$

s_0 : Initial value of s (MPa)
 n: Strain sensitivity exponent
 \hat{s} : Strain resistance coefficient (MPa)
 a: Hardening sensitivity exponent
 h_0 : Hardening constant (MPa)
 s^* : s Equilibrium value in stationary state (MPa)

The parameters of the Anand’s law A , Q , m , n , a , h_0 and s_0 can be determined by tests at constant strain rate and temperature. The internal variable s depends on the hardening state of the material (h_0) and therefore characterizes the microstructural state of the alloy.

I.5.4 Crystal plasticity Model

Phenomenological models are models commonly used to describe the behavior of material at a macroscopic scale. At this scale, the material dimension is large enough to consider the behavior of the material as isotropic and homogeneous. However, the solder joints in electronic assemblies have very small dimensions at the mesoscopic scale. It is necessary to integrate microstructural characteristics into the modeling and the study of the solder joints fatigue. The crystal plasticity approach must be introduced to correctly describe the microstructural aspects. This approach allows the definition of the micromechanical behavior of a single crystal based on crystal plastic deformation. The crystal plasticity is due to the movement of dislocations at the microscopic scale of the single crystal or of the grain within polycrystalline materials. Hill et al.[84] proposed one of the first models of crystal plasticity which was then formulated for digital implantation by Asaro [85]. These models define a relationship between plastic and slip deformation in particular crystal planes and in defined directions and make it possible to link important local characteristics of the microstructure to the effective behavior of the material at the mesoscopic scale.

For high strains, the total strain ε_{total} in the theory of crystal plasticity can be decomposed into an elastic contribution ε_e and a plastic contribution ε_p :

$$\varepsilon_{total} = \varepsilon_e + \varepsilon_p \quad (I.5-11)$$

The elastic behavior is defined by Hooke's law, while the plastic behavior explains the effect of sliding systems by the following equation:

$$\varepsilon_p = \sum_{\alpha=1}^N s^\alpha \gamma_p^\alpha \quad (I.5-12)$$

N: Number of sliding systems
 α : Slip system
 γ_p^α : Slip tensor
 s^α : Schmid tensor

In order to better understand the theory of crystal plasticity, it is necessary to introduce a detailed formulation of this approach. Asaro proposed a conventional formulation of the kinetics of crystal strain where he decomposed the gradient of total strain into 2 parts as it is shown in the equation below:

$$F = F^e \cdot F^p \quad (I.5-13)$$

F: Total strain gradient
 F^e : Tensor of the gradient of elastic strain due to the elastic strain and the network rotation
 F^p : Local plastic strain Tensor

Figure I.5–2 represents the multiplicative decomposition of the transformation gradient.

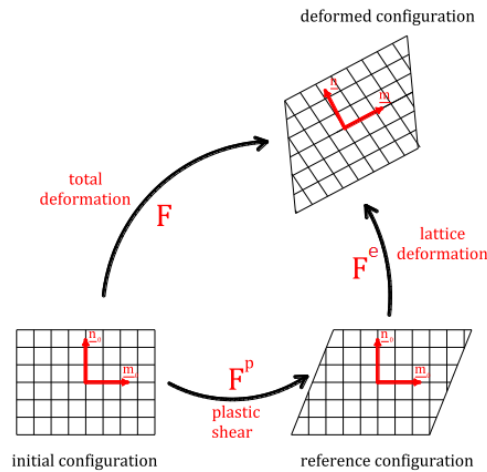


Figure I.5–2: Multiplicative decomposition of the gradient of transformation [85]

The rate gradient tensor (L) is related to the strain gradient by:

$$L = \dot{F} \cdot F^{-1} = L^e + L^p = \dot{F}^e \cdot (F^e)^{-1} + F^e \cdot ((\dot{F}^p) \cdot ((F^p)^{-1}) \cdot ((F^e)^{-1}) \quad (I.5-14)$$

The plastic part of the rate gradient (L^p) can be linked to the rates of plastic slip $\dot{\gamma}_p^\alpha$ on the slip system α by the Schmid's law:

$$L^p = \sum_{\alpha} \dot{\gamma}_p^\alpha m^\alpha \otimes n^\alpha \quad (\text{I.5-15})$$

Where m and n are vectors indicating the slip direction and the normal to the slip plane of the system α , respectively.

The resolved split on the slip system α is given by:

$$\tau^\alpha = T : (m^\alpha \otimes n^\alpha) \quad (\text{I.5-16})$$

Where T is Cauchy stress tensor.

In a given slip system, a viscoplastic power law can describe the flow, and link $\dot{\gamma}_p^\alpha$ and the resolved split τ^α :

$$\dot{\gamma}^\alpha = \dot{\gamma}_0^\alpha \left| \frac{\tau^\alpha}{s^\alpha} \right|^{1/m} \text{sign}(\tau^\alpha) \quad (\text{I.5-17})$$

Where $\dot{\gamma}_0^\alpha$ is the reference constant strain rate, m is strain rate sensitivity parameter and s^α is the internal variable which characterizes the evolution of the critical resolved split under hardening for each slip system. The hardening law is written as:

$$\dot{s}^\alpha = \sum_{\beta=1}^N h^{\alpha\beta} \dot{\gamma}^\beta \quad (\text{I.5-18})$$

$$\text{With } h^{\alpha\beta} = \begin{cases} (\alpha = \beta), & h(\gamma) = h_0 \cdot \sec h^2 \left| \frac{h_0 \cdot \gamma}{\tau_s - \tau_0} \right| \\ (\alpha \neq \beta), & qh_{\alpha\alpha} \end{cases} \quad (\text{I.5-19})$$

$h^{\alpha\beta}$ representing the self-hardening modulus and latent hardening modulus, respectively. The parameters h_0, τ_0, τ_s et q are the initial hardening modulus, the critical split, the saturation split and the latent hardening coefficient, respectively.

The cumulated plastic slip on all slip systems is written:

$$\gamma = \sum_{\alpha} \int_0^t |\dot{\gamma}^\alpha| dt \quad (\text{I.5-20})$$

In order to link F^e to the stress, the stress-elastic strain relation is defined below:

$$T^e = C E^e \quad (\text{I.5-21})$$

$$\text{with } E^e = \frac{1}{2} (F^{eT} F^e - 1) \quad (\text{I.5-22})$$

Where T^e is the stress combined to the elastic strain tensor (Cauchy-Green elastic stress tensor) E^e and C is the 4th order elasticity tensor. The Cauchy stress tensor T is related to T^e by the following relation:

$$\mathbf{T} = (\det \mathbf{F})^{-1} \mathbf{F}^e \mathbf{T}^e \mathbf{F}^{eT} \quad (\text{I.5-23})$$

I.5.5 Synthesis

The characterization of the SAC alloy behavior is an essential step for the study of the durability of electronic packaging. The mechanical stresses undergone by an electronic assembly can be of thermal or mechanical origin, with or without coupling between the two. The establishment of an appropriate SAC constitutive law is important to take into account all types of loading applied to the solder joints during their mission profile.

I.6 Context and objectives of the thesis

Estimating the lifetime of on-board electronic assemblies in aeronautical or automotive applications is essential for their good functioning in real conditions of use. This equipment must indeed be able to perform a required function, under given environmental conditions and for a given time period. This level of reliability is therefore a function of the life profile of each product and it is important to clearly identify the main constraints to which the various assemblies are subjected in order to carry out the appropriate qualification tests.

Results of a statistical study carried out as part of the US Air Force Integrity Program show that more than half of the electronic failures observed are due to temperature variations [86]. The evaluation of the thermomechanical behavior of the constituent materials of the assemblies represents therefore an essential step to guarantee the correct sizing of on-board electronic equipment and their reliability in real conditions of use.

As mentioned earlier, the electronics industry has been using lead-free solder alloys since the banning of lead by the ROHS directives. However, their insertion remains hampered by the lack of understanding of the early failures causes and the uncertainty in the prediction of the solder joints reliability.

The approach based on fracture physics, which consists in identifying the modes (effect by which the failure is identified) and mechanisms (physical processes leading to the failure) of failure by associating them with specific causes, is recommended for the study of the SAC alloy. This is mainly due to the complexity of its initial microstructure which is very dynamic during the use of the assembly. Neglecting the role of the microstructure of the SAC solder joints leads to false estimates of solder joint life expectancy. The impact of tin grain properties (statistical distribution, orientation) on failure modes (ductile, brittle, intergranular, transgranular crack) is crucial to progress in this field.

Establishing the link between the microstructural characteristics of the SAC alloy and its behavior under thermomechanical fatigue is the ultimate goal of this work, according to the physical approach to failure. Several studies well explained SAC solder joints failure mechanism during thermomechanical fatigue [46][54][53][63]. It is characterized by the generation of inelastic deformations in the highly stressed zone leading to the Ag₃Sn particles coalescence as well as the formation of a network of recrystallized tin grains preparing the favorable intergranular propagation cracks path. In these works, they are often interested in the crack propagation phase. However, the link between the SAC alloy microstructural evolution and the crack nucleation phase is not yet well defined until now. Quantitative analysis of the microstructural state triggering crack propagation has also not been revealed. Taking into account quantitative indicators of microstructural damage in prediction models seems to be necessary to ameliorate the accuracy of results. Thus, a better understanding of SAC microstructure degradation is required to progress in the reliability study of lead-free assemblies under thermomechanical fatigue.

A new approach is hence developed in order to evaluate the microstructure effect on the SAC solder joints life service. The solder joint anisotropy and the microstructure evolution were

taken into account for failure analysis and finite element modelling of Pb-free assemblies under thermomechanical fatigue SAC solder to identify microstructural damage criteria that can be exploited in lifetime prediction models. Microstructural analysis has also been used for the assessment of other factors influencing the thermomechanical performance of the electronic assemblies such as the solder geometry and its position in the package.

The next chapter present in more detail the thesis approach with all the tests and techniques necessary to meet the objectives of the thesis.

Chapter II. Research methodology

II.1 Introduction

General context of the study and thesis objectives have been described in the previous chapter. The temperature variations are the main cause of electronic products failure. Knowledge of fatigue failure mechanism for SAC solder joints are thus required to guarantee reliability, predict failure with simulation, and define acceleration factors.

This chapter describes in detail the thesis approach, the aging tests and the methods of analysis with the equipment used. Different test vehicles (TV) composed of several types of components are thus considered. The assembled components are chosen such that they cover several solder joint geometries encountered on real electronic boards. Accelerated thermal cycling test campaign has been carried out to generate a significant number of lifetime results as well as an in-depth microstructural study of the SAC solder joints. The objective is to set up a test which will allow the parallel study of the microstructural evolution and the lifetimes analysis.

A set of preliminary simulations will be also presented to predict the behavior of the various studied electronic components and to determine the various factors that may have an effect on the response of the solder alloy.

II.2 Thesis approach

The evaluation of the durability of electronic assemblies assumes an ability to reproduce conditions as close as possible to real conditions of use. Accelerated tests are recommended by the standards to make the link between the mission profile of on-board equipment and the estimation of its lifetimes. This type of test aims to reproduce the life profile of an electronic assembly while minimizing the cost generated by the test time. These tests must then be correlated to the thermomechanical behavior of the solder alloy in order to identify a dimensioning criterion allowing the development of a corresponding fatigue model. The representativeness of the prediction model therefore depends on the precision of the fatigue criterion, whether it is represented by an equivalent deformation in the case of vibration stresses or energy in the thermomechanical case. In the literature, the identification of this criterion is always done without taking into account the effect of the microstructure of the SAC solder joints. The metrics are always extracted from the modeling at the solder joints scale. However, it has been well explained that the initial microstructure as well as its evolution during accelerated tests has a significant effect on the behavior of solder joints. It is therefore a question of identifying and calculating a relevant fatigue criterion based on the microstructural damage of the solder joints.

Figure II.2–1 schematically presents the organization and the main thesis objectives to reach. The fatigue of the SAC alloy is first studied through an accelerated test campaign allowing the microstructural characterization of the SAC solder joint as well as the analysis of their life service. A link between the measured lifetime and the microstructural state of the solder joints will be established. Microstructural indicators will be then identified to be implemented in numerical simulations and to define a fatigue criterion representative of the microstructural damage of SAC solder joints. Other factors that can affect the reliability of electronic components such as the location of solder joints in the assembly matrix will be investigated. The multi scale modeling will be also used to evaluate the impact of some indicators that cannot be studied by experimental characterization.

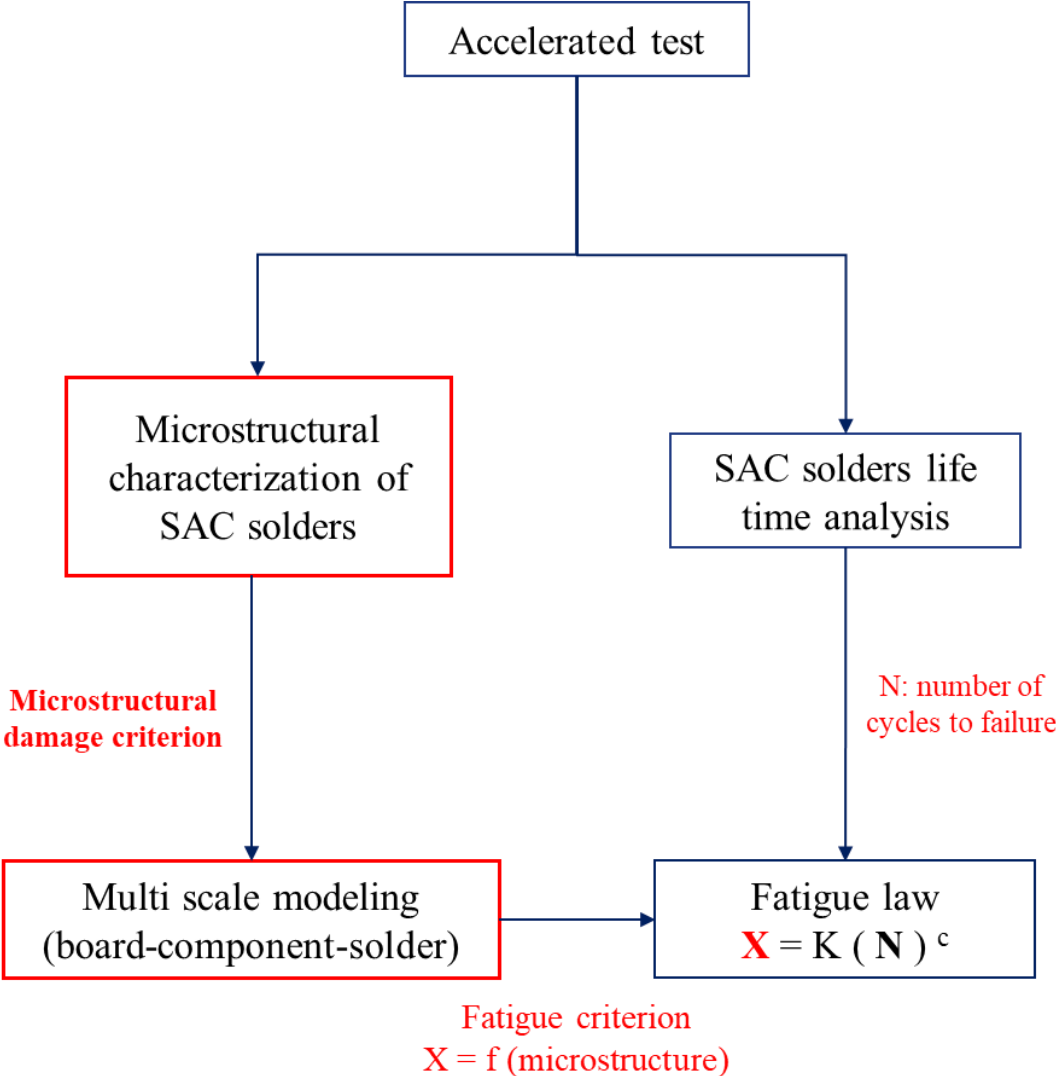


Figure II.2-1: Diagram of the general organization of the thesis with the main objectives

II.3 Experimental approach

II.3.1 Test vehicles and components

The design of the test boards were chosen to:

- Cover the widest field of our partners' applications
- Evaluate the influence of different factors that can have an impact on the durability of SAC solder joints thermomechanical fatigue
- Study the link between the microstructural evolution (kinetics of tin grain recrystallization and Ag₃Sn coarsening) and the average lifetimes calculated from the failures detection

The elements of the assembly: component, solder and PCB are indeed among factors influencing the life of the electronic assembly. Three types of components were thus considered throughout the thesis work according to their dimensions, their constituent materials and their type of interconnection. They have different geometries and CTE values and thus make it possible to cover a wide range of service life.

- CABGA288 (Amkor), 19 x 19 mm body, SAC305 solder balls, 0.48 mm ball diameter, 0.8 mm pitch, solder pads had ENIG finish
- QFN68 (Amkor), 10 x 10 mm body, 0.5 mm pitch, tin finish
- R1206 (Practical Components), 3.2 x 1.6 mm, tin finish on nickel.

The BGA and QFN are dummy but they contain a silicon die (12 x 12 mm for the BGA, 4.5 x 4.5 mm for the QFN). The substrate is a 160×144 mm, 1.6 mm thick multi-layered (four ground copper planes) FR-4 printed circuit board. The characteristics of the FR-4 are given by the manufacturer's data sheet (Table II.3–1). Some were compared with experimental measurements in TMA (thermomechanical analysis) and DMA (dynamic mechanical analysis) carried out in the Continental laboratory. The board had Electroless Nickel Immersion Gold (ENIG) surface finish on non-solder mask defined (NSMD) pads.

Two batches of test vehicles were designed to meet the different objectives of the study. The test boards have voluntarily common points for comparative purposes.

The first lot of boards (B_ROBUSTESSE) was performed with the aim of studying the effect of test condition on the thermomechanical fatigue of SAC solder joints. This aspect was studied only on the BGA components (Figure II.3–1 (a)).

The boards of the second batch (B_FELINE) allowed us to make the link between the different steps of microstructural evolution during thermal cycling and the measured lifetimes of solder joints. These boards contains BGA, QFN and R1206 components and was also useful for the study of the effect of the geometry, the position and the initial microstructure of solder joints (Figure II.3–1 (b)).

SAC solder paste was used to assemble components using the Continental Automotive prototype line with a time above liquidus of 75 s, peak temperature of 245°C, and a cooling rate of 3°C/s (Figure II.3–2). The alloy in the paste is composed of 95.75% Sn, 3.5% Ag and 0.75% Cu. Its composition is very close to the SAC305 consequently we will call it along this work by the SAC305.

Table II.3–1: PCB materials properties

Materials properties	FR-4 IS400	TMA/DMA
T _g (°C)	≥ 150	170
CTE en ppm/K	<p>up to 150°C: 13 according to (x,y) 40 according to z</p>	<p>up to 120°C: 16.7 according to x ; 12.5 according to y. 40.1 according to z</p>
Young Modulus (GPa)	<p>< T_g 25,25 according to (x,y) 22,95 according to z</p>	<p>> T_g 25-30 according to (x,y) 20-25 according to z</p>

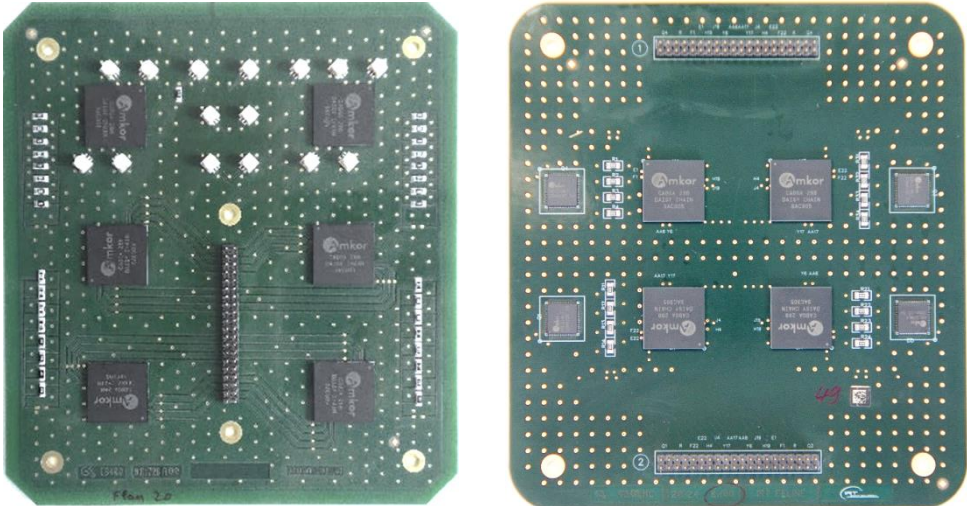


Figure II.3–1: Test vehicles used to study the thermomechanical fatigue of solder joints, (a) B_ROBUSTESSE, (b) B_FELINE

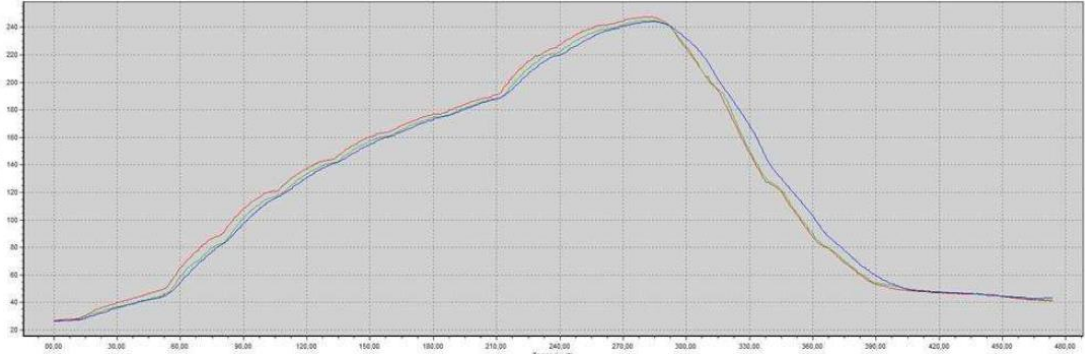


Figure II.3–2: Reflow profile applied for board assembly at partner Continental

II.3.2 Test conditions and plan

The IPC 9701 test and qualification standard recommends an isothermal preconditioning (e.g. 24h at 100°C) before fatigue testing in order to simulate a use period and accelerate thermal aging-related processes (microstructure stabilization). It has also been shown that a prior annealing promotes recrystallization during isothermal cyclic loading. It means that a certain amount of precipitates coalescence and spacing is necessary for recrystallization to take place as it usually does in thermal cycling. In contrast, excessive pre-aging tends to inhibit recrystallization during thermomechanical cycling. This justifies our choice of setting up a controlled test sequence in two steps.

A pre-aging was first performed that induces the microstructural effects (IMC coarsening and spacing) associated to an extended thermal excursion. Two temperatures (100°C, 150°C) and three durations (100h, 500h, and 1000h) were investigated. Some cards have not been stored and remained on their state after reflow soldering (a condition called "pre-aging at 20°C"). Then thermal cycling was applied which generates the strains in solder joints, as well as the strain-enhanced microstructural evolution (recrystallization and IMC coarsening) that leads to failure.

As part of this thesis work, two thermal cycles were also considered according to the TC4 and TC5 test conditions of the IPC-9701[87]. For each of them, the temperature rise and fall rates are set at 10°C.min⁻¹. Two temperature amplitudes are tested with a dwell time of 15 minutes. The effect of pre-aging is sought in the lifetime analysis and in the microstructural evolution characterization of the solder joints over the accelerated tests. To meet the different objectives of the project, some cards are cycled until the failure of the daisy-chains of all the components. The others are sampled on dates which are defined at the start of the test.

Only boards pre-aged at room temperature and at 100°C and which have undergone cycling between -55°C and 125°C are used for analysis of microstructural evolution. A successive sampling of boards was performed until the optical observation of the first total cracks in each type of component. The sampling intervals were adjusted according to the first microstructural analysis results (Table II.3–2). Studies have shown that microstructural degradation as well as crack initiation begin at a low percentage of the lifetime of the assemblies [88]. For this reason, the timing of the first samplings were set based on the estimated average lifetime of the different components under the same accelerated test conditions.

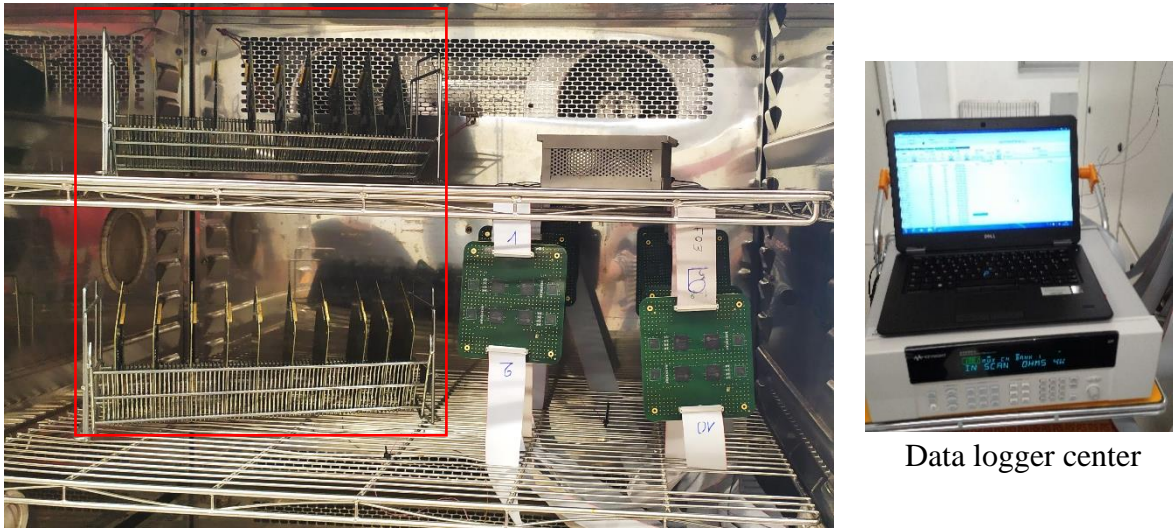
II.3.3 In situ electrical monitoring apparatus

The components and PCB each have daisy-chains allowing the electrical monitoring of the interconnect joints during thermal cycles. Lifetime results can thus be obtained by connecting test vehicles to a Keysight 34980A data logger acquisition unit by 4-point measuring of the electrical resistance of the different daisy-chains (Figure II.3–3).

The B_ROBUSTESSE design included two daisy-chains per BGA package: a short one (48 solder joints) and a long one 240 solder joints (Figure II.3–4 (a)). The idea was to investigate the effect of the number of joints on the electrical resistance increase with time and the measured time to failure.

The B_FELINE test vehicles contains three daisy-chains per BGA: the outer ring (84 joints), the internal ring (60 joints), and a double intermediate ring (144 joints). The BGA footprint and routing are shown in Figure II.3–4 (b) and Figure II.3–5. The objective here was to study the position effect of SAC interconnections and predict the location of the first failure. The solder joints of a QFN component are linked together to form one daisy-chain (68 joints) as presented in Figure II.3–4 (c). For R1206, each group of four components are connected in parallel (Figure II.3–4 (d)).

Sampling for microstructural analysis Failure detection

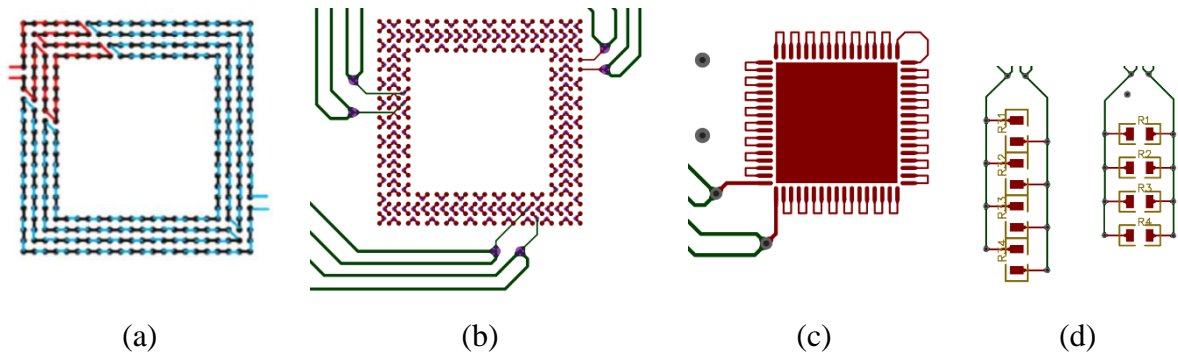


Thermal chamber

Figure II.3–3: Experimental device set up allowing the successive sampling of the boards as well as the measurement of the lifetime of the assemblies under thermomechanical fatigue

Table II.3–2: Test plan for microstructural analysis

Pre-aging	20°C	500h at 100°C
Thermal cycling	[-55 ; 125]°C	
Boards withdrawal time (cycles)	135, 225, 360, 500, 700, 1000,1300, 1500, 1700, 2000, 2300, 2500, 2700, 3000, 3500	



(a) (b) (c) (d)
 Figure II.3-4: Footprint of the (a, b) BGA, (c) QFN and (d) R1206 components

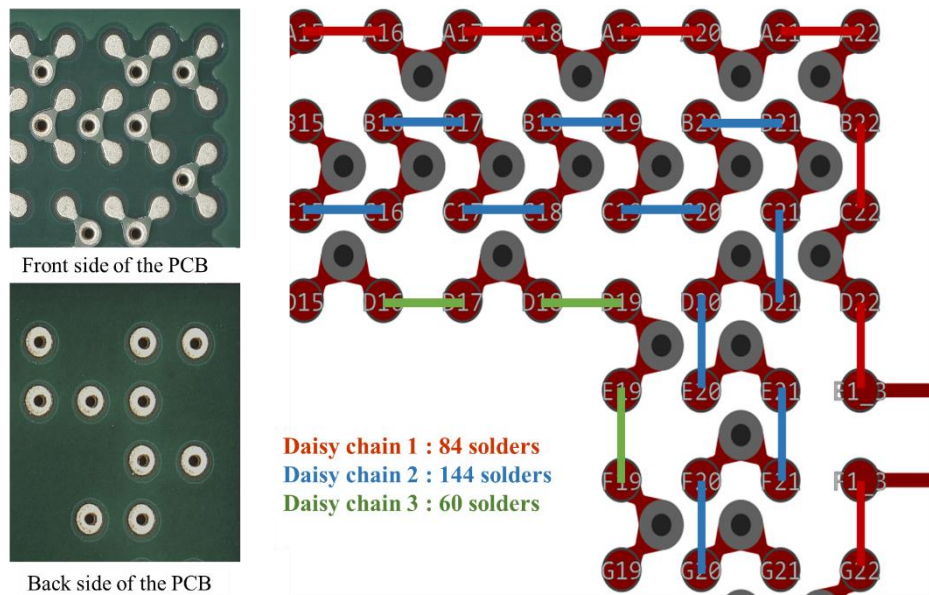


Figure II.3-5: BGA footprint and routing – position of the vias under the component and view of the three daisy-chains in the corner of the component

II.3.4 Microstructural characterization

The board samples are monitored by an optical analysis of different solder joints after cross-sectioning in order to detect cracking as well as the degradation mechanism features. For each board taken out during thermal cycling, a certain number of test components were cut out from the board then cross-sectioned. After that, specimens were encapsulated and subsequently polished. The sample preparation procedure involved mechanical grinding with several SiC papers from grade P80 progressively up to P1200 in order to reach the interest area. A final polishing step is then followed using diamond suspensions. A slight chemical etching at the end of the polishing was applied for the revealing of the microstructure. All finishing steps and the polisher used for the sample preparation are shown in Figure II.3-6 .

A metallographic investigation was then conducted using white/polarized light microscopy and Scanning Electron Microscopy (SEM) observations along with Electron Back Scattered Diffraction (EBSD) analysis. For optical microscopy, a Zeiss Axio Observer optical microscope equipped with a polarizer was used.

At each sampling, several components were observed under the optical microscope. The comparison of the different solder joints at the same level of cycling with white and polarized light allowed us to choose the most critical cases to deepen the microstructural characterization by EBSD. A description of the number of solder joints observed by Optical Microscopy (OM) and analyzed in EBSD for each board taken during thermal cycling is shown in Figure II.3–7.



(a)

Diamond suspension (µm)	Head and plateau rotation (Rpm)	Applied force (daN)	Duration (min)
9	120	2.5	5
6	120	2.5	5
3	120	2.5	5
1	100	2.5	5
¼	100	2.5	5
OPS (Oxide Polishing Suspension)	100	0.5	0.5

(b)

Figure II.3–6: (a) Polisher used during sample preparation (b) Finishing steps applied to reveal the microstructure

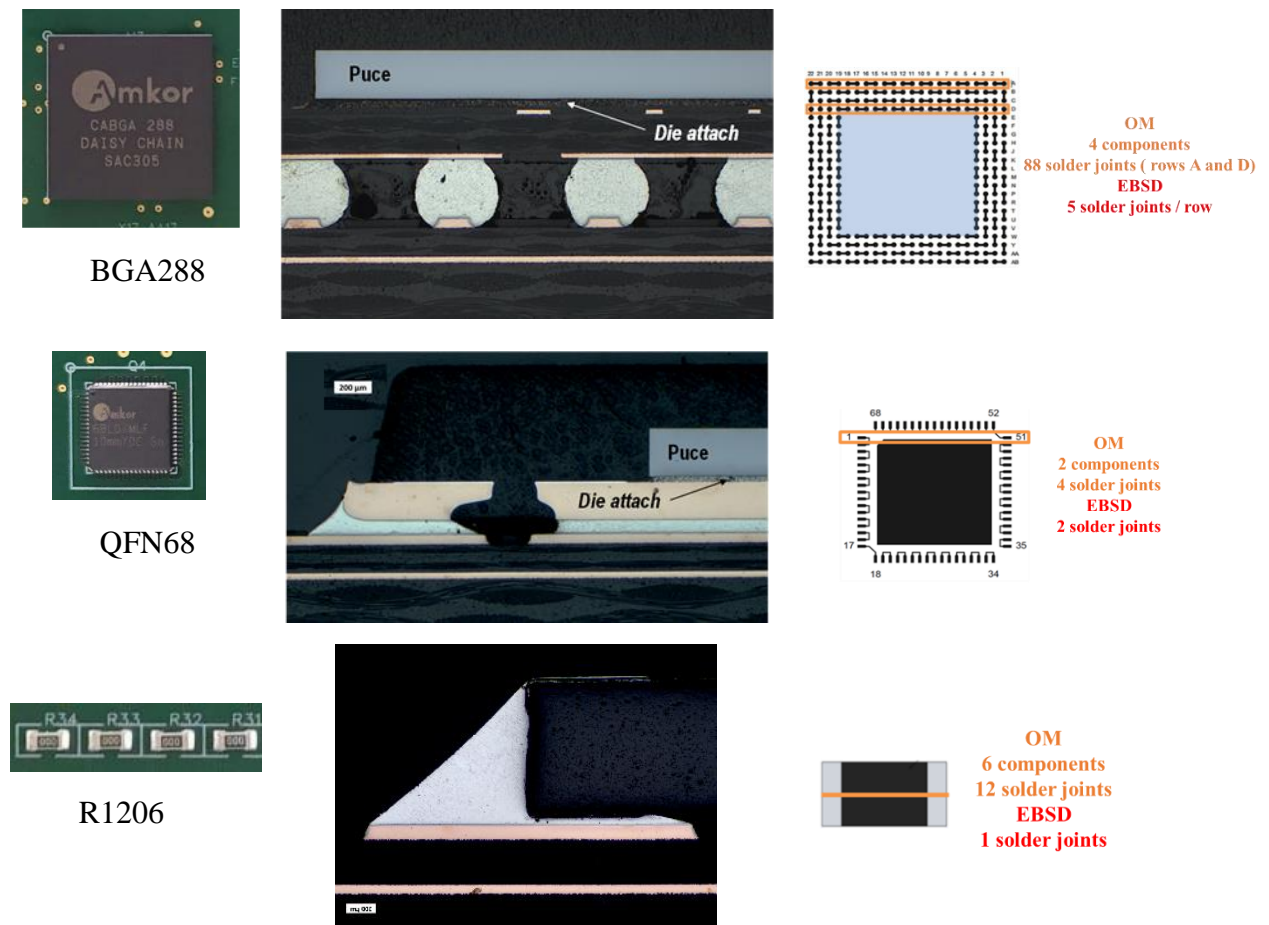


Figure II.3-7: Description of the number of solder joints observed and analyzed in EBSD for each board taken during thermal cycling

EBSD analysis is a technique that allows the study of the microstructural state of a crystalline material. Such an analysis makes it possible to generate several types of information:

- Granulometry (grain size and morphology)
- Crystalline orientations and the material texture
- Crystalline phases
- Local disorientation (internal stress distribution)

It was performed using a Zeiss Supra 55 VP SEM equipped with a detector which records the diffraction images formed during the interaction between the electrons emitted by the SEM column and the crystal lattice of the specimen. EBSD data were then post-processed using the Aztec and Channel 5 softwares from Oxford Instruments to reproduce all data in the form of maps.

When the incident electron beam interacts with the surface of the material, a portion collides with the nuclei of the atoms in the sample and is returned in a direction close to that of the incident beam. These electrons constitute the backscattered beam. Among the backscattered electrons, some will diffract on the crystalline planes of the sample by following Bragg's law:

$$n\lambda = 2d \cdot \sin(\theta)$$

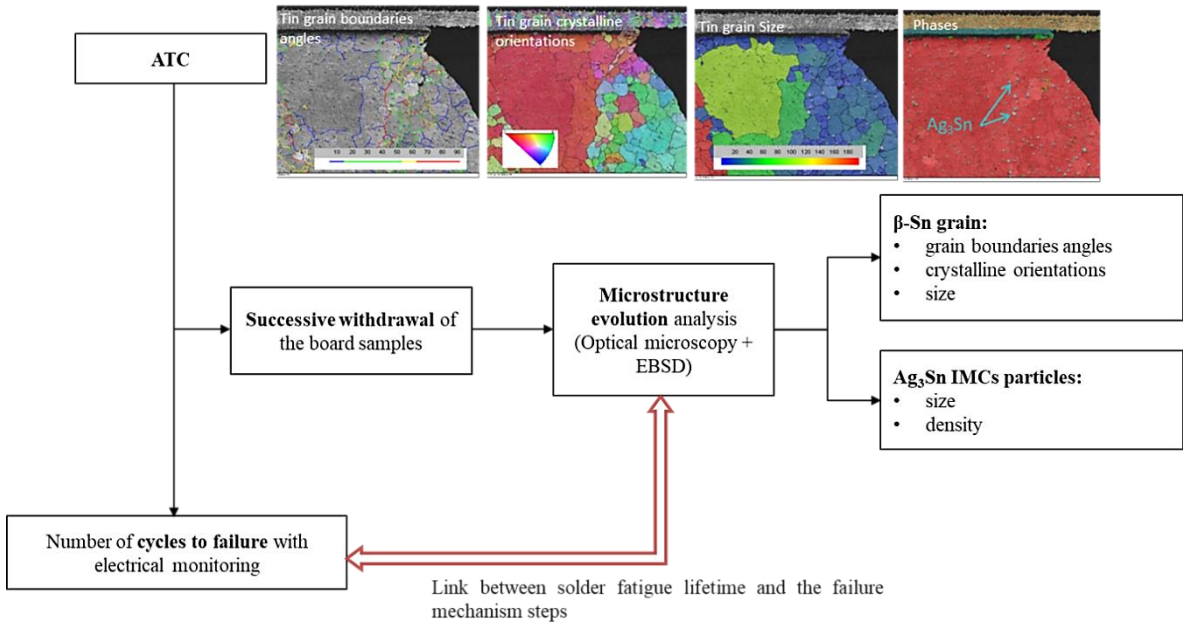


Figure II.3–9: Procedure for evaluating the microstructural evolution of SAC305 interconnections

II.3.5 Synthesis

The experimental approach considered for the study of the reliability of electronic assemblies in thermomechanical fatigue is detailed in this paragraph. An accelerated thermal cycling campaign was carried out in order to determine the link between each step of the microstructural evolution and the lifetimes of the SAC solder joints. Two thermal cycles have been selected according to the TC4 (-55°C/125°C) and TC5 (-55°C/100°C) test conditions of the IPC-9701. An isothermal pre-aging was also performed to get closer to real conditions of use. Two temperatures (100°C, 150°C) and three durations (100h, 500h, and 1000h) were investigated. Other test boards have not been stored and remained on their as-reflowed state (a condition called "pre-aging at 20°C"). Three types of components, BGA, QFN and R1206 will be studied. The in situ electrical monitoring coupled to the microstructural characterization through the optical microscopy and the EBSD technique will allow the investigation of the SAC solder joints damage under thermal cycling.

II.4 Preliminary numerical simulations

Before launching the test campaign, a set of finite element simulations was carried out in order to qualitatively predict the mechanical behavior of the components considered. Different factors may have an impact on the behavior of the SAC solder joint during accelerated thermal cycling. The design and the materials properties of the assembly as well as the as-reflowed microstructure of the SAC solder joints seem to be the most predominant for the study of thermomechanical fatigue of lead-free assemblies.

The setup of this simulation flow is a primary task to overcome before fatigue characterization as durability of solder joint depends on geometrical and differential stress of a stack up. The ultimate objective resides in normalizing the lifetime of a solder joint regarding its stress state.

II.4.1 Modeling at the scale of the Board

(a) *Description of the model*

To anticipate the mechanical behavior of the different studied components, a global model of the board was reproduced. The dimensions are those of the substrate and the components considered for the manufacture of the test vehicle (B_FELINE). This design was chosen for this study since it allows the study of several types of components

Due to the symmetry of the test vehicle, only a quarter was considered. It is also important to note that a simplified geometry has been modeled to reproduce the role of solder joint for each type of package. Figure II.4–1 shows the global model used for evaluating the test vehicle behavior.

Simulations were based on simple elastic models on ABAQUS software. Table II.4–1 summarizes the different materials properties of each part of the assembly. The considered solder alloy was the SAC305.

The boundary conditions are determined by two symmetry planes. A fixed point was applied at the lower face of the substrate center. A tie constraint condition was chosen to ensure the connection between the different assembly parts. This type of constraint allows fusing together two regions with different meshes on the surfaces. A temperature drop from the reflow point (230°C) to the ambient (25°C) followed by one thermal cycle (-55/125°C) has been applied on the model.

The model was optimized, mainly by refining the mesh of the PCB in the component assembly areas. The elements used for this analysis are the C3D8R elements. It is a general purpose linear brick element, with one reduced integration point.

Table II.4–1: Mechanical properties of assembly materials [90]

Materials properties	PCB	R1206	QFN	BGA	SAC305
Young Modulus E (GPa)	22(x,z) 10(y)	280	19	10, 25<T<165°C 1, 175<T<230°C	50, 50°C 45, 125°C 0.1, 230°C
CTE (ppm°/C)	18 (x,z) 70 (y)	6.8	25 (x,y) 35 (z)	14, 25<T<165°C 68, 175<T<230°C	22
Poisson ratio ν	0.28 (xy,zy) 0.11(xz)	0.23	0.27	0.22	0.35

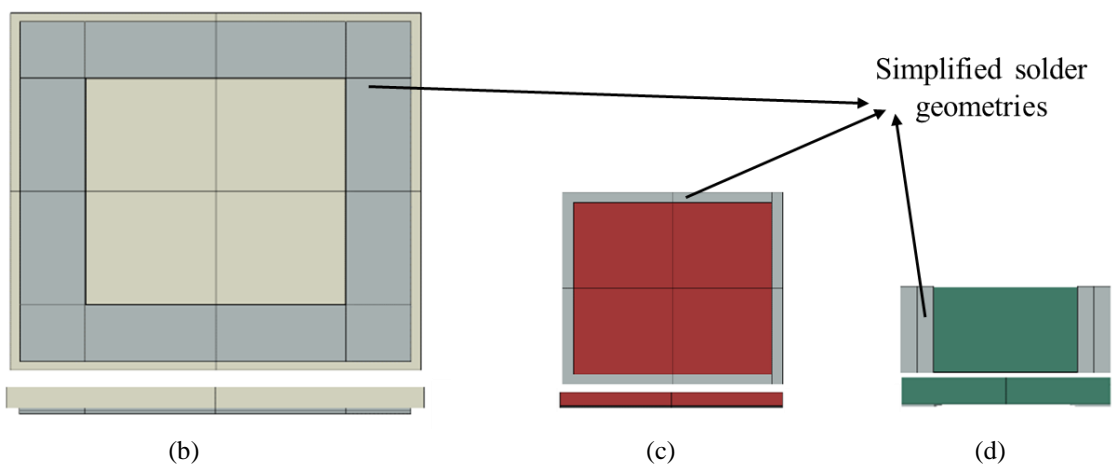
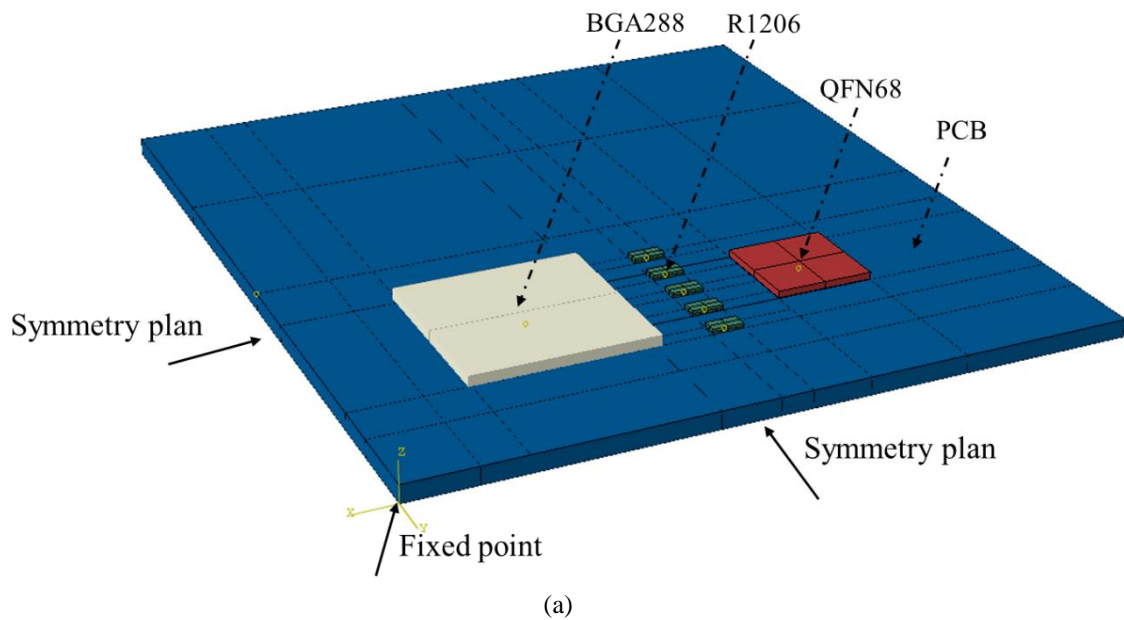


Figure II.4–1: Model of PCB board with three types of components with different solder geometries (b) BGA (c) QFN and (d) passive component

(b) Comparison between the SAC solder stress states in the BGA, QFN and chip resistor components

As the test vehicle is subjected to thermal cycles, the solder balls are mainly stressed in shear. Figure II.4–2 shows that BGA component seems to be the most stressed region compared to the QFN and the passive packages. However, the Von Mises stress distribution validates that the SAC solder alloy represents the most critical part in the test board. The Maximum value of the Von Mises stress was measured on the solder joints of the passive component. The second most strain solder joints are those of BGA component. The solder alloy of the QFN component has the lowest level of stress. These results assume that the solder joints of the R1206 component will present the first failures during the accelerated thermal cycling, then the BGA and finally the QFN.

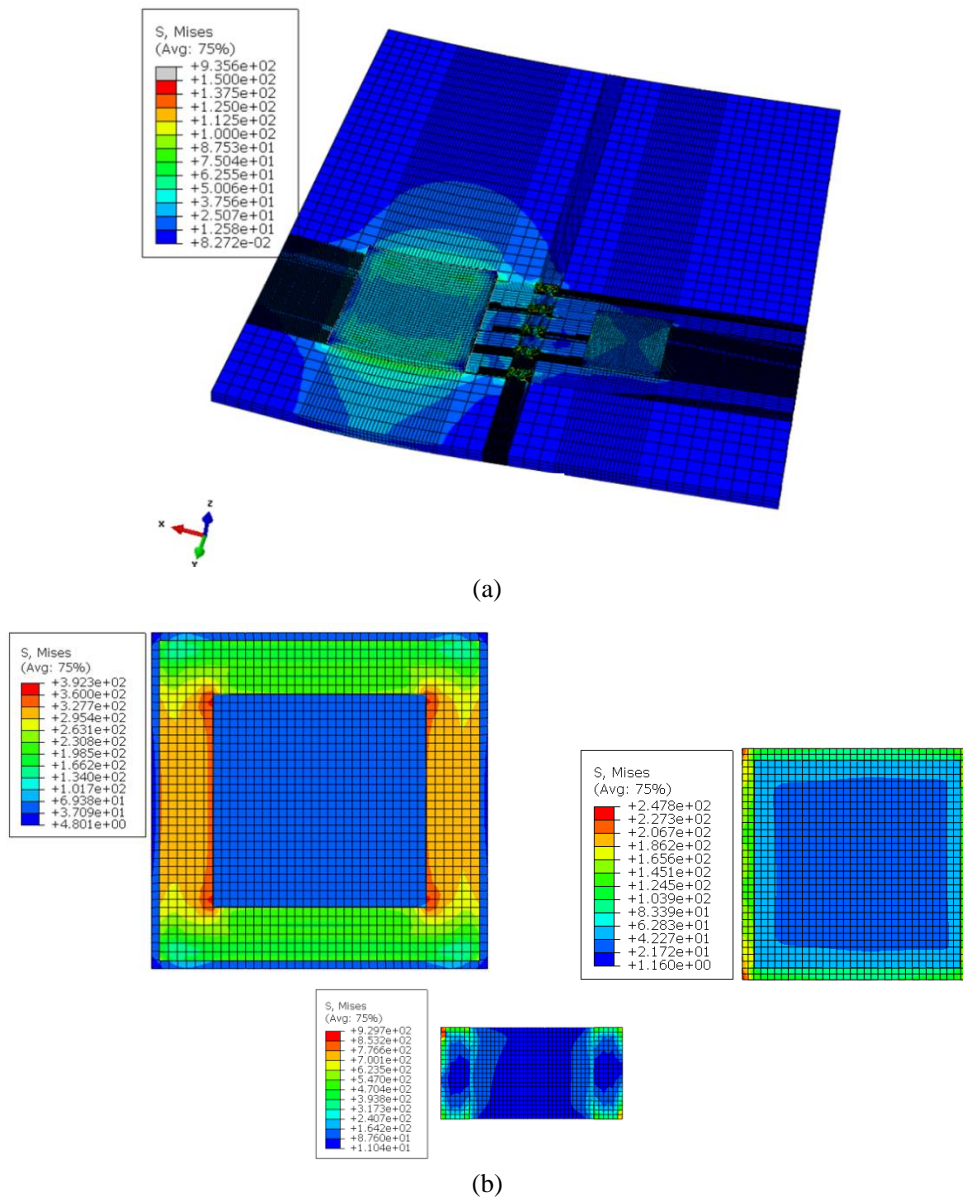


Figure II.4–2: Distribution of the Von Mises stress (MPa) at 125°C (a) board level (b) SAC alloy level

(c) *Effect of the component position*

The effect of the component position was also studied using this simplified model. A second configuration was simulated. It was defined by modifying the symmetry planes near the QFN component side (red and green plans shown in Figure II.4–5). Results show the same Von Mises stress distribution on the SAC alloy level of the different studied components. Table II.4–2 validates that the interconnections of the R1206 components remains the most strain geometries compared to the BGA and the QFN. We can conclude that the two configurations present the same thermomechanical behavior.

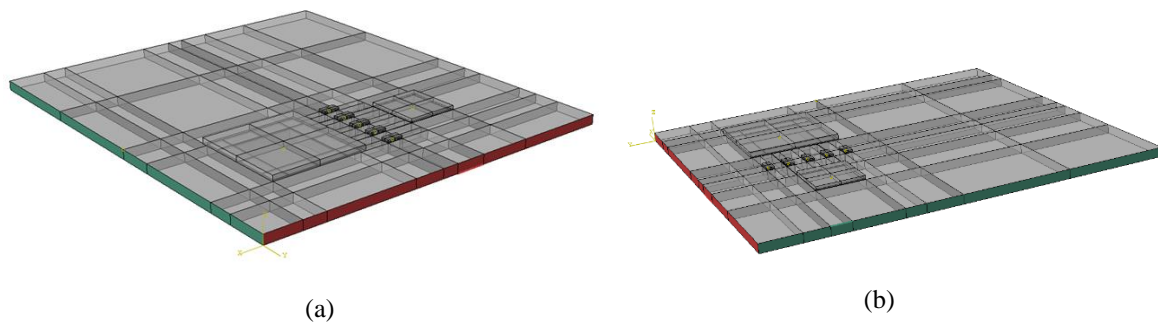


Figure II.4–3: Two different board designs (a) BGA component in the center (b) QFN component in the center

Table II.4–2: Maximum Von Mises stress in the different studied components

Configuration	$\sigma_{VM\ BGA}$ (Mpa)	$\sigma_{VM\ QFN}$ (Mpa)	$\sigma_{VM\ R}$ (Mpa)
(a)	326	180	378
(b)	324	167	383

II.4.2 Impact of the tin grain anisotropy on thermomechanical behavior of Lead-Free Solder Joints

Due to the complex as-reflowed microstructure coupled with the highly anisotropic properties of the tin phase, the mechanical properties of solder joints are strongly anisotropic and will affect their reliability under thermal loading. For these reasons, predicting the first failed joint is quite difficult. It may be more or less randomly located and not always at the position of highest global strain or distance to neutral point [21].

Many elements need to be considered in a model to predict the lifetime of lead-free solder joints in field conditions. To investigate the effects of anisotropy of coarse-grained joints, some authors already considered the microstructure in their models [91] ; Lovberg et al. showed the influence of the grain orientations of neighboring single grained joints on the stress/strain state on the corner joint [92].

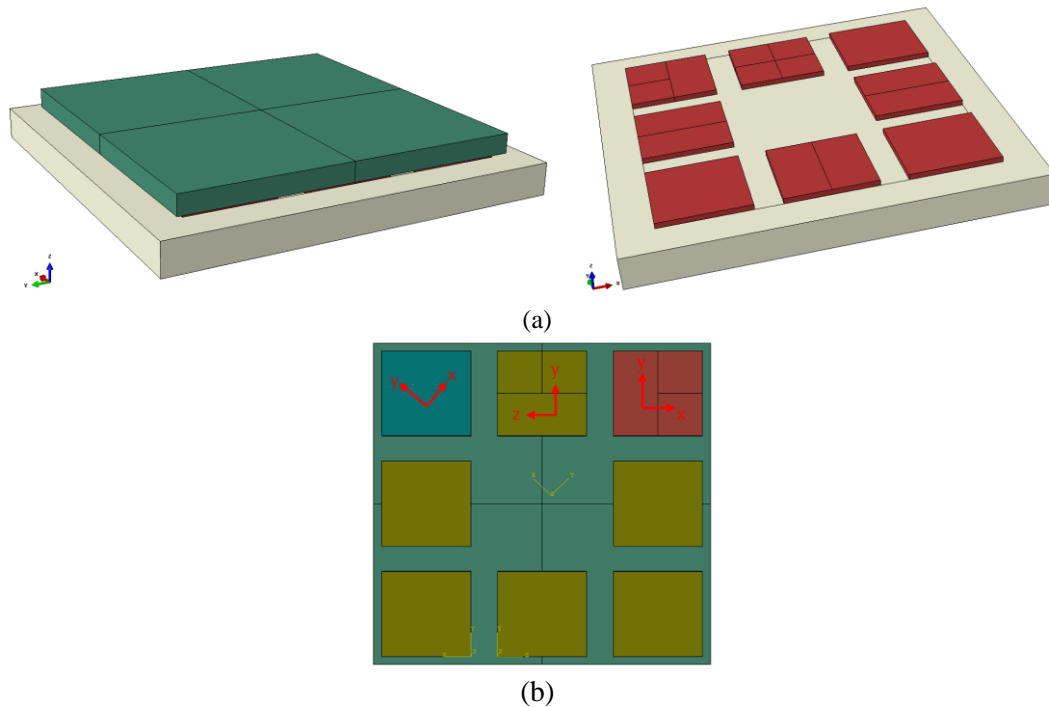


Figure II.4-4: Simplified BGA model used for studying the effect of the crystalline orientations and morphologies of SAC solder joints (a) square blocks of SAC, (b) considered SAC blocks orientations

In this part, the influence of different combinations of single-grained joints and poly-grained joints on the stress state of the solder joints in a BGA is investigated by simulations. A simplified BGA model with anisotropic properties was set up to simulate thermomechanical loads. Orientations and morphologies of the solder joints are parameterized with several configurations taking into account three tin orientations and two morphologies (single-grain, polygrains). In this model SAC interconnections were represented by square blocks (Figure II.4-4 (a)).

The three considered orientations are shown in Figure II.4-4 (b) and characterized by:

- A c-axis parallel to the substrate (red orientation)
- A c-axis perpendicular to the substrate (yellow orientation)
- A c-axis making a 45° to substrate (green orientation)

The anisotropic elasticity of the solder alloy was implemented in ABAQUS through the elastic coefficient matrix in stiffness. The PCB and the BGA were considered as linear elastic materials.

(a) *Impact of the tin crystalline orientation*

On this section, we considered that each solder block has one crystalline orientations. This is representative of the macro-grained morphology with a single tin crystalline orientation (single grain). We aim to have preliminary leads for the study of the effect of crystalline orientation on the thermomechanical behavior of SAC solder joints.

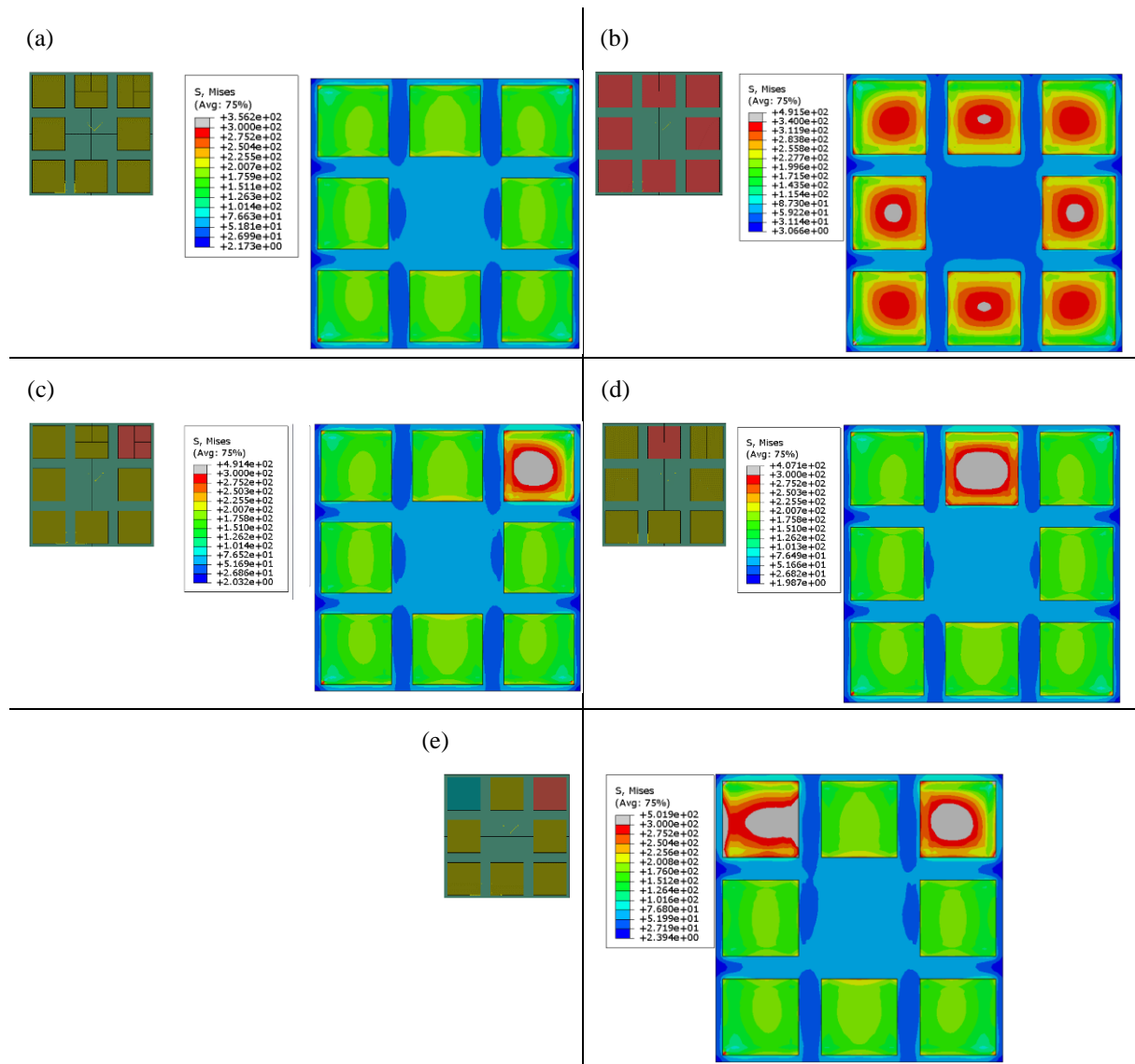


Figure II.4-5: Impact of the tin grain orientation on the Von Mises stress state of the SAC solder block (a) all solder blocks having a c-axis perpendicular to the substrate (b) all solder blocks having a c-axis parallel to the substrate, (c, d) one solder having a different orientation compared to its neighbors, (e) two solder joints with two different orientations compared to the others solder joints

We started first by implementing the same orientation for all the solder blocks. Results show that the stress level depend on the tin grain orientation. Red and yellow orientation presents the highest and the lowest Von Mises stress value respectively (Figure II.4-5 (a) and Figure II.4-5 (b)). We can also see that the stress distribution depends on the position and orientation of the solder block.

Then, we only changed the orientation of a single block and the others kept the same crystalline orientations. The objective here is to study the effect of crystal orientation on the position of the most stressed solder joint. Figure II.4-5 (c) and Figure II.4-5 (d) emphasize that there is one particular orientation which is more detrimental than the other ones. We can clearly observe that the highest strain block has the red orientation and it is not the one under the component corner. That is, the crystalline orientation has an effect on the location of the failure in the package.

On the other hand, having of combination blocks with different orientation seems to increase the maximum value of the Von Mises stress. The highest level of stress was calculated when we implemented three different orientations (Figure II.4–5 (e)). Results show also that the presence of different orientations make more difficult to localize the position of the highest stressed joint

(b) Tin grain morphology

Solder joints can have also the poly grained morphology characterized by the presence of few tin grain with different crystalline orientations. The idea is to understand the effect of polygrains structure on the behavior of the SAC solder joint. In this part, the corner solder block has been divided into two or three partitions and each partition has a different orientation. Three configurations are presented here to illustrate the effect to have several tin grains in a solder joint (Figure II.4–6).

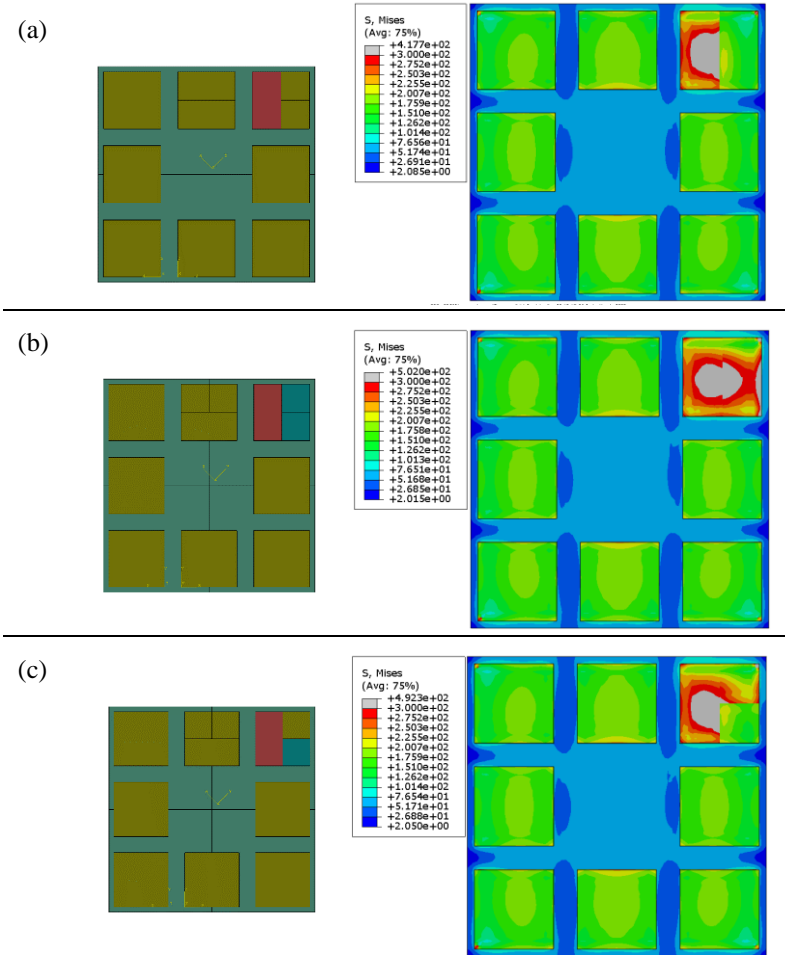


Figure II.4–6: Effect of the polygrained morphology of the corner solder joints under thermal cycling, (a, b) corner solder having two crystalline orientations (c) corner solder having three crystalline orientations

The presence of two or more different orientations in the solder block generates a discontinuity in the Von Mises stress distribution. This discontinuity can be a weak point leading to early solder joint failure

Unfortunately, the model used in this study is oversimplified. It does not make it possible to determine the most critical morphology between the single grained or polygrained structures. However, it highlights the need to take into account the as reflowed tin grain microstructure in the reliability study of solder joints under thermomechanical fatigue.

II.4.3 Synthesis

Preliminary simulations have been carried out to anticipate the thermomechanical behavior of the test board and the different factors that must be considered in the study of the reliability of SAC solder joints. Results show that solder joints in the passive components are the most stressed next in the BGAs and finally in the QFNs. It is therefore assumed that the durability of the R1206 component will be the lowest and that the QFN package will present the longest lifetime. On the hand, taking into account the as-reflowed microstructure in simplified FE models reveals its impact on the thermochemical behavior of SAC solder joints. The stress distribution in a SAC solder joint depends on its crystalline orientation and morphology. The microstructure seems to have an effect on the location of critical joints in the package. Some orientations/morphologies may be detrimental for the reliability of SAC solder joints under thermal cycling.

II.5 Conclusion

The microstructure of solder joints appears to play an important role in the behavior of electronic assemblies. In this chapter, all the experiments allowing studying this aspect and carried out during this thesis have been described in detail.

Three types of components (BGA288, QFN68 and R1206) have been chosen with different solder geometries and to cover a different range of durability. Isothermal storage followed by thermal cycling is the accelerated aging test considered to study the thermomechanical reliability of SAC solder joints. For the isothermal aging two temperatures (100°C, 150°C) and three durations (100h, 500h, and 1000h) were investigated. Some boards have not been stored and remained on their as-reflowed state (a condition called "pre-aging at 20°C"). Two thermal cycles were also considered according to the TC4 and TC5 test conditions of the IPC-9701.

Traditionally thermal cycling tests are performed to determine the number of cycles to fail; then a microstructural analysis on the failing components is done to study the phenomena leading to the failure. In this study, failure detection by electrical monitoring and microstructural analysis of components were carried out in parallel with the aim of defining the link between solder fatigue lifetime and the failure mechanism steps.

The physical approach to failure, which requires an in-depth study and a good understanding of the failure mechanisms active in the joints of a given component and for particular conditions, is gaining ground and is strongly recommended by researchers. This is mainly due to the complexity of SAC solder materials which exhibit a very dynamic microstructure

Along the test, a successive sampling plan was performed to characterize failure kinetics of lead-free solder joints under accelerated thermal cycles. The board samples are followed by an optical analysis of different solder joints in order to detect cracking as well as the degradation mechanism features. The comparison of the different joints at the same level of cycling with bright and polarized light allowed us to choose the most representative cases to deepen the microstructural characterization by EBSD analysis. The main objective is to study microstructural features evolution of SAC305 solder joints as β -Sn grain size and crystallographic orientation, grain boundary angles and the size of Ag₃Sn intermetallic compound (IMC).

Preliminary finite element simulations was also carried out in order to qualitatively predict the test board behavior during the ATC and anticipate the test vehicle behavior under the ATC and the effect of the SAC microstructure on thermomechanical solder joints response. Simulations show that the R1206 component seems to be the first to fail compared to the QFN and BGA packages. They also highlighted the need to consider the as-reflowed microstructure to provide FE models allowing an accurate prediction of the location of critical solder joints.

The next chapter will focus on the detailed description of the failure mechanism of solder joints in thermomechanical fatigue. In fact, this work is necessary to understand the effect of microstructural evolution in SAC solder joint cracking and to allow then the establishment of direct link at each stage of the microstructure changes and the solder joints lifetimes.

Chapter III. Role of tin grain recrystallization and Ag₃Sn intermetallic coalescence in SAC305 solder cracking during thermomechanical fatigue

III.1 Introduction

Thermomechanical fatigue rupture of SAC solder joints induced during temperature gradients is the main cause of electronic assembly failures. Interconnections microstructure evolves considerably throughout thermal cycles. The gradual change in the properties of the lead-free alloy initial microstructure is responsible for solder joints performance loss. Thermomechanical fatigue of lead-free solder joints is always associated with intergranular cracking. When a lead-free solder joint is exposed to thermal cycling, viscoplastic strains are possibly generated leading to the formation of new β -Sn grains characteristic of the recrystallization phenomenon. A recovery process takes place prior to recrystallization where the stored energy can be released by forming low angle grain boundaries ($<15^\circ$) [4]. As high strains develop in the solder joints, the created dislocations annihilate and rearrange to form sub-grain boundaries (dislocation walls). These dislocation cells (sub-grains) can then grow due to thermally activated and strain-enhanced Ag₃Sn coalescence, decreasing their surface energy, and rotate to create a network of higher angle grain boundaries leading to recrystallized β -Sn grains. This network represents a high stressed area that provides favorable intergranular crack propagation paths until failure. As it appears that recrystallization and Ag₃Sn is the primary damaging process involved in thermomechanical fatigue of SAC solder joints, each step leading to the creation of recrystallized grains, and possibly solder crack, should be fully understood.

An in-depth study aiming at providing an accurate description of SAC305 microstructure degradation during thermomechanical fatigue testing will be presented in this chapter: each process leading to fatigue cracking will be investigated. The main objective is to study the link between the early steps of SAC solder joints microstructure evolution and the crack development. To do this, we will start by characterizing the kinetics of each phenomenon separately and without taking into account the interaction between them. Then, we will establish a correlation between the evolution stages of the different phenomena to define the role of recrystallization and Ag₃Sn coarsening on the cracking kinetics.

First, the typical microstructure of the solder joints were identified from cross-section analysis made on components after assembly by reflow. Observations under an optical microscope in polarized light and EBSD analyzes were carried out in order to understand and quantify the microstructural characteristics of the interconnection joints. It is also very important to understand the isothermal storage effect on the as-reflowed microstructure of SAC interconnections since it is a treatment recommended by the standards recommended by standards for board level reliability testing

The second part is interested in the detailed description of the phenomena which characterize the microstructural evolution of the SAC solder in different types of components subjected to temperature cycles. A campaign of accelerated tests in a thermal chamber with a successive sampling of test vehicles are carried out in order to generate sufficient microstructural data allowing the characterization of the different stages of SAC solder joints microstructural changes under thermomechanical loading.

The last part of this chapter aims to follow the stages of cracking in lead-free solder joints under thermomechanical fatigue and identify the role of microstructural evolution in joints failure mode. A correlation between the microstructural evolution and crack propagation is presented in order to well describe lead-free solder joint failure mechanisms under thermomechanical fatigue.

III.2 As-reflowed SAC solder joint microstructure

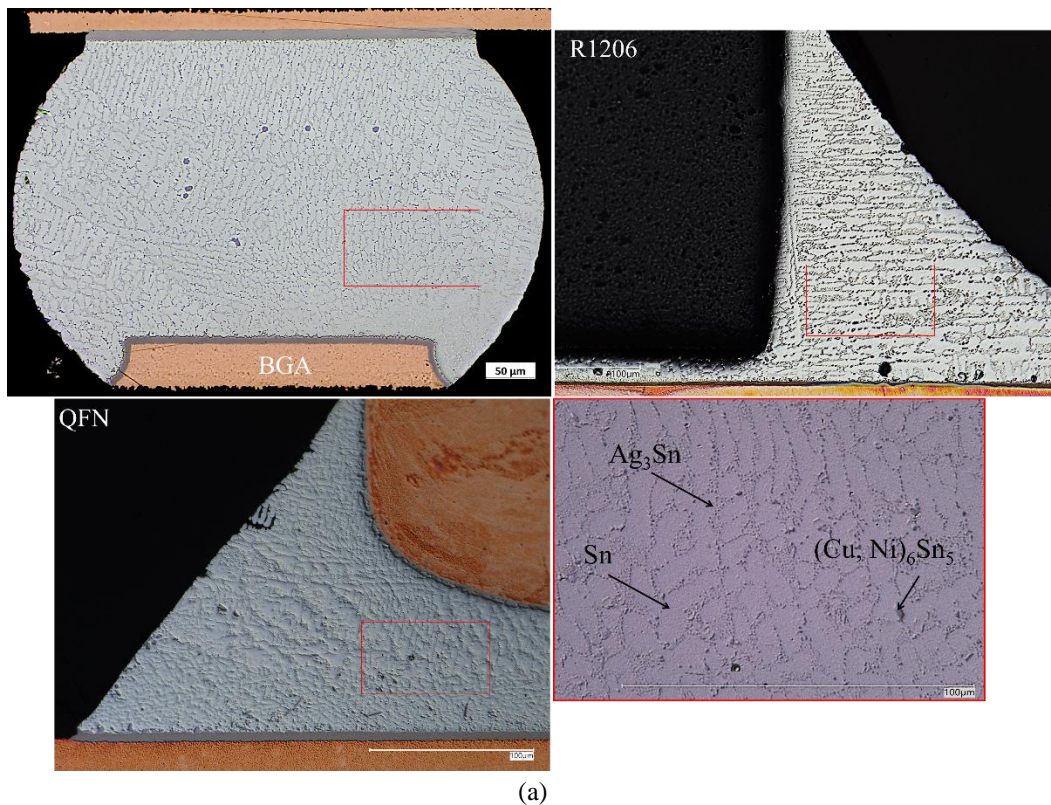
III.2.1 SAC solder joints composition and microstructure

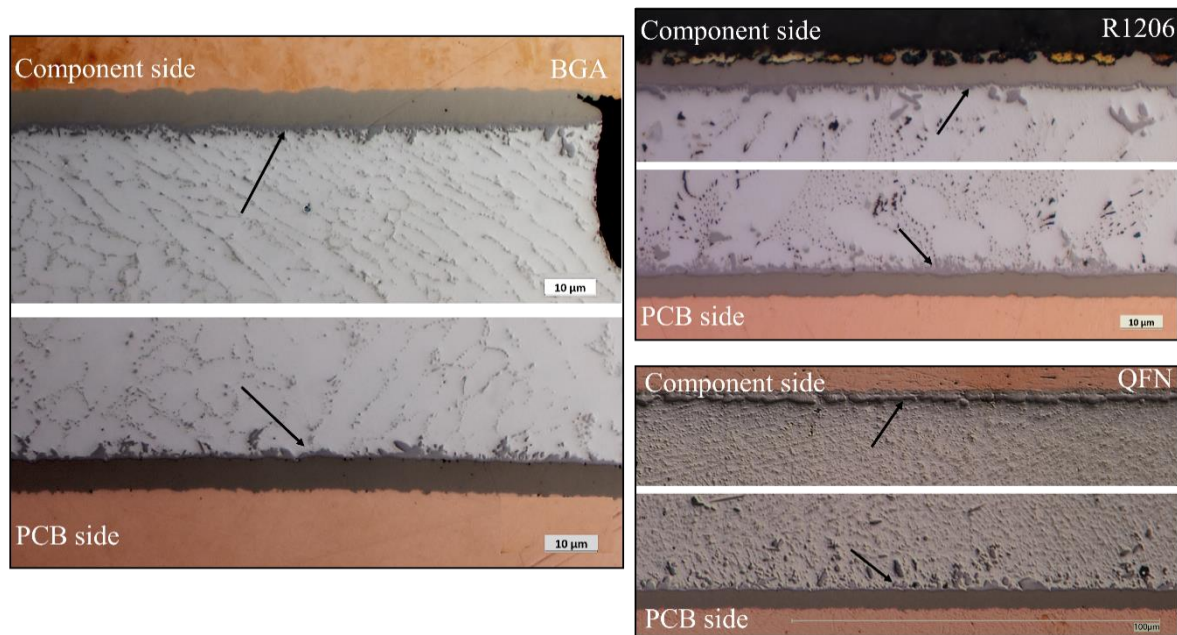
SAC solder joints behavior study under thermomechanical cycling requires first the characterization of their as-reflowed microstructural state. The previous bibliographic study highlighted the effect of the as-reflowed SAC305 interconnections microstructural characteristics on the components reliability in thermal cycling [31][68][93]. It is therefore a question here of corroborating the complexity of this microstructure from micrographic sections made at the level of various surface mount (SMT) components assembled by reflow. The objective is to define the various microstructural parameters of our components in the initial state which can have an impact on the solder behavior during the thermal cycling test.

As a first step, it is necessary to ensure that the solder joints have the expected microstructure. Micrographic sections were thus made and observed under an optical microscope in white light. Figure III.2–1 shows that the as-reflowed microstructure presents:

- Pro-eutectic β -Sn tin matrix in the form of dendrites (Figure III.2–1(a)),
- Intermetallic precipitates in the interdendritic spaces (Figure III.2–1(a)),
- Intermetallic layers at the interfaces with the components and the PCB (Figure III.2–1(b)).

This microstructure is the same whatever the type of component. The intermetallics composition depend on the finish layers of each assembly.





(b)

Figure III.2–1: As-reflowed microstructure observed in the different studied components (a) the tin matrix with the intermetallic precipitates in the inter-dendritic spaces, (b) the intermetallic layers at the interfaces on the components and the PCB sides

Figure III.2–2 presents EDS cartographies of as-reflowed R1206 solder joints. In addition to tin, they reveal the presence of Ag, Cu, Ni and Au in the intermetallics of the solder bulk. For the interfaces, there is only Cu and Ni.

The different crystalline phases are identified by EBSD according to their crystallographic diffraction pattern. Figure III.2–3 show that the inter-dendritic spaces regardless the solder joint geometry present:

- Eutectic Sn-Ag zone that is composed of nanoscale Ag₃Sn precipitates with circular shape embedded in a pure β-Sn matrix. They are distributed homogeneously throughout the solder.
- Cu₆Sn₅ intermetallic compounds, which are larger than Ag₃Sn particles and with more defined geometric shapes. The presence of nickel in these precipitates depends on the amount of dissolved nickel from the component and PCB finish.
- AuSn₄ particles that are weakly detected and certainly come from the Au existing in the finish layer on the PCB side, which has dissolved in the solder.

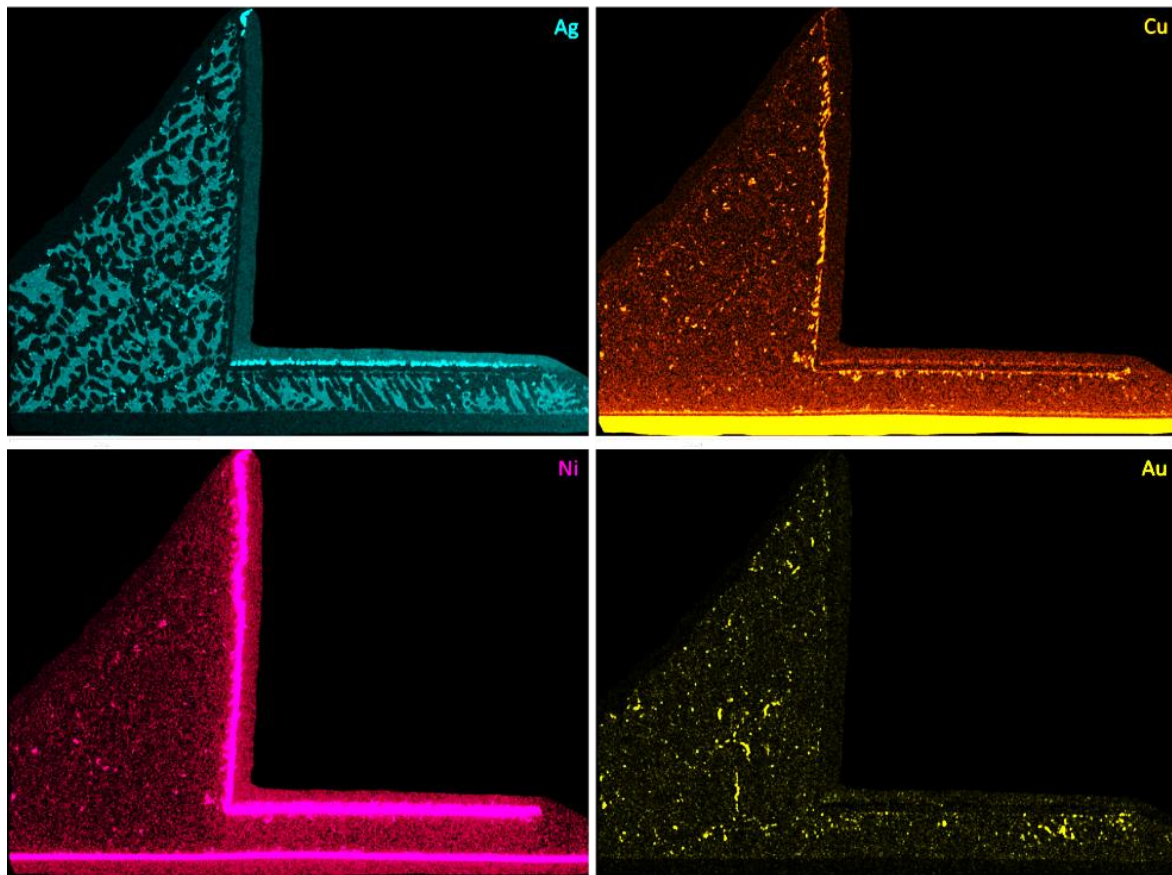


Figure III.2-2: EDS maps showing the different chemical element detected in a chip resistor SAC solder joint after reflow

The SAC alloy also forms an intermetallic layer during the soldering process by reaction with:

- Sn (QFN) or Ni (BGA, resistor) finish on the component side,
- Ni finish on the PCB side.

These layers are composed of Cu₆Sn₅ and Ni₃Sn₄ or a mixture of these IMCs depending on the quantity of nickel. During analyses of the various solder joints, phases containing substitute elements cannot be differentiated from the “pure” phases because the crystal geometry remains identical. This means that the designation Ni₃Sn₄ actually encompasses all the variants of the (Ni, Cu, Au)₃Sn₄ type phases. Likewise, the designation Cu₆Sn₅ includes all phases of (Cu, Ni, Au)₆Sn₅ type and the designation AuSn₄ represents all phases of (Au, Ni, Cu)Sn₄ type.

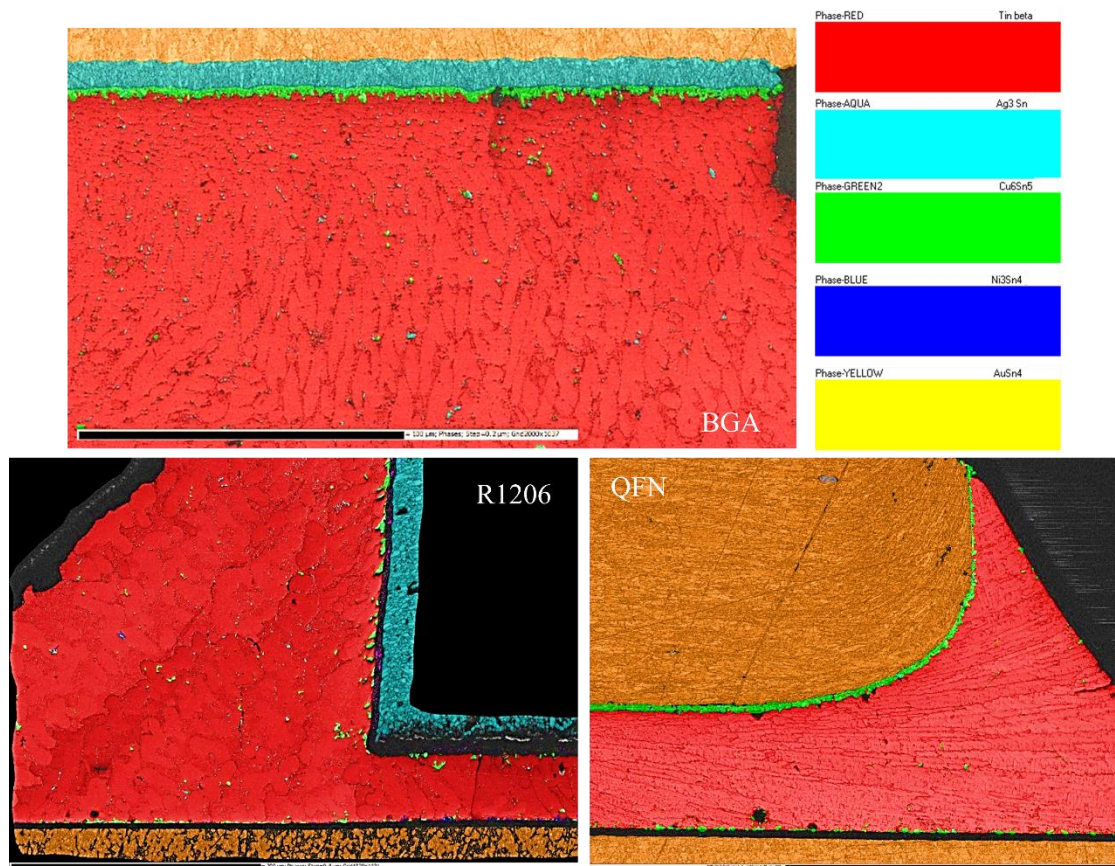


Figure III.2-3: Crystalline phase's maps of BGA and QFN solder joints

III.2.2 SAC solder joints tin grain structure

(a) Description of tin grain morphologies

SAC solder joints microstructure after reflow is characterized by varied morphologies. It is interesting to note that, as has been demonstrated from the literature study, SAC305 interconnection joints after reflow systematically exhibit a macrograin morphology. The birefringence properties of tin make it possible to distinguish under polarized light grains with different crystal orientations. By this way, we get more information on lead-free solder joints microstructure.

Observations show that this macro-grain morphology is existing regardless of the analyzed component (BGA (Figure III.2-4 (a)), QFN (Figure III.2-4 (c)), R1206 (Figure III.2-4 (d))). It is characterized by the presence of one or more β -Sn grains with different random crystalline orientations. In a more specific case, solder joints with only single-grained (one orientation) or a cyclic twinned structure are normally observed when solidification occurs at not too large undercooling. In cross-sections of BGA solder joints with cyclic twins, they sometimes have an appearance of a beach ball consisting of three different crystalline orientations (Figure III.2-4 (b)).

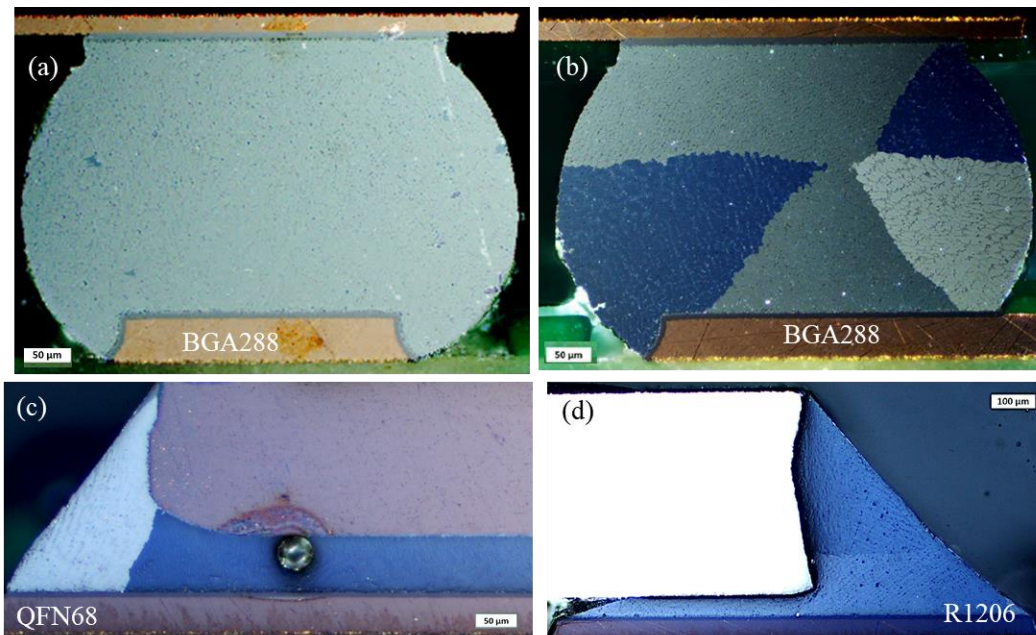


Figure III.2-4: Various tin grain morphologies observed in as reflow solder joints in different type of components, (a) single-grain (b) cyclic twin (c, d) poly-grains

Another mentioned morphology in literature that can also appear after assembly is the mixed structure which presents both the cyclic and interlaced twinned morphologies and consists in three major twin orientations. The polarized light observation of the different studied solder joints highlight the presence of this morphology (Figure III.2-5 (a) and Figure III.2-5 (b)). The interlaced regions is punctual and often located at the nucleation site near the solder pad (component or PCB side). Observation show that they did not exhibit a dendritic structure and are in fact characterized by a high density of Ag₃Sn particles of larger sizes randomly distributed in the tin matrix (Figure III.2-5 (c)). The interlaced areas are therefore more resistant to deformation and thus have a higher hardness [53]. These features can be considered beneficial if the solder joint has a fully interlaced structure. However, partially interlaced regions in mixed morphology, having different material properties than the rest of the solder joint, can increase the risk of early failures [31]. In this work, this morphology was not detected in the chip resistor solder joints.

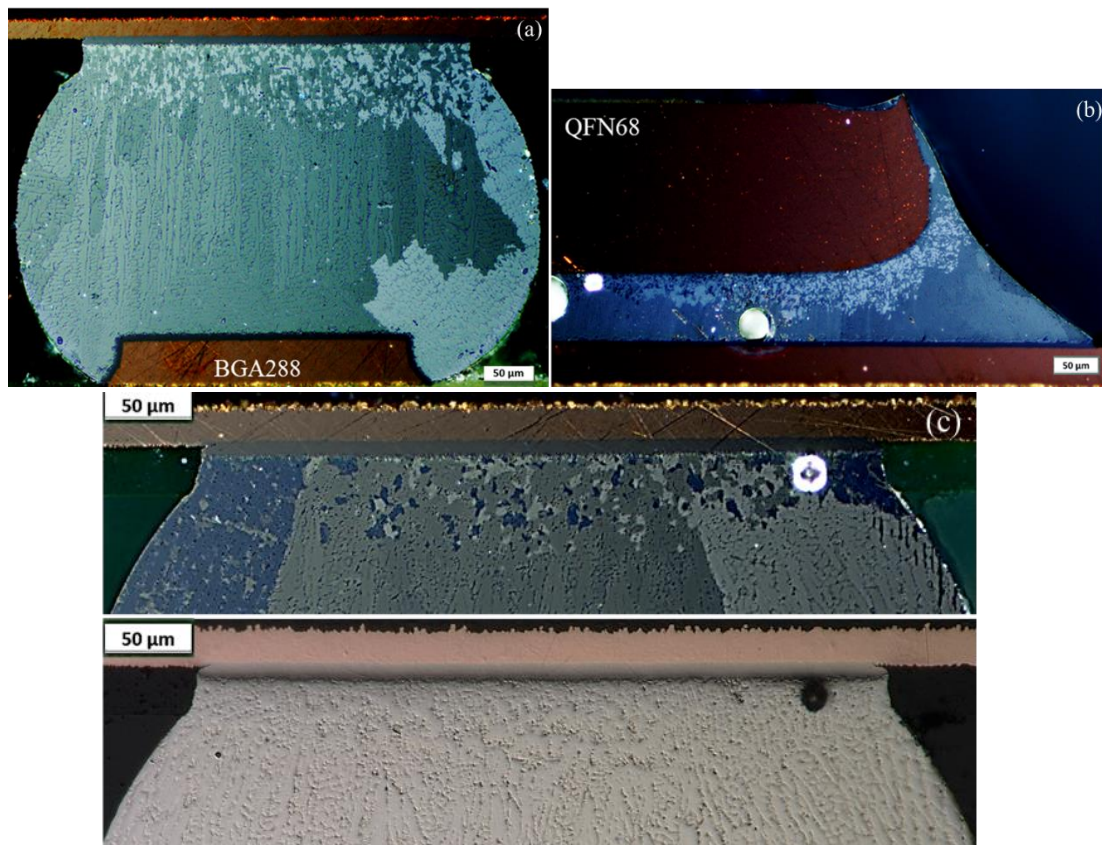


Figure III.2-5: Characterization of tin grain mixed morphology, (a, b) polarized light observation BGA and QFN solder joints , (c) Ag₃Sn particles distribution in the interlaced region

(b) *Tin grain morphologies distribution*

As the initial microstructure is expected to have an impact on the thermomechanical response of lead-free solder joint due to tin grain anisotropy, a quantitative study was made to identify the predominant morphology in the different studied components (BGA, QFN and chip resistor).

During polarized light observation, the color of a grain will depend on the polarization of the light. Consequently, grains with different orientation will have slightly different colors. Furthermore, the colors of the grain will change gradually when we rotate sample in the cross-sectioned plane. Figure III.2-6.a show that at certain angles two grains may have the same color despite that they have different orientations. Some samples having more than a grain may be mistaken for single-grained, if they are not in the good rotation during the inspection. This may also lead to an overestimation of the fraction of single-grained solder joints. However, the interlaced structure was always detected at any angle of the sample rotation (Figure III.2-6.b). In this work, all the observations were carried out without rotating the sample given the long time that the inspection of each joint can take.

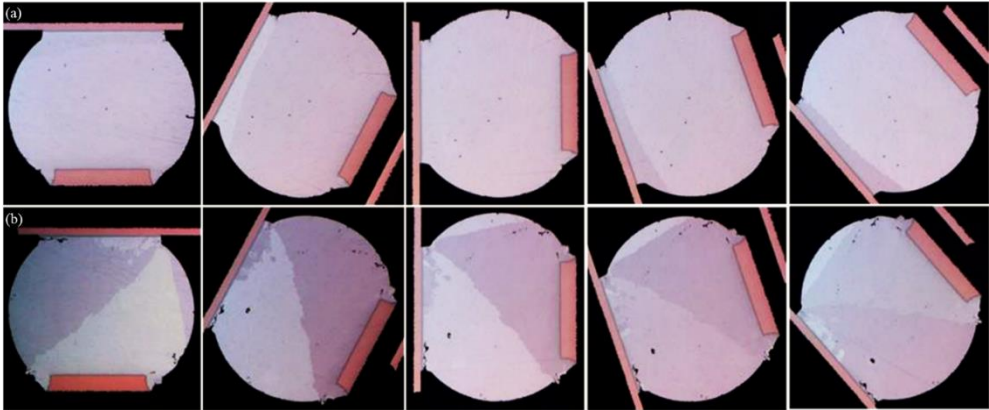


Figure III.2-6: Sample rotation effect on tin grain orientation detection by polarized light observation [31]

The cross-section plan can also have an impact on the identification of morphologies present in the solder joints. BGA components with two different cross-section plans were examined to better understand the plan observation effect in the estimation of data morphologies. In this part, BGA components come from ROBUSTESSE boards designed for a test plan allowing a large number of observations on non-cycled boards. Some components have undergone different isothermal storage conditions. The effect of isothermal aging on the tin morphology has been verified on some components. Observations showed that the morphology of tin grain does not evolve during isothermal storage.

First, cross-sections were done in parallel to an edge of the cross-sectioned components. The goal was that the cross-sectioning plan should be close to the middle of the solder joints. This classic mode of observation, provides access to both the morphology of the tin in each solder joint as well as the properties of the interfaces but a polishing step is necessary to move on to the next row of bumps.

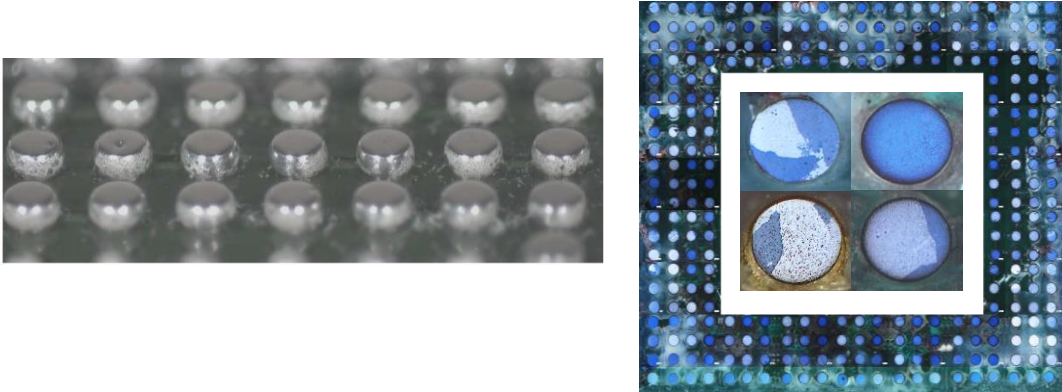


Figure III.2-7: Observation of BGA solder joints by the top view

Since it is quite time consuming to make several cross-sections going from one row to another in each analyzed component, another cross-section plan was used to collect more quickly tin morphology data in all the joints of a component. BGA components have been polished from above to access in a single cross-section the information on the morphology of all the joints. 288 bumps per cross-section can be observed compared to 22 joints for the 1st mode (Figure III.2–7).

Table III.2–1 summarizes the results of the morphology distribution in some considered components. The single grain morphology have been reported to be predominant with a fraction that may range up to 88% in the BGA solder joints. However, this fraction is little lower in the top view mode compared to the classic observation mode (80%). The percentages do not exceed 12% for the macro-grained morphology with several crystalline orientations (poly-grains) at any observation mode. These percentages can present an overestimated/underestimated since those observations have been performed in a single cross-section plane.

Additionally, solder joints exhibiting a cyclic twin morphology in the cross-section plane may have a part showing an interlaced structure in other portions of the solder joint. Similarly, solder joints having a fully interlaced twinned structure in a cross-section may actually have a mixed structure (interlaced + cyclic twinned), although this is less likely since the interlaced region is usually rather small. Thus, the solder joints fraction with a mixed morphology may be underestimated and the fraction of interconnections with an all interlaced structure overestimated. Consequently, and given that the observations showed the weak presence of tin twin phenomena (intertwined or cyclic) in our solder joints, the distribution data of the different morphologies presenting the structure of tin twins were reported together in a single column. The percentages do not exceed 15% in this case

Table III.2–1: Distribution of various tin grain structure in BGA solder joints of ROBUSTESSE board

Observation mode	BGA component pre-aging condition	Percentage of various tin grain structure		
		Macro-grained		interlaced, cyclic twinned and mixed
		single-grained	poly-grained	
sectional view	100°C – 500h	84	12	4
	100°C – 1000h	87	9	4
	150°C – 500h	88	4,5	7,5
	150°C – 1000h	85	10	5
top view	As-reflowed	73	12	15
	As-reflowed	80	11	9

The occurrence of the different morphologies in components depends on solder volume, alloy composition, surface finish and cooling rate. The effect of solder geometry on the distribution of tin grain morphologies was also studied by making micro sections on the Feline board (test vehicle with BGA, QFN and R1206 components). The images were taken in the classic observation mode. Cross-section show that single-grained, poly-grained and mixed structure were the only present structures.

Another observation attracted our attention is that the BGA solder joints do not have the same tin grain morphology distribution compared to the BGA_ROBUSTESSE components despite the assembly of the two batches of cards (ROBUSTESSE, FELINE) was made with the same reflow profile using the same solder paste. However, the two batches were not assembled at the same time. 58% of BGA solder joints present a mixed structure compared to fractions of 33% for the single-grained morphology and 9% of solder joints having the poly-grained structure.

QFN Solder joints showing single-grained are rare (4%) with practically equal distribution between SAC solder with poly-grained and mixed structure (50% and 46% respectively).

The absence of the mixed structure on the chip resistors solder joints was validated with the count data of tin grain morphologies distribution. In this solder geometry, the single-grained structure was also the most present with a fraction of 63% compared to 37% of poly-grained interconnections.

Table III.2–2: Distribution of various tin grain structure in BGA, QFN and R1206 solder joints of FELINE board

Component type	Percentage of various tin grain structure		
	Macro-grained		mixed
	single-grained	poly-grained	
BGA	33	9	58
QFN	4	50	46
R1206	63	37	0

(c) Characterization of tin grain morphologies by EBSD technique

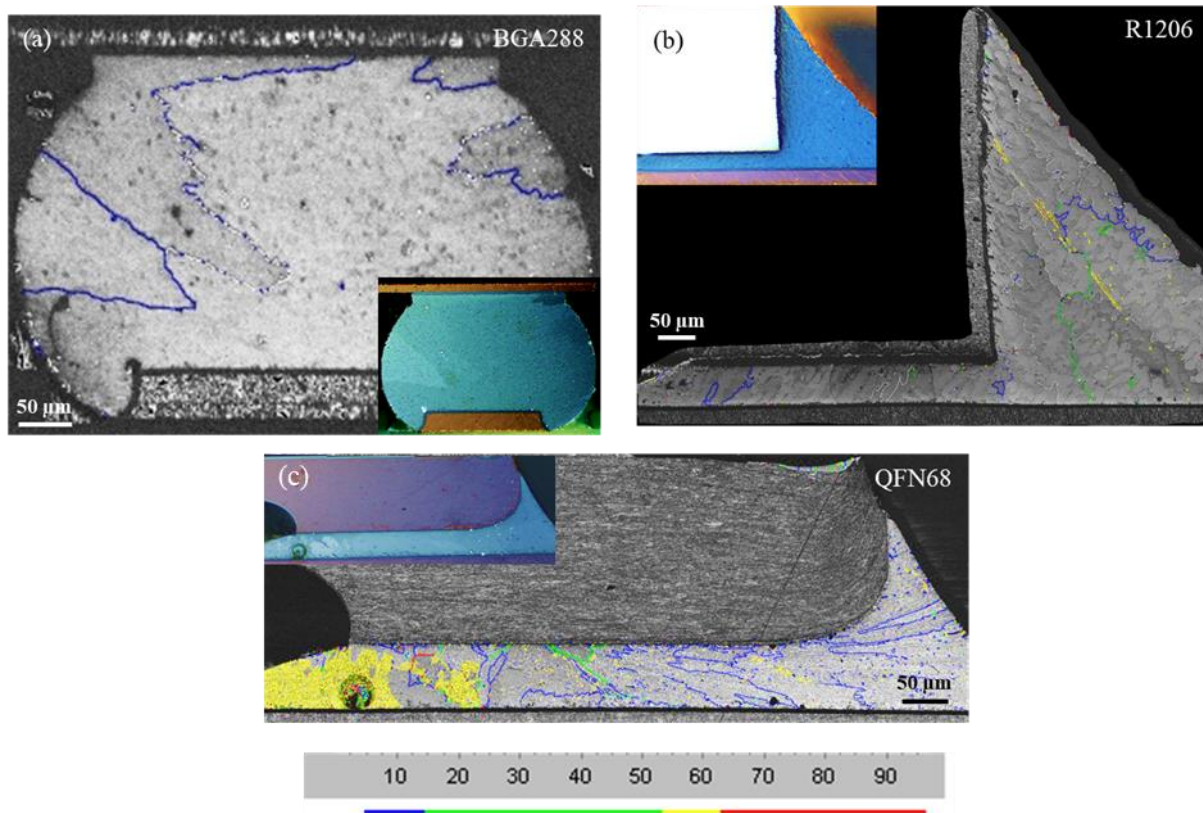


Figure III.2-8: Tin grain boundary angles maps in different solder joint geometries, (a) BGA solder joint, (b) R1206 solder joint, (c) QFN solder joint

Observation under polarized light is very useful for highlighting the different morphologies but does not allow them to be quantified. The technique of backscattered electron diffraction (EBSD) provides access to a quantitative characterization of the grain boundary angles, the crystalline orientation and the grain size with high spatial resolution.

Grain boundary angles analysis by EBSD allows illustrating the spatial distribution of all detected grain boundaries. Figure III.2-8 presents the different angle intervals convention used in this work:

- [2°; 5°[= white,
- [5°; 15°[= blue,
- [15°; 55°[= green,
- [55°; 65°[= yellow
- [65°; 90°] = red,

The comparison between polarized light images and the grain boundary angles cartographies shows that the misorientation limit below which we cannot distinguish two neighboring grains under an optical microscope depends on the geometry of the solder joint (Figure III.2-8).

For BGA joints, only white boundaries with angles <5° may possibly not be distinguished under polarized light (Figure III.2-8 (a)). In the case of the QFN and passive components solder

joints, the disorientation between two grains not detected by polarized light can have a greater angle going to a value around 55° (green and blue grain boundaries in Figure III.2–8 (b) and Figure III.2–8 (c)). Over this value, the differences in orientation between two neighboring grains are observable. These results show that the identification of tin grain structure by polarized light observation can underestimate the fraction of interconnections having poly-grained structure. However, it allows the interlaced and cyclic twinned structure detection.

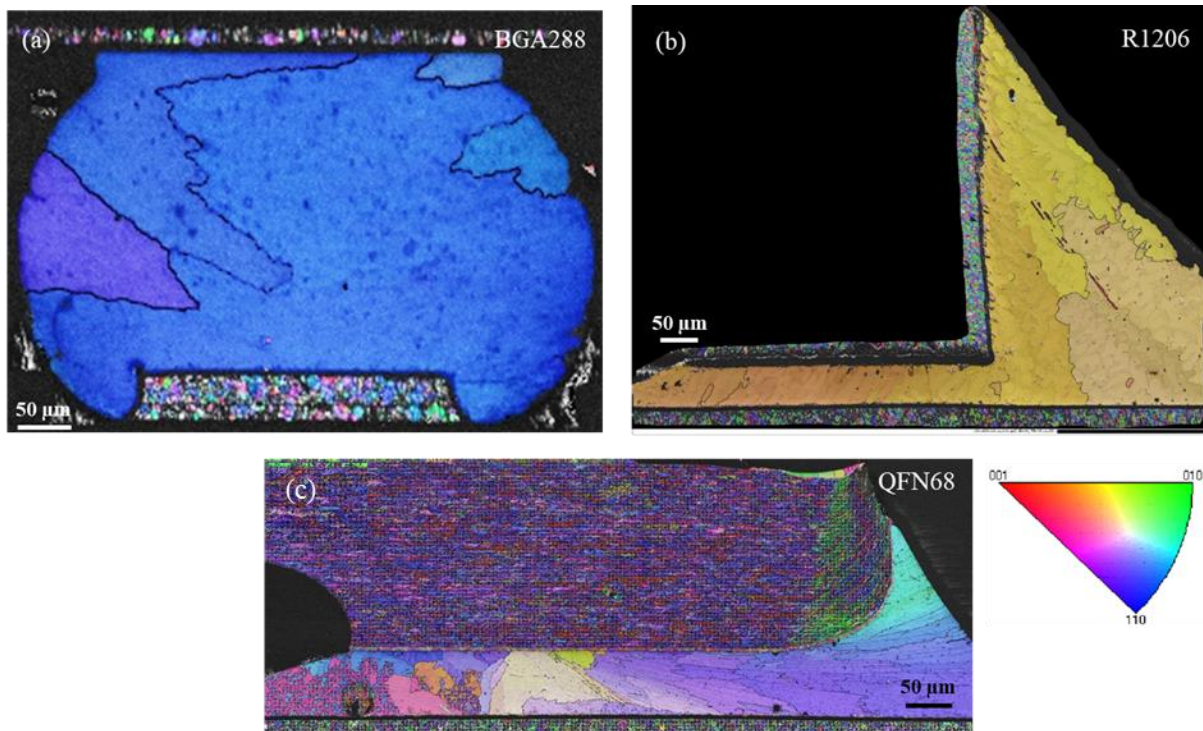


Figure III.2–9: Tin grain crystallographic orientation maps in different SAC solder joint geometries, (a) BGA solder joint, (b) R1206 solder joint, (c) QFN solder joint

Beyond the tin grain boundaries angles characterization, we must be interested in the solder joints crystallographic texture of the different tin grain structure. Studies cited in the bibliographical section have shown the dependence of the mechanical properties on the tin crystal direction. The anisotropy of a solder joint can therefore be quantified by identifying the crystallographic orientation of each grain. EBSD data can be used to characterize the crystallographic texture of SAC solder joints by generating IPF (Inverse Pole Figure) crystal orientation maps. They represent the grains orientation with respect to a given direction of observation. In general, there are three directions of observation:

- X corresponding to the horizontal of the map
- Y to the vertical and
- Z to the normal to the sample surface.

These three directions of observation X, Y and Z respectively give rise to three crystal orientation maps named IPF-X, IPF-Y and IPF-Z. For these three maps, the orientation of a grain relative to the observation axis is color coded. In the case of tin, a tetragonal-type crystal lattice material, there are by convention three reference orientations denoted [001], [010] and [110]. The grains having exactly these orientations along a certain observation axis will be colored respectively in red, green or blue on the IPF map associated with this observation axis. Figure III.2–9 presents the IPF_x maps showing the various tin grain crystalline orientation that can be present in the studied components.

The superposition of the grain boundaries angles and the IPF crystal orientation maps visually highlights the different tin grain structures present in lead-free solder joints. Figure III.2–8.a, Figure III.2–8.b, Figure III.2–9.a and Figure III.2–9.b allow to recognize the poly-grained morphology in the BGA and R1206 chip resistor with a slight misorientation (maximum angle of 15°) between two neighboring grains. However, a very particular type of structure after reflow was encountered in the QFN solder joint. We have qualified it with a noticeable gradient in crystal orientation and a clear substructure in the form of long slats. Since the variations of orientations remain moderate and progressive, this microstructure could be characterized as a "**distorted**" macro-grained morphology. This specificity probably linked to the cooling conditions of the solder in this geometric configuration.

Figure III.2–8.c and Figure III.2–9.c show a QFN solder joint having a particular structure. It looks close to the mixed structure with the concentration of interlaced twinned structure with grain boundaries angle around 60° (yellow lines) in the right part. The other parts of the solder are characterized by the presence of β-Sn sub-grains (misorientation <5°) and low disorientated grains (<15°) in the form of very elongated slats which appears to be a very large-scale dendritic microstructure.

The IPF maps provide only a visual representation of the spatial distribution of the textured areas of a material. However, to get a more quantitative estimation of the textures, it is necessary to convert the crystal orientation maps into actual reverse pole figures. The principle is to transfer the orientation of each pixel of an IPF map into the standard stereographic triangle which will ultimately be made up of a point cloud. Three inverse pole figures (along X, Y and Z) are thus obtained from the three crystal orientation maps (IPF-X, IPF-Y and IPF-Z). Then the post-processing software splits the standard stereographic triangle into small elementary areas and calculates the density of points contained in each of the fragments of the triangle. The three inverse pole figures are then colored according to the local point density (in each fraction of the triangle). The texture of a material is evaluated in terms of MUD (Multiples of Uniform Density). Typically, if an inverse pole figure has a MUD_{max} greater than 2 in a given region, the material at the origin of the pole figure could be considered as textured in the direction of the pole figure. Conversely, a MUD_{max} less than 2 will be an indicator of a material with little or no texture, and if the MUD_{max} also remains below this threshold for the 2 other reference directions of the orthonormal coordinate system, the grains of this material will be said "equiaxis".

The measurement of the MUD_{max} on the three interconnections presented above show that as-reflowed SAC solder joints are generally textured. However, the MUD_{max} value depends on initial tin grain morphologies. We observe that the QFN solder has a much less textured microstructure than the chip resistors and BGA solder joints (Figure III.2–10). This helps once more to highlight the presence of the unusual QFN interconnection morphologies with a mixture of an interlaced and unusual deformed macro-grained structure.

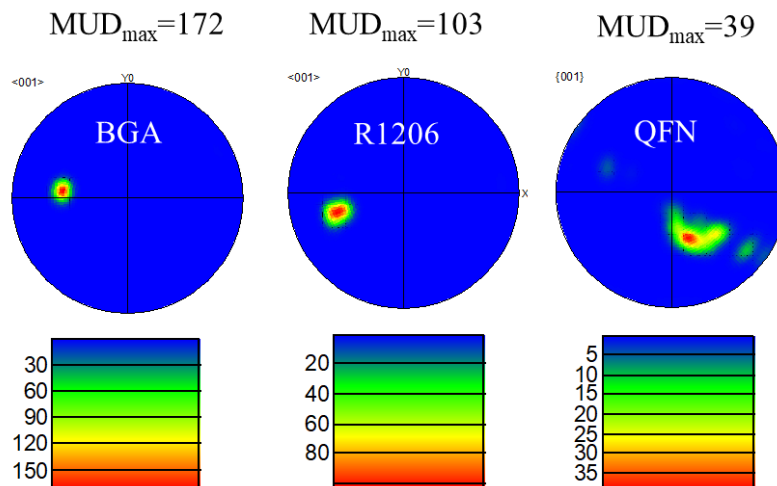


Figure III.2–10: MUD_{max} measurements in the BGA, R1206 and QFN solder joints

The size of each tin grain is also an important indicator to characterize the different solder joint morphologies. In this work, it was determined by calculating the diameter of its equivalent circle. Figure III.2–11 presents the tin grain size maps according to a color code ranging from blue for the smallest grains, to red for the largest depending on the different studied solder joints geometry. Measurements show that the tin grain size in BGA and R1206 components having the macro-grained structure is of the same order of magnitude as the solder joints (equivalent diameter $> 50 \mu\text{m}$ in Figure III.2–11 (a) and Figure III.2–11 (b)).

The analysis of the deformed macro-grained structure characteristic of the QFN solder joints call attention to the presence of very small tin grain ($10 \mu\text{m}$) in addition to macro grains (Figure III.2–11 (c)). For the region showing mixed morphology, as presented in the literature, it is a form of twinning phenomenon which are characterized by a rotation of 60° around the axis $[001]$ of the Sn crystal lattice. In this case, the tin grain boundaries will have an angle approximately of 60° . Thus, the particle size analysis is carried out by considering that all the subdomains linked by a twin symmetry relationship like a part of the same grain.

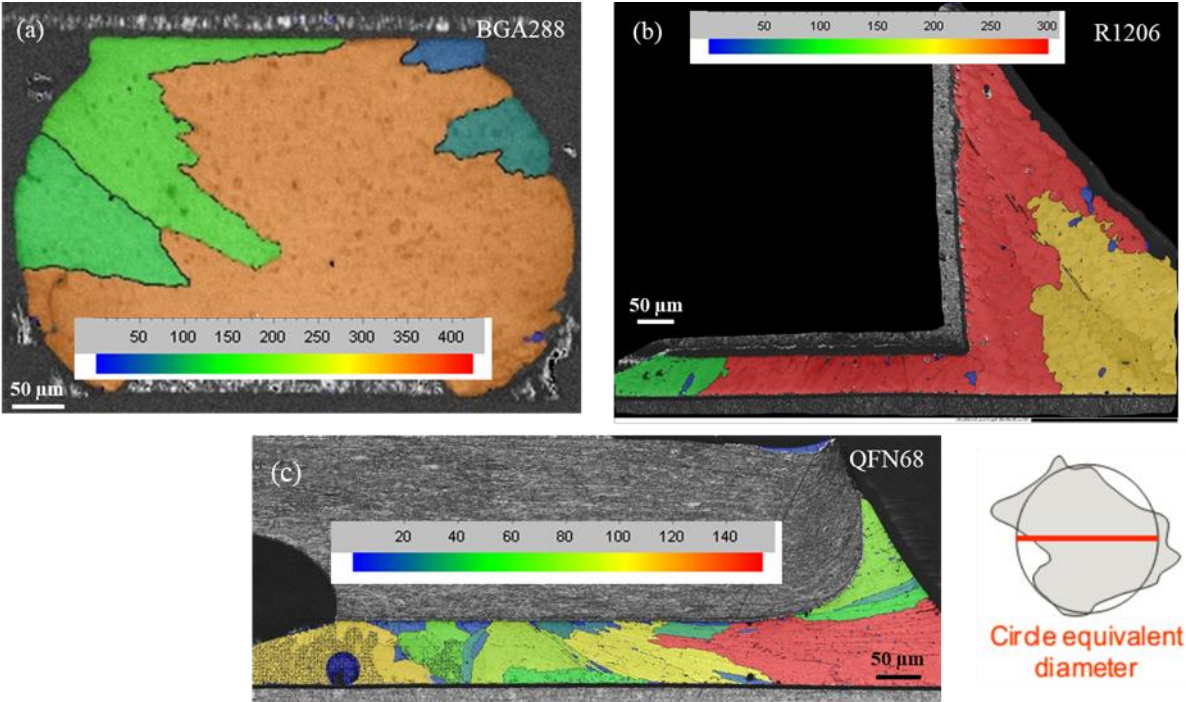


Figure III.2-11: Tin grain size maps in different solder joint geometries, (a) BGA solder joint, (b) R1206 solder joint, (c) QFN solder joint

The cyclic tin twin phenomenon was also observed on some joints with scratches that could not be removed even after the polishing finishing step (Figure III.2-12 (a)). The force applied to the samples during the mechanical polishing step can generate joint deformations leading to the appearance of twin phenomena (Figure III.2-12 (b) and (Figure III.2-12 (c)). The EBSD analysis of certain solder joints showing no scratches when observed in polarized light reveals the presence of this type of defect. Care must be taken thereafter not to confuse this defect with the appearance of new tin grains during microstructural evolution.

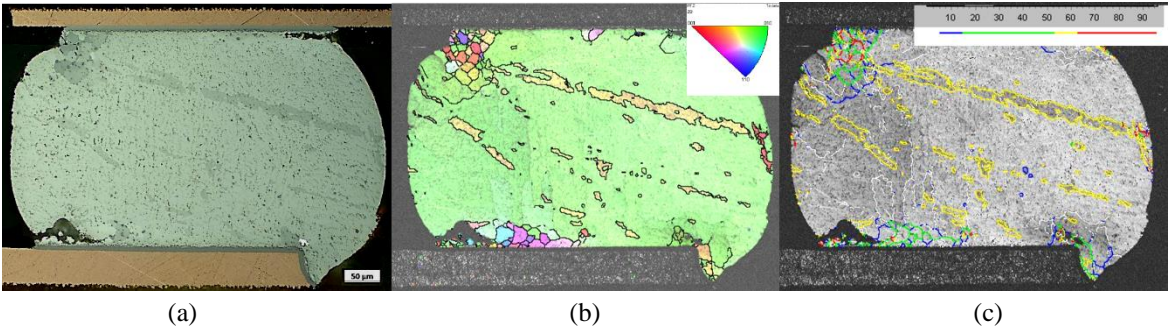


Figure III.2-12: Observation of BGA SAC solder joint with a polishing defect, (a) polarized light observation, (b) crystalline orientation map, (c) grain boundary map

III.2.3 Isothermal pre-ageing effect on SAC305 solder joints microstructure

Isothermal pre-ageing is a recommended condition in board level reliability testing for approaching real applications of electronic assemblies [94].

It has been reported that the annealing process during the pre-aging treatment alters the morphology and the distribution of dispersed intermetallic compound (IMC) particles in the solder joints. The coarsening of these particles can apparently facilitate the Sn grain boundary mobility due to less effective pinning on dislocation movements [24][95]. The fine IMC particles, present in a non-aged microstructure, are able to decelerate microstructural evolution under thermomechanical stress by blocking Sn grain boundary movements during recrystallization [96].

In this part, we focused on the effect of pre-ageing on the microstructure of SAC solder joints after reflow [97]. Some components, which have undergone a hot pre-ageing without being cycled in temperature, have been encapsulated for studying the precipitate coarsening in bulk solder and interfacial intermetallic layer thickening.

The intermetallic coalescence was firstly confirmed in various aged specimens with optical microscopy. Thermal aging is expected to cause precipitate coarsening in bulk solder and interfacial intermetallic layer thickening through diffusion phenomena. The small precipitates dissolve into the matrix and re-precipitate at the larger ones [98]. The diffusion phenomenon is thermally activated, thus occurs in the whole solder joint. The observation of the microstructure of solder joints with different heat treatment conditions highlighted the coalescence phenomenon of the bulk precipitates and the weakening of the dendrite structure described above. Figure III.2–13 shows the effect of different isothermal storage conditions on the BGA solder joints. The inter-dendritic distribution of Ag₃Sn nano-particles is retained and smaller precipitates remain in the majority. However, the increase in time and temperature of treatment makes it possible to produce some precipitates of larger size to the average by coalescence of the smallest. The coalescence and the increase in the spacing between the Ag₃Sn precipitates are visually more important for the highest temperature (150°C). However, Ag₃Sn particles evolution has been more difficult to perceive for pre-aging at 100°C. Observations show also that the pre-aging of R1206 and QFN solder joint pre-aged at 100°C during 500h has no effect on their initial structure.

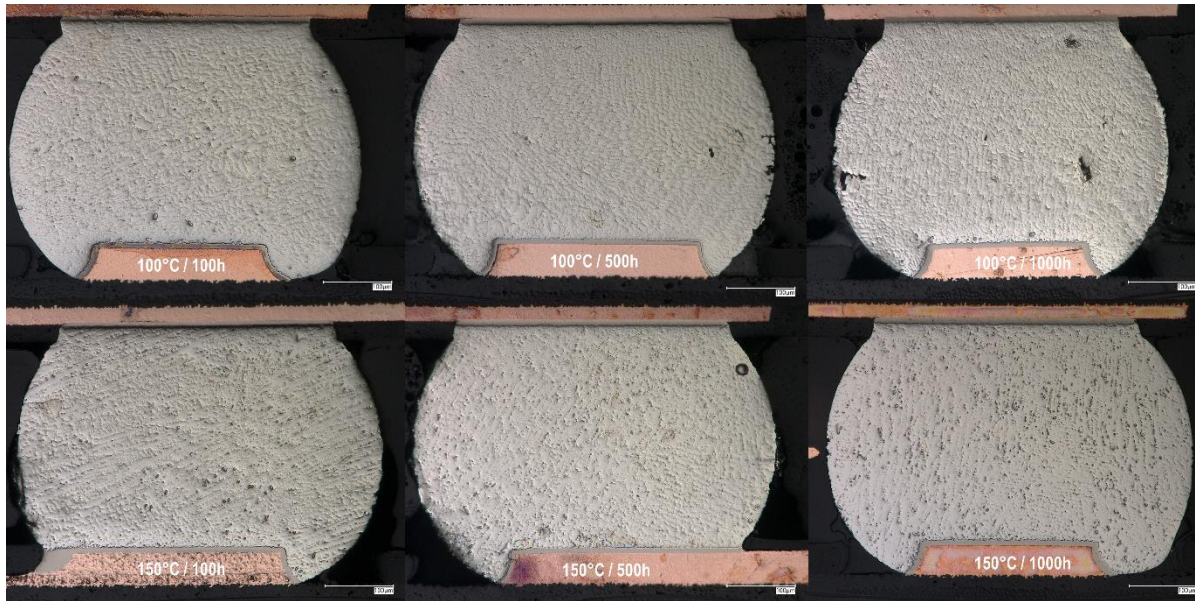


Figure III.2–13: Evolution of the microstructure of BGA solder joints with different isothermal aging conditions (100h, 500h and 1000h at 100°C and 150°C)

The effect of isothermal aging on the precipitate distribution and the tin dendritic structure is even clearer through chemical/ crystallographic data. Silver mapping with Energy Dispersive X-ray Spectroscopy in the upper part of single-grained solder joints illustrates the decrease in precipitate density with aging and the depopulation of the interdendritic spaces (Figure III.2–14). From EBSD crystal phase analysis, the evolution of the different Ag₃Sn grain size categories was quantified (Figure III.2–14(d)). The proportion of the smallest detected grains (area between 0.22 and 0.65 μm^2) drops with aging (up to 44% after 1000h at 150°C) and the weight of other categories increases. After aging at 100°C and 150°C during 1000h, larger precipitates (area > 2 μm^2) are detected while they do not exist with room temperature aging. The coalescence is therefore more important as aging duration and temperature get higher enabling the diffusion.

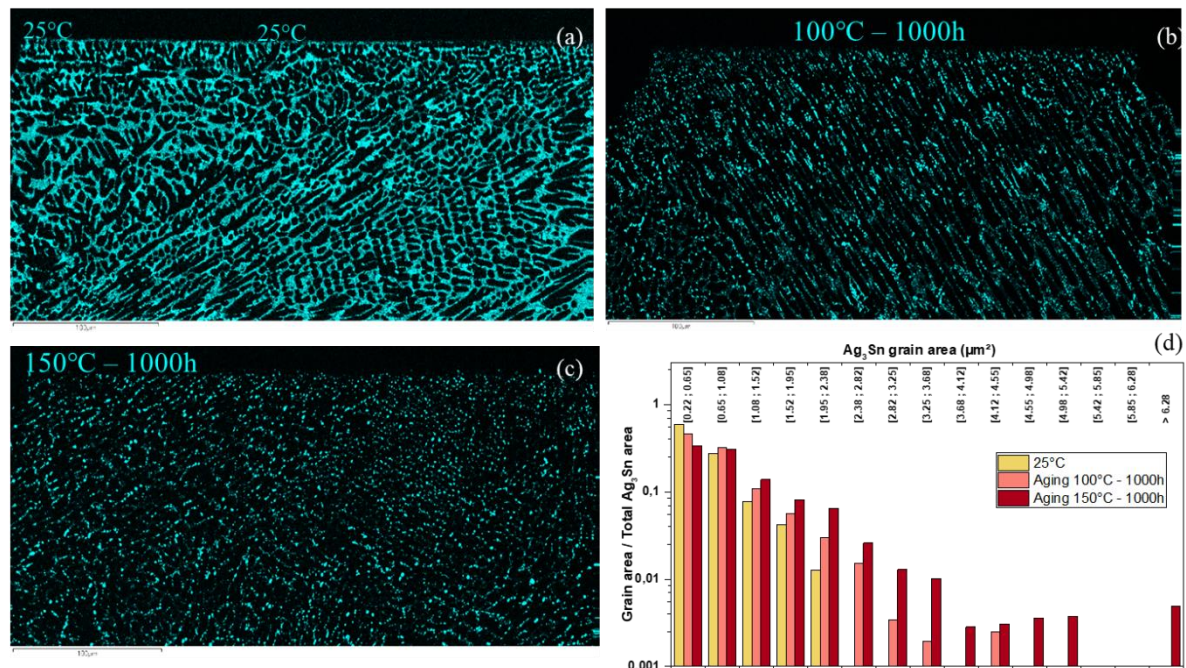


Figure III.2-14: Ag₃Sn precipitate coalescence during isothermal aging, silver EDS mapping with room temperature aging (a), after 1000h at 100°C (b), 1000h at 150°C (c), evolution of Ag₃Sn precipitate population in function of grain area (EBSD data) (d)

The second aspect to consider in microstructural evolution under the isothermal ageing is the thickening of the intermetallic layers. In this work, the increasing of layer thickness was not clearly observed. The values measured by image analysis vary between 1.5 and 3.5 μm without any effect of storage time or temperature having been demonstrated. It is difficult to see a difference in layer thickness between the initial state and the two longest aging conditions in Figure III.2-15. On the other hand, this figure makes it possible to highlight once again the evolution of the distribution of Ag₃Sn particles in the solder joints bulk (more precisely in the zone close to the interface with the component).

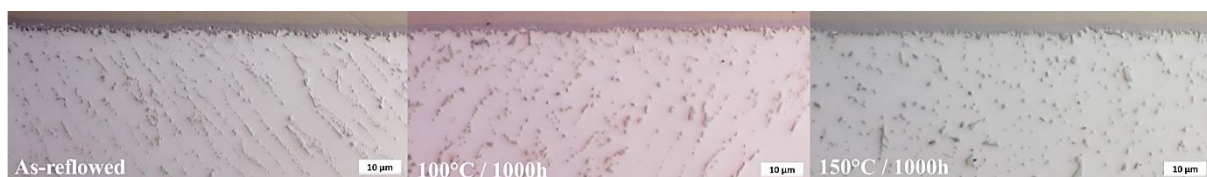


Figure III.2-15: intermetallic layers evolution under isothermal ageing

In our study, isothermal pre-aging does not appear to have a significant effect on intermetallic interfaces. This is an unexpected result when compared to those in the literature [39]. It is assumed that the nickel finish has prevented diffusion at the interface.

III.2.4 Synthesis

The solder microstructure investigation was carried out on the as-assembled state and after isothermal aging. Cross-sectioning, optical microscopy and EBSD allowed identifying

the typical as-reflow SAC dendritic microstructure made of a β -Sn matrix and Ag₃Sn precipitates filling the interdendritic spaces. Macro-grained, cyclic twinned and mixed tin morphologies were observed in the different considered solder geometries. As the initial microstructure is expected to have an impact on the solder mechanical behavior due to tin anisotropy, a quantitative analysis under polarized-light microscopy was made on several components to study the tin grain structures distribution. From a global point of view, the macro grain morphology proved to be predominant in different solder geometries (BGA, QFN and chip resistor). EBSD technique was used to characterize grain boundary angles, crystalline orientations and grains size the various observed tin grain structures. It highlights the presence of unusual deformed macro-grain structure in the as-reflowed QFN interconnections.

For the isothermal aging, the intermetallic coalescence coupled with a loss of the joint dendritic structure was confirmed in various aged specimens through optical microscopy and chemical/ crystallographic data. However, no effect was observed on the evolution of intermetallic interfaces thickness. For the following section, the storage condition for 500h at 100°C was chosen in order to accelerate the thermal cycling without modifying too much the initial properties of the lead-free interconnections.

III.3 Thermal cycling effect on pre-aged SAC305 solder joints microstructural

III.3.1 Global recrystallization of tin grains

Microstructural analyses on different types of components (BGA, QFN and chip resistor) taken out of the thermal chamber along the test allowed us to set up the successive steps of recrystallization and its propagation in the solder joint. The recrystallization study was conducted using polarized light images and data from EBSD analyzes.

Observations were focused on the high strain regions since microstructural changes begin in geometric singularity zones of the assembly (near the solder pads for the BGA and underneath the QFN and R1206). Images of entire joints were also taken in order to collect as much information as possible on the location and advancement of microstructural evolution phenomena.

Since the EBSD technique is more difficult to implement, the first step was to proceed with an inspection of the evolution of the tin grains in order to identify upstream cases of apparent recrystallization by optical microscopy in polarized light. With the hypothesis that tin birefringence properties allow the distinction of the new grains having crystalline orientations different from the initial orientation, the objective is to identify over time the early stages of tin grains changes during thermal cycling [-55°C,125°C].

(a) BGA solder joint

For BGA solder joints, optical observations showed that microstructural evolution appears to start at 1000 cycles. Figure III.3–1 presents polarized light images carried out on samples taken successively from the climatic chamber at different cycling level (225, 500, 1000 and 1300 cycles).

Before 1000 cycles, the thermal cycling effect is not detectable. New crystalline orientations of tin grain begin to appear on the sample which has been subjected to 1000 cycles. Recrystallization is evident on the solder joint sampled at 1300 cycles. The apparent absence of recrystallized grains on samples taken at 225 and 500 cycles does not necessarily mean that the tin grains did not evolve during thermal cycling.

Since the analysis of the as reflowed microstructure has shown the difficulty of detecting by polarized light observation all the grain boundaries present in the various interconnections, the same samples present in Figure III.3–1 were analyzed by EBSD to validate the microstructural state of each joint after such a number of cycles.

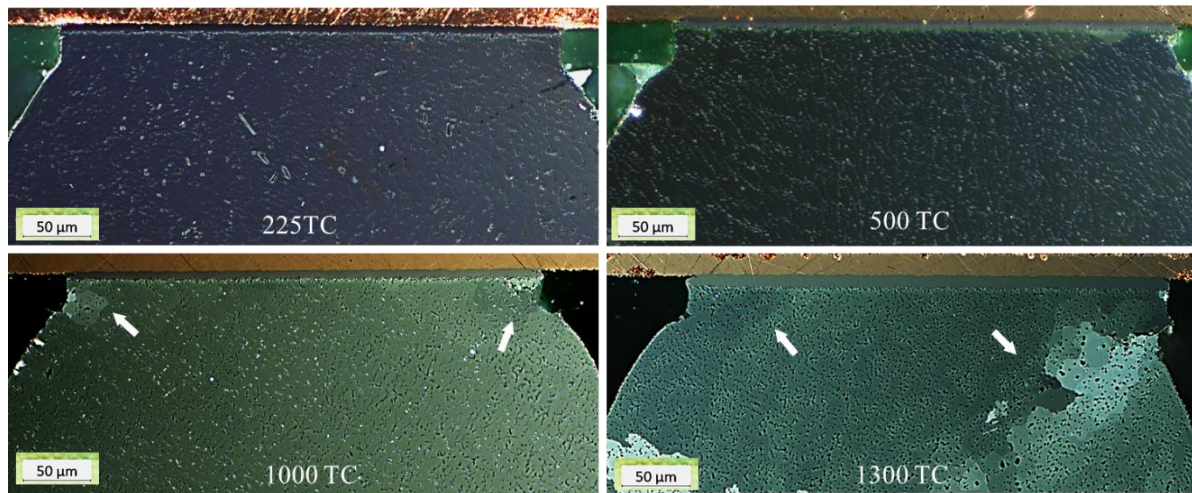


Figure III.3-1: Microscopy optical inspection of BGA solder joints with different number of thermal cycles by Polarized light observation

Tin grain boundary angles mapping showed that BGA SAC solder joints evolution already started before 225 cycles. It begins with the recovery process characterized by the formation of β -Sn sub-grains (misorientation $<5^\circ$) and low disorientated grains ($<15^\circ$) in the high strain regions. Figure III.3-2 shows the first stages of the recovery process (white and blue lines) observed in few cycled solder joints (225 cycles). The comparison with the as reflowed microstructure validates that this process was activated due to thermal cycling.

Figure III.3-3 (a, b, c, d, e, and f) illustrate that the solder joints microstructure still remains in the recovery phase with an increase in low angle boundaries number (blue lines) during the first 1000 cycles. During this process, the tin grains do not change their initial crystalline orientation. The comparison between the optical image and EBSD maps of joint subjected to 1000 cycles shows that in some cases recovery process can be observed by polarized light. Grain boundaries angle present at this time probably had angles which tend towards the superior bound value of the low angle interval (15°).

In the course of further thermal cycling, the microstructure keeps evolving gradually and the recrystallization process begins. Sub-grains grow to reduce their surface energy and facilitate their rotation due to thermal activation and deformations generated in the damaged area. Grain boundaries with larger angles ($>15^\circ$) appear and delimit new tin grains leading to the creation of more or less equiaxed grain structures with random crystalline orientations.

Figure III.3-3 (g) and Figure III.3-3 (h) shows that the recrystallization has developed by the formation of new grain orientations (purple, red, and green) limited by high angle grain boundaries (green lines). The absorption of dislocations into dislocation walls is the origin of the gradual increase in misorientation of low angle boundaries and their transformation into high angle boundaries. It is interesting to note that the recovery process operates also after the nucleation of the recrystallization preparing the favorable environment for the recrystallization spreading in the bulk of the solder.

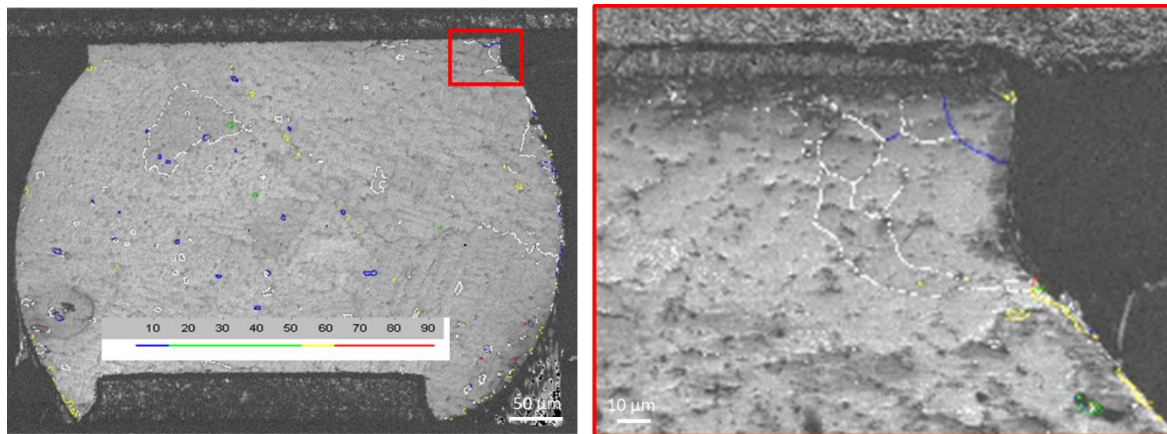


Figure III.3-2: Recovery process revealed by grain boundary angles mapping in the BGA solder joints corner taken at 225 cycles; white sub-boundaries ($[2^{\circ}; 5^{\circ}]$) and blue boundaries ($[5^{\circ};15^{\circ}]$)

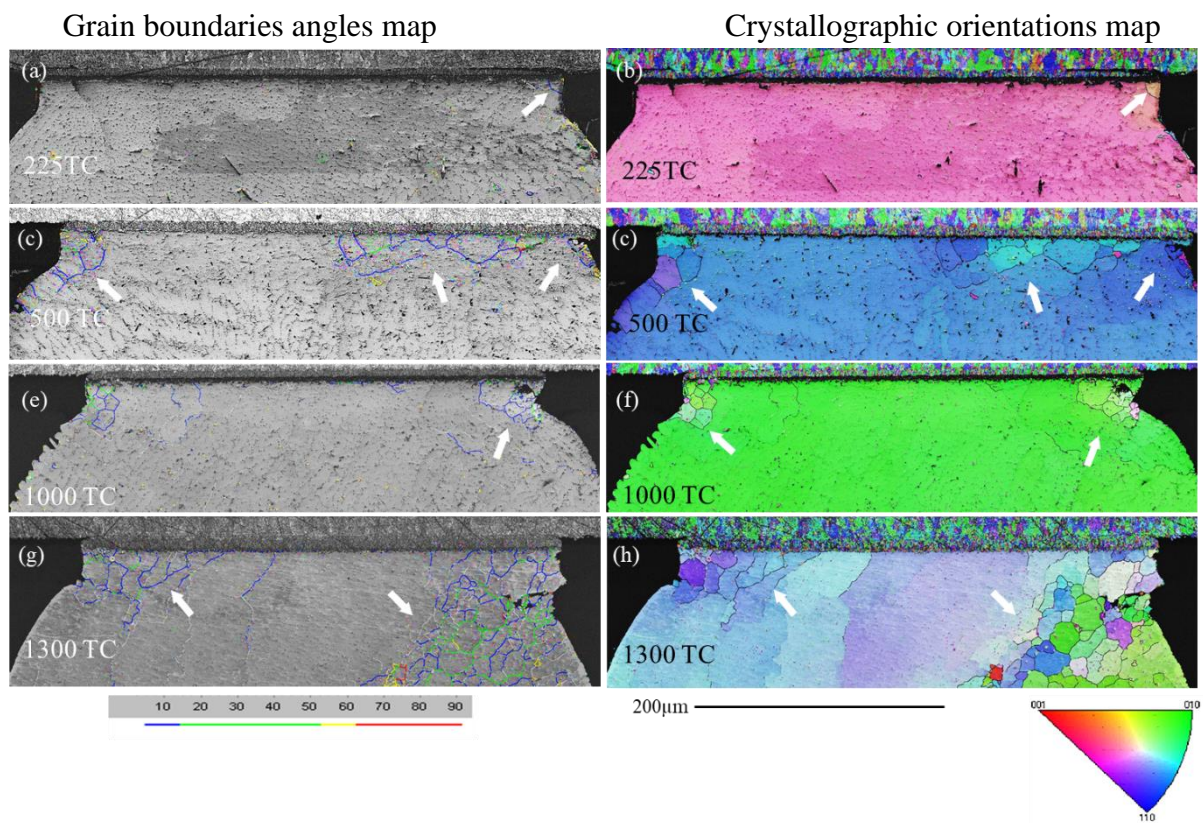


Figure III.3-3: Characterization of BGA solder joints tin grains evolution during thermal cycling by EBSD analyses with grain boundaries maps showing the low angle ($[5^{\circ};15^{\circ}]$) and high angle ($[15^{\circ};55^{\circ}]$); (a, b, c, d, e, f) recovery process, (g, h) recrystallization with rotation of new tin grains

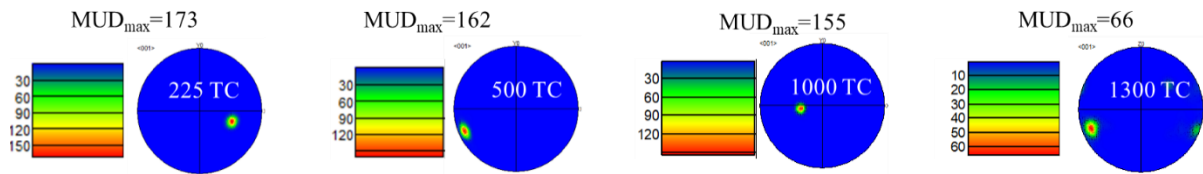


Figure III.3-4: Evolution of the MUD_{max} value in the BGA solder joints under thermal cycling

The progressive formation of a network of more and more highly misoriented recrystallized grains induces the attenuation of the initial macrograin texture. The pole figures show that the strong crystallographic texture observed after reflow gradually disappears as the thermomechanical damage accumulates during the cycles. Despite the slight decrease in the MUD_{max} during the recovery phenomenon (first 1000 cycles), it is clear that the joint retains its crystallographic texture. The loss of this texture is greater during the recrystallization phenomenon characterized by a high density of highly disoriented grain boundaries.

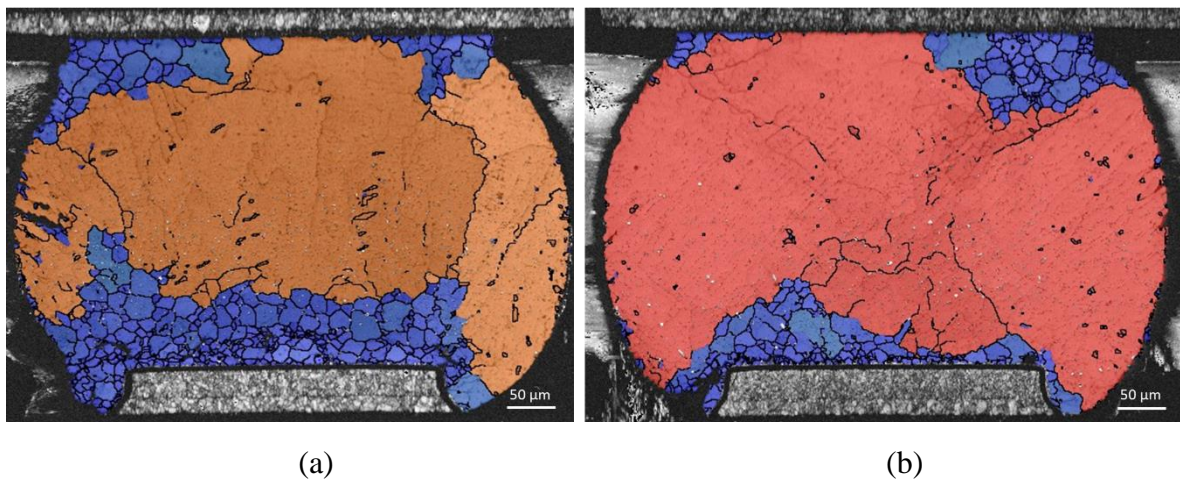


Figure III.3-5: Propagation of the network of recrystallized tin grains (blue) on the BGA solder joints taken out at 2300 TC (a) and 2000 TC (b)

Samples analysis with different thermal cycles show that this change in the microstructure often starts in the solder corner near the pad on the package or PCB side. Then, the recrystallized volume gradually expands from the solder corners toward the center, across the joints neck near the interfacial region of the interconnection until total recrystallization of the highly strain region (Figure III.3-5 (a)). Occasionally, recrystallization can spread across the diagonal of the bump between two opposite corners up to the junction of the two sides of the interconnection ((Figure III.3-5 (b)). These observations are consistent with previous work [15][29][54].

(b) *Chip resistor solder joint*

The polarized light inspection step was carried out on all the geometries studied. It also allowed us to highlight the evolution of tin grains on the R1206 solder joints. Figure III.3–6 presents polarized light images of solder joints with three different levels of cycling (135, 500 and 700 cycles). Microstructural changes are evident in the solder joint taken from thermal chamber after 700 cycles. New tin grains with orientations different to the parent orientation are clearly observed in Figure III.3–6 .

The verification of the evolution of the tin grains on the same samples was developed by the EBSD technique in order to identify the first microstructural changes of R1206 solder joints during thermal cycling and examine the recovery and the recrystallization of tin grains [99].

Tin grain boundaries maps highlighted once again that observation of recovery process is not always possible in polarized light. Figure III.3–7(a) and Figure III.3–7 (b) highlight that solder joint taken at 135 cycles was already in a recovery state. Large number of low angle boundaries (blue lines) are present under the component. However, its examination by polarized light did not reveal a microstructural change.

Tin grain boundaries maps illustrate also the nucleation of R1206 interconnections recrystallization after 500 cycles (Figure III.3–7 (a) and Figure III.3–7 (b)). A gradual lattice rotation has formed into high angle grain boundaries from low angle boundaries during thermal cycling, which characterizes the tin grain recrystallization of the already recovered microstructure. Gradual lattice rotation occurred in the transition from the parent pink orientation to several orientations (red, blue, yellow). This microstructural change was difficult to detect by optical microscopy despite the start of the new tin grains rotation.

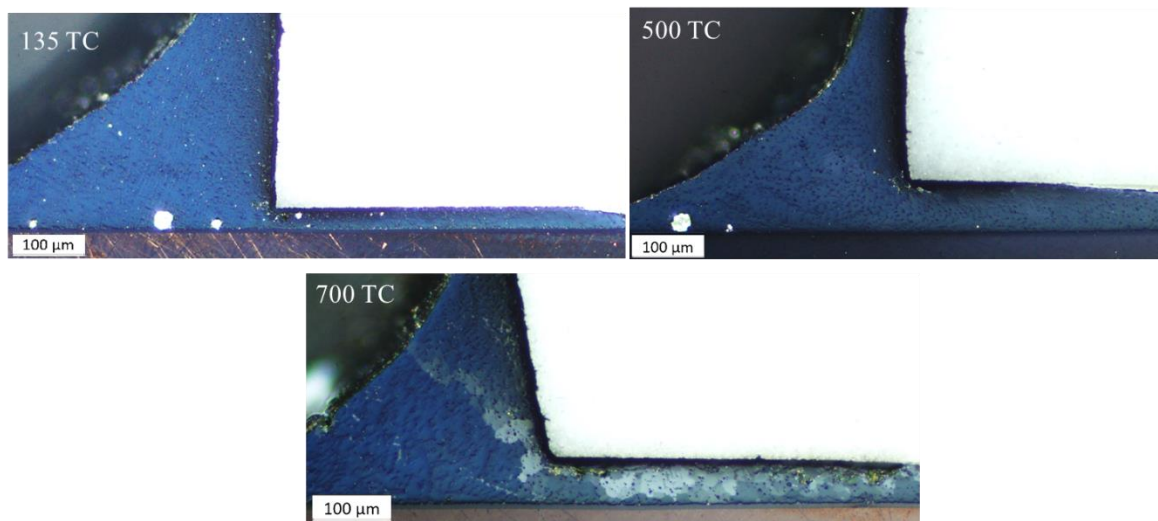


Figure III.3–6: Microscopy optical inspection of R1206 solder joints with different number of thermal cycles by Polarized light observation

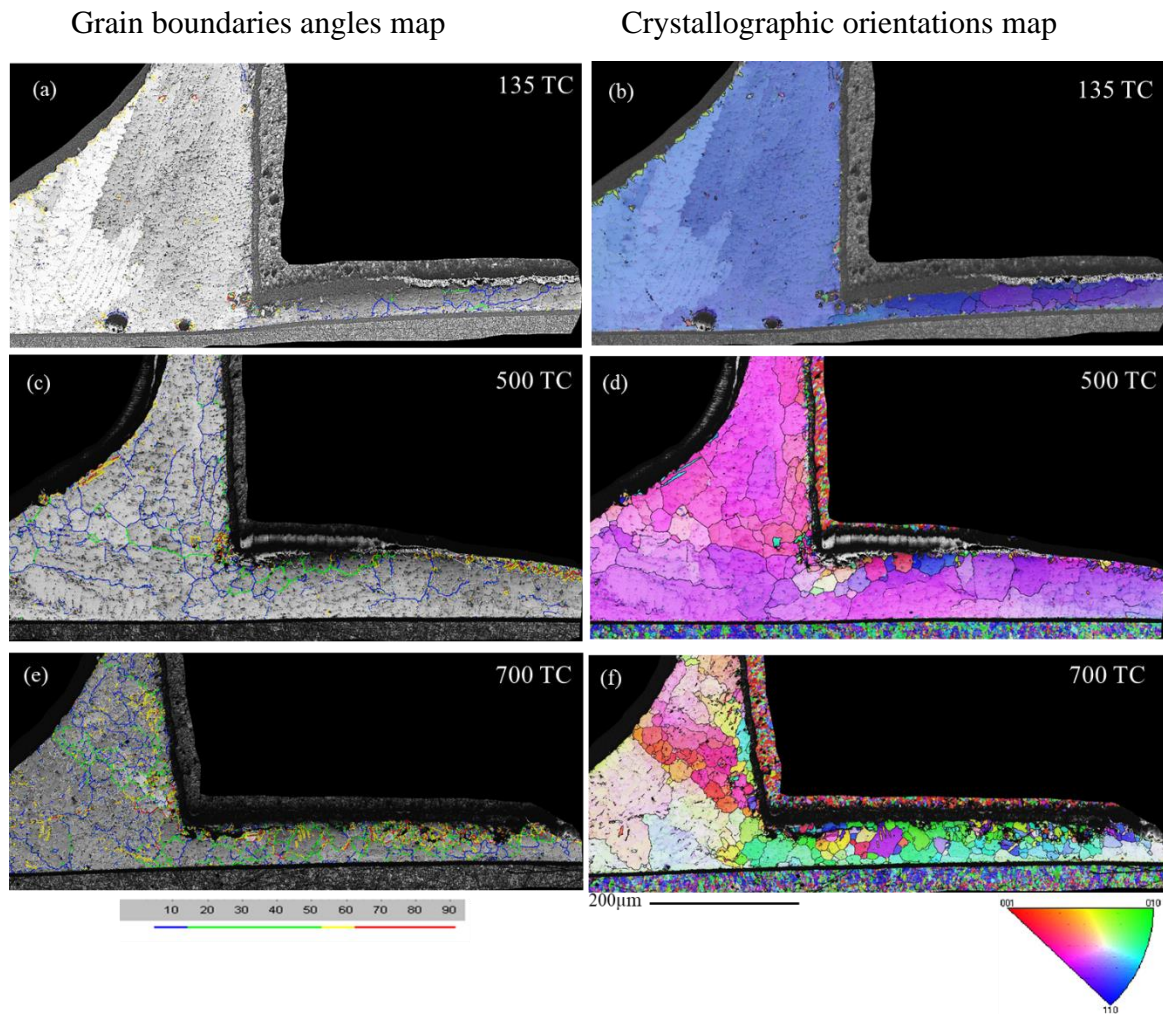


Figure III.3-7: Characterization of R1206 solder joints tin grains evolution during thermal cycling by EBSD analyses (a, b) recovery proces , (c, d, e, f) recrystallization

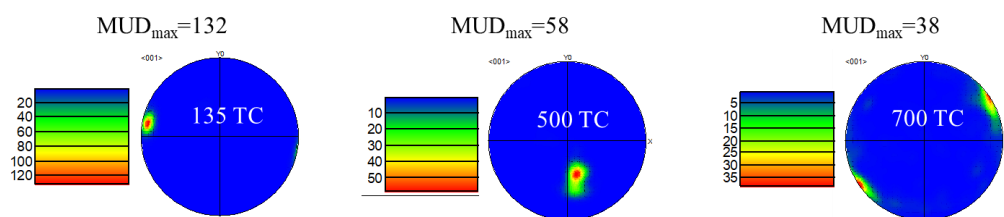


Figure III.3-8: Evolution of the MUD_{max} value in the R1206 solder joints under thermal cycling

The loss of crystallographic texture has been clearly demonstrated by the measuring of the MUD_{max} value during thermal cycling. Figure III.3-8 shows the pole figures associated with solder joint present in Figure III.3-7. It highlights the decrease of the MUD_{max} after 500 cycles ($132 > 58 > 38$). This microstructural evolution developed first in the highly constrained area under the component. Then, the network of the new recrystallized grains spreads across along the component interface or the diagonal of the solder meniscus.

(c) *QFN solder joint*

Until now, works that focus on the description of the failure mechanism of QFN SAC solder joints are rare. They often consider that QFN interconnections present the same behavior as other solder joint geometries [100].

In the QFN geometry, polarized light observations revealed that tin grains evolution started about 700 cycles (Figure III.3–9). The complex microstructure observed on as reflowed QFN solder joints did not allow us the identification of the first steps of tin grain evolution. Even with an accurate EBSD analysis, it was difficult to spot the phenomena of recovery and recrystallization of tin grains on the various samples taken out at low levels of thermal cycling (before 1000 cycles). The presence of low disorientated tin grain ($<15^\circ$) in the as reflowed QFN solder joint compromises the detection of the first steps of the SAC interconnections microstructural evolution based on the appearance low grain boundaries angles during the recovery process of aged components.

Figure III.3–10 presents the results of the EBSD analyzes carried out on three QFN solder joints taken at different number of cycles (135, 500 and 1000 cycles). Grain boundaries with low angles ($<5^\circ$, white lines) were observed on solder taken at 135 cycles. They were located in a high strain region on the component side. This suggests the activation of the recovery process under the thermal cycling effect. During this phase, the rotation of the tin grains is not detected, which means that the tin grains still have the same crystalline orientations than in the initial state (Figure III.3–10 (a) and Figure III.3–10 (b)).

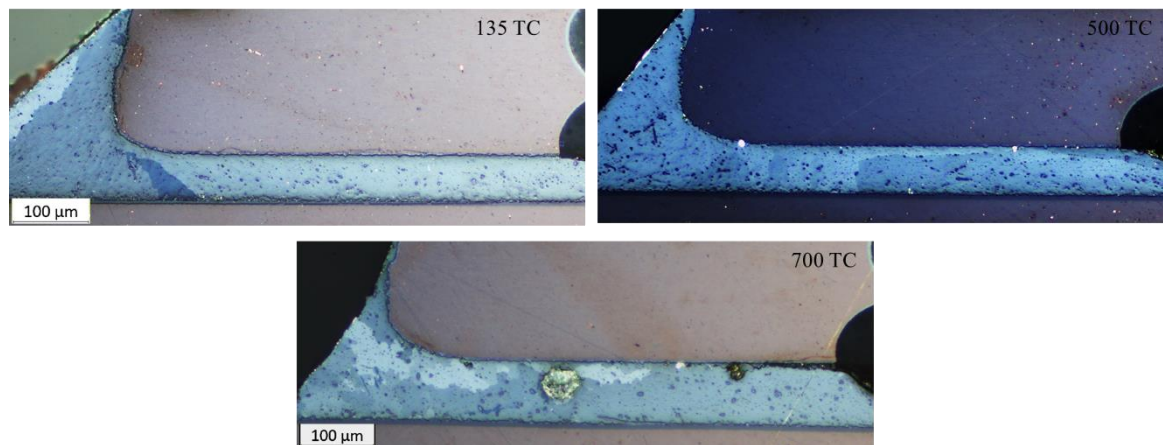


Figure III.3–9: Microscopy optical inspection of QFN solder joints with different number of thermal cycles by Polarized light observation

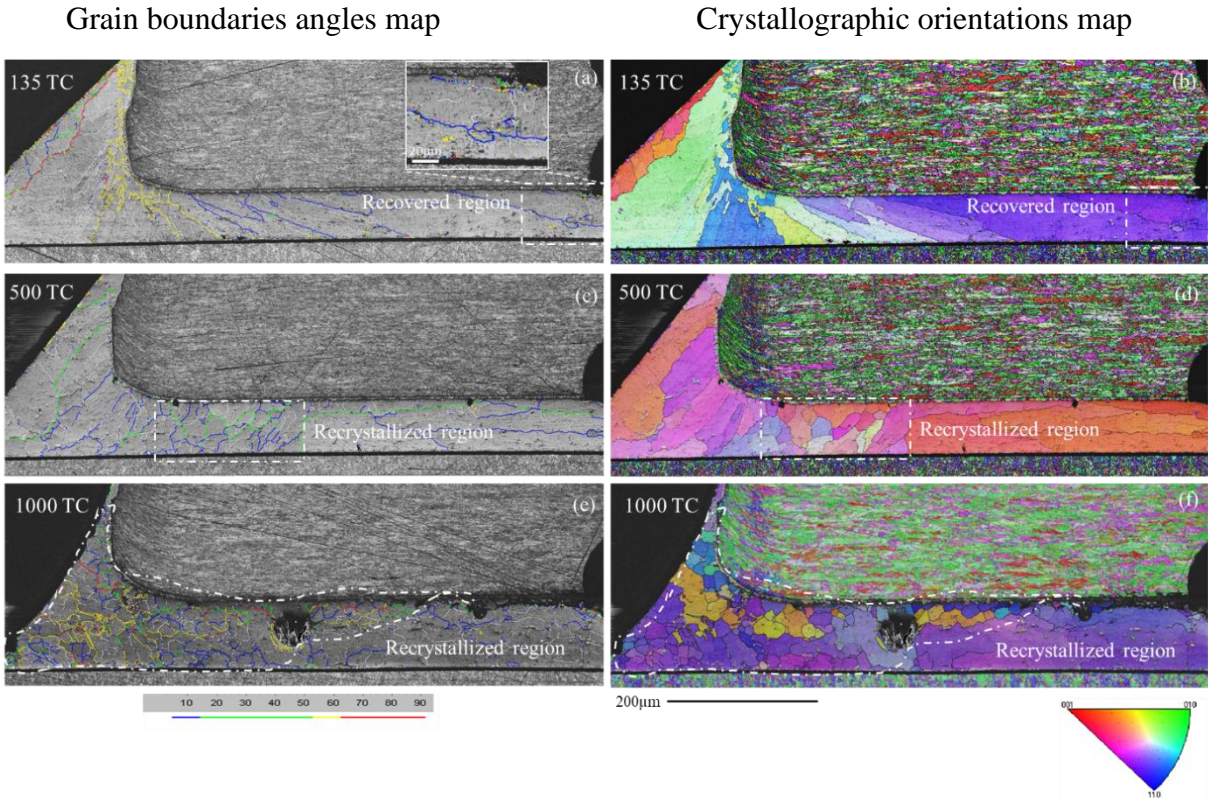


Figure III.3-10: Characterization of R1206 solder joints tin grains evolution during thermal cycling by EBSD analyses, (a, b) recovery process (c, d, e and f) recrystallization phenomenon

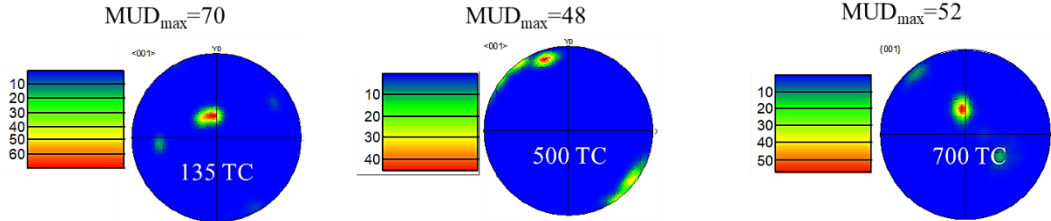


Figure III.3-11: Evolution of the MUDmax value in the QFN solder joints under thermal cycling

Figure III.3-10 (c) and Figure III.3-10 (d) show that tin grain recrystallization process seems to start after 500 cycles with the formation of some high angle boundaries ($[15^\circ; 55^\circ]$, green lines) limiting new tin grains having an orientation little different from the neighboring parent orientation. It is assumed that the slight variations in orientation of the central zone must be induced by recrystallization despite the fact that we can still distinguish the initial microstructure characterized by the unusual "deformed" macro-grain. The polygon (circular) shape of these grains also allows their differentiation from the grains present in the initial state having a more elongated (elliptical) shape

Tin grain recrystallization is more evident in QFN solder joint taken out after 1000 cycles. Figure III.3-10 (e) illustrates that the microstructure is almost entirely traversed by high angle grain boundaries ($>15^\circ$, green and red lines), which highlights an advanced state of recrystallization. The high number of disorientated boundaries was correlated with new

crystallographic orientations (purple, yellow, red and orange) different to the blue parent orientation (Figure III.3–10 (f)). The presence of low disorientated grain boundaries (<15°, white and blue lines) at this state shows that the recovery and recrystallization are operating simultaneously.

The study of the crystallographic texture did not make it possible to highlight the effect of thermal cycling as in the other studied solder joints despite the slight decrease in mudmax observed after 500 cycles. On this type of component, a very particular type of microstructure after reflow was encountered. We have qualified it with a noticeable gradient in crystal orientation and a clear substructure in the form of long slats. This orientation gradient will also affect the values obtained for the max MUD and this lamellar substructuring (slats disoriented around 7 to 8°) will impact the detection of the recrystallized grains (threshold left by default at 5°).

III.3.2 Local recrystallization of tin grains

Another scale of recrystallization attracted our attention during the microstructural analyzes of the different solder geometries during thermal cycles. It is a local recrystallization that is often found around voids or at tin and intermetallic interfaces.

When solder joints have a variation of section or a defect or a void, precipitate harder or less hard than the rest of the material, a concentration of stresses can locally occur. While we think to be in the elastic domain, solder joint enters locally in the plastic domain. It can thus occur a local hardening. This phenomenon is one of the main causes of the creation of cracks in fatigue phenomena.

In the case of precipitates, this phenomena is called the Particle Stimulated Nucleation (PSN) mechanism [101]. During deformation, areas of high density of dislocations and disorientations develop around the second phase particles to accommodate the difference in plastic behavior. This mechanism only occurs for precipitates with a diameter greater than 1µm and results in a random distribution of the recrystallization seeds. This PSN mechanism therefore tends to reduce the sharpness of the texture in the areas where it occurs.

Figure III.3–12 illustrates the local recrystallization observed in BGA solder joints taken out at 1300 and 1500 cycles. A network of high disorientated tin grain with random crystalline orientations was highlighted by EBSD analysis. The new recrystallized grains have a very small size compared to new tin grain appeared during the phenomenon of global recrystallization presented in the previous section.

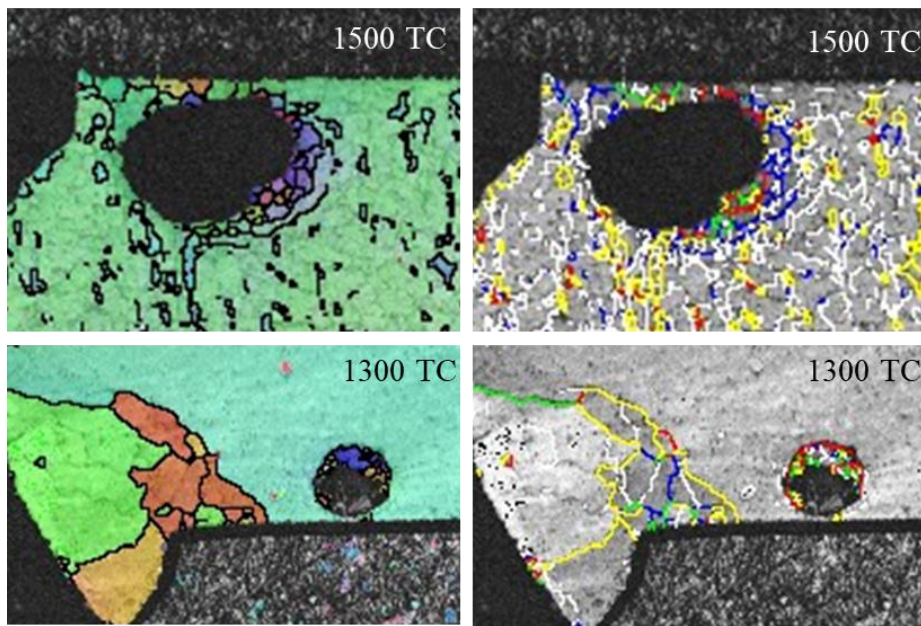


Figure III.3–12: Tin grain local recrystallization revealed by EBSD mapping

III.3.3 Ag₃Sn particles coarsening

Ag₃Sn IMCs coalescence is the other microstructural phenomenon that characterizes the thermomechanical damage. Under cycling, diffusion occurs and Ag₃Sn IMCs in the solder joints coarsen; smaller IMC particle coalesce to produce larger size particles which leads to a loss of dendritic structure and reduces the ability of the particles to block dislocation movements by the pinning effect. This will decrease the precipitation hardening and make the solder softer. Ag₃Sn precipitates will undergo coalescence activated by temperature but above all by the deformations generated during thermal cycling. This phenomenon will therefore be more local than during hot pre-aging and will be located in the high strain region.

The Ag₃Sn particles evolution was highlighted by the observation of solder joints with different level of cycling. EBSD crystal phase analysis coupled to silver mapping with Energy Dispersive X-ray Spectroscopy allowed us to highlight the phenomena of Ag₃Sn coarsening in BGA solder joints (Figure III.3–10). While the microstructure of the solder joint after reflow exhibits an organized distribution of nanoscale Ag₃Sn intermetallics in interdendritic spaces, the damaged regions consist of larger particles less densely dispersed. Some large particles are present in the solder taken after 1000 cycles, which shows the increase in Ag₃Sn IMCs diameter. The coalescence of this particles is all the more important on the sample having undergone 1700 cycles; the high strain regions present larger sizes particles with a clear disappearance of the nano-Ag₃Sn IMCs.

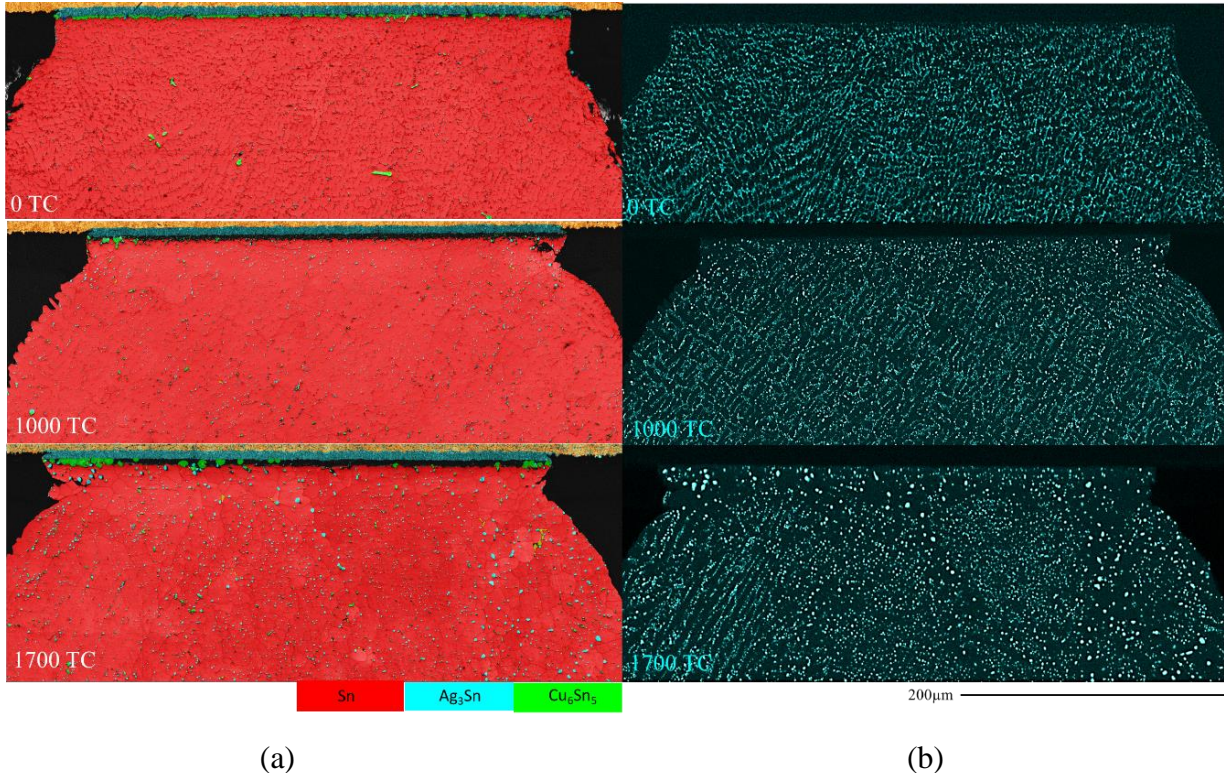


Figure III.3–13: Characterization of Ag₃Sn particles evolution in BGA solder joint during thermal cycling, (a) crystalline phases maps (b) silver EDS maps

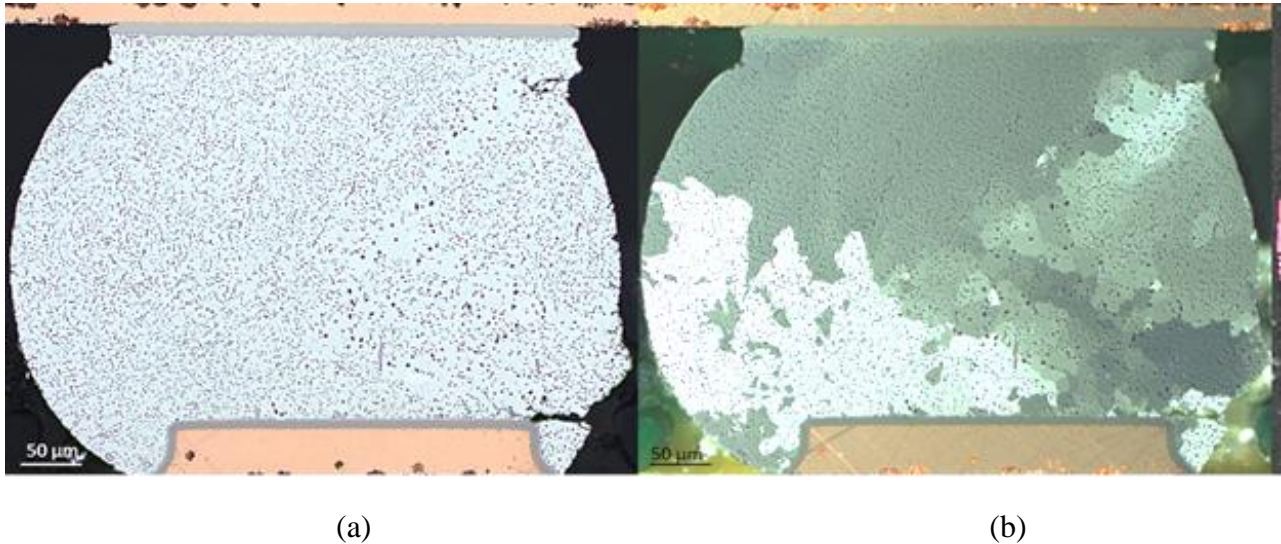


Figure III.3–14: Correlation between Ag₃Sn coarsening and tin grain recrystallization on a BGA solder joint taken out after 1300 cycles (a) white light observation (b) polarized light observation

Under thermal cycling, recrystallization is favored by the appearance of large incoherent precipitates, sufficiently spaced apart, which act as a source of dislocations and locally create very strong distortions of the crystal lattice. The dislocations can indeed move and involve foreign atoms during the recovery. There may therefore be a migration of species with segregation at the grain boundaries. However, the damaged zones are characterized by the

progressive formation of recrystallized grains which are strongly disoriented. This observation therefore suggests that the local coalescence of Ag_3Sn IMCs induced by thermomechanical deformations is controlled by grain boundary diffusion.

However, small precipitates present in the initial microstructure are close together which slow down the recrystallization process. They promote a homogeneous distribution of the dislocations with sub-grains which are not very disoriented with respect to one another. This absence of local disorientation of the crystal lattice can considerably reduce the germination of recrystallization. They are very effective at anchoring sub-joints and can even prevent them from shifting.

The observation of Ag_3Sn particles coalescence is always coupled with the detection of tin grains recrystallization. Larger particles were mainly located at tin grain boundaries. Figure III.3–14 shows the correlation between coarsened region and tin grains recrystallization observed in BGA solder joints taken out after 1300 cycles.

For the chip resistor and QFN solder joints, Ag_3Sn particles coarsening was also observed during cycling. It is also localized in the high strain region on the component side. Figure III.3–15 and Figure III.3–16 illustrate the appearance of larger Ag_3Sn particles with the loss of the dendritic structure characteristic of the as-reflowed state of R1206 and QFN SAC solder joints. Polarized light observation highlights also the recrystallization of tin grains in the coarsened regions.

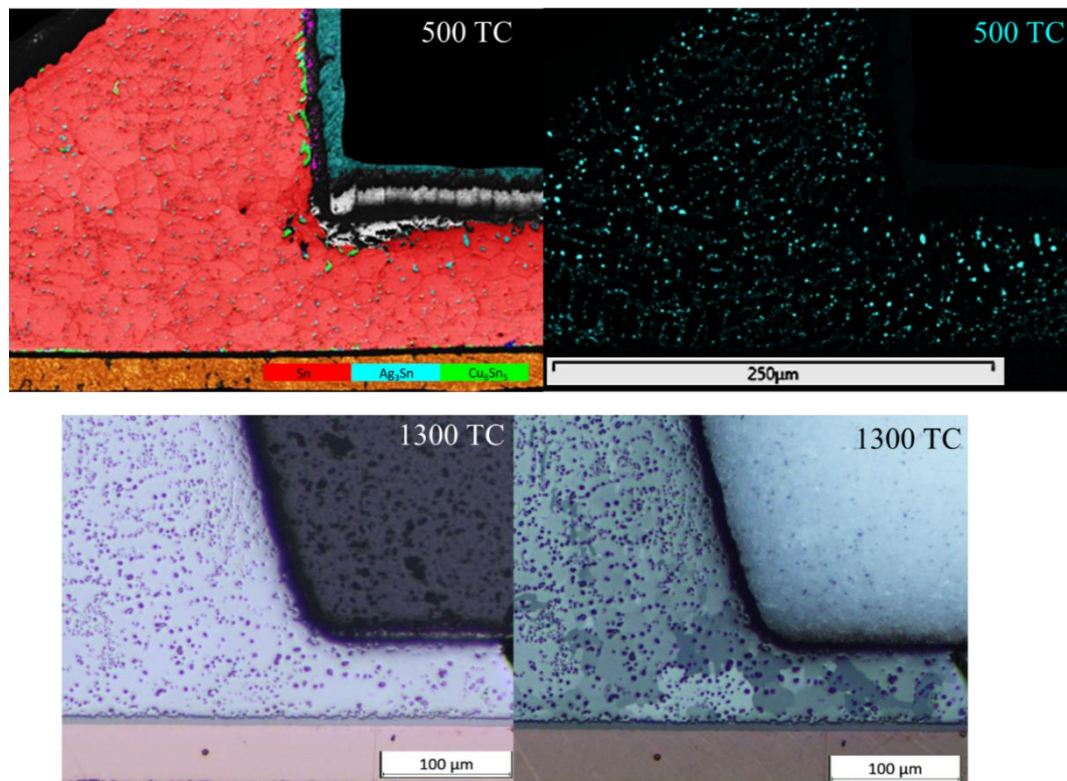


Figure III.3–15: Ag_3Sn particles coarsening in passive component solder joint at 1300 cycles

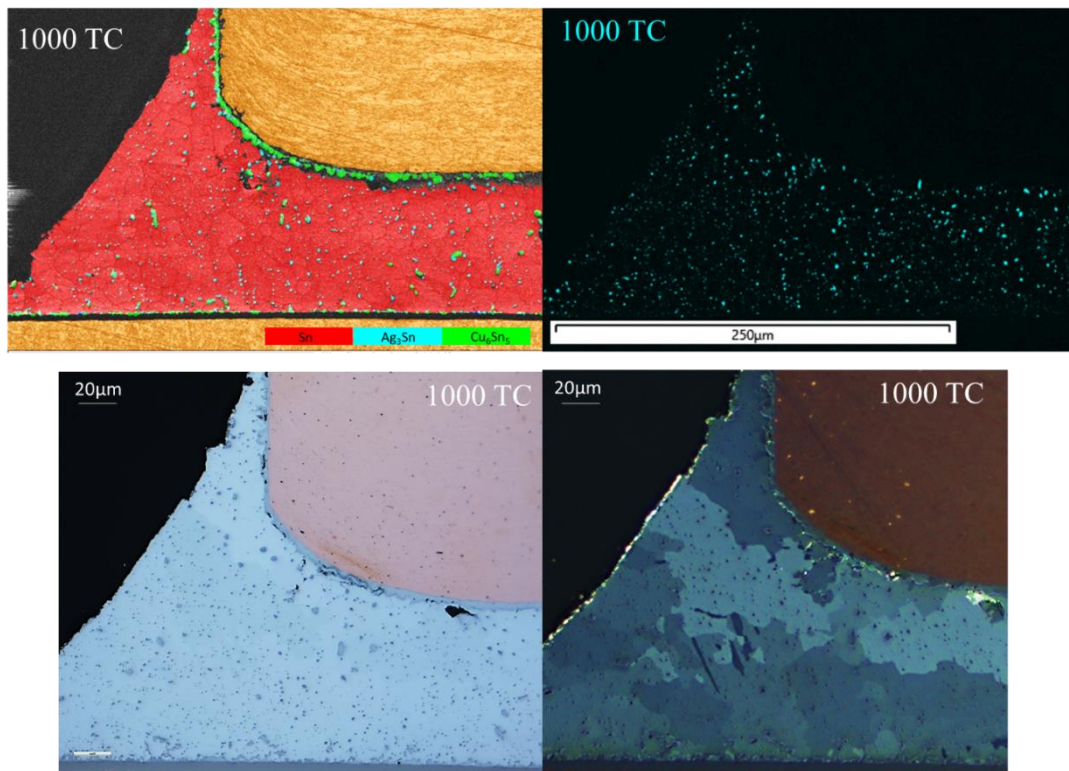


Figure III.3-16: Ag_3Sn coalescence in QFN solder sampled at 1000 cycles

III.3.4 Synthesis

BGA, QFN and R1206 solder joints are characterized by the same microstructural behavior during thermomechanical fatigue. Two consecutive microstructural phenomena occur during the evolution of tin grains under thermal cycling: recovery followed by recrystallization. The recovery process seems to be a prerequisite for the initiation of recrystallization but remains operative along the test. The rearrangement of the dislocations created by the inelastic deformations in fact generates the formation of weakly disoriented sub-grains. This cellular structure then undergoes rotations as thermal cycling progresses, thus leading to the creation of highly disoriented recrystallized grains. The coalescence of Ag_3Sn intermetallics is another phenomenon activated by temperature and deformations. It seems to facilitate the nucleation of the phenomenon of recrystallization. The role of these phenomena on the failure mode of the various studied components is the purpose of the following section.

III.4 Role of tin grain recrystallization and Ag₃Sn intermetallic coalescence in SAC305 solder cracking during thermomechanical fatigue

The formation of cracks in a lead-free solder joint during thermomechanical fatigue is usually reported as consisting of two steps. First, tin grain recrystallization coupled to Ag₃Sn particles coarsening occur in the part with highest strain. Then intergranular cracks will grow in the boundaries between the grains in the recrystallized zone until a complete crack has formed. These steps are well described in different researches [46][52][53][54]. However, crack initiation phase in SAC solder joints are not clearly characterized up to now. The objective of this section is to study the role of recrystallization and Ag₃Sn intermetallic coalescence in SAC305 solder crack development from their nucleation until the formation of total cracks.

III.4.1 Crack initiation

To characterize the crack initiation, observations were carried out on samples with little number of cycles (< 500 cycles). Crack initiation phase seems to appear very early and take a few cycles. For the QFN and chip resistor components, it was already detected on solder joints taken at 135 cycles. Crack initiation was observed in BGA solder joints sampled from 225 cycles.

Crack initiation often occurs in the geometrical singularity of the assembly. The stress concentration generated, either near the BGA solder pads on the component or PCB sides or underneath the QFN and chip resistor components, is the main cause of crack initiation. The presence of relatively large intermetallic particles in these highly stressed areas appears to facilitate also the crack initiation. The very first were observed to start at an interface between tin and its precipitates whatever the solder joint geometry.

EBSD mapping was made to characterize the crack initiation zone. The crystalline phases map shows the presence of (Cu, Ni)₆Sn₅ near the crack initiation site which can cause local brittleness in the solder. Crystallographic orientations and grain boundary maps also revealed that crack initiation was associated with a localized recrystallization of tin. The presence of intermetallic compounds in the high strain region of the solder can generate a stress concentration which can cause a local recrystallization at their interfaces with tin and facilitate the appearance of the first micro cracks.

It is also interesting to note that in some solder joints the crack initiation could take place before recrystallization and as soon as the recovery phase (formation of β-Sn sub-grain boundaries without the rotation of new grains). Figure III.4–2 illustrates the presence of low disorientated tin grain boundaries (<15°) which means that solder joint is in the recovery phase. This result shows that crack initiation probably does not require SAC solder joints global recrystallization.

Role of tin grain recrystallization and Ag₃Sn intermetallic coalescence in SAC305 solder cracking during thermomechanical fatigue

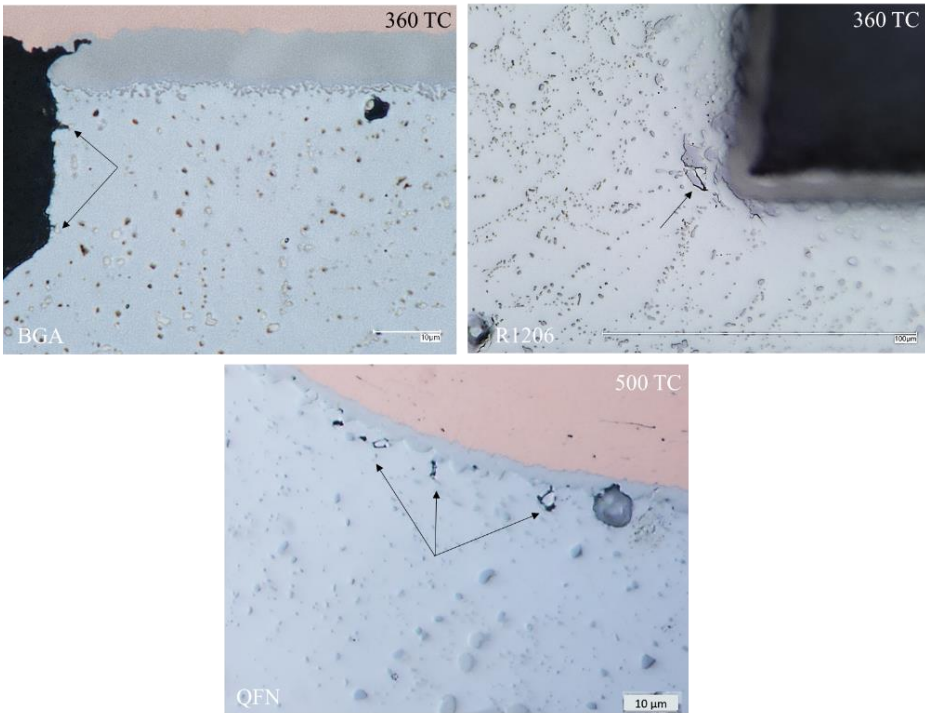


Figure III.4-1: Crack initiation at the interface between tin and (Cu,Ni)₆Sn₅ intermetallics

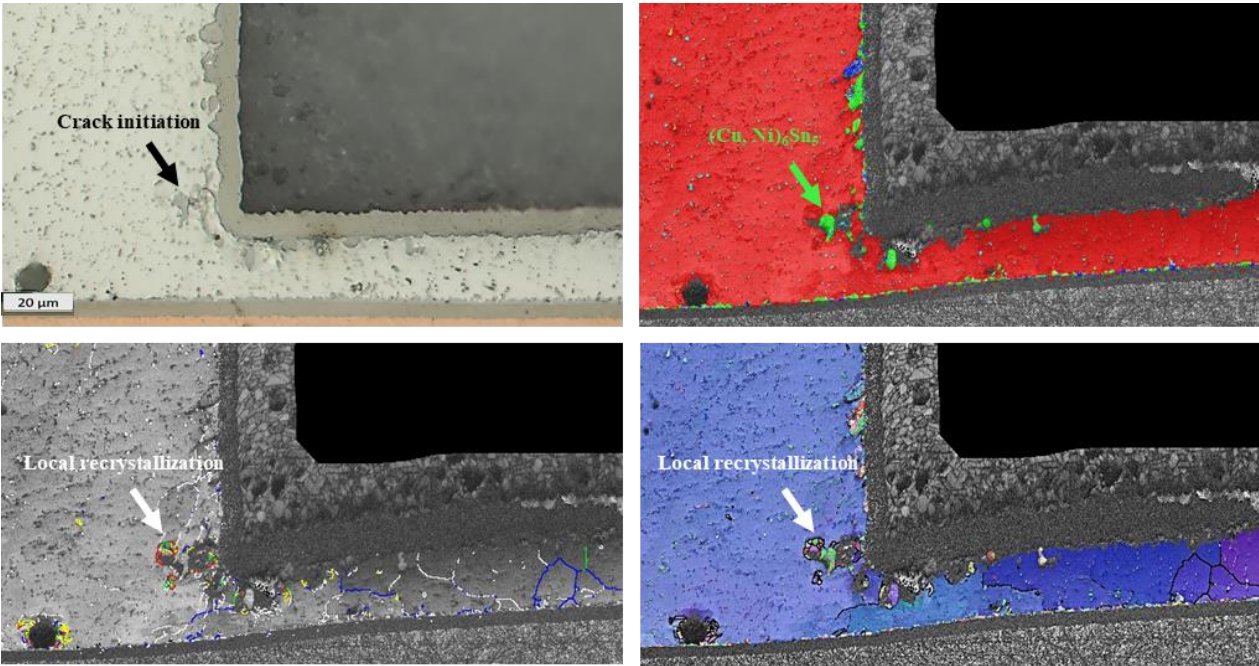


Figure III.4-2: Characterization of crack initiation site observed in chip resistor solder joint taken out at 135 cycles

III.4.2 Crack propagation

Crack propagation characterization was made from sampled boards taken after 500 cycles. The failure analysis revealed the presence of different damage mechanisms under thermal cycling depending on the different interconnections.

The known thermomechanical fatigue mechanism was observed in the BGA and chip resistor solder joints. Optical observations and EBSD analyzes of the crack propagation paths analysis show the intergranular nature of thermomechanical fatigue failures. Cracks often propagate in recrystallized zones (between the highly disoriented tin grain boundaries) with a low density of Ag₃Sn particles. As Ag₃Sn particles coarsening takes place, the dislocation motion is favored. After reflow, finely dispersed Ag₃Sn precipitates can proceed as barriers to the viscoplastic strain-induced dislocations motion and inhibit SAC305 solder degradation by dislocation pinning process. However, with larger spacing between Ag₃Sn IMCs, the dislocations are no longer blocked, the largest particles can constitute good nucleation sites and recrystallization is accelerated. Moreover, Ag₃Sn precipitates tend to move towards high-disoriented grain boundaries as coalescence occurs. This migration weakens the grain boundaries leading to intergranular crack propagation. This failure mode is induced by a sliding mechanism at the grain boundaries due to the shear stresses generated during the cycles.

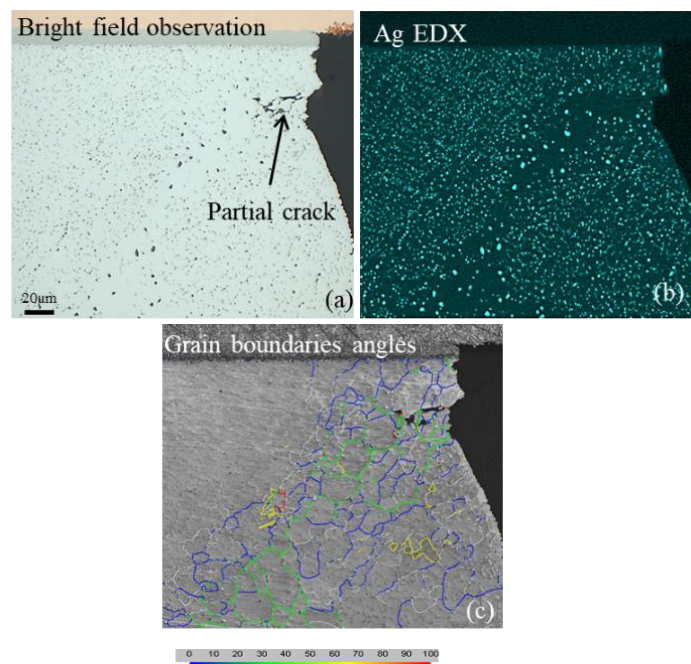


Figure III.4–3: Favorable intergranular crack path in BGA solder joint after 1300 cycles, (a, b) Ag₃Sn coarsening and migration, (c) network of highly misorientated recrystallized β-Sn grains

Analysis of BGA components show that fatigue cracks start to propagate on solder joint taken out after 1000 cycles. Several crack propagation paths have been observed and seem to be in competition:

- “Horizontal” propagation, between the two top corners or the two bottom corners (Figure III.4–4 (a)),

- “Diagonal” propagation, between two opposite corners (Figure III.4–4 (b)),

Some joints have two horizontal cracks at the same time and diagonal cracking has mainly been observed in the corner joints. Crack propagation follows the recrystallized areas but seems to do not need a total recrystallization of the highest strain region. Figure III.4–4 (c) illustrates the presence of partial crack in locally recrystallized region. This assumes that crack propagation and tin grain recrystallization operate at the same time.

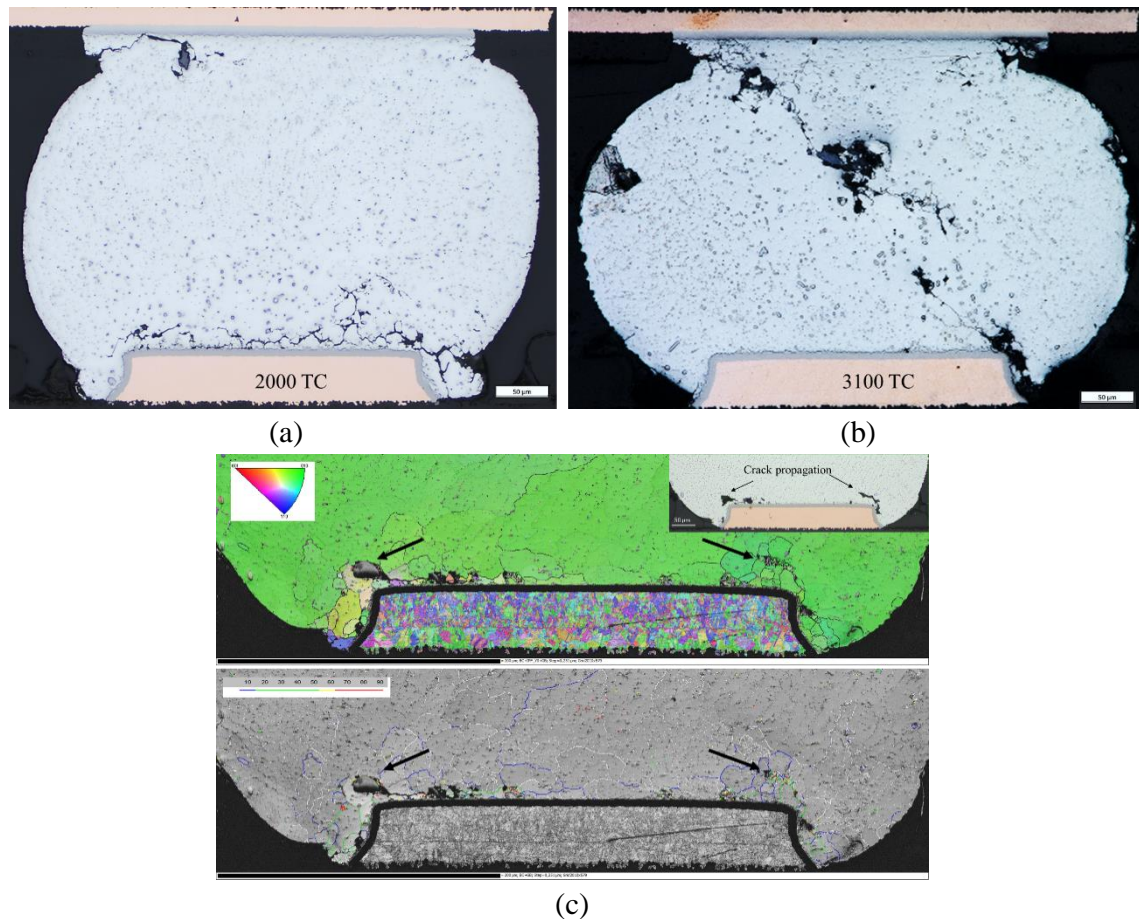


Figure III.4–4: Intergranular crack propagation in BGA solder joint (a) horizontal propagation (b) diagonal propagation, (c) partial cracks in locally recrystallized areas

In the chip resistor solder joints, intergranular crack propagation was observed along the component edge on samples have been cycled for more than 500 times. The crack is initiated under the component where the inelastic deformations generated during the thermal cycles are the most important, then propagates in the part of the solder going up on the side of the R1206 components following two preferred directions: along the component (Figure III.4–5 (a)) or through the solder according to the diagonal (Figure III.4–5 (b)). The presence of defects like the voids in high strain region can facilitate the recrystallization in these zones and reduces the distance traveled by the crack. Consequently, the cracking path will pass in a privileged way through this defect

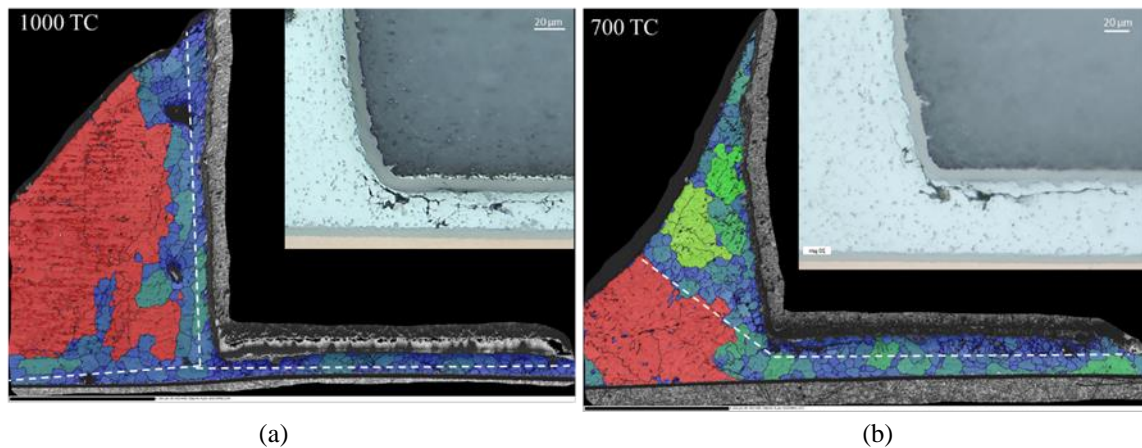


Figure III.4–5: Recrystallized tin grains (blue) and favorable intergranular crack paths in chip resistor solder joints (a) along the component and through a voids, (b) according to the diagonal

It is also interesting to note that a high proportion of small β -Sn grains was observed along the intergranular crack path. These grains can result from a local recrystallization process due to the high stress concentration at the crack tip during propagation; temperature and viscoplastic deformations are always present, allowing a recrystallization on a local scale at the crack tip. We can say that it is a phenomenon of recrystallization of grains already recrystallized before crack propagation. This shows that crack propagation occurs at the same time with a local recrystallization at the crack tip. The same process repeats itself until total crack.

Characterization of cracks development highlights that intergranular crack propagation take an important number of thermal cycles to start after the crack initiation observation. The fact that propagation of cracks was not observed earlier hypothesizes that it requires a well-defined microstructural damage criterion [102]. Tin recrystallization degree and Ag₃Sn density seem to be the two factors allowing the identification of common microstructural damage criterion in different geometries of SAC solder joints. A more complete study of these two parameters will be presented in the following chapter.

However, the failure analysis of QFN interconnections revealed the presence of other damage mechanisms under thermal cycling. A competition between the usual thermal fatigue mechanism and interfacial cracking mechanism was observed in the QFN solder joint. It is a mixture of different failure modes with brittle interfacial cracks between IMC and solder bulk and ductile intergranular cracks along the high disorientated grain boundaries (Figure III.4–6 (a)). Figure III.4–6 (b) shows that failure appear to initiate by the development of interfacial crack underneath the component then they propagate towards the intergranular crack. Recrystallization and Ag₃Sn coarsening were often observed as essential for the intergranular crack mode. However, they do not appear to be a fundamental for the interfacial failure mode (Figure III.4–6 (b)). This mixed mode is usually due to shear stress that generates considerably higher solder bulk plastic deformation compared to the tensile stress located at the interface IMC-solder bulk [103].

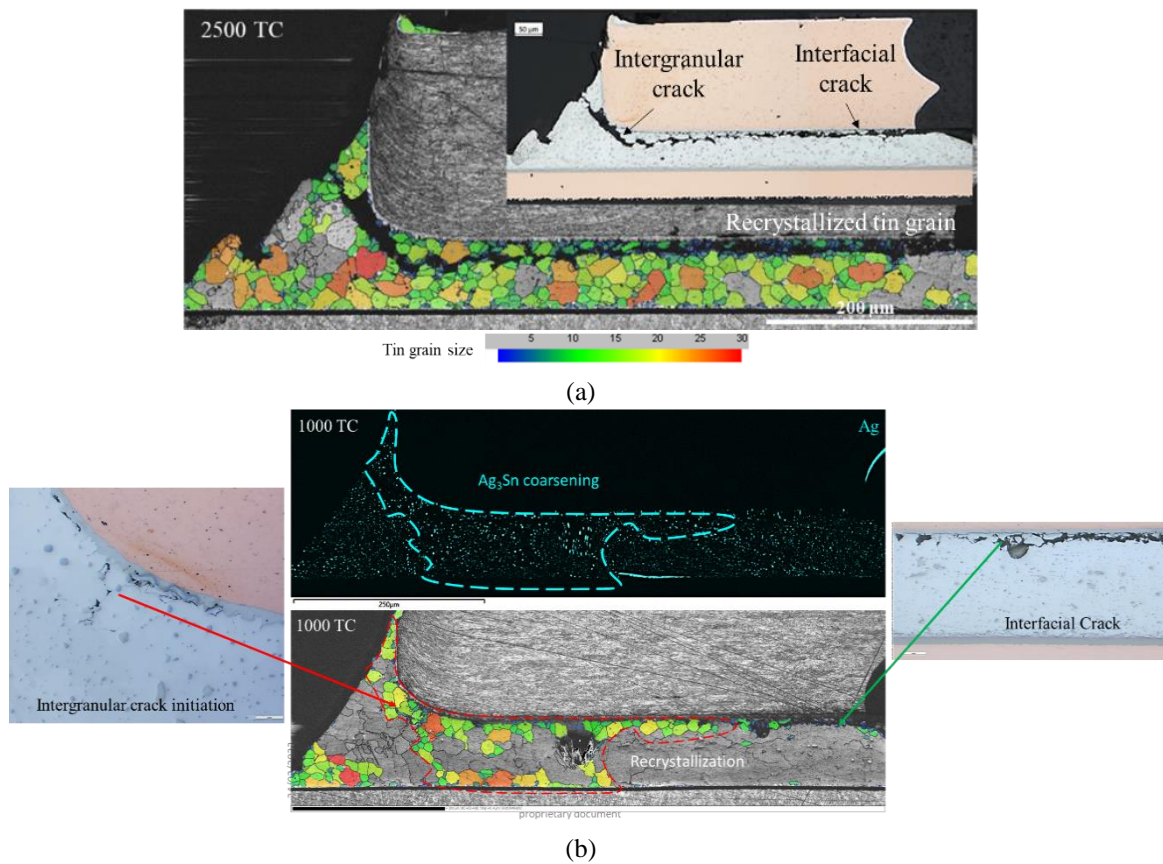


Figure III.4-6: Correlation between the mixed failure mode observed on QFN solder joints, tin grain recrystallization and Ag₃Sn coarsening

A total interfacial cracks were also observed in the QFN solder joint. Micro interfacial cracks were seen to initiate at the interface between solder and intermetallic layers on the component side then they develop during the cycling into a macro cracks along the solder. Therefore, the region around IMC solder interfaces becomes excessively brittle and fails rapidly. Figure III.4-7 shows the interfacial crack mode observed in QFN solder joint taken out at 1500 cycles. EBSD analysis of this solder shows the absence of tin grain recrystallization along the crack path. This validates once again that the recrystallization process is not the responsible phenomenon leading to crack propagation. This failure mechanism often happens when the solder is subjected to tensile loading [103].

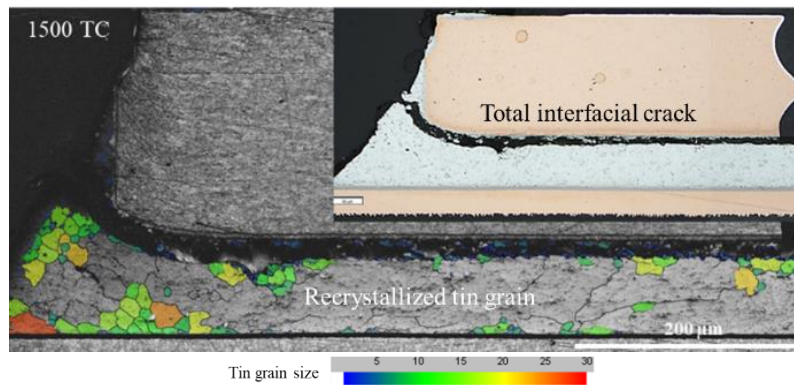


Figure III.4–7: Correlation between the interfacial failure mode observed on QFN solder joints and tin grain recrystallization detected by EBSD maps

Hence, failures in solder due to cyclic shear loading are a mixture of ductile-brittle mode with a higher percentage of bulk ductile damage and more important fatigue lifetime than interconnections subjected to tensile stress and having brittle failures behavior. FE analysis could be a way to highlight the competition between tensile and shear stresses in QFN solder joints. Accurate thermomechanical properties of the package materials are also needed.

III.4.3 Synthesis

The role of the microstructural evolution on the SAC solder joints cracking under thermal cycling is defined in this section. Observations show that crack initiation can appear before the onset of the microstructural evolution. This means that crack initiation does not require a change in the SAC alloy microstructure. This result has not been revealed in the literature until now

On the other hand, the study of the crack propagation of the different studied solder joints geometries highlights the presence of two failure mechanisms.

Tin grain recrystallization and Ag₃Sn particle coarsening are the two microstructural phenomena preparing a favorable cracking path in the first mechanism. Fatigue cracks in this case propagate by a sliding mechanism at the grain boundaries. The failure mode observed is thus intergranular crack which agree with the literature. Another finding, it is that crack propagation and tin grain recrystallisation operate at the same time and crack propagation do not need a total recrystallization of the high strain region. Previous work indicates that crack propagation first requires full crystallization of the crack path [15][53].

The second mechanism does not need microstructural evolution to occur. Micro cracks appear at the interface between solder bulk and intermetallic layers and make this region brittle. Then, they propagate under thermal cycles into a total crack along the solder. This failure mode present an interfacial brittle crack. A competition between these two failure mechanisms may be the cause of appearance of a mixed failure mode. This mechanism was observed only on the QFN solder joints. It should be noted that until now the detailed description of the failure mechanism of QFN solder joints has not been revealed in previous studies.

III.5 Conclusion

This chapter has made it possible to characterize the as-reflowed microstructure of SAC305 interconnections and its evolutions under thermomechanical loading. The main objective was to well describe SAC solder failure mechanism and to identify the microstructural changes responsible for cracking under thermal cycles.

The tin grain structure in lead-free solder joints to as-assembled BGA, QFN and chip resistor components may vary a lot and is affected by a large number of parameters. Tin grain structure distribution study highlights the significant presence of the macro-grained morphology (90% in some cases). The undercooling condition during solidification is critical for the grain structure in solder joints. The interconnections' geometry appears to affect tin grain morphology. An unexpected distort macro grain structure was observed in QFN solder joints.

The chronology of the accelerated thermal tests corresponds to a successive sampling of the test towards the microstructure evolution of the various SAC305 considered solder joints. In the considered temperature range, the SAC305 alloy mainly made up of tin is indeed likely to undergo a recovery process followed by recrystallization. These phenomena were also accompanied by various microstructural changes having an impact on the thermomechanical damage of SAC305 solder joints. The Ag₃Sn intermetallics will first grow and allow the movement of the dislocations in the zones of high deformations. The formation of low disoriented sub-grains will then evolve towards a network of recrystallized β -Sn grains exhibiting strong crystalline disorientations at the grain boundaries. Thus, the main failure mode observed is intergranular cracking by a sliding mechanism at the grain boundaries. Thus, the first failure mechanism observed in SAC305 interconnections is characterized by the propagation of cracks by a sliding mechanism at the grain boundaries. This intergranular failure mode was marked in the BGA and chip resistor solder joints.

Observations highlight also that crack initiation occurs at the interface IMCs and tin during the recovery process. The presence of large (Cu, Ni)₆Sn₅ and Ag₃Sn particles in the highest strain region can cause local brittleness in the solder which causes fatigue crack initiation. This phase takes a few hundred cycles before cracks begin to propagate. This assumes that a well-defined recrystallization degree coupled with a threshold Ag₃Sn particles density value is required to provide favorable intergranular propagation path. The evolution of tin grain recrystallization degree and Ag₃Sn particles density under thermal cycles will be presented in the next chapter in order to define a SAC305 interconnections common microstructural damage criterion.

The failure analyzes showed the appearance of another failure mechanism on QFN solder joints under thermomechanical fatigue loading. Cracks often occur at the interfaces between the solder bulk and the intermetallic layers and do not require microstructural evolution. It is an interfacial failure mode with brittle nature that often happens when the solder joint is subjected to tensile loading.

A mixture of the intergranular crack and the interfacial crack was also observed in the QFN solder joint. This mixed mode seems to be more damaging than the interfacial mode due to shear stress that generates considerably higher solder bulk plastic deformation compared to the tensile stress located at the interface IMC-solder bulk.

This findings show that QFN interconnections have a different behavior compared to lead-free solder joints in other components (BGA, chip resistor) during thermomechanical fatigue. This difference may be due to the package geometry or its material properties (aspect ratio, copper lead-frame and epoxy molding compound). As the initial microstructure is expected to have an effect on the thermomechanical behavior of lead-free solder joint due to tin anisotropy, the unusual complex as-reflowed microstructure encountered in QFN solder joints can also have an impact on their behavior and may cause a different response compared with other type of assemblies.

These different characterizations constitute the basis of the work developed in the rest of this manuscript. The next chapter will treat more in detail the effect of SAC305 solder joints geometries on the reliability of lead-free assemblies under thermomechanical fatigue. The solder joints lifetimes' data and the evolution of different microstructural parameters (recrystallization degree, Ag₃Sn particles density, crack length) will be investigated to determine a common microstructural damage criterion promoting the crack development.

Chapter IV. Identification of SAC alloy microstructural damage criterion

IV.1 Introduction

The degradation of mechanical properties of SAC solder alloys are the result of the microstructural evolution during thermomechanical testing. The most well-known and widely observed changes are the tin grain recrystallization and coarsening of the Ag_3Sn intermetallic compounds (IMCs) present in the eutectic regions between β -Sn dendrites. In most of the prior investigations, microstructural changes during aging have been investigated by comparing the micrographic sections of interconnections subject to different numbers of thermal cycles. In the current work, quantitative analyses will be presented to characterize the dynamic of the tin grain recrystallization and Ag_3Sn particles coarsening.

This chapter combines in-situ monitoring, failure analysis and microstructural investigation in order to understand the link between the lead-free solder fatigue lifetime and the failure mechanism during thermal cycling. The fine EBSD analysis of the solder joints after a relatively low number of thermal cycles allows the search for degradation indicators in three different SAC solder geometries and the identification of the microstructural state promoting the crack propagation. The considered components in this study are the BGA, QFN and the R1206 packages assembled on the FELINE boards having undergone pre-aging for 500h at 100°C followed by thermal cycles between -55 and 125°C . This approach aims to identify a common microstructural damage criterion for SAC solder joints that governs failure by intergranular cracking.

The first part focuses on the definition of the parameters developed along this chapter and used to assess the SAC solder joints behavior during thermomechanical loading. The measured lifetimes, the crack ratio, the size of the recrystallized grains and the degree of recrystallization, the equivalent diameter of the Ag_3Sn intermetallic particles and their density are the considered parameters to define microstructural damage criterion representative of SAC solder joints thermomechanical fatigue.

A new approach, based on the microstructural characteristics of the SAC alloy, will be then presented to assess the thermomechanical reliability of lead-free electronic assemblies. The correlation between the lifetime's data and the crack evolution measurements will be first useful to identify the most important phase in the life service of the SAC solder joints. The evolution of each microstructural parameter under thermomechanical testing will be then studied to identify the microstructural state of this phase. The comparison of the behavior of the three solder geometries (BGA, R1206 and QFN) will be finally established to define common microstructural degradation indicators allowing the prediction of the performance loss of SAC305 solder joints in thermal cycling.

IV.2 General approach for assessing the reliability of solder joints

This part aims to define the different indicators allowing the quantitative evaluation of the state of the SAC solder joints microstructural damage. Measurements were carried out on samples removed from the oven at different times of the thermal cycle. The components considered are therefore representative of different levels of damage. The measurement process will be described in detail in order to make the direct link between the measured microstructural damage criterion and the SAC solder thermomechanical reliability.

IV.2.1 SAC solder joints lifetimes

During thermal cycling, solder joints cracking is characterized by an increase in electrical resistance of the daisy-chains due to the progressive opening of the circuit. The failure criterion chosen for this study is based on the IPC-9701A standard describing failure as a 20% increase in the initial electrical resistance of each daisy chain for five consecutive measurements.

The criterion is applicable to the QFN and BGA components daisy-chains in which the solder joints are in series (Figure IV.2–1 (a)). For the R1206 components, considering that the electrical monitoring was done by group of four components mounted in parallel, an offset of the resistance base line is expected at each electrical opening (Figure IV.2–1(b)).

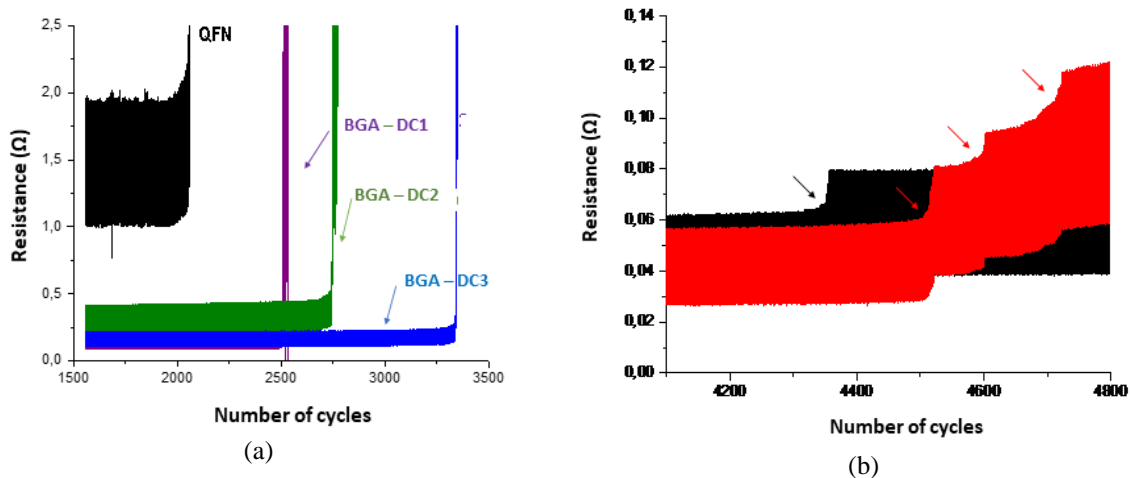


Figure IV.2–1: Resistance monitoring and failure detection in daisy-chains, BGA, QFN (a), chip resistors (b)

Electrical continuity measurement results were then analyzed to obtain the lifetime of each package assembled on the test boards. This set of lifetimes is then used to get the number of cycles to failure for a 63.2% failure rate.

A 2-parameter Weibull distribution is thus used to model the number of cycles to failure:

$$F(t) = 1 - e^{-\left(\frac{t}{\eta}\right)^\beta} \quad (\text{IV.2-1})$$

where $F(t)$ is the cumulative failure distribution function or failure rate, η the characteristic life (number of cycles to failure for 63.2% of failed specimens) and β the shape parameter.

However, a 3-parameter Weibull distribution can be also used to model the number of cycles to failure. Indeed, a 3-parameter distribution presents a better correlation than with a 2-parameter in some cases [97], thanks to the Anderson-Darling statistics (A^2 parameter named AD on the Weibull plots).

$$F(t) = 1 - e^{-\left(\frac{t-\gamma}{\eta}\right)^\beta} \quad (\text{IV.2-2})$$

where $F(t)$ is the cumulative distribution function, γ is the location parameter or “failure-free life”, η and β are the scale and shape parameters respectively. The addition of γ and η gives the number of cycles to failure for 63.2% of failed specimens, which is equivalent to the characteristic life in a 2-parameter distribution.

Minitab software was used to plot the different Weibull distributions and determine the different parameters.

IV.2.2 Measurements of crack propagation

In order to correlate between the crack development and the failure detection results, crack ratio (I_{crack}) was defined by the formula below (IV.2-3). It was also used as a criterion for the definition of microstructural damage indicators by making the link with the kinetics of the evolution of the microstructure of the solder joints of the different studied components.

Each length measurement was repeated 3 times with an uncertainty not exceeding 1%. The length of the crack is measured as a line from the starting point to the tip of the crack.

For the total length of the crack, the lengths of the measured crack segments are added. Individual small crack length (C_i) along the crack path shall be summed and contribute to the total length of the crack. If the crack has any contact with a void present in the solder joint, then the complete diameter, D_i , of the void contributes to the crack length.

The total length (100%) of the solder joint, defines the reference length used to calculate the crack ratio I_{crack} . It was defined as the visible crack length and the shortest remaining distance to the nearest solder joint surface (L_i).

$$I_{crack} = \frac{\sum C_i + \sum D_i}{\sum C_i + \sum D_i + \sum L_i} \quad (\text{IV.2-4})$$

In case of several crack paths, the most critical (longest) crack (%) is taken into account according to the following rule:

The most critical crack path = the shortest remaining length

Figure IV.2–2 shows an example of a BGA solder joint observed after 2300 cycles with two different crack paths. The first path present the shortest remaining length ($(L_1+L_2)_{path 1} < L_2_{path 2}$). In this case, we take into account the crack ratio of path 1.

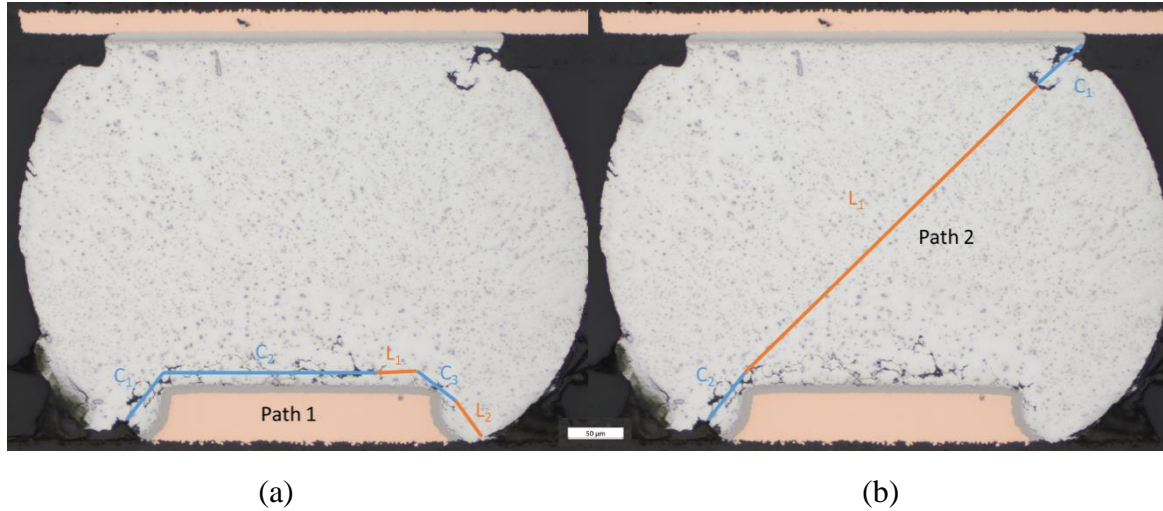


Figure IV.2-2: BGA solder joint with two crack paths (a) crack propagation near the PCB side (path1), (b) crack propagation along the diagonal (path 2)

The evolution of the average crack ratio is finally plotted as function of the cycle's number. The average crack ratio represents the average of the crack ratios of solder joints sampled at the same level of cycling.

$$\text{Average crack ratio}_k = \frac{\sum_i^{N_k} I_{\text{crack},i,k}}{N_k} \quad (\text{IV.2-5})$$

k is the sample withdrawing date and N_k is the samples total number for each withdrawing

IV.2.3 Definition of microstructural damage indicators

The results of the previous chapter show that SAC solder joints cracking needs a favorable microstructural state to trigger its propagation. Tin grains recrystallization and Ag_3Sn precipitates coalescence are probably the two microstructural processes allowing the identification of SAC alloy microstructural damage criterion.

EBSD analyzes make it possible to quantify SAC interconnections failure mechanism by following the evolution of Ag_3Sn particles and tin grains during thermal cycling. The data from the EBSD analyzes are provided under either a set of maps of different types (crystalline phase, crystalline orientation, tin grain size, etc.) or an excel table in which all the grains of all the phases detected are indexed as well as their parameters (area, equivalent diameter, coordinates, Euler angles, etc.). A Scilab program was developed in order to post-process the raw data from the excel files and to extract the indicators which characterize the Ag_3Sn particles coarsening and the tin grains recrystallization.

For recrystallization, the first step is to identify the recrystallized grain size and measure its evolution during the thermal cycling. The recrystallized grain size was calculated with the same approach used in the previous chapter by calculating the diameter of its equivalent circle.

Then, the program calculates the surface occupied by the recrystallized grains in order to trace the evolution of the recrystallization degree. Along this work, the recrystallization degree ($D_{Recrystallization}$) was defined as follows:

$$D_{Recrystallization} = \frac{A_{recrystallized\ region}}{A_{solder}} \quad (IV.2-6)$$

The recrystallized area of an interconnect joint is defined as the cumulative areas of all recrystallized grains.

$$A_{recrystallized\ region} = \sum A_{recrystallized\ grain} \quad (IV.2-7)$$

A graph showing the evolution of recrystallization degree during cycling is finally drawn based on all analyzes carried out on samples removed from the climatic chamber at different times of the thermal cycle.

The same approach was applied to highlight the dynamics of the Ag_3Sn particles coalescence. We started by characterizing the evolution of Ag_3Sn precipitates size. However, the smallest detected intermetallics had a diameter of the order of a tenth of a micron against ten microns for the largest. Therefore, the study of the Ag_3Sn IMCs has been established on the particles density rather than their surface percentage. The density of Ag_3Sn precipitates is then plotted as a function of their size and the cycling. It is presented as:

$$D_{Ag_3Sn\ particles} = \frac{Ag_3Sn\ particles\ number}{Solder_{area}} \quad (IV.2-8)$$

EBSD analyzes were carried out at different magnifications depending on the region studied and the geometry of the solder joints. At a low magnification, the results may lack precision for very fine particles like Ag_3Sn IMCs and consequently some data are not usable. In this case, the EBSD analyzes were post-processed manually on ImageJ software from only tin grain size maps in order to measure the solder area and the recrystallized area (Figure IV.2–3). Then the equation (IV.2-8) is used to determine semi-quantitatively the recrystallization degree of SAC solder joints using. The comparison of the results from the calculations made by ImageJ with those of the Scilab code shows that the measurement uncertainty is 1%.

The main goal of low magnification analyzes is to collect as much information as possible and compare the microstructural evolution in the various neighboring joints. This allows us either to identify the location of the first failure or to study the different effects affecting SAC solder joint behavior (neighboring interconnection joints, the morphology of the tin grains and of their crystal orientations).

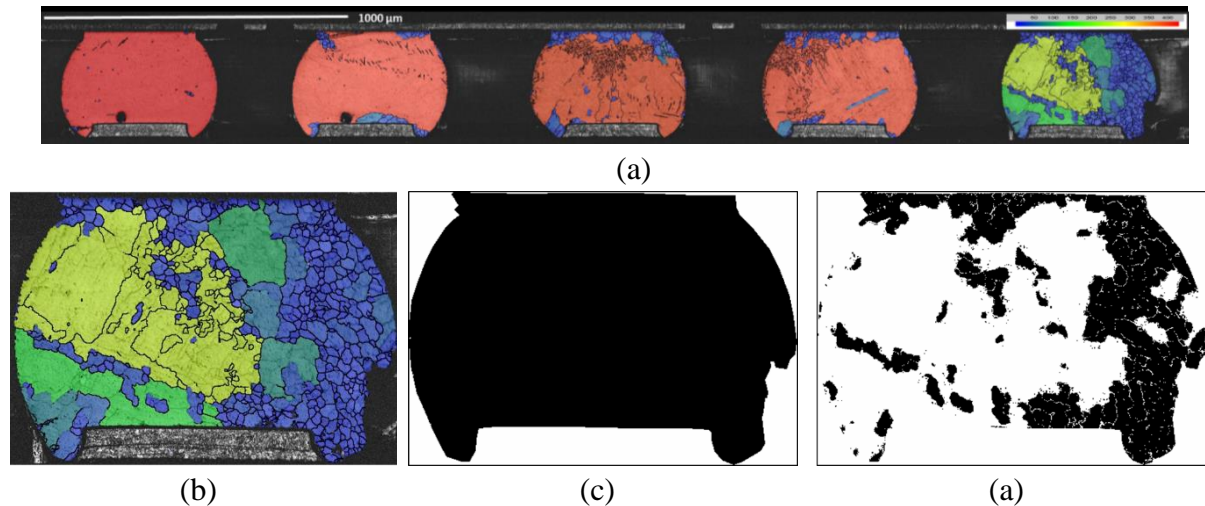


Figure IV.2-3: Identification of recrystallized degree by ImageJ software , (a) EBSD analysis of multiple BGA solder joints with low magnification, (b) Choice of solder to be analyzed, (c) Solder area (d) Recrystallized area

IV.2.4 Synthesis

This section aimed at defining all parameters that will be afterwards used to define the microstructural damage criterion allowing the evolution of the reliability of SAC solder joints under thermomechanical fatigue. All the measurement steps have been well described in this section. The definition of the damage criterion will be based on the measurement of the service life of the solder joints by electrical monitoring, the study of the crack development phases and the analysis of the evolution of the microstructural indicators. The correlation between these different considered parameters will allow first to evaluate the method of detection of electrical failure set by the standards in relation to the dates of appearance of the cracks, then to identify the microstructural state favorable to the crack propagation phase.

The following section will represent the results of the analysis of the lifetimes of the three components studied.

IV.3 Lifetimes analysis results

The purpose of this part is to be able to collect the maximum of data allowing the comparison with the results of the failure analysis and the microstructural study considering that the measurement of lifetimes by electrical monitoring is the method recommended by the standards to evaluate the durability of solder joints subjected to thermomechanical loads.

QFN, BGA and R1206 components were electrically monitored for a thermomechanical fatigue life analysis of SAC solder joints. These packages present different material properties, geometries and locations solder which allow covering a wide range of durability (Figure IV.3–1). Results validate that the different studied types of solder joint presents different characteristic lifetime [104]. Table IV.3–1 summarizes all the data from electrical monitoring results and considered during this study (Number of cycles of the first and the last detect failures, the Weibull parameters). The Weibull plots of the three studied components are shown in Figure IV.3–2 [104].

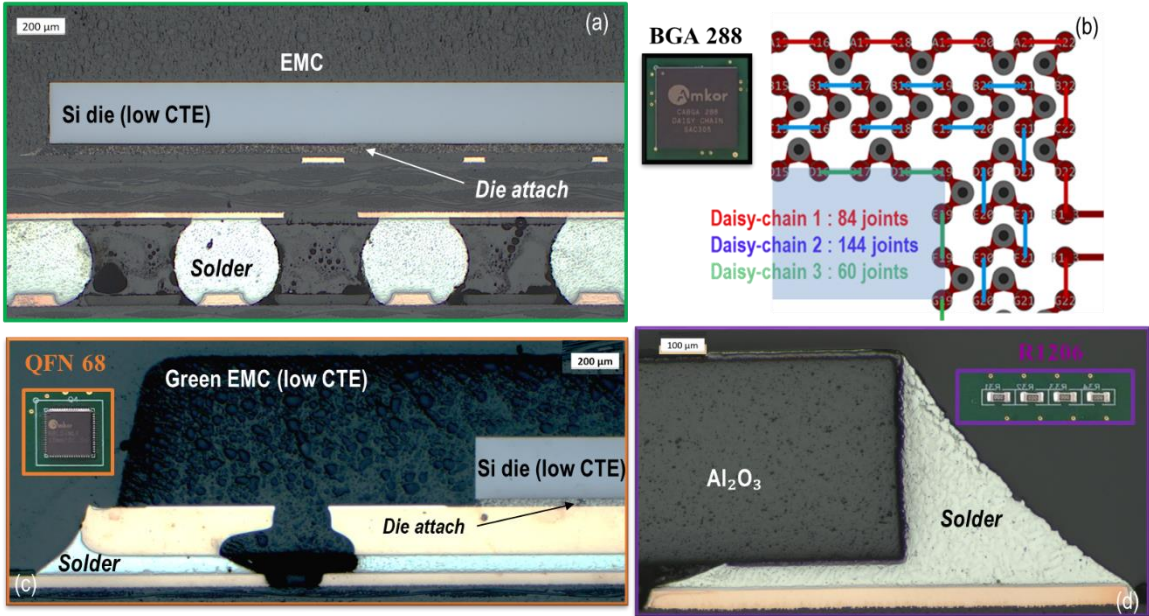


Figure IV.3–1: Characterization of the different studied components after the reflow process (a) Microsection on the BGA under the die edge (b) BGA footprint showing the three considered daisy-chains, (c, d) Microsection of QFN and R1206 respectively.

IV.3.1 R1206 solder joints lifetimes

The characteristic life of the R1206 component is 5151 cycles and the 1st failure was detected at 3900 cycles (Table IV.3–1). Under the specific experimental conditions, the R1206 component present the highest durability compared to the BAG288 and the QFN68 packages (purple plot in Figure IV.3–2). Monitoring the electrical continuity of a four R1206 components group mounted in parallel can delay the detection of failure. Crack development section will allow us to verify the accuracy of these results.

Table IV.3–1: Thermal cycling lifetime analysis results

	QFN68	BGA288			R1206
		DC1	DC2	DC3	
1 st failure	1436	2689	2595	2091	3900
Last failure	2367	4785	4191	3671	5787
Weibull parameters	$\beta = 7$ $\eta = 1919$	$\beta = 8,8$ $\eta = 4226$	$\beta = 9,6$ $\eta = 3707$	$\beta = 8,4$ $\eta = 3100$	$\beta = 9,9$ $\eta = 5151$

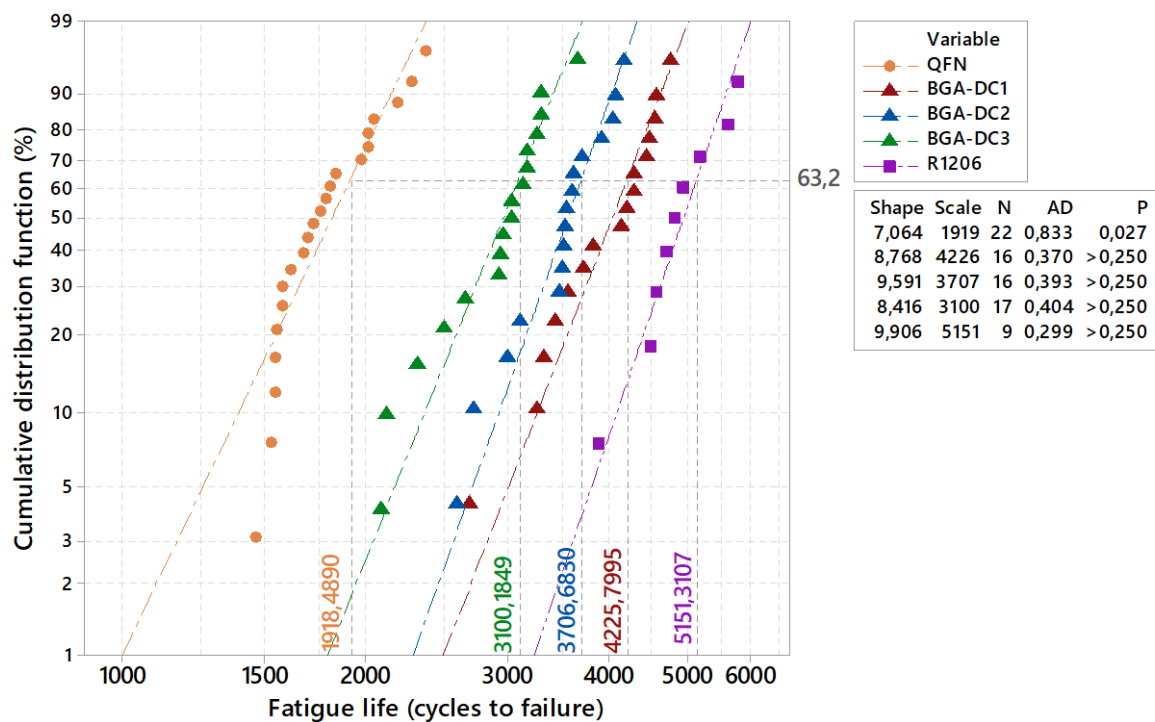


Figure IV.3–2: Weibull distributions for the BGA, QFN and R1206 components: thermal cycling from -55°C to 125°C

IV.3.2 BGA288 solder joints lifetimes

For BGA component, the electrical resistance measurements were carried out on the three daisy-chains (Figure IV.3–1 (b)) throughout the cycling test in order to detect the location of the first failures. It appears that the inner ring (daisy chain 3) of solder joints (green Weibull distribution in Figure IV.3–2) has the lowest characteristic lifetime compared to the other two daisy chains. This means that the first failures are more likely to occur under the edge of the silicon die and not under the corner of the component. The presence of the silicon die at the level of the internal ring generates significant shear stresses due to its low Coefficient of Thermal Expansion (CTE), which can change the critical positions of the first BGA solder ball to fail. We call it the “die shadow” effect, which means that the proximity to the die (low CTE of 3 ppm/K compared to that of the PCB) prevails over the distance to the center of the package

in the location of the first failure [90]. This result highlights that the distance from the neutral point (from the center of the components to the corners) is not the only unfavorable factor in terms of interconnection position. The study of the electronic assemblies reliability should not be based only on geometric considerations but earlier by taking into account the properties of each material present in the package.

IV.3.3 QFN68 solder joints lifetimes

The QFN component seems to have a different behavior compared to lead-free interconnections in other components (BGA, R1206) during thermomechanical fatigue. The three-parameter distribution seems to fit better with the curvature adopted by the experimental data. It is also possible to interpret the failure distribution as the combination of two populations involving competition between two different failure mechanisms.

A detailed description of the different phenomena leading to the failure of QFN interconnections was carried out in the previous chapter in the part. The results clearly show the presence of two mechanisms leading to different cracking modes (interfacial and mixed modes). Considering these two different failure modes in the plotting of the Weibull distributions validates the presence of two populations (Figure IV.3–3). An early number of cycles to failure characterize the first population (black points). However, a late failure detection was identified on the second population (red points). CTE measurements of the QFN component by TMA/DMA confirmed the use of a "green" package with a low CTE (6 ppm/K compared to that of the BGA). This type of component presents a different design and materials properties compared to the other packaging's, which may explain the different behavior of the QFN solder joints.

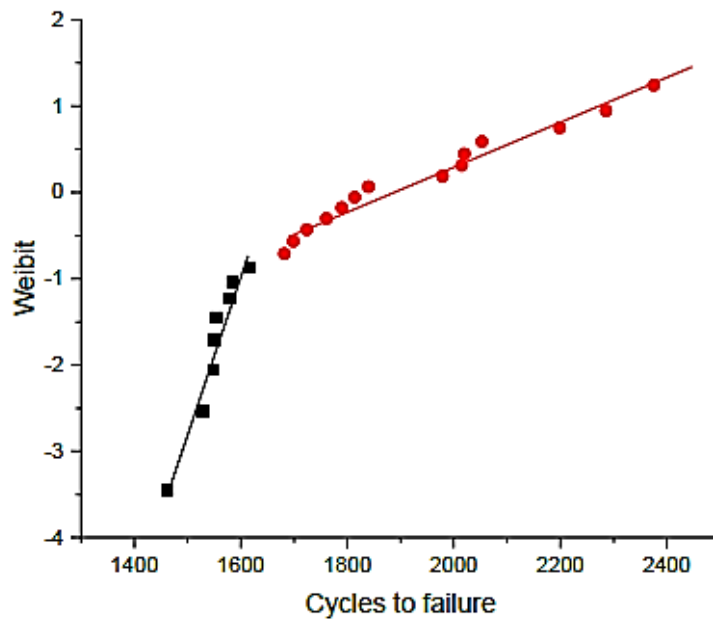


Figure IV.3–3: QFN solder joint Weibull distribution with two slopes

IV.3.4 Synthesis

The lifetime's results as well as the failure mechanism analysis presented in the previous chapter validate the presence of different SAC solder behaviors leading to two types of cracks:

- Common intergranular cracking, characteristic of the failure of BGA, QFN, and R1206 solder joints, a consequence of the tin recrystallization and coalescence of Ag_3Sn precipitates
- Interfacial cracking, rather transgranular, not requiring recrystallization to develop and present only on the QFN interconnections.

The package design (solder geometry and position, aspect ratio and assembly dimension) and its material properties (copper lead-frame and epoxy molding compound) present crucial parameters affecting the thermomechanical reliability of SAC solder joints under thermal cycling.

A semi-quantitative investigation is the goal of the next section to better understand the SAC alloy thermomechanical behavior and determine the link between SAC solder lifetimes and the crack development.

IV.4 Crack evolution

This part focuses on the evaluation of the nucleation time and propagation rate of cracks in BGA, QFN and R1206 component board assemblies under thermal cycling condition. A correlation between the crack development steps and results of failure detection by electrical monitoring is also investigated in order to identify the most important phase on the SAC solder joints lifetimes. Crack measurement has been carried out on samples taken out successively during the testing.

The crack ratio was calculated with the formula defined in section IV.2.2 and the evolution of the average crack ratio as a function of thermal cycles was plotted for the three solder geometries. The crack initiation and propagation phases were identified as following:

Crack nucleation phase : *Crack ratio* < 20%

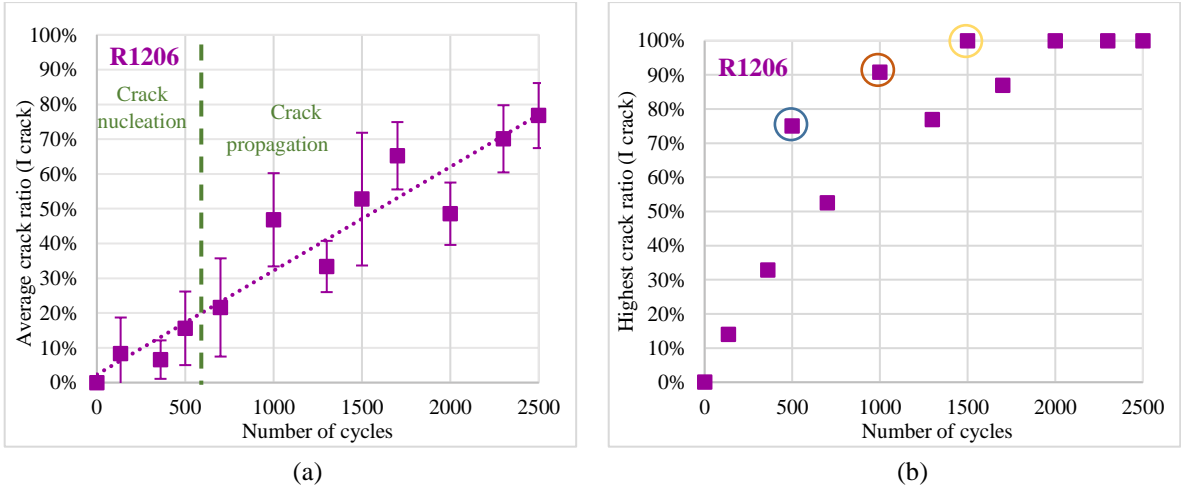
Crack propagation phase: *Crack ratio* = > 20%

A green line has been drawn on the next results graphs to highlight the transition to the crack propagation phase. We made also the choice to define a solder joint lifetime measured by optical microscopy. It is the first number of thermal cycles when the cracking ratio reaches 100% (total crack).

IV.4.1 R1206 solder joint

Figure IV.4–1. (a) shows the average crack ratios of the R1206 solder joint as function of the number of thermal cycles. Between 8 and 12 samples were used to calculate each point from the graph. The nucleation of cracks in the interconnections of the R1206 board assemblies started very early and take on average about 600 cycles.

An important scatter was observed in the evolution of the average crack ratio (Figure IV.4–1 (a)), which means that solder joints can present a different state of cracking at same number of cycles. It is possible that some as-reflowed solder joints have defects that can influence the crack rate such as the presence of voids and a substandard shape of the solder. These imperfections can cause early failures of lead-free assembly.



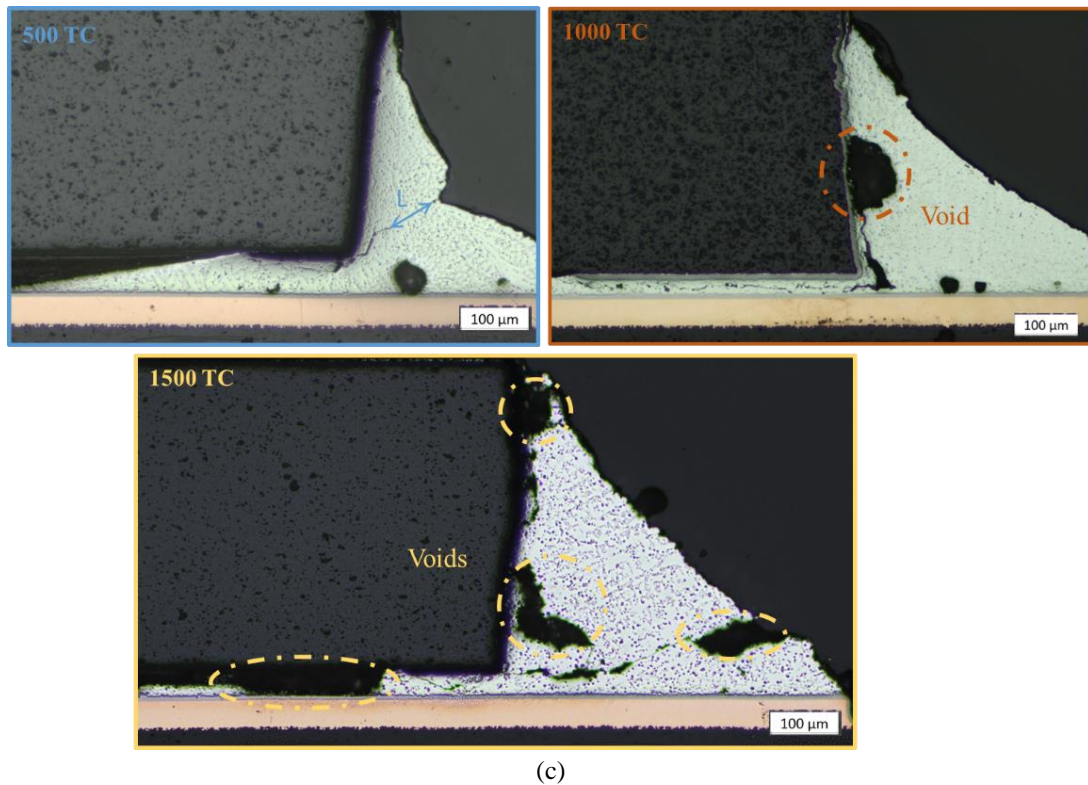


Figure IV.4–1: Characterization of crack propagation in R1206 interconnections under thermal cycling (a) average crack ratio evolution, (b) crack ratio in the most critical joint at different level of cycling, (c) crack inspection by optical microscopy.

The crack ratio evolution under thermal cycling was analyzed on the most cracked R1206 solder joints to validate this hypothesis (Figure IV.4–1 (b)). As expected, the crack propagation phase in the critical joints starts earlier compared to that identified from measurement of average crack ratio: after 360 cycles according to the crack ratio criteria (\Rightarrow 20%). The values measured on the samples taken at 500, 1000 and 1500 cycles are higher than those respectively found at 700, 1300 and 1700 cycles. Crack inspection by optical microscopy of the sample taken out 500 cycles shows that the solder presents a different shape with a short remaining distance (L). For the solder joints, undergone 1000 and 1500 cycles, voids with large diameters were observed on the crack propagation path (Figure IV.4–1 (c)).

Figure IV.4–1 (b) allows also the identification of the chip resistor lifetime by optical inspection (1500 cycles). This means that the crack nucleation phase in the most critical solder joints (360 cycles) represent only about 24% of the lifetime of R1206 interconnections and that the rest of service life is controlled by crack propagation.

IV.4.2 BGA solder joint

The evolution of the average and highest crack ratio were also plotted in the BGA solder joints. Measurements were carried out only on the corner solder joints under the component edge (the corner of the daisy chain 1 shown in Figure IV.3–1 (b)). It is the most critical position reported in the literature. For each level of thermal cycling, between four and six samples were used.

Figure IV.4–2 (a) shows that crack growth in the BGA interconnections thermal cycling starts out almost immediately but relatively slowly (500 cycles). Then, crack development accelerates quite suddenly after 1000 cycles that seems to coincide with the number of cycles typically required to activate tin grain recrystallization and Ag_3Sn coarsening. The measured standard deviation present can be due either to the imperfections appeared after the assembly process as was the case of the R1206 interconnections or to the measurements carried out on solder joints observed from the same component. If a corner joint begins to crack earlier than another corner joint, this can generate different stress levels/distribution and therefore different cracking states.

Figure IV.4–2 (b) shows that the first total crack on the BGA corner joints appear about 2300 cycles which represents the BGA lifetime calculated by optical microscopy. The crack nucleation phase of the most critical interconnections takes about 500 cycles i.e. about 21% of the optical lifetime. It should also be noted that analysis of the most critical solder joints highlights that total cracks of corner interconnections are often near the PCB side (Figure IV.4–2 (b)). The crack propagation phase represents also the most longer step on the corner solder joints lifetimes of the BGA288 package

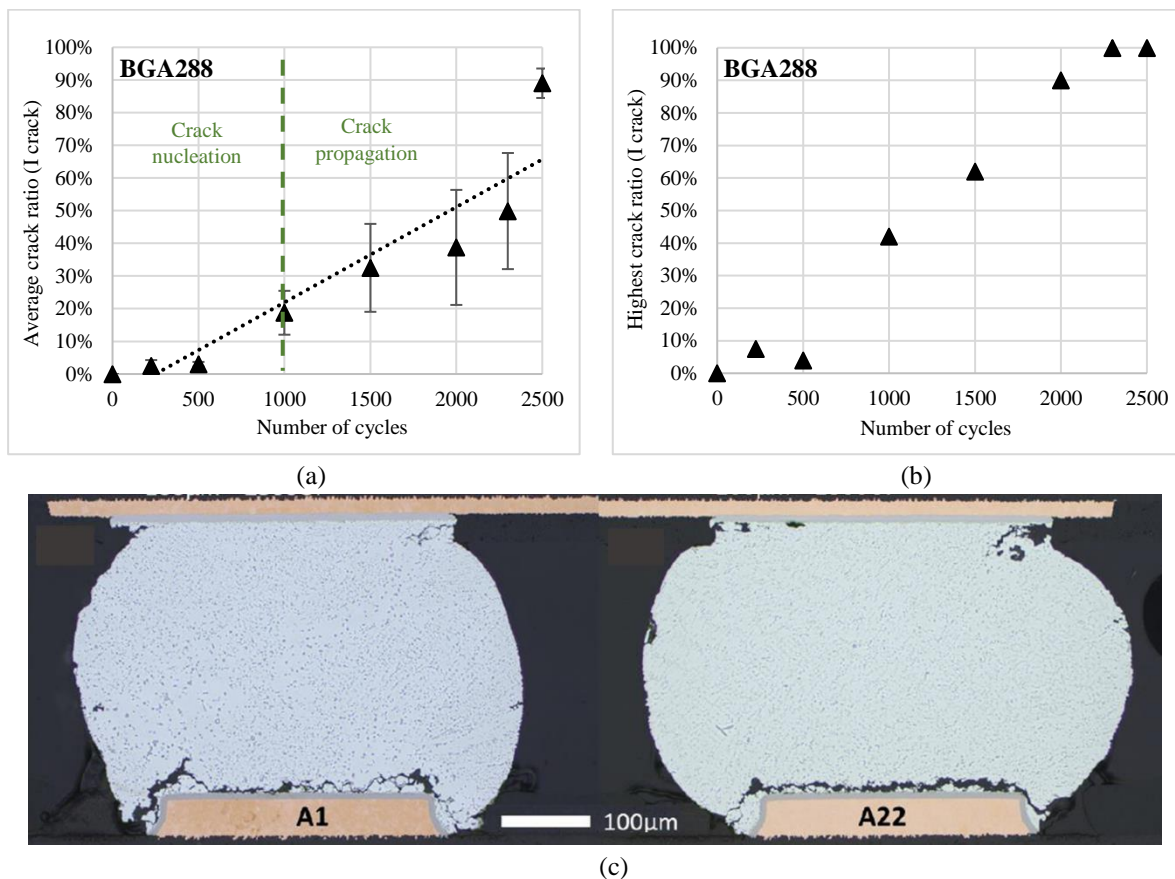
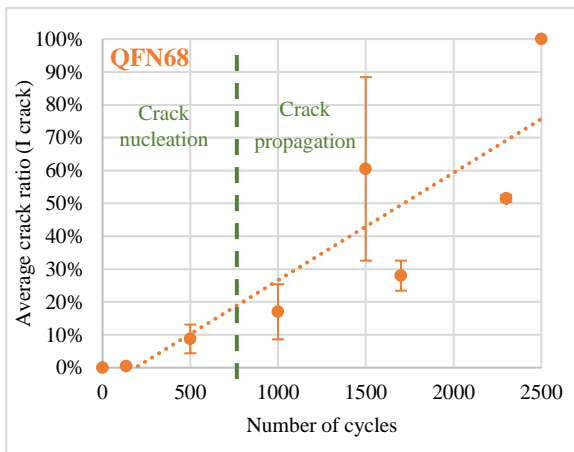


Figure IV.4–2: Characterization of crack propagation in corner joint of BGA component under thermal cycling (a) average crack ratio evolution, (b) crack ratio in the most critical joint at different level of cycling (c) Total crack observed near the PCB on the corner solder joints taken out after 2300 cycles

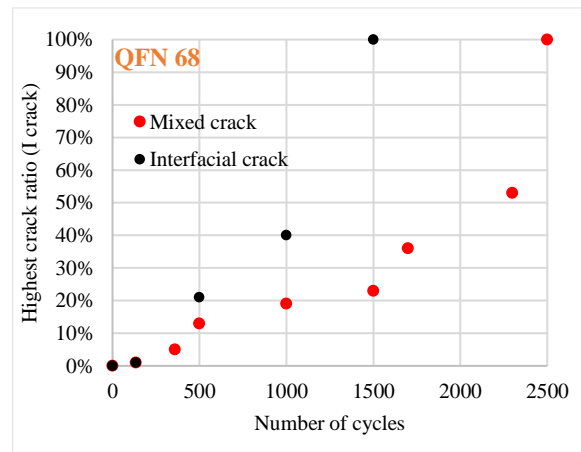
IV.4.3 QFN solder joint

The number of samples considered for the study of the QFN interconnections is between 4 and 6. Analysis of the QFN solder joints taken at different number of thermal cycling highlights the increase of the average crack ratio during thermal cycling (Figure IV.4–3 (a)). The crack propagation phase starts after 500 cycles. This is the number of cycles after which the QFN solder joints reach 20% cracking. The study of the failure mechanism of QFN solder joints under thermal cycling showed the presence of two types of cracking (interfacial and mixed crack, previous chapter). This means that the evolution of the average crack ratio does not allow studying the crack evolution according to its nature. The high standard deviation measured during these analysis can be caused by the presence of two cracking behaviors.

The crack ratio evolution measured on the most critical solder was plotted with considering the presence of two cracking types. Figure IV.4–3 (b) shows that the propagation of interfacial cracks seems to be faster than the mixed cracks development. The crack nucleation phase takes 500 cycles for the first mode compared to 1000 cycles in the case of mixed one. A slower propagation phase was observed for mixed cracking. The mixed crack is characterized by a combination of the interfacial and the intergranular cracking modes. The intergranular crack propagation appears to decrease the propagation rate. The formation of a network of highly disoriented tin grains with coarsened Ag_3Sn IMCs is required to facilitate the intergranular crack propagation. However, interfacial crack propagation does not need SAC solder joints microstructural damage. Figure IV.4–3 (b) reveals that the first interfacial total crack happen at 1500 cycles (Figure IV.4–3(c)). However, the mixed total crack was detected at 2500 cycles (Figure IV.4–3 (d)). The crack propagation phase represents 80% and 91% of the measured lifetimes by optical microscopy respectively. It is the longer step on the life service of the QFN interconnections.



(a)



(b)

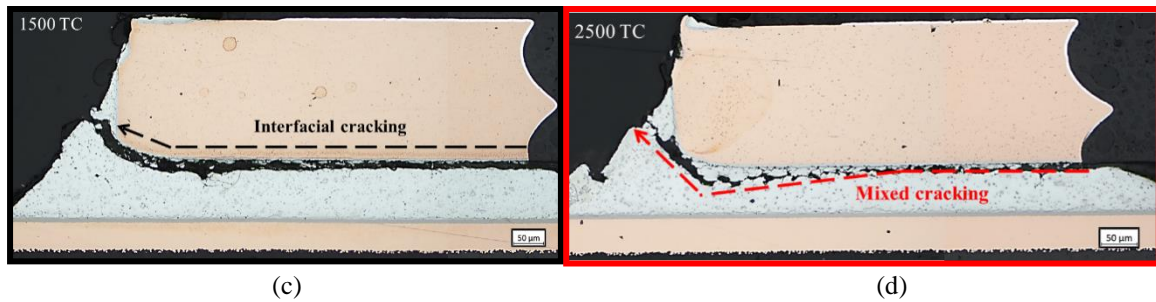


Figure IV.4-3: Characterization of crack propagation in QFN solder joints under thermal cycling (a) average crack ratio evolution, (b) crack ratio in the critical joint at different level of cycling (c) total interfacial crack observed on solder taken at 1500 cycles (d) observation of the mixed cracking mode on solder subject to 2500

IV.4.4 Correlation with lifetimes results

Table IV.4-1 summarizes all data used to establish the correlation between the lifetimes results and the crack propagation measurements. The lifetimes measured by optical inspection does not correlate with lifetimes results identified by electrical monitoring. Crack evolution measurement shows that the R1206 package does not present the highest reliability. First total crack were observed on the R1206 components taken out at 2000 cycles. This number of cycles is very low compared to the first detected failure (3900 cycles) as well as the characteristic lifetimes measured by electrical continuity (5151 cycles). The parallel assembly of the chip resistor components, chosen when designing the board, seems to be the cause of the delay in electrical failure detection. The in situ monitoring was also unreliable for the detection of the very first failures in the case of the passive components.

Electrical continuity data may be more useful in the case of BGA components. The time of the first detected failure (2689 cycles) is close to the date of observation of total cracks (2300 cycles) although the characteristic lifetime was too high (4229 cycles).

Correlation between the crack evolution on the QFN solder joints and the lifetimes analysis shows that the total cracks observation (1500 cycles) corresponds to the number of cycles of 1st electrical failure (1436 cycles). The characteristic lifetime (1919 cycles) remains always away from the date of total cracks formation. Two populations were presented in the Weibull distribution of the QFN (Figure IV.3-3). The number of cycle of their appearance correlate with the dates of observation of the two types of cracking. The interfacial cracking mode is characterized by the first total cracks appearance (before 1500 cycles) which is associated with the first population (black points) in the QFN Weibull plots. Total intergranular crack happens later on thermal cycling (2500 cycles). This cracking mode seems to be the cause of failures on the red population.

Table IV.4–1: Correlation between results of crack measurement and electrical failures

Number of cycles	R1206	BGA DC1	QFN	
			Intergranular	Interfacial
Crack propagation in the most cracked solder	360	1000	1000	500
1 st observed total crack = optical lifetimes	2000	2300	2500	1500
1 st electrical failure	3900	2689	1700	1436
Characteristic lifetime	5151	4226	1919	

These results show that failure detection by electrical monitoring can be useful for the detection of the very first total cracks. However, it does not allow in any case following the steps of crack propagation. The dates of observation of crack propagation appearance are far from the various events detected by electrical monitoring.

IV.4.5 Synthesis

The nucleation and crack propagation phases have been identified in the R1206, BGA and QFN components under thermal cycles thanks to the cracking criterion defined at the beginning of the section. The number of cycles after which the nucleation of cracking was observed in the various joints therefore proves to be very low in comparison with the optical or electrical measured lifetimes. This means that the life service of the solder joints is controlled by the propagation of crack. The interfacial crack propagation seems to be faster than the intergranular one that causes early failure in the QFN solder joints.

It is important to recall that the main purpose of this section is to identify the transition times to the crack propagation phase in our own components so that we can then correlate them with microstructural evolution. The intergranular cracking represents the only and common failure mode observed on the BGA and R1206 interconnections. A significant population of the QFN joint failed by the mixed mode of cracking where intergranular propagation occurs. A major study has therefore been undertaken in the next sections to characterize the microstructural indicators changes that govern the recrystallization and Ag₃Sn coarsening of realistic SAC joints and lead to the transition to the crack propagation phase in our packaging's

IV.5 Tin grain recrystallization

Tin grain recrystallization phenomena is a primary process for the SAC solder joint crack propagation. Quantitative analyses were carried out to identify the size of the recrystallized grain and the degree of recrystallization promoting the crack development under thermomechanical loading.

IV.5.1 Characterization of the BGA solder joint evolution

(a) *Identification of recrystallized tin grain equivalent diameter*

The size of the tin grain is an important indicator allowing the characterization of the microstructural damage of SAC solder under thermomechanical loading. Measurements of the tin grain size and its evolution with thermal cycles were investigated to better understand the dynamics of the recrystallization phenomenon.

Analysis of highest strain regions (near the component or PCB sides) of the BGA solder joints highlighted that the equivalent diameter of the recrystallized grains is between 1 and 30 μm . Figure IV.5–1 (b) shows an example of the EBSD grains size map carried out near the BGA component taken out at 1700 cycles (Figure IV.5–1 (a)). We can clearly observe that the network of recrystallized grains have a blue color (size between 1 and 30 μm). It is considered that a grain having a diameter greater than 30 μm as the remainder of a macro grain resulting from the after reflow state and which is not yet completely recrystallized (green and red grains in Figure IV.5–1 (b)). For this reason, a visual filter has been applied to the grain size maps to better highlight the evolution of this parameter during thermal cycling (Figure IV.5–1 (c)). It is also interesting to note that whatever the level of the cycling of the BGA solder joints, the grain size remains in the same range (Figure IV.5–1 (d)).

The grains were then classified by size intervals and the evolution of the recrystallization degree of each range under thermal cycling was studied. The objectives is to determine the dominant recrystallized grain sizes at the time of crack propagation and verify whether a certain diameter can favor cracking of SAC solder joints. Results shows a synchronized increase of all the ranges of recrystallized grains (Figure IV.5–2). This observation allows us to conclude that there are no grain size which promotes cracking compared to others and assumes that the kinetics of recrystallization is fast; the size of the β -Sn grains quickly reaches a threshold value from the diameter remains constant.

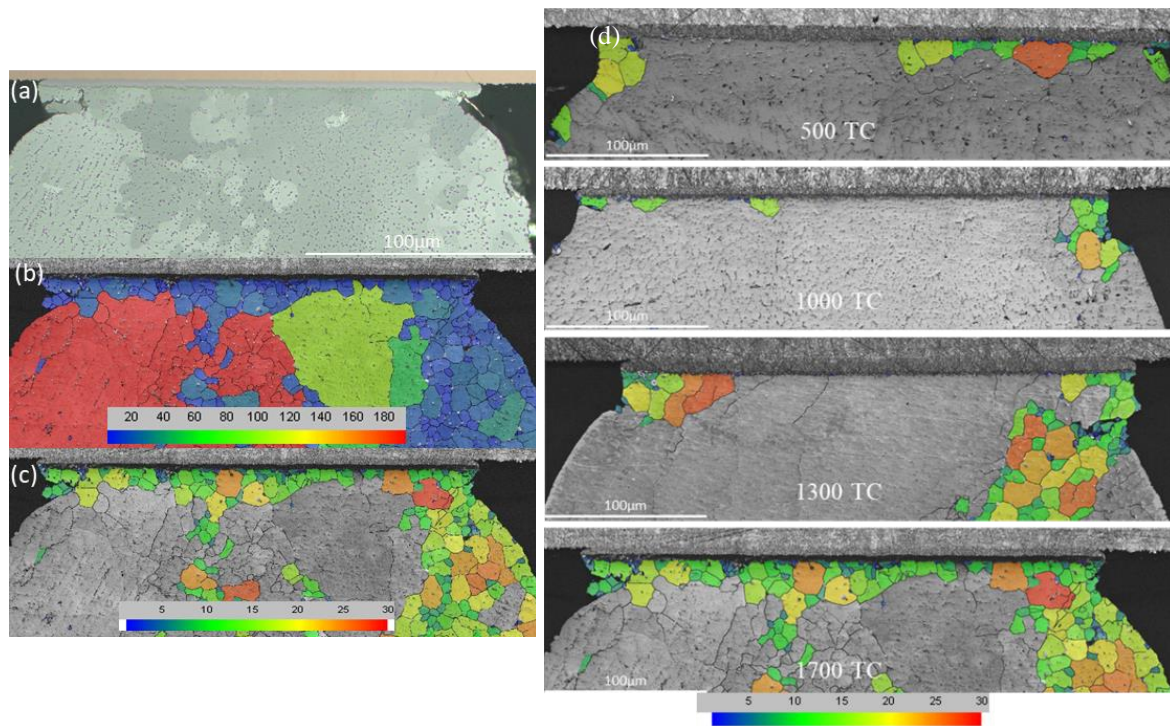


Figure IV.5–1: Characterization of recrystallized tin grains in the BGA component side, (a), (b) and (c) identification of the tin grain size, (d) evolution of the tin grain size under thermal cycling

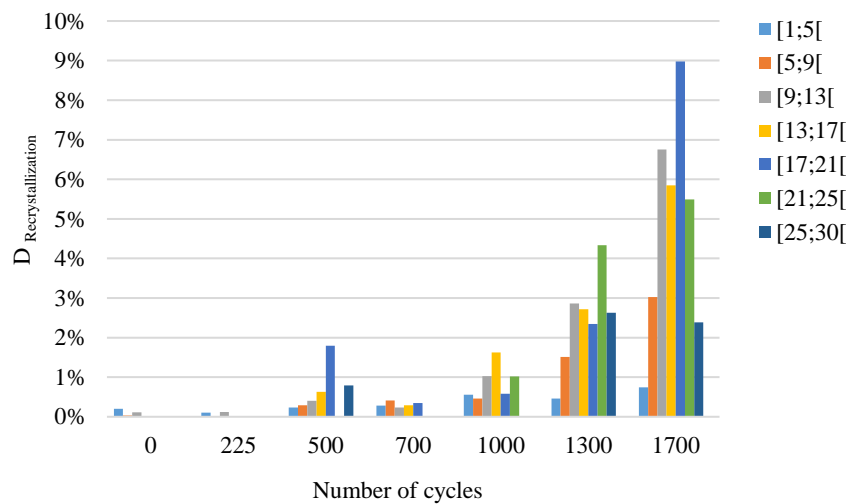


Figure IV.5–2: The evolution of the recrystallization degree of the different tin grain size ranges under thermal cycling

(b) *The evolution of the recrystallization degree with thermal cycles*

Measurements of the evolution of the degree of the recrystallization was carried out on the BGA components taken at different level of the thermal cycling until the observation of total cracks. EBSD analyses have been conducted in order to better understand the role of the recrystallization on the crack propagation (Figure IV.5–3 (a) and Figure IV.5–3 (b)). The highest strain areas were selected to be analyzed during thermal cycling: Blue frame for area near the component edge and black frame for the PCB side region (Figure IV.5–3 (b)).

Figure IV.5–4 represents the curves of the evolution of the degree of recrystallization during the thermal cycling of the studied zones. The recrystallization begins almost immediately within the first thermal cycles but relatively slowly then it accelerates quite abruptly after 1000 cycles. The degree of the recrystallization remains after that practically constant until the end of the cycling. We can also observe that the degree of the recrystallization is higher near the PCB side. It reaches 37% compared to the maximum value calculated of the component side (16%). It is assumed that the stresses submitted by the studied BGA solder joints on the PCB side are higher than on the component side.

The correlation between the crack development and the recrystallization degree evolution shows that the phenomenon of recrystallization was present during the crack development. A low degree of recrystallization was measured during the crack nucleation phase. Then, cracks propagation near the PCB/component sides only started after 1000 cycles with an important increase in the recrystallization degree. The fact that crack propagation does not begin earlier shows that it requires a well-defined recrystallization amount to provide favorable intergranular generation paths. This correlation shows that BGA solder joint cracking and recrystallization develop simultaneously and that crack begins to propagate even before reaching total recrystallization.

It is also important to note that total cracks were located only along the PCB side on joints that have been cycled for more than 2300 times (Figure IV.4–2 (c)). This means that the highest degree of recrystallization near the PCB side allows the propagation of partial cracks until total failure of the solder joints. The observation time of total cracks (2300 cycles) corresponds to recrystallization degree of about 35% of studied region (Figure IV.5–4). However, optical observations and EBSD maps highlight that total cracks are often present in a completely recrystallized region. It should be kept in mind that the degree of recrystallization depends on the area of the studied region. The recrystallization zone that will lead to total cracking is narrower than we have studied, yet it is in this zone that 100% recrystallization occurs. Thus, the degree of recrystallization on the analyzed area is always less than 100%. Consequently, we can assume in our study that a total recrystallization (100%) of the crack propagation zone on the PCB side happens from 1300 cycles when the curve reaches steady state (about 35% of recrystallization of the studied area).

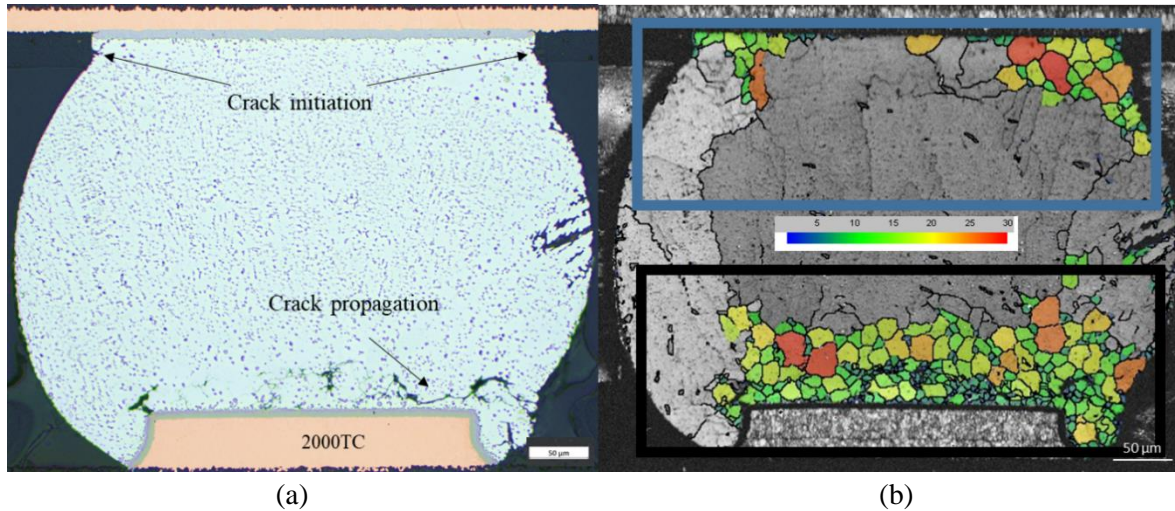


Figure IV.5-3: Correlation between the crack development and the tin grain recrystallization (a) optical observation of cracks, (b) Recrystallized tin grain size maps

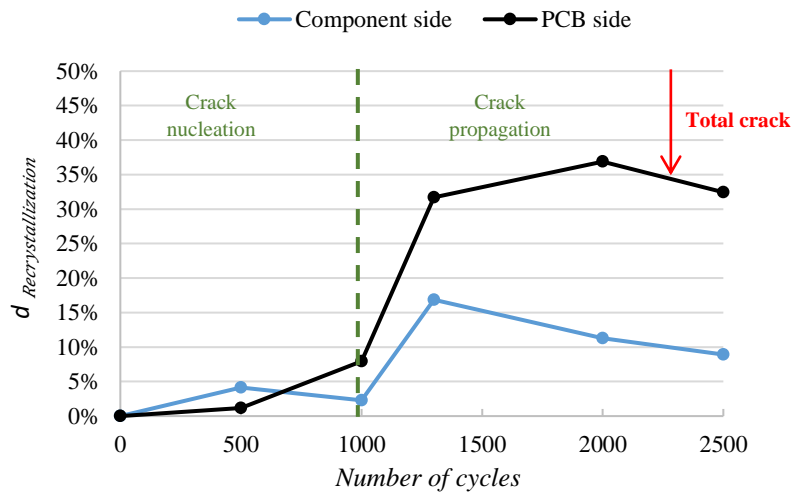


Figure IV.5-4: The evolution of the recrystallization degree of the BGA solder joints under thermal cycles and as function of the intergranular crack development

The low rate of recrystallization reached on the component side seems to be not sufficient to have a complete propagation of the cracks. No total crack or completely recrystallized areas were observed on the component side. The increase in recrystallization degree contributed to the transition to the crack propagation phase but the value reached at steady state was not sufficient to have total cracks and represents partial recrystallization of the crack propagation area. After 1000 cycles, the recrystallization no longer evolves with thermal cycling which prevents from going as far as total cracking of the component side.

It should be remembered here that the solder balls analyzed in this part of the study are located under the component corner. Since the quantitative study of the microstructural evolution and the measurement of the lifetimes of the solder joints were carried out in parallel, it was considered that the most critical joints are located under the corner of the components as reported in the literature. However, the electrical detection of BGA component failures has shown that the balls under the die are the ones that fail first. Consequently, it can be assumed

that total cracks happen earlier in the joints under the die edge. The appearance of these cracks can change the location of the highest strain region on the corner interconnections. The behavior of each solder joint may depend on the response of the other joints present in the BGA component matrix. The behavior of the balls close to the corner ball as well as that of the joints positioned under the edge of the die is presented in the next chapter.

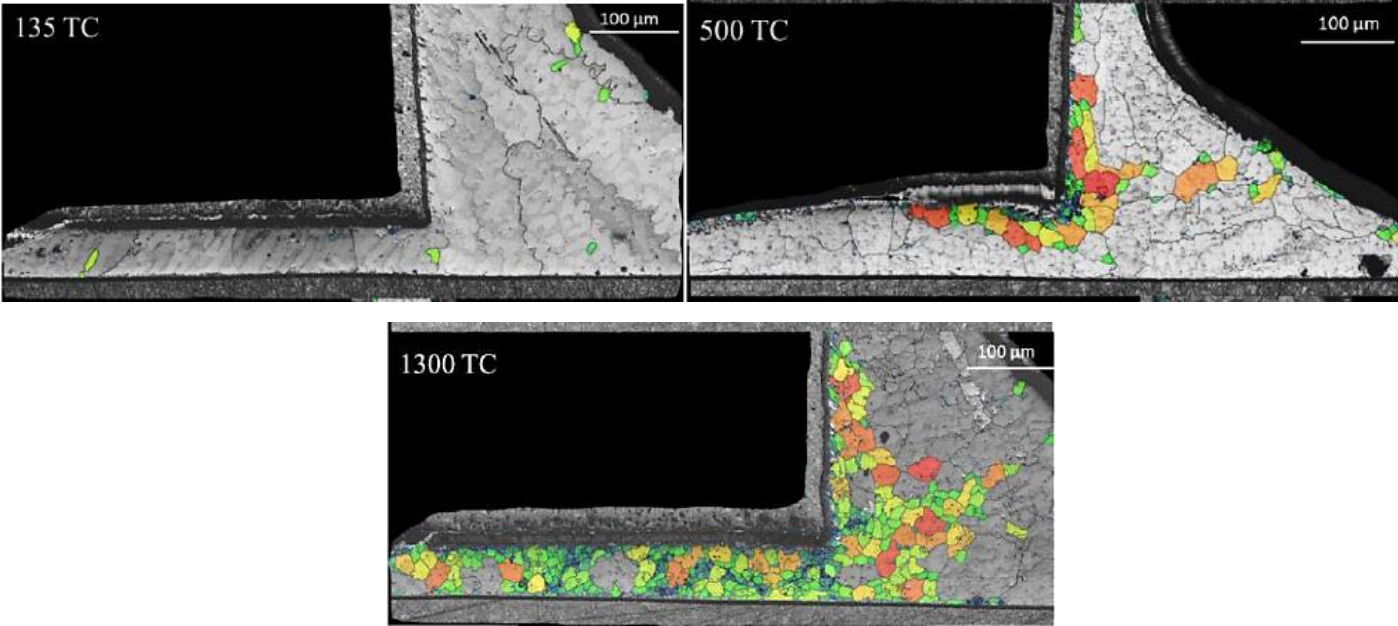
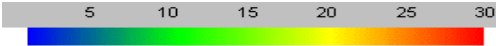
IV.5.2 Comparison with the R1206 and QFN solder joints geometries

The same study was carried out on the R1206 and QFN components to compare the SAC alloy behavior on different solder geometries. The highest strain regions of these components were analyzed to characterize the evolution of the tin grain size and the recrystallization degree as function of the solder joint geometries. It should be kept in mind that one of the objectives of this chapter is to define a common microstructural criterion allowing the evaluation of the state of damage of various interconnections geometries.

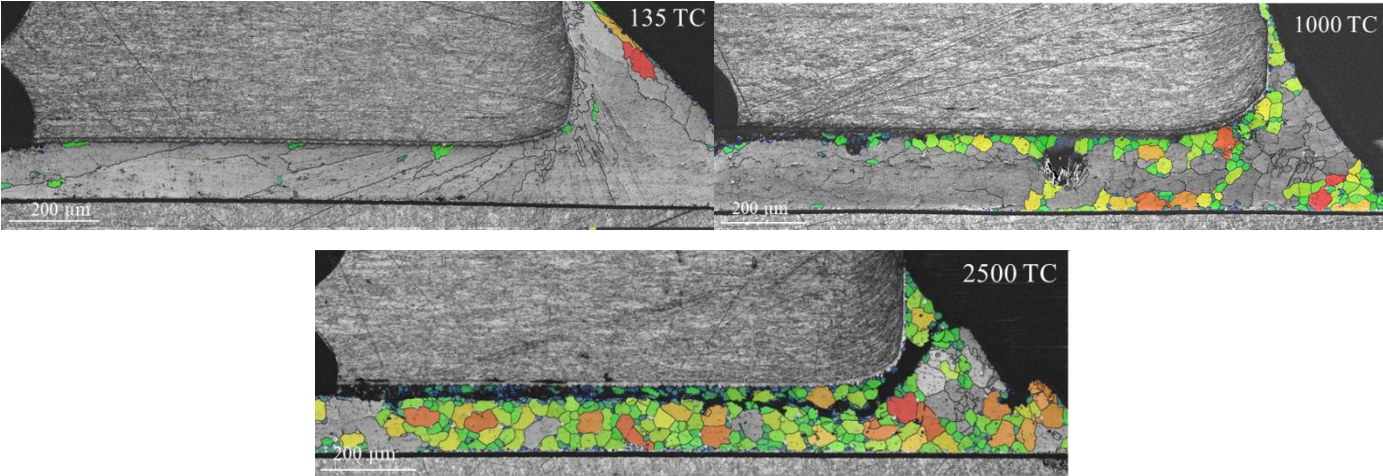
(a) *Tin grain equivalent diameter*

Analyses of the R1206 and QFN solder joints taken out at different levels of thermal cycling reveal that the recrystallized grain present the same range size as the BGA solder joints. Figure IV.5–5 (a) and Figure IV.5–5 (b) present the tin grain size mapping of R1206 and QFN interconnections with different microstructural state damage: weak, partial and total recrystallization of the crack propagation region. The diameter of recrystallized grains is between 1 and 30 μm whatever the level of the thermal cycling and the solder joint geometry. Observations show high proportion of small β -Sn grains along the intergranular crack path. These grains is supposed to be the result of a local recrystallization of the largest recrystallized grains at the crack tip due to the high stress concentration. This assumes that the crack crosses the grains with the largest diameter and therefore grains having a diameter of about 30 μm can be considered as the grains responsible for crack propagation.

Results highlight that the size of the recrystallized grains does not depend on the solder geometry but it is a feature of the solder alloy. Therefore, this indicator can be considered as a microstructural damage criterion that can be implemented in numerical simulations to improve the accuracy of the prediction results since tin grain recrystallization is a common process responsible for the failure of different lead-free solder geometries.



(a)



(b)

Figure IV.5–5: Recrystallized tin grain size maps at different thermal cycles (a) R1206 (b) QFN68

(b) *Degree of recrystallization evolution*

In this part, only the recrystallization degree near the PCB side for the BGA component was considered since it was the region of the total cracks appearance. The choice of the zones analyzed for the QFN and R1206 components was made with the aim of being able to follow all the stages of the formation of the intergranular crack propagation path.

The comparison of the evolution of the degree of recrystallization in the three studied geometries shows that the BGA interconnections seems to have a particular behavior compared to those of the R1206 and QFN. Figure IV.5–6 highlights that the solder joints of the R1206 and the QFN components are characterized by a linear evolution of the recrystallization degree as a function of the number of thermal cycles. However, a stationary phase was observed after a certain number of cycles when analyzing the BGA solder joints. The resistance and QFN solder joint geometries are closer than that of BGA. This may be the origin of the similar behavior observed on these two types of solder.

The correlation between the crack development measurements and the recrystallization degree evolution in the different solder geometries shows that the recrystallization evolves synchronously with crack evolution. It is present from the crack nucleation phase to the appearance of total crack which once again validates that the development of intergranular cracks does not require a complete recrystallization of the propagation path.

The recrystallization degree promoting crack propagation is of the same order of value for the BGA and the R1206 components (8% and 10% respectively). The higher rate of recrystallization measured at the time of transition to the crack propagation phase on the QFN solder joints (27%) may be due to their particular cracking mode. Indeed, QFN interconnections are characterized by a mixed cracking mode which is a combination of interfacial and intergranular cracks. In this configuration, intergranular cracks may require a higher degree of recrystallization to promote intergranular crack propagation.

The total recrystallization of intergranular crack propagation path in QFN and R1206 geometries is only reached at the time of observation of total cracks. As explained in the case of the BGA geometry, the maximum recrystallization degree value for each geometry can represent a state of complete propagation path recrystallization. The areas of the analyzed regions are generally larger than the propagation path area. The very low evolution of the recrystallization degrees calculated on the R1206 samples taken after 2000 cycles (total cracking of the joints) shows that the recrystallization no longer evolves and reaches to a saturation phase. At this step, we can consider that the crack propagation path is completely recrystallized.

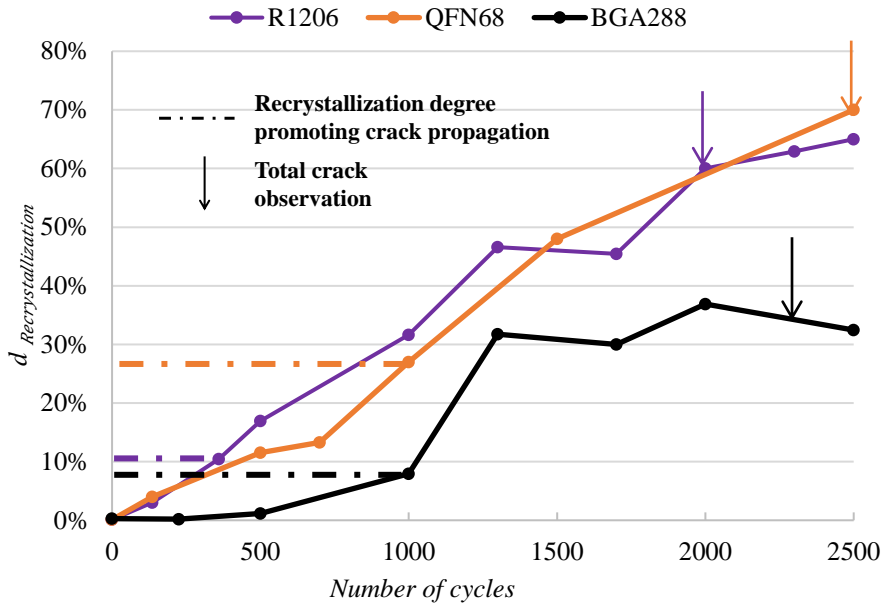


Figure IV.5–6: The recrystallization degree evolution as function of the solder joint geometries

IV.5.3 Synthesis

The quantitative analysis of the phenomenon of tin grain recrystallization has made it possible to study the evolution of the recrystallized grains size and the recrystallization degree of the BGA, QFN, and R1206 solder joints under thermal cycles.

The measurements show that the equivalent diameter of recrystallized grains is between 1 and 30 μm . This range does not depend on the solder geometry and does not evolve under thermal cycling. We can then consider that the recrystallized grain size is a characteristic of the solder alloy which can be implemented in numerical models to improve the accuracy of life prediction results.

The correlation between the evolution of the recrystallization degree and the crack development in the three studied components shows that a well-defined degree of recrystallization is necessary to trigger crack propagation. This rate is of the same order for the BGA and R1206 geometries which are characterized by a common purely intergranular cracking mode. For QFN solder joints, the crack propagation seems to require a higher recrystallization degree. This can be explained by their particular cracking mode which is a mixture between the interfacial and intergranular modes.

IV.6 Ag₃Sn coarsening

Ag₃Sn IMCs coalescence is the other microstructural phenomenon that characterizes the thermomechanical damage. Under cycling, Ag₃Sn IMCs in the solder joints coarsen; the largest particles grow in size while smaller particles dissolve which leads to a loss of dendritic structure. This will decrease the precipitation hardening and make the solder softer, which facilitates the recrystallization [10]. The detailed description of the solder failure mechanism during cycling, established in chapter 3, shows that the coalescence of Ag₃Sn particles is activated in the BGA, and R1206 interconnection geometries. Quantitative analyses of the size and the density of the IMC particles were performed with all of EBSD data at different levels of the ATC in order to identify the indicators underlining the state of microstructural damage activated by the Ag₃Sn coarsening. Measurement steps were outlined before in section IV.2.3.

IV.6.1 Characterization of the BGA solder joint evolution

(a) *Changes of Ag₃Sn particles size*

Among the different studied packages, this part focuses on the BGA components. We started by the characterization of the evolution of Ag₃Sn IMCs equivalent diameter. On the same approach applied in the previous section, the two most stressed regions in the case of a BGA joint (near the component/PCB sides) have been analyzed along the ATC and until observation of total cracks (Figure IV.6–1). The measurements were carried out on the balls under the component corner.

The analyzed regions during the first cycles were typically chosen to be interdendritic regions with a heavy concentration of IMC particles, characteristic state of the as-reflowed solder joints. Samples taken later in the cycling and presenting larger particles mainly localized at the level of the recrystallized zones were chosen to characterize the change in the diameter of the IMCs during the microstructural damage.

The variations of the average equivalent IMC diameter as function of the number of thermal cycles are shown in Figure IV.6–2. It is evident that the average size of the Ag₃Sn particles increase with increasing cycling time. The appearance of larger particles seems to be more noticeable on the PCB side. This observation correlates with the results of tin grain recrystallization analyzes which validates that the level of stress applied by the PCB on the corner joints is higher than that generated by the component.

Nonetheless, a high standard deviation was observed during measurement of the average equivalent diameter with an increase in its value all along the thermomechanical cycling. This shows that Ag₃Sn particles presenting at the as-reflowed state have scatter diameters and the appearance of larger particles makes their distribution more dispersed. The Ag₃Sn particles density seems to be the most suitable parameter highlighting the Ag₃Sn IMCs coarsening during thermomechanical loading.

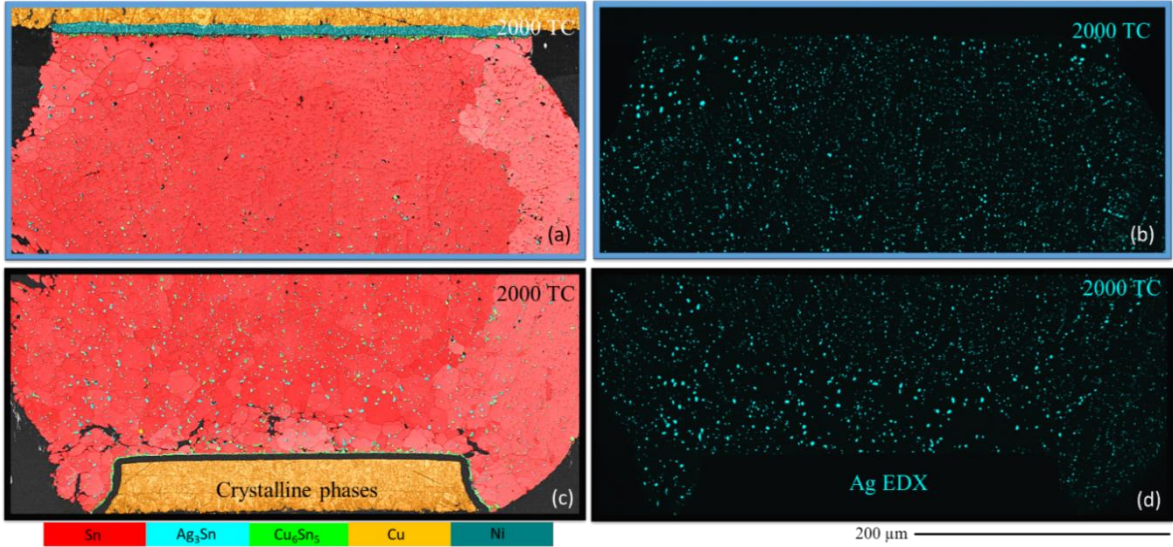


Figure IV.6-1: Coarsening of Ag_3Sn particles on a BGA solder joints taken out after 2000 cycles

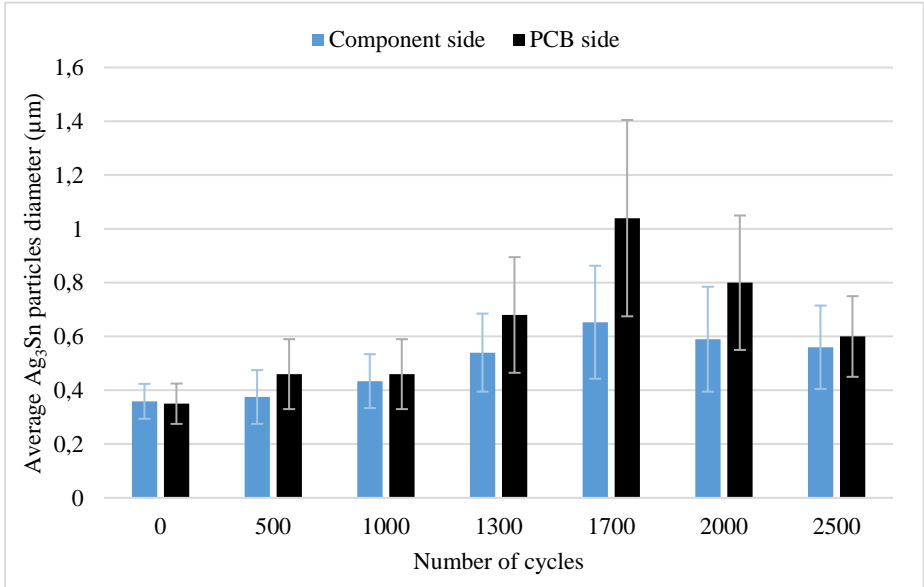


Figure IV.6-2: Evolution of the Ag_3Sn particles equivalent diameter on the BGA solder during thermal cycling

(b) Evolution of Ag_3Sn particles density

To better define the dynamics of IMCs evolution and to make a link with the tin grains recrystallization phenomenon as well as the development of cracks in the solder joints, a monitoring of Ag_3Sn particles density has been established by generating different equivalent diameter intervals. The objective is to refine as much as possible the identification of the Ag_3Sn particles density and size.

Assessments reveal that the values of the equivalent diameter are between 0.2 and 3.3 μm . Since these particles have nano metric diameters, the evolution of the IMCs density were considered for four intervals: [0.1; 1[, [1; 2[, [2; 3[and [3; 4] μm with an increment of 0.1 μm in each interval. This choice was applied to obtain results allowing comparison with QFN and R1206 geometries.

Figure IV.6–3 shows the evolution of Ag_3Sn particles density, near the PCB side of the BGA solder joints under thermomechanical cycling, for the different studied diameter intervals: the histograms present the density of each population belonging to this interval and the curves show the evolution of the density of all the particles present in this interval.

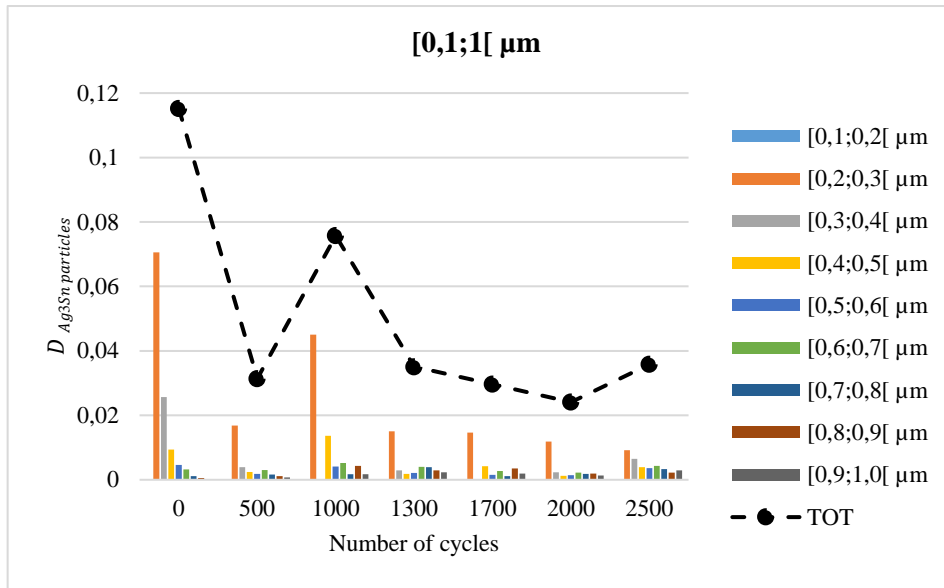
We can clearly observe that we have two different IMCs behaviors according to their diameters. The Ag_3Sn density decreases with increasing the number of thermal cycles for particles having a diameter less than 1 μm (Figure IV.6–3 (a)). This highlights that the smallest Ag_3Sn dissolve under thermal cycling so that the larger particles start to appear which leads to a loss of the dendritic structure.

Figure IV.6–3 (b, c, and d) reveal an increase in the density of particles with an equivalent diameter superior to 1 μm which validates the formation of bigger precipitates. The date of their appearance depends on their size. The smaller the IMCs, the earlier the density increase is observed. Indeed, the density rises significantly from the first thermal cycles up to 500 cycles for precipitates with diameters between 1 and 2 μm . Particles with diameters belonging to intervals [2; 3[and [3; 4] μm appear later after 1000 cycles.

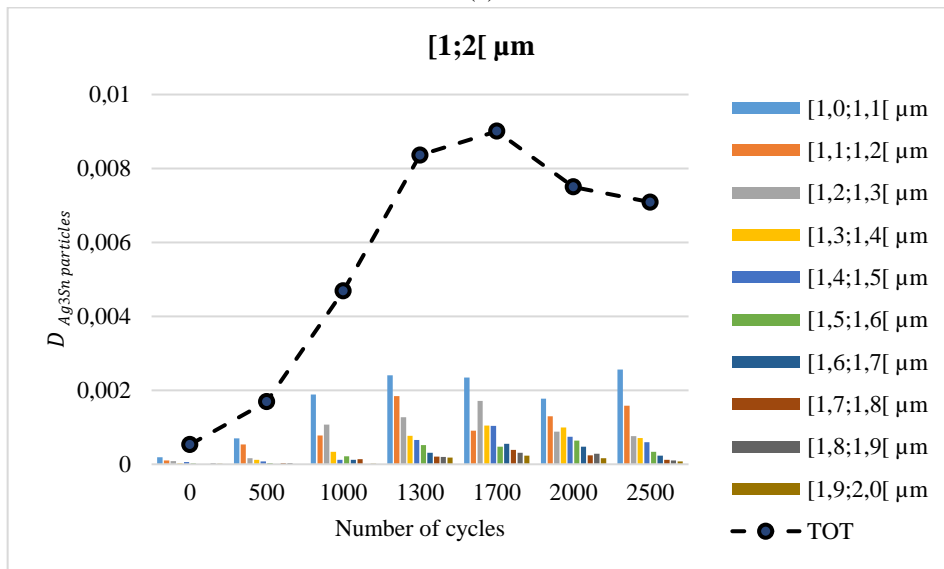
However, it is interesting to underline that the measured total density of the largest particles remains too low compared to the density value of the nanometric particles. This category seems to be the predominant population even after the application of a high number of thermal cycles. The decrease in its total density throughout thermal cycling causes continuous softening of the highest strain region of the solder joints. As the coarsening of Ag_3Sn particles occurs, the density of the smallest precipitates decreases and their ability to block dislocation movements is reduced. IMCs present on the as-reflowed state are finely dispersed and can indeed operate like barriers to the viscoplastic strain-induced dislocations motion and inhibit solder joints damage by dislocation pinning process.

The high strain regions show that large IMCs have coalesced where tin grain recrystallization takes place and high angles grain boundaries are created (Figure IV.6–4). This observation assumes that strain-enhanced Ag_3Sn coalescence is controlled by grain boundary diffusion. With the increasing size of Ag_3Sn precipitates coupled with the lower density (more important spacing between particles), the dislocations are no longer blocked, the largest IMCs can constitute good nucleation sites and recrystallization is thus promoted.

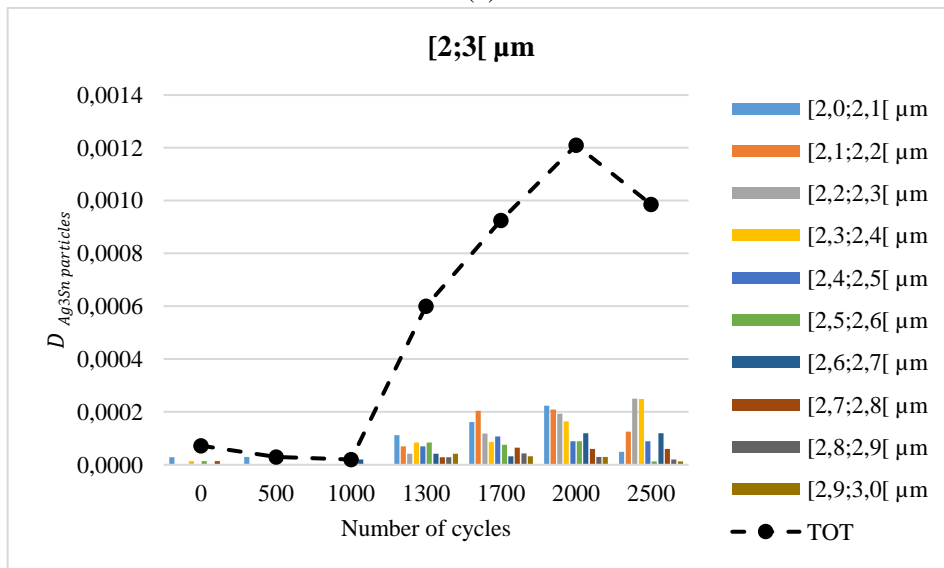
The evolution of the Ag_3Sn particles density has been correlated with the recrystallization degree and the crack phases in order to understand the effect of the largest precipitates growth on the tin grain recrystallization and the crack propagation. The Ag_3Sn IMCs density were measured at different level of cycling near the component and the PCB sides for the considered equivalent diameter intervals to associate with the recrystallization degree results.



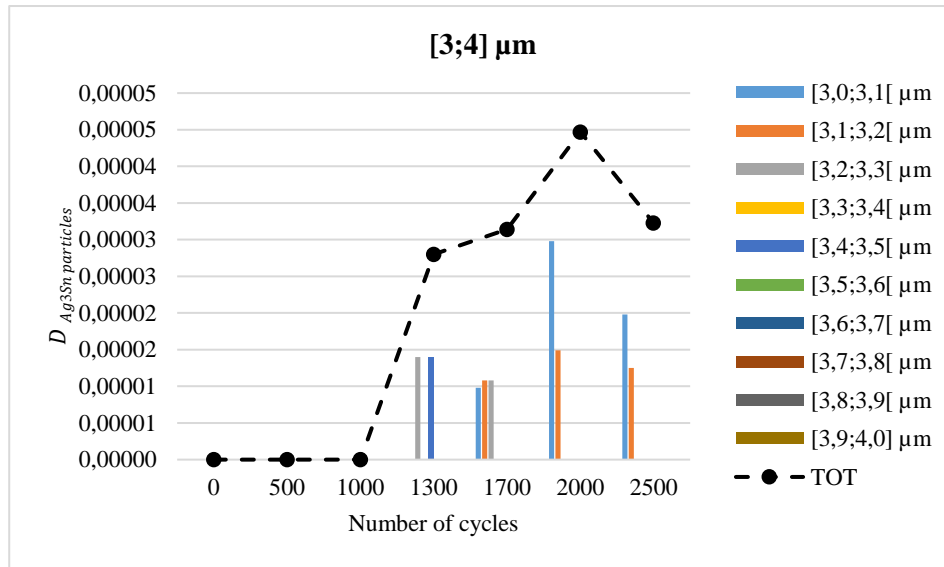
(a)



(b)



(c)



(d)

Figure IV.6-3: Characterization of the Ag₃Sn density and size evolution on the PCB side of the BGA solder for the four considered diameter intervals (a) [0,1 ; 1[μm, (b) [1 ; 2[μm, (c) [2 ; 3[μm and (d) [3 ; 4] μm

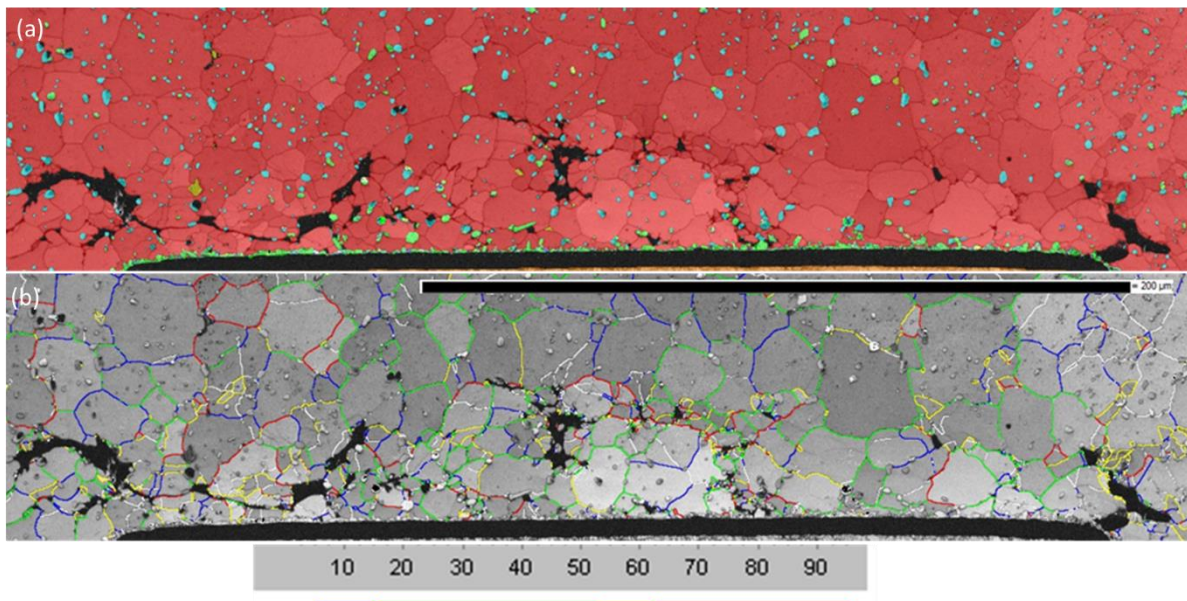


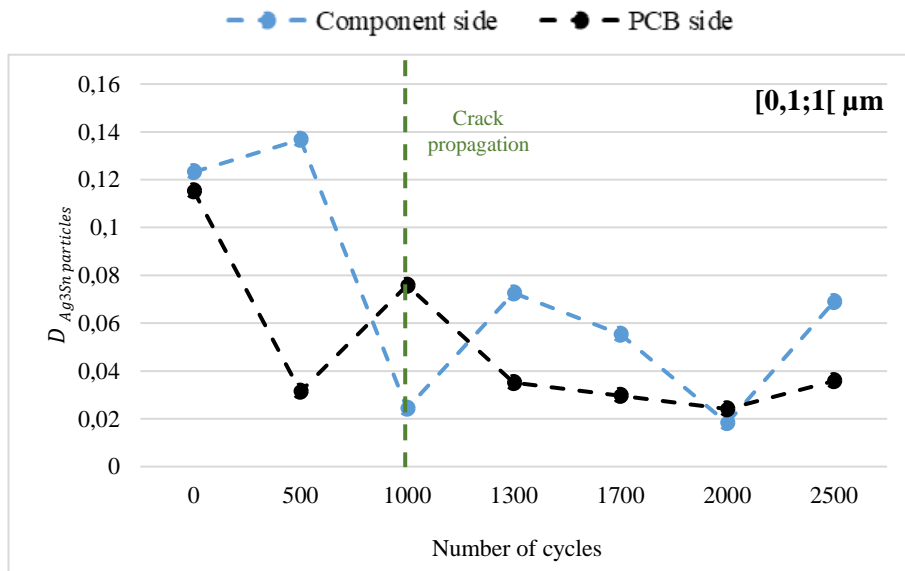
Figure IV.6-4: Strain-enhanced Ag₃Sn coalescence controlled by grain boundary diffusion (a) crystalline phases map, (b) grain boundaries map

Figure IV.6-5 shows first that the highest region near the component side present the same Ag₃Sn particles behavior of the PCB side during thermomechanical loading. The densities in the two studied regions are of the same order of magnitude. The coalescence of Ag₃Sn particles does not seems to be affected by the stress level applied by the PCB as observed during the analysis of the evolution of the recrystallization.

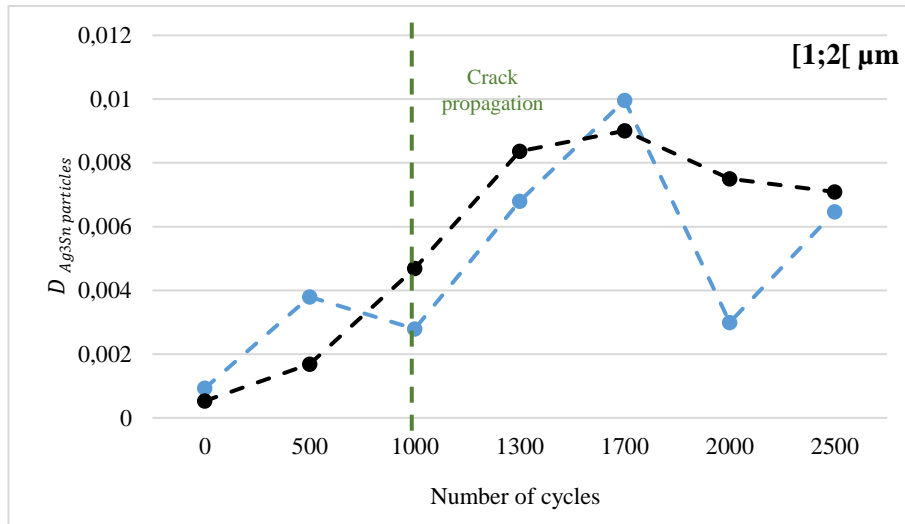
The correlation between the Ag_3Sn particles density and the recrystallization degree shows that the two phenomena appear simultaneously. Measurement highlight a significant increase of the recrystallization degree after 1000 cycles. This moment corresponds also to the beginning of the crack propagation phase. The lowering of smaller particles (between 0.1 and 1 μm) is remarkable from the first cycles of thermal testing (before 1000 cycles). However, after 1000 cycles, the density of this category reached a more or less steady state. This suggests that the density value measured at permanent state represent the lower threshold density of the finest particles promoting recrystallization.

The link between the recrystallization and the growth of the largest particles has been also revealed. The density of particles having diameter between 1 and 2 μm increases gradually under thermal cycling and synchronously with the recrystallization degree. After 1000 cycles, the density of these particles category multiplied by 5 which shows that the presence of these particles accelerates the tin grain recrystallization and consequently the crack development.

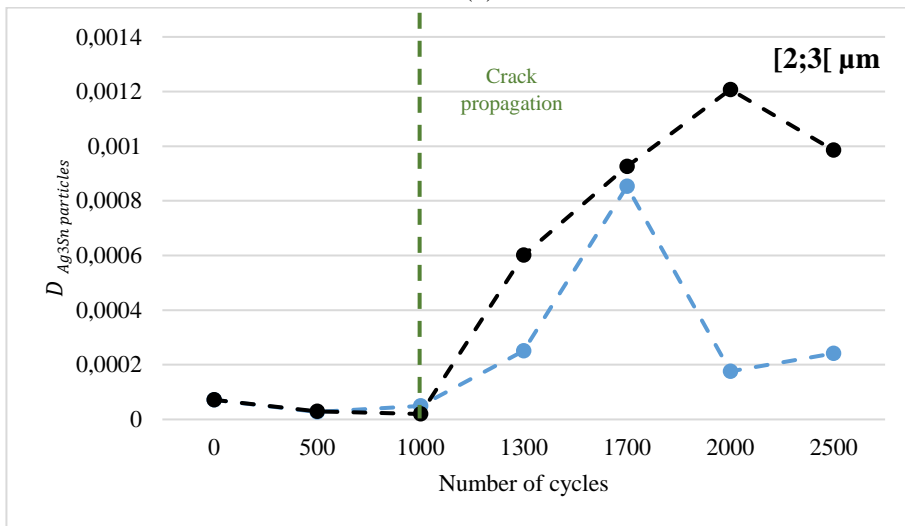
Bigger precipitates with diameters superior to 2 μm are detected only on samples taken out after 1000 cycles. The date of the appearance of this population corresponds to the time when the highest recrystallization degree was measured. This observation assumes that the largest IMCs constitute the most favorable particles for the tin grain recrystallization of the BGA solder joints. This population can be also considered as a factor that triggers crack propagation; the correlation with the measurements of the crack evolution shows that these particles appear at the phase of crack propagation.



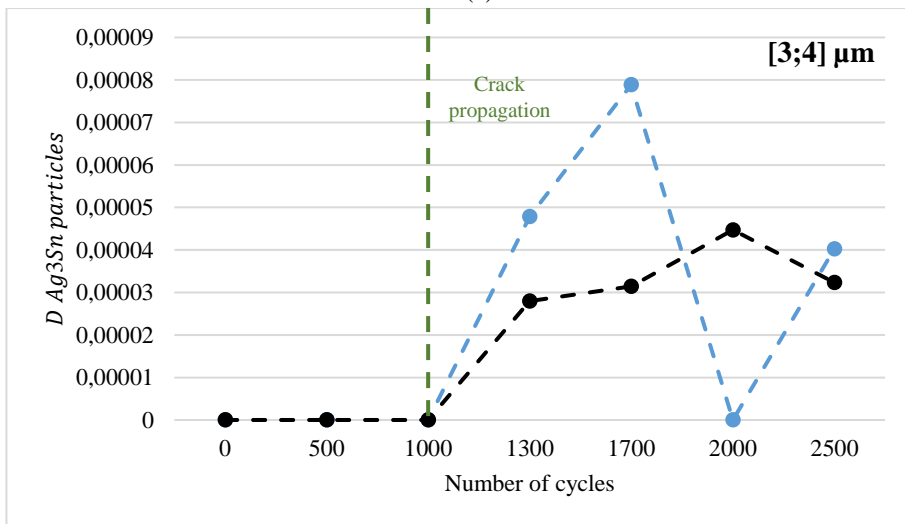
(a)



(b)



(c)



(d)

Figure IV.6–5: The evolution of the total density of Ag_3Sn particles in the BGA solder joints on the component and PCB sides for the four considered diameter intervals (a) $[0,1 ; 1[\mu m$, (b) $[1 ; 2[\mu m$, (c) $[2 ; 3[\mu m$ and (d) $[3 ; 4 \mu m$

IV.6.2 Comparison with the R1206 and QFN solder joints geometries

The quantitative analysis of the evolution of Ag_3Sn particles was also carried out on the QFN and R1206 components. Figure IV.6–6 shows the analyzed regions for this comparative study. This choice was made to validate the effect of the solder joint geometry.

During an EBSD acquisition, the detection threshold of Ag_3Sn particles depends on several parameters such as the width and height of the analyzed field, the resolution and the step size applied. The study of different solder geometries will surely affect these parameters and therefore the detection threshold of Ag_3Sn IMCs. The parameters applied for the analysis of the R1206 and QFN solder joints made it possible to detect Ag_3Sn particles having a diameter greater than $0.4\ \mu\text{m}$. However, the finest detected particles on the BGA interconnections have an equivalent diameter of $0.2\ \mu\text{m}$. The maximum equivalent diameter for the three analyzed geometries does not exceed $4\ \mu\text{m}$.

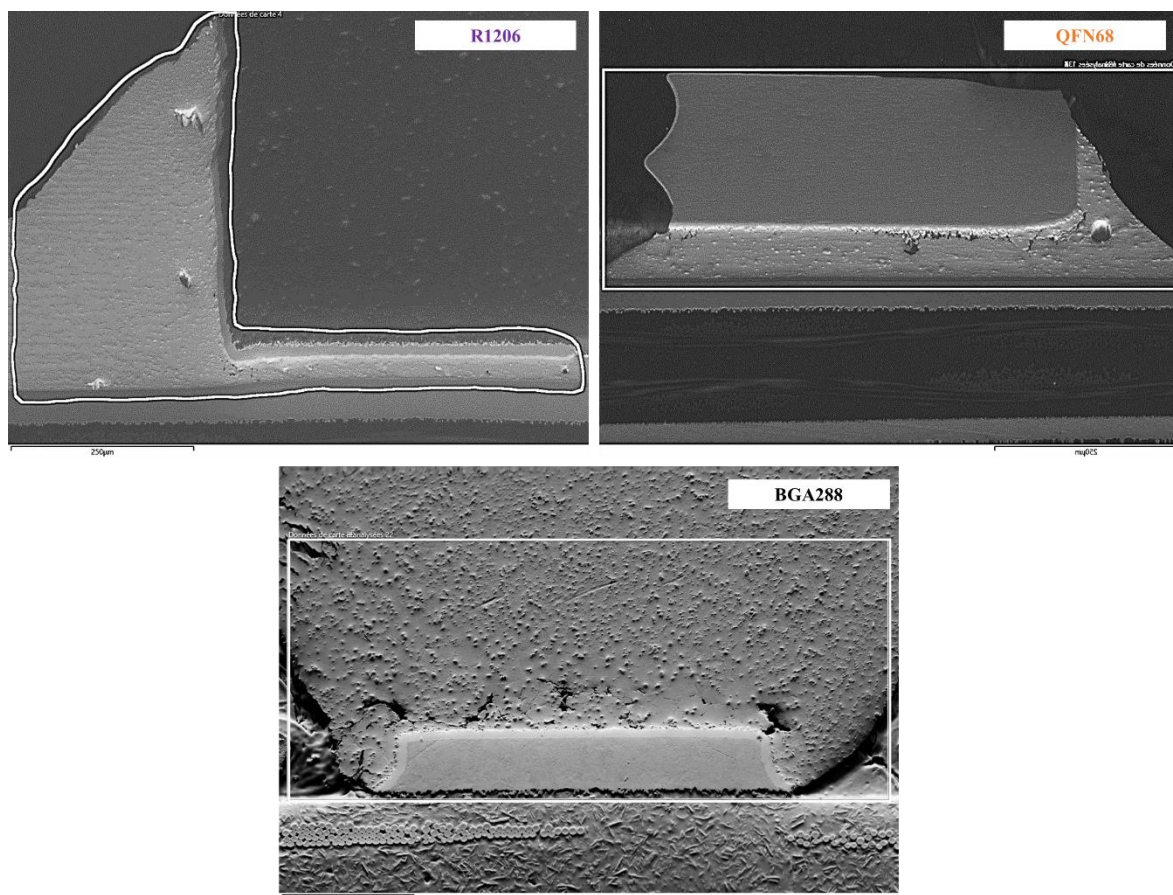


Figure IV.6–6: EBSD acquisition zone for each studied geometry

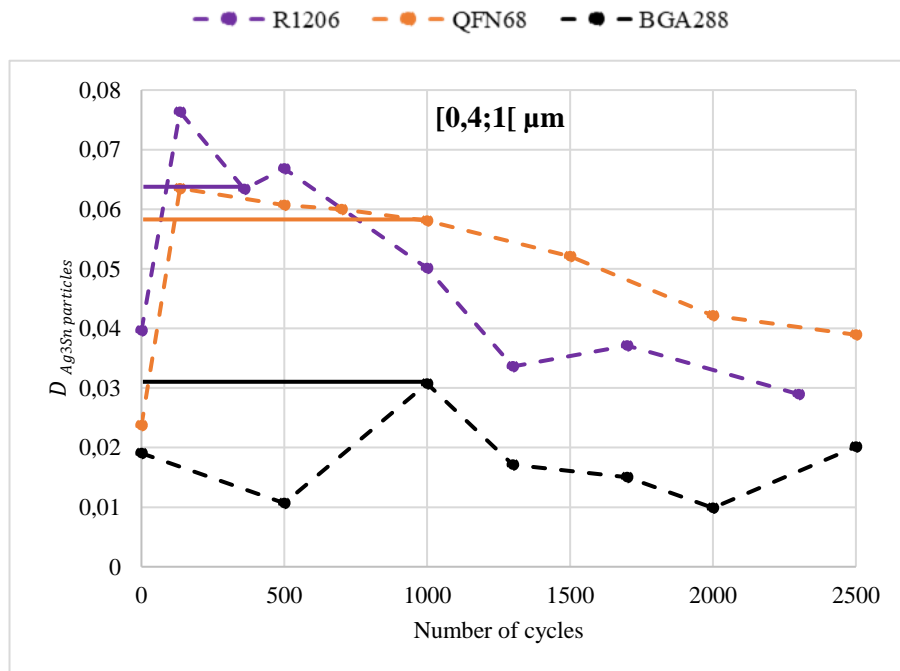
It is necessary to have a common diameter threshold allowing the treatment of the same populations of Ag_3Sn particles detected on the R1206, QFN and BGA solder joints. The study of the evolution of the density of the BGA Ag_3Sn particles having a diameter belonging to the interval $[0.4; 1[$ (black curve shown in Figure IV.6–7 (a)) shows that it presents the same behavior of those of the interval $[0.1; 1[$ (black curve shown in Figure IV.6–7 (a)). This assumes that particles with diameter inferior to $0.4\ \mu\text{m}$ do not affect the density evolution of Ag_3Sn

population having a diameter between 0.4 and 1 μm . We can then consider only this population ([0.4; 1[) to compare the behavior of the finest particles in the different studied solder joints. For larger particles, the diameter intervals [1; 2[, [2; 3[and [3; 4] μm were considered.

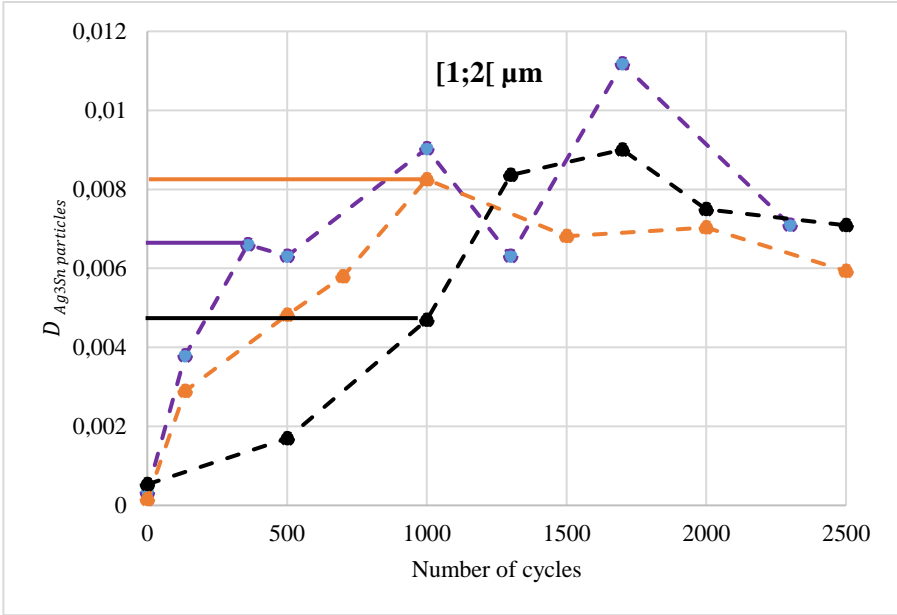
Measurements of the evolution of the Ag_3Sn IMCs density during thermal cycling show a similar behavior for the four diameter intervals on the R1206, QFN and BGA solder joints (Figure IV.6–7). The overall effects are shrinkage of smaller particles, and growth of larger particles.

Indeed, during the first cycles, an increase of the density of Ag_3Sn with a diameter between 0.4 μm and 1 μm was observed (Figure IV.6–7 (a)). This can be related to the coalescence of intermetallics having a diameter lower than the resolution of the EBSD analysis. Then, the density of this population decreases to promote the appearance of larger precipitates. This softens the solder alloy which accelerates the tin grain recrystallization under thermal cycles.

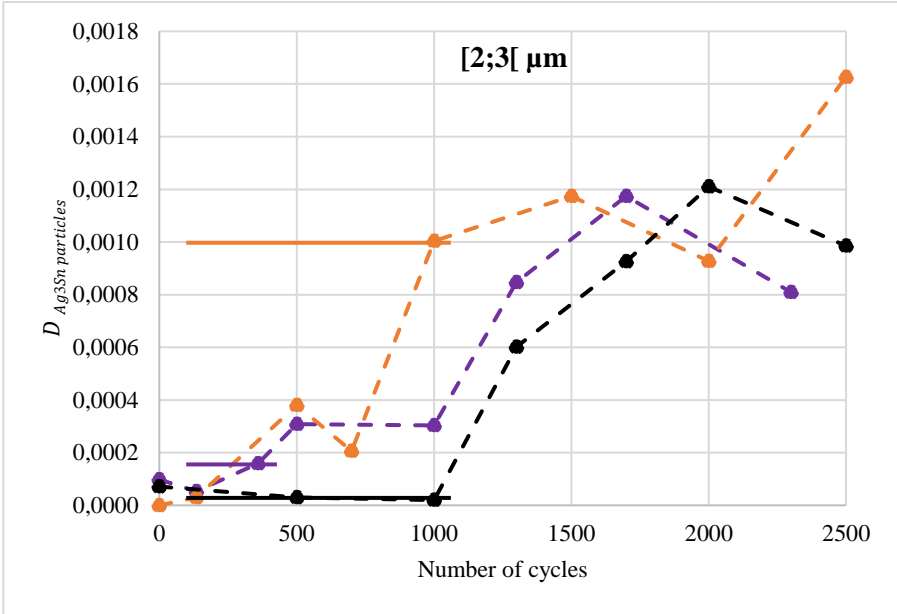
The growth of particles with higher diameter occurs at different times in the thermal cycle. The smaller the intermetallics, the earlier their density increase was observed. For precipitates with diameters between 1 and 2 μm , the density increases significantly from the first thermal cycles. The appearance of this population seems to be faster in the R1206 and QFN compared to the BGA geometry. At 500 cycles, the densities measured in the QFN and R1206 geometries are 3 and 4 times greater respectively than that of the BGA joint. After 1000 cycles, the density of this population no longer evolves and reaches a maximum value. This aspect has been observed in three types of solder. The maximum value of the density is of the same order in the three geometries. The density of these particles increases simultaneously with the recrystallization degree of tin grains.



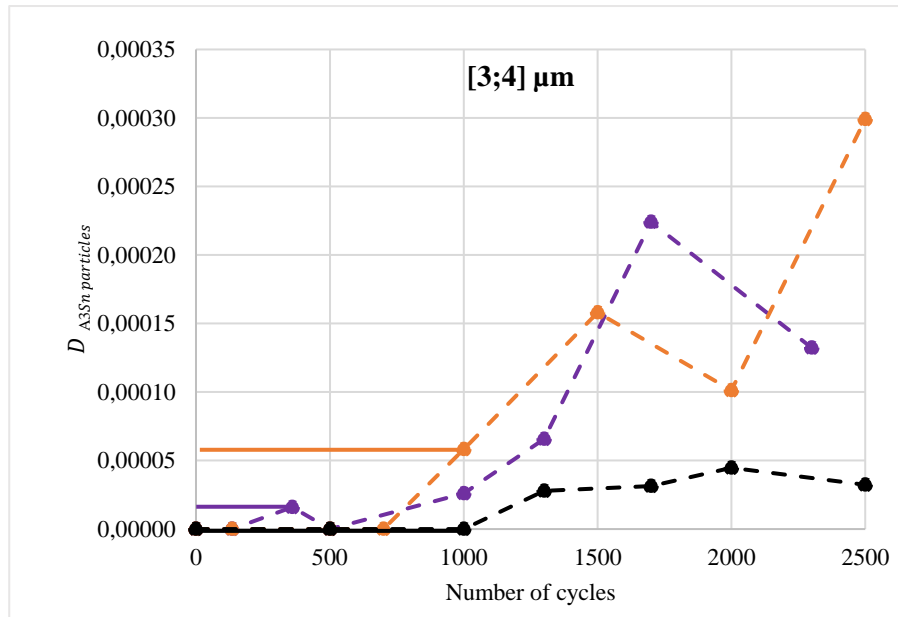
(a)



(b)



(c)



(d)

Figure IV.6-7: The evolution of the total density of Ag₃Sn particles in the R1206, QFN and BGA solder joints for the four considered diameter intervals (a) [0,4 ; 1[μm, (b) [1 ; 2[μm, (c) [2 ; 3[μm and (d) [3 ; 4] μm. (The continuous lines correspond to the densities promoting crack propagation on the different geometries)

For bigger precipitates with diameter superior to 2 μm, the coarsening phenomenon is mainly observed later in thermal cycling where the recrystallization degree reaches its maximum values for the three geometries. That is when the cracks start to spread which means that this population plays a favorable role in the intergranular crack propagation.

IV.6.3 Synthesis

The evolution of the size and the density of Ag₃Sn particles under thermomechanical loading was studied in the BGA, QFN and R1206 components. Measurements show that Ag₃Sn particles involved in the SAC microstructural damage have equivalent diameters between 0.4 and 4 μm whatever the solder geometries. This interval can be considered as a microstructural damage indicator common to the three studied geometries. The evolution of the Ag₃Sn density under thermal cycles is characterized by a decrease in the finest particles ([0,4; 1[μm) and an increase in the largest ones ([1; 4] μm). Precipitates with a diameter greater than 2 seem to be the most favorable for tin grain recrystallization. The date of their appearance correlates with the moment when the highest recrystallization degree was measured. It should be noted that the BGA, QFN, and R1206 geometries present the same behavior. The measurement of the equivalent diameter ranges of the Ag₃Sn particles and their densities can then be used to evaluate the damage state in a solder joint subjected to thermal cycles.

IV.7 Conclusion

A new approach for the assessment of the thermomechanical behavior of the lead-free solder joint has been described in this chapter. It combines electrical failure data, characterization of crack development and microstructural investigations through EBSD analysis to understand the link between fatigue life of lead-free solder and failure mechanism during thermal cycling. The main objective was to define a common microstructural criterion representative of the fatigue of different solder joints geometries subjected to accelerated temperature cycles.

Solder fatigue life analysis results allowed the comparison of the behavior of the different studied component (BGA, QFN and R1206). Lifetime results validate the different behavior of QFN solder joints. This was also observed in the previous chapter where a detailed description of the failure mechanism of the different studied solder joints under thermal cycling was established.

The lifetimes obtained from a standard electrical detection criterion were put into perspective with the crack evolution characterization to determine the most important phase on the SAC solder joint life service. Crack measurements emphasize that crack nucleation phase do not exceed 24% of SAC solder lifetime and that the crack propagation phase controls the durability of lead-free interconnections. On the other hand, the analysis of the crack evolution shows that the as-reflowed state of the SAC solder joints has a significant effect on their thermomechanical behavior. Observation shows that the presence of voids can accelerates the crack propagation which seems to be one of the causes of early failures appearance which agrees with literature. This highlights the necessity of inspecting the voids distribution after the assembly process. The interfacial cracks can be responsible of premature failure. Measurements have shown that their propagation is faster than intergranular cracks.

However, the intergranular cracking represents the most observed failure mode on BGA, QFN and R1206 solder joints under thermal cycling. The tin recrystallization and the Ag_3Sn coarsening previously described in chapter III are common processes necessary for the intergranular crack propagation in the different solder geometries. The size of recrystallized grains and the degree of recrystallization, the size of Ag_3Sn particles and their density have been defined as microstructural indicators allowing monitoring the microstructural change of the SAC solder alloy. The correlation between the evolution of these indicators and the crack development under thermal cycles was presented to define the microstructural state promoting the crack propagation.

The quantitative analysis of tin grain recrystallization shows that the equivalent diameter of recrystallized grains is between 1 and 30 μm for the BGA, QFN and chip resistor component and whatever the level of cycling. The recrystallized grain size can be considered as a feature of the solder alloy. The grains having 30 μm seem to be responsible for the crack propagation and therefore need to be implemented in numerical models to improve the accuracy of life prediction results. The correlation between the evolution of the recrystallization degree and the crack phases highlights that crack propagation does not need total recrystallization of the high strain region. A well-defined degree of recrystallization is required to trigger crack propagation.

This degree is of the same order for the BGA and R1206 geometries which are characterized by a common purely intergranular cracking mode. A higher recrystallization degree is required for the crack propagation on QFN solder joints. This can be due to their different behavior characterized by the mixed cracking mode which is a competition between the interfacial and intergranular cracks.

The study of the evolution of the size and the density of Ag_3Sn particles in the BGA, QFN and R1206 components shows that particles involved during the microstructural damage have equivalent diameter between 0.4 and 4 μm . The behavior of these particles under thermal cycles is similar for the three studied geometries. The density evolution of these particles during the thermal cycles shows a decrease for the particles having a diameter inferior to 1 μm and an increase of those with diameter superior to 1 μm which is representative of the loss of dendritic structure.

Therefore, the size of recrystallized grains and the recrystallization degree, the size of Ag_3Sn particles and their density can be used as a way of measuring the aging state of solder joint presenting a similar cracking mode.

Chapter V. Different factors affecting solder joint reliability under thermomechanical fatigue

V.1 Introduction

A myriad of factors can influence the thermomechanical performance of SAC solder joints. The results from chapters 3 and 4 emphasize that QFN solder joints have different behavior compared to the BGA and R1206 joints. The material properties and the design of the assembly may have an effect on the thermomechanical behavior of lead-free package. The SAC alloy microstructural state before thermal cycling and the position of the solder joints in the electronic package are also influent parameters to the reliability of electronic assemblies. In this chapter, a study of these parameters will be presented in order to identify those that should be considered in the prediction of the SAC solder joints lifetime.

Accelerated testing, failure analysis, microstructural investigation and finite element modelling are the considered tools in this chapter to evaluate the impact of each factor on the SAC interconnections response under thermomechanical loading. The microstructural damage indicators identified in the previous chapter will also be used to quantitatively analyze the different aspects on the BGA, QFN and R1206 components.

The effect of isothermal pre-aging will be the first aspect studied in this chapter since this condition can influence the SAC solder properties. Lifetimes data and microstructural characterization will be used to study the impact of isothermal aging on the thermomechanical durability of SAC solder joints. The influence of the SAC solder joint location under thermal cycling will be then investigated by studying the behavior of several solder joints at different position on the BGA components. Finally, the as-reflowed microstructure of the SAC alloy will be also studied as a factor having an important role to progress on the reliability study of solder joint under thermal loading.

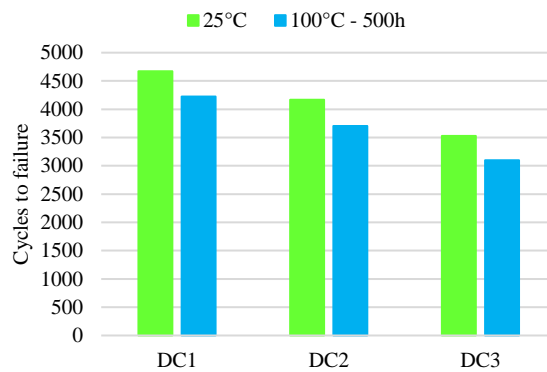
V.2 Effect of pre-aging on SAC solder joint under thermal cycling

V.2.1 Lifetime's analysis

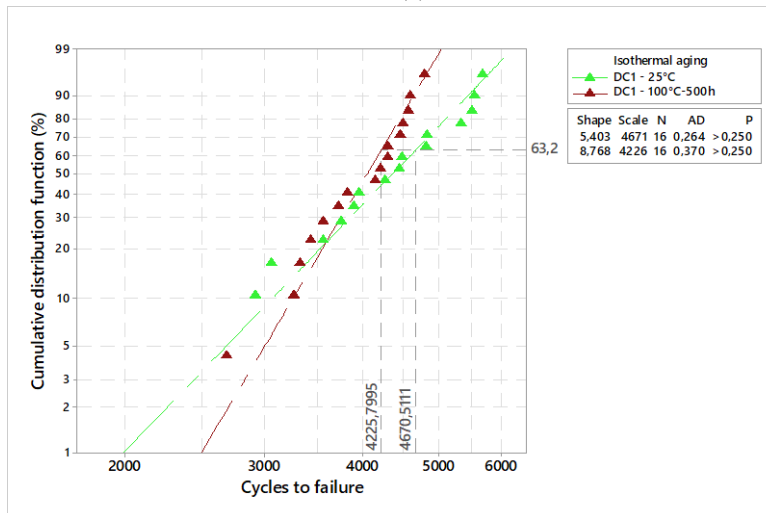
(a) *Effect of pre-aging as function of solder geometries*

i. BGA component

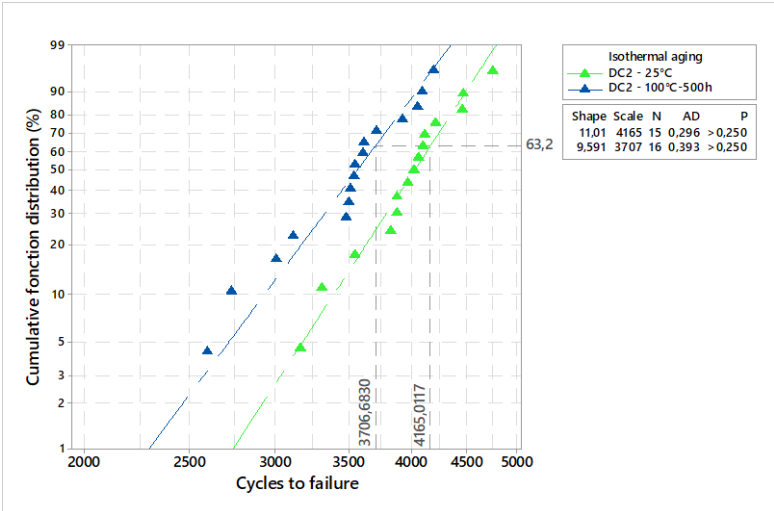
The effect of pre-aging on the lifetime of BGA joints was studied for the three daisy chains. Figure V.2–1(a) confirms a moderate reduction (10-12%) of the characteristic lifetime with aging at 100°C in the various rings. The Weibull distributions allow easily the revelation of this effect on the two internal daisy chains (Figure V.2–1 (c) and Figure V.2–1 (d)). The analysis of the results is more complex for daisy-chain 1 (external balls) because the dispersion of failures is very wide for boards aged at room temperature (Figure V.2–1 (b)).



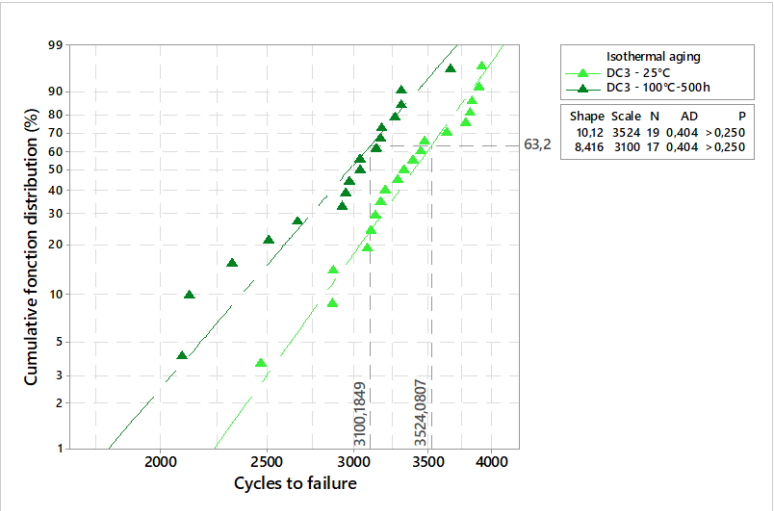
(a)



(b)



(c)



(d)

Figure V.2–1: Effect of pre-aging at 100°C on the lifetime of BGA joints in the different daisy-chains (a) number of cycles to failure of each daisy chain for a pre-aging at 25°C and at 100°C- 500h (b) Weibull distribution of daisy chain 1 (DC1), (c) Weibull distribution of daisy chain 2 (DC2), (d) Weibull distribution of daisy chain 3 (DC3)

ii. QFN component

Storage at 100°C does not seem to have any impact on the thermal cycling life of QFN solder joints. Comparing the results, the fatigue lives do not seem to be impacted by isothermal pre-aging. This is an unexpected result when compared to those in the literature; from these results, we can validate that in our study the heat treatment has no effect on the as-reflowed microstructure of the QFN solder joints.

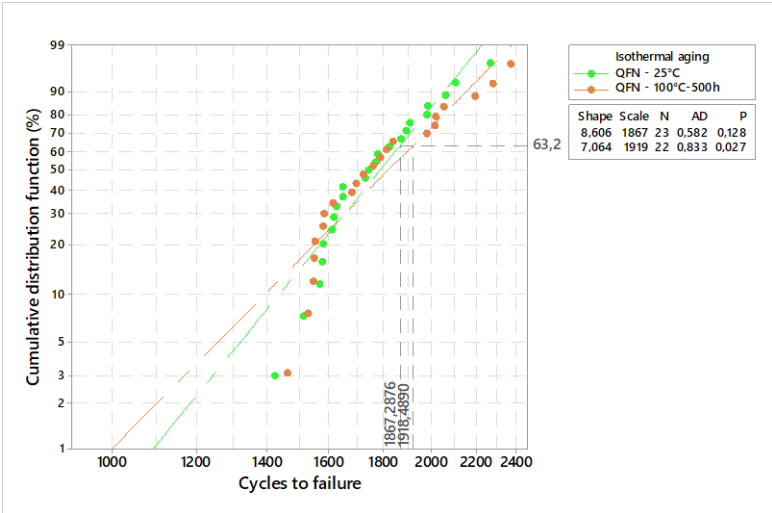


Figure V.2-2: Effect of pre-aging at 100°C on the lifetime of QFN solder joints

iii. R1206 component

As explained in section IV.4.4 , the parallel connection of the resistors 1206 has delayed the failure detections. It did not provide enough data for the pre-aging condition at 20°C for quantitative analysis (Table V.2-1). However, we can consider that the pre-aging at 100°C has accelerated the failure detection since the same failure criterion was applied for both conditions.

Table V.2-1: Failure dates in resistor daisy chains connected in parallel

	Number of cycles to failure
Pre-aging at 20°C	3740, 4354
Pre-aging at 100°C	3900, 4520, 4600, 4723, 4838, 4954, 5189, 5641, 5787

(b) Effect of different pre-aging and thermal cycling conditions

In this section, only the BGA solder joints were considered. Two temperatures (100°C, 150°C) and three durations (100h, 500h, 1000h) were investigated. ATC was performed between -55°C and 100°C (TC1) and between -55°C and 125°C (TC2). A 3-parameter Weibull distribution was used to model the number of cycles to failure. A better correlation was found with a 3-parameter distribution than with a 2-parameter one [97].

Comparing the results for the components exposed to the two thermal cycling tests, the fatigue lives are significantly longer in TC1 than in TC2 (Table V.2–2). For identical isothermal aging conditions, the acceleration factor between the two cyclic loading conditions is between 1.6 and 1.8. The fatigue life was slightly impacted by a prior aging at 100°C.

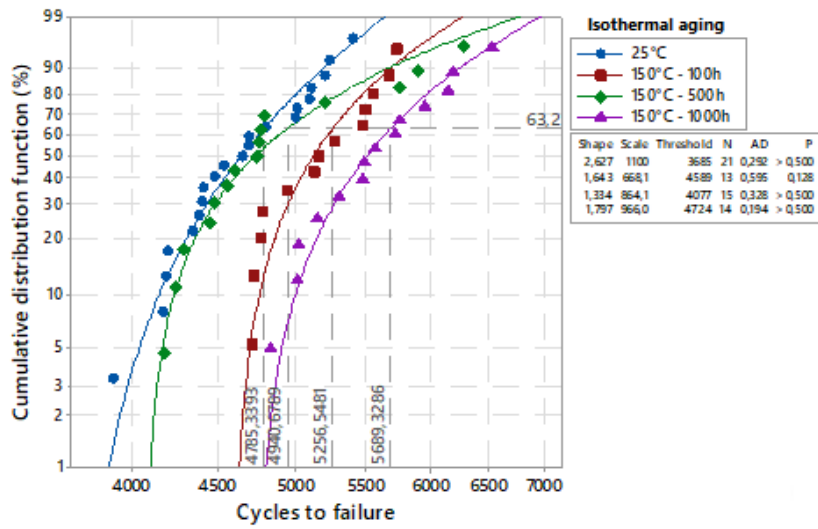
From one aging condition to another, the variations of the $\gamma + \eta$ value did not exceed 18% for TC1 and 11% for TC2. In each TC condition, a small life improvement was observed after 100h of aging at 100°C. These mild aging conditions must have removed residual stresses in the joints.

Nevertheless, extended exposure at 100°C proved to lower the solder lifetime. With a thermal aging at 150°C, the fatigue lifetime unexpectedly increased. The variations are moderate (<19%) but the longest lifetimes were measured for the most severe aging conditions (1000h at 150°C). These results imply a time and temperature dependent failure of the solder joints.

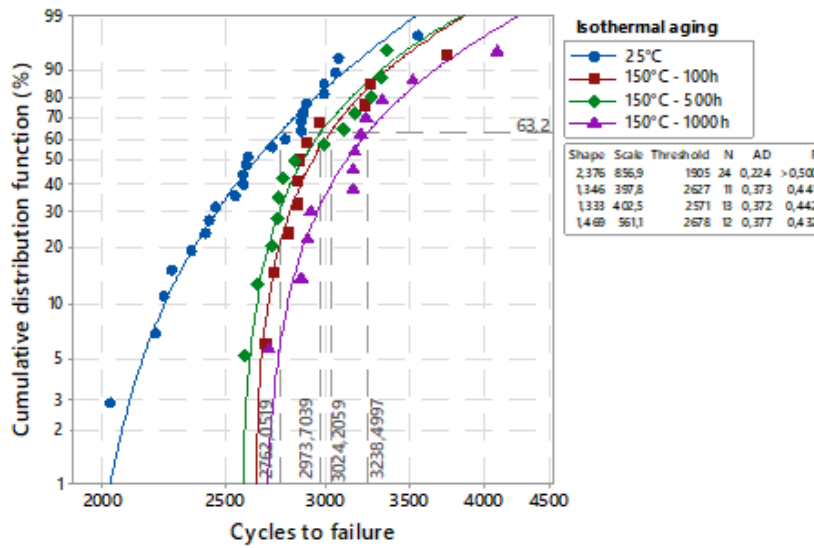
Table V.2–2: Thermal cycling failure data, with different prior isothermal aging conditions

Test conditions	Weibull parameters		
Thermal cycling –55 °C ↔ 100 °C	Shape β	Scale η	Threshold γ
Aging at 25 °C	2.6	1100	3685
100 h at 100 °C	1.8	761	4237
500 h at 100 °C	1.4	775	3463
1000 h at 100 °C	1.8	1012	3236
100 h at 150 °C	1.6	668	4589
500 h at 150 °C	1.3	864	4077
1000 h at 150 °C	1.8	966	4724

Test conditions	Weibull parameters		
Thermal cycling –55 °C ↔ 125 °C	Shape β	Scale η	Threshold γ
Aging at 25 °C	2.4	857	1905
100 h at 100 °C	1.4	604	2358
500 h at 100 °C	2.3	580	2084
1000 h at 100 °C	2.4	600	2080
100 h at 150 °C	1.3	398	2627
500 h at 150 °C	1.3	403	2571
1000 h at 150 °C	1.5	561	2678

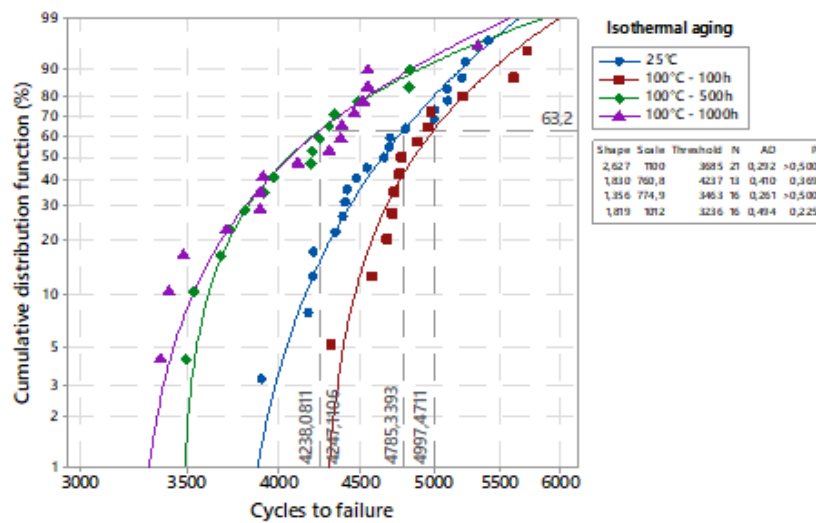


(a)



(b)

Figure V.2-3 Effect of prior aging at 100 °C on failure in BGA solder joints, thermal cycling from - 55°C to 100°C (a), from - 55°C to 125°C (b)



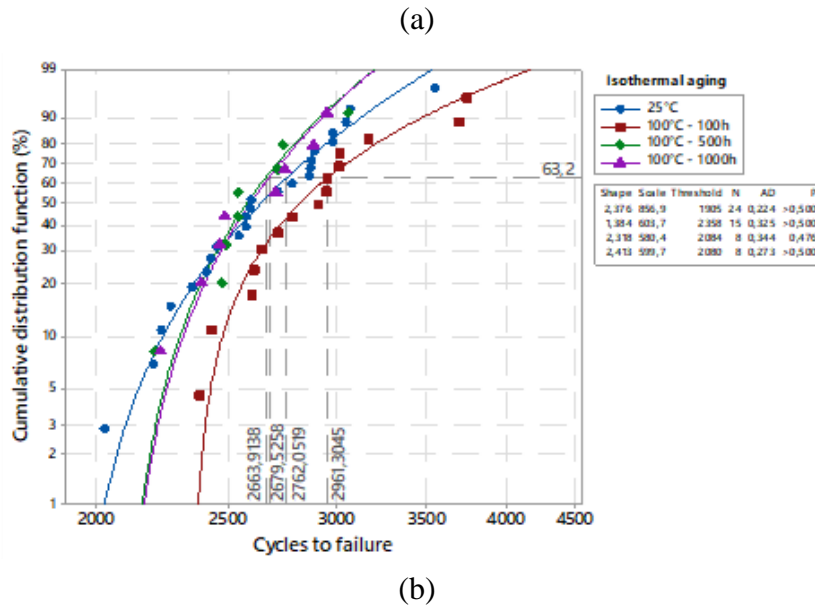


Figure V.2–4: Effect of prior aging at 150°C on failure in BGA solder joints, thermal cycling from -55°C to 100°C (a), from -55°C to 125°C (b)

V.2.2 Microstructural and failure analysis

The analysis of specimens in which failure had been electrically detected revealed that the main failure mechanism involved tin recrystallization and strain-enhanced precipitate coarsening. The combination of these microstructural processes led to intergranular cracking that starts in the solder neck and propagates in the near-package or near-PCB region. No difference in failure was noticed between the TC1 and TC2 conditions. The strong microstructural degradation and cracking were already noticeable before failure detection (Figure V.2–5).

Unlike isothermal aging, thermal cycling induces precipitate coalescence in a more important, strain-dependent and localized way [105]. The solder recrystallized and coarsened area provides a favorable path for crack propagation. At the solder level, the failure mechanism also seemed to be the same regardless of the prior aging conditions. As the SAC alloy softens with aging and Ag₃Sn coarsening, its creep strain rate increases [44][105]. It is then possible to explain that the microstructure evolution caused by a prior aging can make solder joints fail faster in thermal cycling [44][98].

On the other hand, the prolonged lifetimes that were measured after aging at 150°C suggest that there may be a threshold in precipitate density and softening beyond which the solder can withstand more strain before cracking. A local creep and hardness characterization of the aged solder joints could confirm these differences in mechanical properties and their dependence on microstructure [106]. In this case, solder may not be necessarily the weak point of the assembly and cracks could initiate first elsewhere.

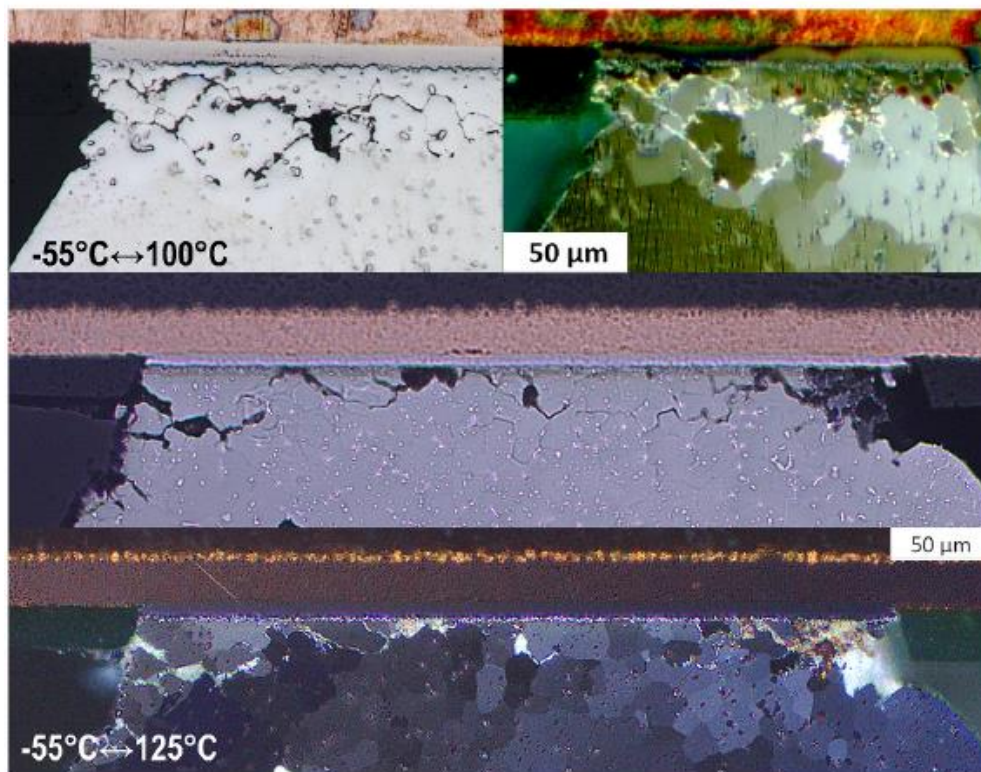


Figure V.2-5: Recrystallization and precipitate coarsening assisted failure of solder joints in thermal cycling, - 55°C to 100°C (TC1) and - 55°C to 125°C (TC2), white and polarized light observation after electrical failure detection

Cracking in the laminate was specifically investigated in order to explain the variations in fatigue life. This phenomenon is known to occur more easily in thermal cycling with lead-free assembly processes [107][108] and non-solder mask defined (NSMD) pad configuration [109]. Even very small PCB cracks induced by the soldering process could change the dominant failure mode in thermal cycling from solder cracking to pad cratering. Laminate cracking may lower the stress on the solder joints resulting in a longer fatigue life. Akbari et al. showed that very small cracks in the PCB may reduce accumulated creep strain and work in the solder joints [110]. Hence, there is a risk of life overestimation in accelerated testing in comparison with field conditions that imply milder conditions [108]. No crack was found in the resin substrate on the package side. However, several partial cracks were observed on the PCB side after various aging and thermal cycling conditions (Figure V.2-6). The largest number of cracks was found in samples that experienced the harshest aging conditions (1000 h at 150°C). Thermomechanical analysis carried out on aged and non-aged PCB samples (Table V.2-3) revealed that the initial glass transition temperature ($T_g=149^\circ\text{C}$) had undergone a shift of 17°C after 1000h of exposure at 150°C. An aging of the board laminate near its T_g might modify its structure and induce a degradation of its mechanical properties. The softening of the solder alloy and the modification of the PCB material could explain that cracking occurs first in the laminate under the solder pad.

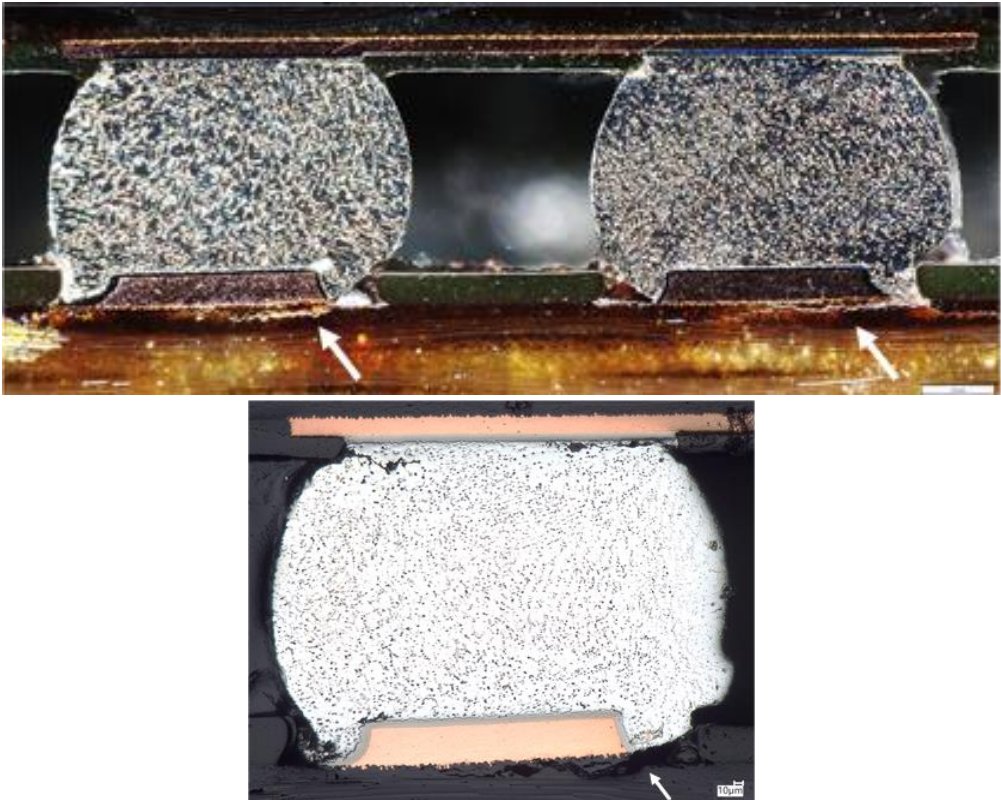


Figure V.2–6: Laminate cracks under solder pads after harsh isothermal aging (1000h at 150°C) followed by thermal cycling (-55°C to 100°C)

Table V.2–3 Coefficient of thermal expansion (CTE, in ppm/K) and glass transition temperature (T_g) measurements on the board material before and after severe isothermal aging.

Aging conditions	CTE _x		CTE _z	
	[20; 120]°C	T < T _g	T _g	T > T _g
25 °C	16.7	40.1	149 °C	189
150 °C – 1000 h	15.4	47.1	166 °C	221

V.2.3 Synthesis

This section deals with the effect of isothermal prior aging on the solder microstructure and fatigue lifetime of the BGA, QFN and chip resistor components. The tested aging conditions (time, temperature) induced various differences in thermal cycling failure data. Even if the complete propagation of cracks was detected and observed in recrystallized regions of solder joints as usual, the fatigue lifetimes were slightly lowered by aging at 100°C and increased by aging at 150°C. It can be explained by the softening of the solder being replaced as the weakest part and delaying the failure after cracking occurred in the PCB laminate.

V.3 SAC solder joint location effect under thermal cycling

The location of a solder joint is a very important factor for the lifetime of lead-free electronic assemblies under thermomechanical conditions. Lifetimes results presented in the previous chapter show that the BGA solder joints under the die edge have the lowest durability compared to the other interconnections located elsewhere. However, even with these data, it is not possible to predict the first failure position. Failure analysis and microstructural investigations were carried out on the interconnections under the component edge and those under the die edge to better understand the effect of the solder location on the thermomechanical BGA package behavior and to correlate with lifetimes results.

V.3.1 Solder joint behavior under component edge

We started by an optical inspection of all solder joints present under the component edge. Observations were made on components taken out successively during thermal cycles to localize the very first cracks. The analyses show that the most evolved solder joints are the closest ones to the corner of the component.

The studied balls under the component edge (row A) are the five ones close to the package corners because these positions seem to be the most vulnerable to thermal cycling due to their distance from the neutral axis. The symmetry of the component makes it possible to consider that the positions A1 – A5 are equivalent to the positions A22 – A18. In this part, EBSD analysis were carried out with low magnitudes allowing the study of the five solder joints for different levels of thermal cycles. The recrystallization degree was thus calculated for each solder joint with the ImageJ software. The measurement steps were described in detail in the previous chapter.

Figure V.3–1 shows the evolution of the recrystallization degree under thermal cycling and as a function of the SAC solder joints positions. A trend appears since the most damaged balls in the row A are almost systematically those located at the corners of the components (red bars which represent position A1 or A22 in Figure V.3–1 (b)). This therefore confirms the results of the literature according to which, in the BGA components, the distance to the neutral point is a factor which accelerates the kinetics of recrystallization. From the cracking point of view, the observations up to 3000 cycles have shown that only the solder joints at the corner of the component have total cracks. This validates that the corner joints represents the most critical position under the component edge (row A).

However, we can clearly see that the second most recrystallized solder is not necessarily located near the corner interconnections. For example, Figure V.3–1 (b) and Figure V.3–1 (c) reveal that the second highest degree has been measured for the samples taken at 2700 in the solder A4. It is also interesting to note that the recrystallized grain size is always in the same range identified previously at any position of the joint.

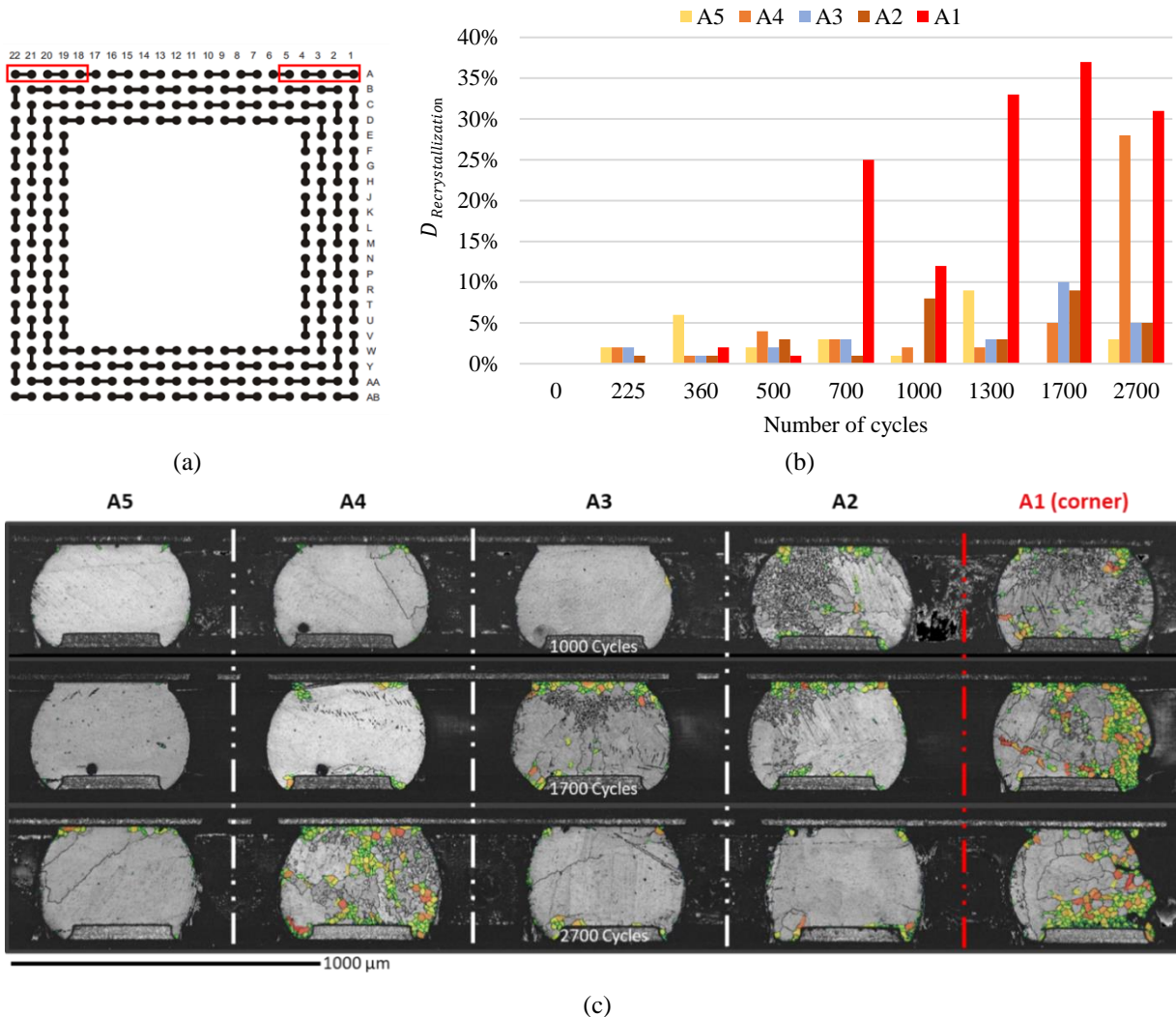


Figure V.3–1: Influence of the solder position under the component on the recrystallisation degree evolution during thermal cycling (a) position of the analysed solder joints in row A (b) histogram of degree of recrystallization as a function of the position of the solder joint (c) recrystallized tin grain size maps of samples taken out at 1000, 17000 and 2700 cycles

V.3.2 Solder joint behavior under silicon die edge

The lifetime analysis revealed that the first failure date and the average lifetime of the inner daisy-chain solder joints were lower than those of the other interconnections (die shadow effect). Microstructural analyses showed that the failure mechanism is based on the same microstructural phenomena, whatever the position in the balls matrix. However, it is the path of the cracks which varies from one characteristic position to another, which seems to be directly related to stress distribution differences (Figure V.3–2). The stress responsible for damaging of the component corner solder seems to be the maximum shear stress, which causes the propagation of recrystallization in the diagonals and not only at the interfaces with the PCB and the component. Contrary to what is observed in row A, the recrystallized solder joints appear to be distributed more homogeneously on the internal ring and not only at the die corner.

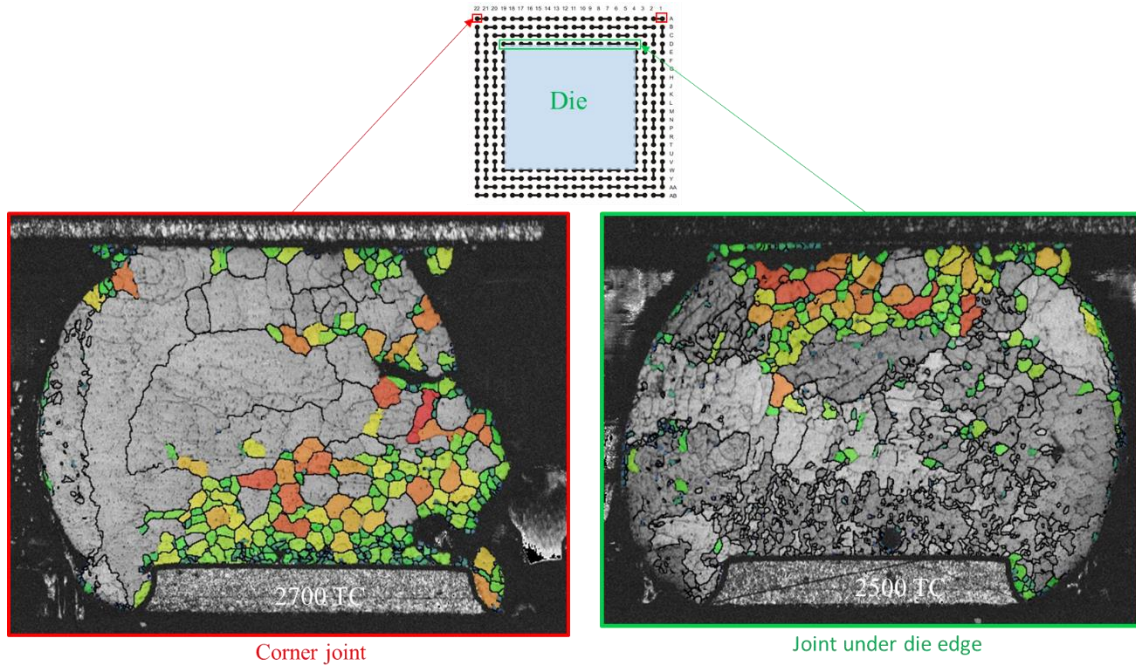


Figure V.3-2: Comparison of the location of recrystallization and cracking under thermal cycling between two characteristic positions in the BGA matrix

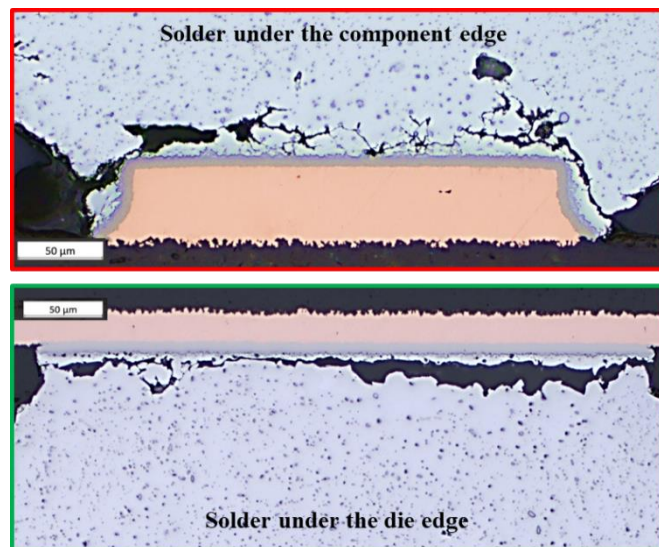


Figure V.3-3: Total cracks observation on the BGA corner solder and

The recrystallization of solder joints under the die edge develops most of the time on the upper side of the joint, i.e. near the die side. It is important to note that the recrystallized grain size is not impacted by the position of the solder joint. The same grain size range was found on the solder joints under the die edge

The recrystallized distribution is often correlated with crack propagation paths. The cracks of the most critical solder (A1) under the component edge propagate down the joint near the PCB or follow a diagonal path. The cracks of the solder joint located under the die edge develops in the upper part of the solder joint near the die side.

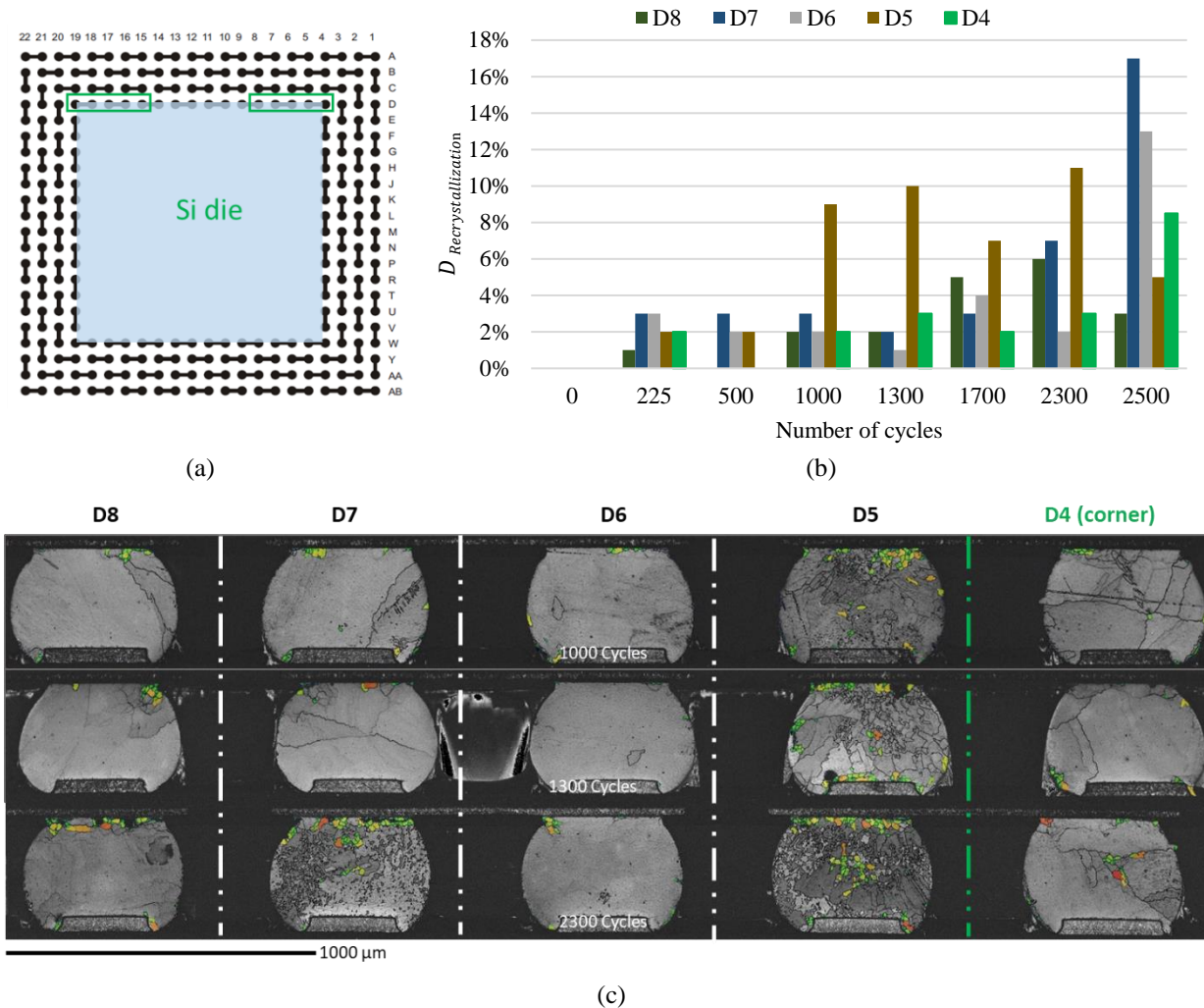


Figure V.3-4: Influence of the solder position under the die edge on the recrystallisation evolution during thermal cycling (a) position of the analysed solder joints in row D (b) histogram of degree of recrystallization as a function of the position of the solder joint (c) recrystallized tin grain size maps of samples taken out at 1000, 1300 and 2300 cycles

The cracking in the joints below the edge of the die appears to be straight compared to known intergranular cracking (Figure V.3-3). Tensile stress is often the cause of this mode of cracking. This assumes that the interconnections under the component edge and those under the die edge are not subject to the same type of stress. The propagation rate of this type of crack can be higher than that of intergranular propagation. Total cracks will therefore appear first in the joints under the die which can clarify the results of failure detection by electrical monitoring. However, the microstructural analyzes at different thermal cycling allowed us to correlate between the main phenomena of microstructural damage (tin grain recrystallization and Ag_3Sn particles coarsening) and the development of the crack under the joints under the die. It can then be considered as intergranular cracking mode.

On the other hand, the micro-sections carried out within the inner row did not show any preferential position for cracking. Several total cracks can be observed at different positions of the row under the die edge. Conversely, observations of the outermost ring identified the corner joint as the one that always cracked first. Analysis of the recrystallization degree evolution has

been also investigated in order to better understand the behavior of the SAC interconnections under the die edge (row D). The results presented here are only those of the five solder joints under the corner of the silicon die (positions D4 – D8 and D15 – D19 shown in Figure V.3–4(a)) to study the effect of distance from the neutral axis.

Figure V.3–4(b) shows the evolution of the SAC solder recrystallization degree under thermal cycling on studied positions. It reveals a more or less homogeneous increase in the degree of recrystallization of the five analyzed positions. The most recrystallized solder is not the located under the die corner and no position seems to be preferential to the development of recrystallization. This correlates with total cracks observations where no position appears to be critical to the failure of the interconnections under the die. From these results, we can conclude that the distance of a joint located under the die edge to the neutral axis does not represent a factor which accelerates the failure of the solder joints.

It is also interesting to note that the comparison between the maximum values degrees of maximum recrystallization reached by the joints located on the rows A and D shows that the degree of recrystallization is much more important on the joints under the component edge than on under the die (37% and 17% respectively). This can be explained once again by the different stress distributions applied on each joint.

V.3.3 Finite element simulation

Numerical modeling is a good tool to better understand the origin of the different behaviours of the solder joints under the die edge compared to those under the corner of the component. Due to the symmetry of the BGA package, only a quarter has been modeled in order to lighten the simulation model and reduce the calculation time. The dimensions are those of the BGA component assembled on our test vehicles. Figure V.3–5 shows the different elements considered in the FE model. This model was optimized, mainly by refining the mesh only of the solder joints.

A temperature drop from the reflow point (230°C) to the ambient (25°C) followed by one thermal cycle (-55/125°C) has been applied on the model. A fixed point allowing to block the displacements in the three dimensions of space is applied to the lower face of the PCB.

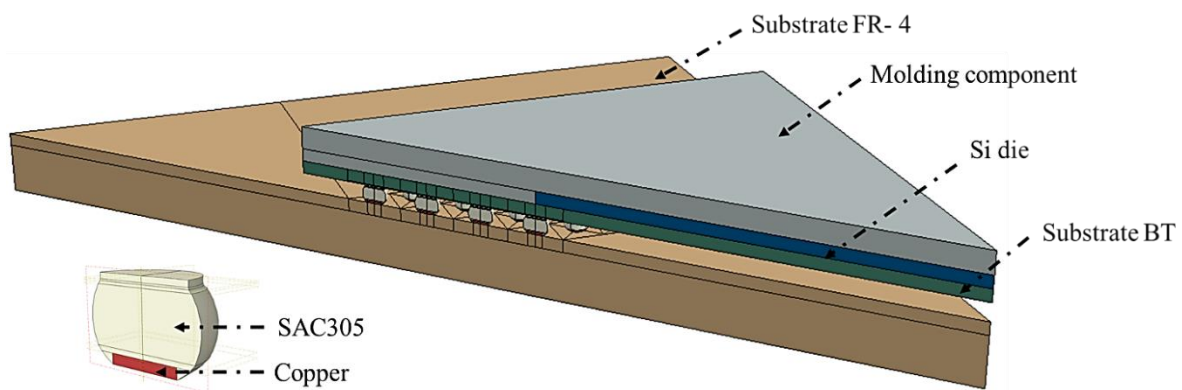


Figure V.3–5: BGA assembly model

Table V.3–1 and Table V.3–2 show the material properties of each element considered on the BGA package. Anand's law was chosen to model the creep behavior of the SAC solder joint. All other materials have a linear elastic behaviour. Two types of component molds were used in this study (mold A and mold B). Mold A has a different materials properties on the first step of loading (temperature drop) compared to the thermal cycle. However, the materials properties of the Mold B are constant throughout the two steps. The equivalent creep strain was calculated in this study.

A first configuration using the Mold A properties was generated to locate the critical joint in the BGA component. This configuration presents the closest properties to the reality and what is often found in bibliographical studies

Simulation results show that the critical solder ball is under the component corner (Figure V.3–6 (a)). The calculations clearly show the effect of the distance to the neutral point. The farthest balls from the center of the component are the most strained solder joints. Observations confirm that critical solder joints under the component edge are often located in the corner. However, lifetime analysis revealed that solder joints under the component edge do not necessarily have the lowest durability and those under the die edge are the most critical.

This shows that the properties used in this configuration do not allow the accurate prediction of the location of the critical joints leading to the failure of the BGA component. A second configuration has therefore been studied by considering the mold B. The goal was to simplify the model and identify the effect of the mold properties on the location of the critical joint.

Table V.3–1: Thermo-elastic properties implemented in the FE model [90]

Materials		Young's modulus (GPa)	Poisson ratio	CTE (ppm/°C)
Substrate FR-4		25 (x,z)	0.18 (xy,zy)	18 (x,z)
		22 (y)	0.15 (xz)	50 (y)
Substrate BT		26 (x,z)	0.39 (xy, zy)	15 (x,z)
		11 (y)	0.11 (xz)	52 (y)
Mold	A	10, 25<T<165°C 1, 175<T<230°C	0.25	18, 25<T<165°C 120, 175<T<230°C
	B	10	0.25	18
Si die		131	0.28	2.8
Copper		120	0.34	17
SAC305		50, 50°C 45, 125°C 0.1, 230°C	0.35	22

Table V.3–2: Parameters of the viscoplastic Anand model for the SAC305 alloy [79]

A	ξ	h ₀	n	s	m	a	Q	R
1.08e3	0.0558	9.5e8	4.6e6-3	1.04e6	0.162	1.56	69e3	8.32

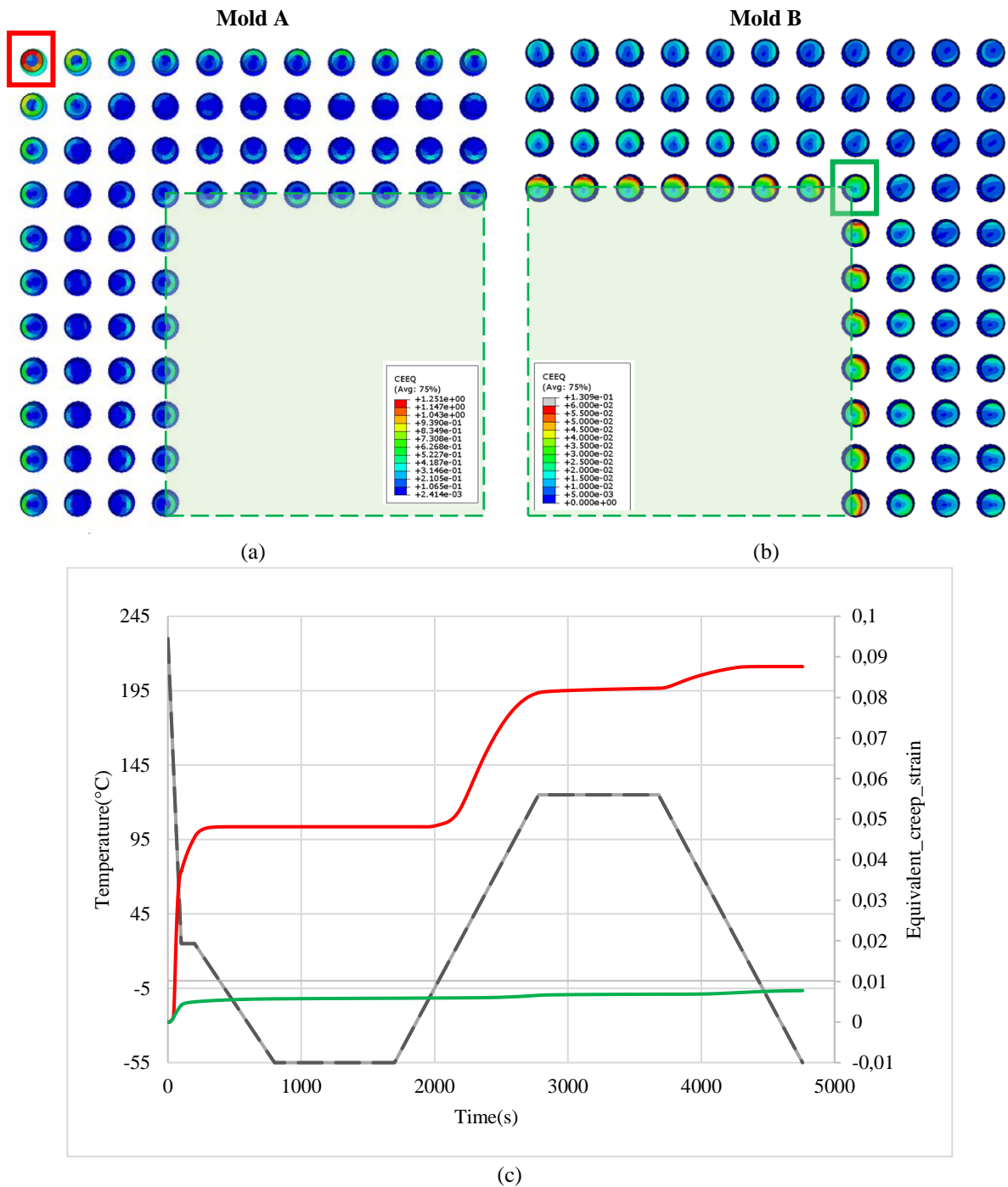


Figure V.3-6: (a) Equivalent creep strain distribution on BGA sold joints of the first configuration (Mold A), (b) Equivalent creep strain distribution on BGA sold joints of the second configuration (Mold B), (c) evolution of the maximum equivalent creep strain on the component corner solder joint of model with Mold A (red curve) and the die corner solder joint of model with Mold B (green curve)

FE simulations by implementing the properties of Mold B show that the equivalent creep deformation is maximum in solder balls located under the edge of the die. Thus, these balls are clearly identified as the most stressed balls in the assembly. These results correlate with the results of failure detection by electrical monitoring where it has been found that the solder joints at the die edge present the shortest lifetimes. However, no position under the die edge appears to be critical and all balls are subjected to nearly equal strain levels. Observations validate that the cracks are not necessarily under the die corner but they appear randomly on the different balls at the die edge. The microstructure of these solder joints seems to play an important role in the location of crack appearance. This aspect will be discussed in more detail in the next paragraph.

On the other hand, the level of equivalent creep strain measured on the die corner solder joint of simulation with Mold B (green curve) seems to be very low compared to the component corner solder joint of model with Mold A (red curve). The stress applied by the die seems to be evenly divided over all the solder joints present on its edge which can explain the low level of equivalent creep strain observed on these joints. The properties considered for the Mold B can be also the cause of this result.

These observations show that the good characterization of each material properties of the assembly is an essential task for the accurate prediction of affect the location of the most strained solder joints.

V.3.4 Synthesis

A comparison between the behavior of solder joints located under the die edge and those under the component edge has been made in this section to study the effect of the solder joints position on the reliability of lead-free assemblies under thermal cycling. Results show that the distance to the neutral point does not always identify the position of the critical solder joint. The die shadow effect was a more detrimental factor than the DNP and no position appears to be detrimental for the solder joint cracking under the die edge.

It is also interesting to note that the most cracked solder in this study present the mixed morphology. Thus, the effect of the as-reflowed microstructure on thermomechanical behavior of SAC solder joints will be presented in the next section.

V.4 Effect of the as-reflowed microstructure

Another factor influencing the thermal cycling behavior of solder joints is their initial microstructure. The microstructure of SAC solder joints after reflow is characterized by diverse tin grain morphologies with random crystalline orientations. Due to this complex as-soldered microstructure and coupled with the highly anisotropic properties of the tin grain, the thermomechanical response of SAC solder joints greatly depends on the morphology and crystal orientation of its Sn grains [111]. The effect of these two factors on the SAC solder joint behavior will be investigated in this section. The study was conducted only on the BGA components.

V.4.1 Impact of the crystalline orientation on thermomechanical behavior of mono-grained SAC solder joint

(a) *Finite Element Model of BGA solder joints*

i. Description of the model

A model of a quarter Chip Array BGA with anisotropic properties is set up to simulate thermomechanical loads to generate a finite element model that allows implementation of different combinations of grain orientations. All the solder joints were considered to have the single-grain morphology. A temperature drop from the reflow point (230°C) to the ambient (25°C) followed by one thermal cycle (-55/125°C) has been applied on the model.

We have chosen to model the two extreme orientations reported in the literature (c-axis parallel and perpendicular to the substrate) with another third orientation with a c-axis which makes a 45 degree angle to the board surface.

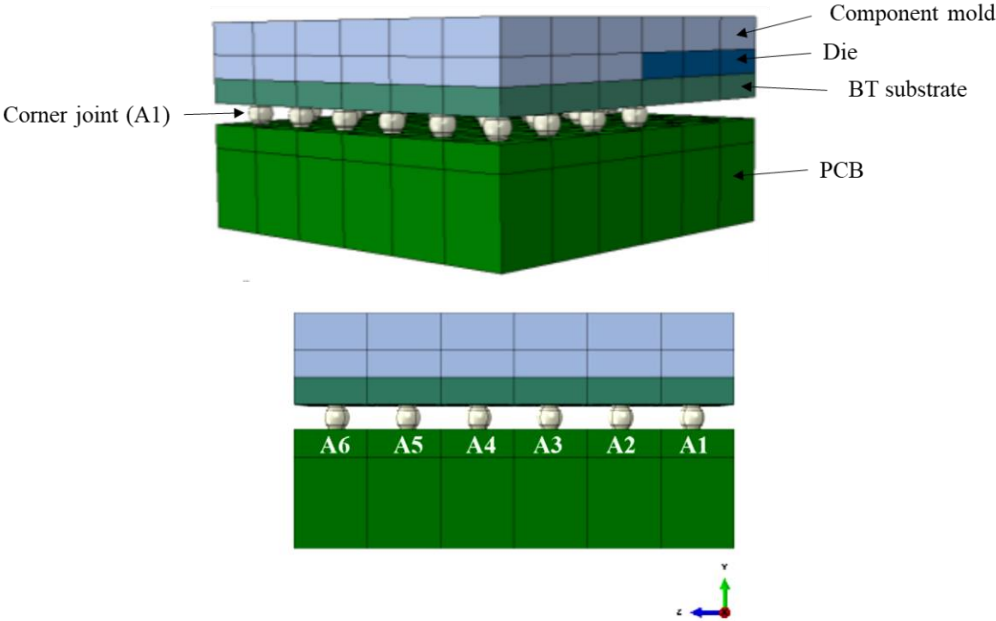


Figure V.4–1: Model of a quarter of a BGA component

Anisotropic properties of β -Sn were implemented in ABAQUS through its elastic coefficient matrix in stiffness form. This matrix is defined by 6 independent constants due to the tin crystal symmetry:

$$\begin{pmatrix} C_{11} & C_{12} & C_{13} & 0 & 0 & 0 \\ C_{12} & C_{11} & C_{13} & 0 & 0 & 0 \\ C_{13} & C_{13} & C_{33} & 0 & 0 & 0 \\ 0 & 0 & 0 & C_{44} & 0 & 0 \\ 0 & 0 & 0 & 0 & C_{44} & 0 \\ 0 & 0 & 0 & 0 & 0 & C_{66} \end{pmatrix} \quad \text{V.4-1}$$

Table V.4–1 presents the tin elastic coefficients used in the FE model.

Table V.4–1 : Elastic Constants (GPa) of tin used in numerical analysis [25]

Parameter	C_{11}	C_{22}	C_{33}	C_{44}	C_{44}	C_{66}	C_{12}	C_{13}	C_{23}
	72.3	72.3	88.4	22.0	22.0	24.0	59.4	35.8	35.8

In order to change the orientation of the solder joints in the model, the elements of the joint are rotated using Euler angles. This rotation is done according to a first rotation φ around the z-axis, followed by θ around the new x-axis and finally Ψ around the updated z-axis and based on the rotation matrix:

$$R = \begin{pmatrix} c_3c_1 - s_3c_2s_1 & -c_3s_3 - s_3c_2c_1 & s_3s_2 \\ s_3c_1 + c_3c_2s_1 & -s_3s_1 + c_3c_2c_1 & -c_3s_2 \\ s_2s_1 & s_2c_1 & c_2 \end{pmatrix} \quad \text{V.4-2}$$

Where c_1, c_2, c_3 and s_1, s_2, s_3 are the cosine and sine of the rotation angles φ, θ and Ψ .

All other materials in the model were modelled as linear elastic (Table V.3–1).

ii. Influence of crystalline Orientation on the stress state of the corner joint

In order to assess the influence of orientations on the stress state of the corner joint, three different cases of grain orientation are modelled. In all three cases, all joints have the same orientation. The results show that the component corner joint is always the most critical in any configuration as shown in Figure V.4–2.

Figure V.4–3 shows the stress state in the corner joint as a function of orientation. The stress state in the solder joints strongly depends on their orientations. Although the highest stressed area was in the neck of the joint for all orientations, we noted a variation of the maximum Von Mises stress between 5% and 15% depending on orientation. Tegehall et al. argued that the orientation has an impact on the behavior of the corner joint and therefore on its degree of recrystallization [68]. Therefore, the orientation of the solder joint plays a significant role in the time to recrystallization and subsequently in the fatigue life of the solder joints.

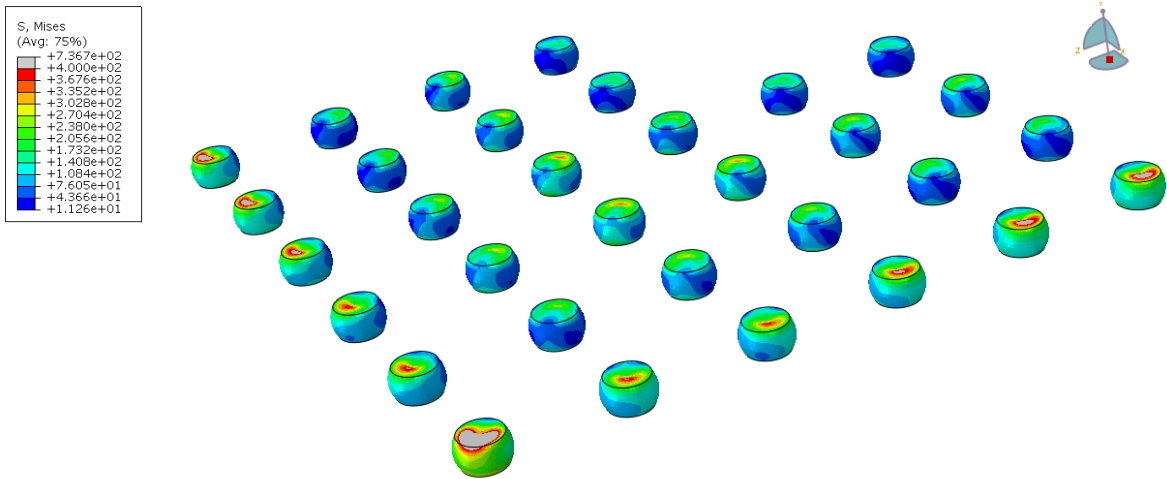


Figure V.4-2: Von Mises distribution on the solder joints of the BGA component

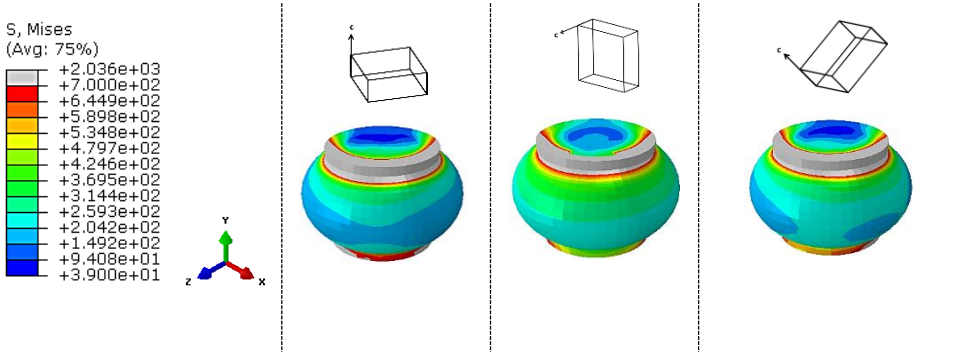


Figure V.4-3: Von Mises stress in the corner joint as function of c-axis orientation

iii. Effect of the orientation of the corner joint on the neighboring balls

The objective from this part of the study is to understand the impact of corner joint orientation on the stress state of neighboring joints. We studied also three configurations but only by changing the orientation of the corner joint; the neighboring bumps orientations are defined by a c-axis parallel to the substrate for each simulation. For the corner joint (A1), the three orientations chosen at the beginning of this section were implemented.

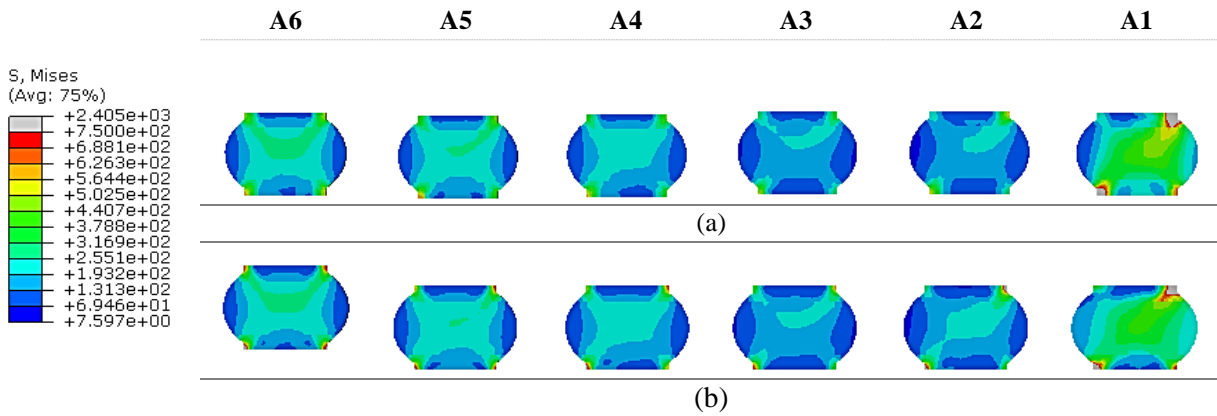


Figure V.4-4: Effect of the c-axis orientation of the corner joint A1 on the neighboring bumps; (a) A1 with a c-axis orientation parallel to the substrate, (b) A1 with a c-axis orientation perpendicular to the substrate

Results of two configurations are presented in Figure V.4-4. Balls of the first range of the FE model were cut in half to show the representative stress state of each solder joint. As expected, we can observe that the corner joint with a c-axis orientation parallel to the substrate is more stressed than that with a c-axis orientation perpendicular to the substrate which validates that orientations with very high CTE value are more detrimental to the fatigue life than orientations with low CTE values.

This figure also shows that the stress state of their surrounding balls was impacted by the orientation of the corner joint. This effect is more remarkable on the stress distribution of the joints A2 and A5 and depends on the value of the variation of the orientations from one bump to another.

These observations show that orientation has an important effect on the behavior of the solder joints and therefore it influences their fatigue life.

iv. Simulations of combinations of different orientations

To get closer to reality and have a more representative model, different cases of joint orientation combinations were modelled. Each case is characterized by a random c-axis orientations distribution; the crystal orientations implemented are also those defined at the beginning of this paragraph.

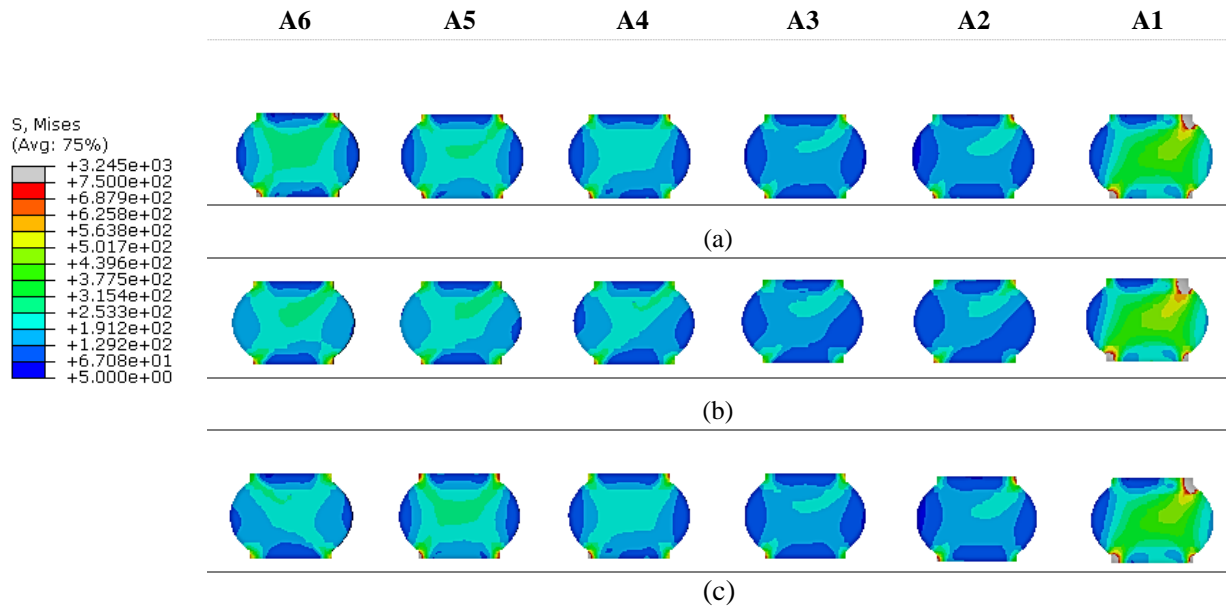


Figure V.4-5: Stress distribution in each joint of the outermost range of the model of three different combinations of grain orientation

Simulations of three different combinations of bumps orientations are presented in Figure V.4-5. As shown in this figure, by generating more realistic combinations, the effect of crystalline orientation on the behavior of the joints became clearer. Due to the combined effect of orientation of joint, its position and orientations of neighboring bumps, the stress distribution of each solder joint is unique and locations of most stressed joints change from one combination to another.

On the other hand, by comparing the stress levels along the simulations carried out in this study, we observed that a model which contains joints with different orientations has a higher stress level (Figure V.4-5) with differences of 37% compared to the stress level observed in the simplest cases (Figure V.4-3) and 25% for configurations where the orientation of the corner joint has been modified (Figure V.4-4).

These results explain the dispersion in times to failure and lead to the conclusion that fatigue life of an area array component will be strongly affected by the initial microstructure of solder joints. For that, it is necessary to make lifetime predictions based on a certain combination of joint orientations.

(b) EBSD maps as function of the c-axis orientation

This work was also supported by a statistical study of crystalline orientations of solder joints having different number of thermal cycles. In order to determine the influence of the tin grains orientations on thermomechanical behavior of the SAC305 solder joints, a color code has been applied to the EBSD maps of crystal orientations at different levels of thermal cycling. The blue and red colors represent the two extreme orientations (c-axis parallel and perpendicular to the substrate respectively). A color gradient characterizes the intermediate orientations. Figure V.4–6 reveals that most of the joints has an orientation of the c axis greater than 30°.

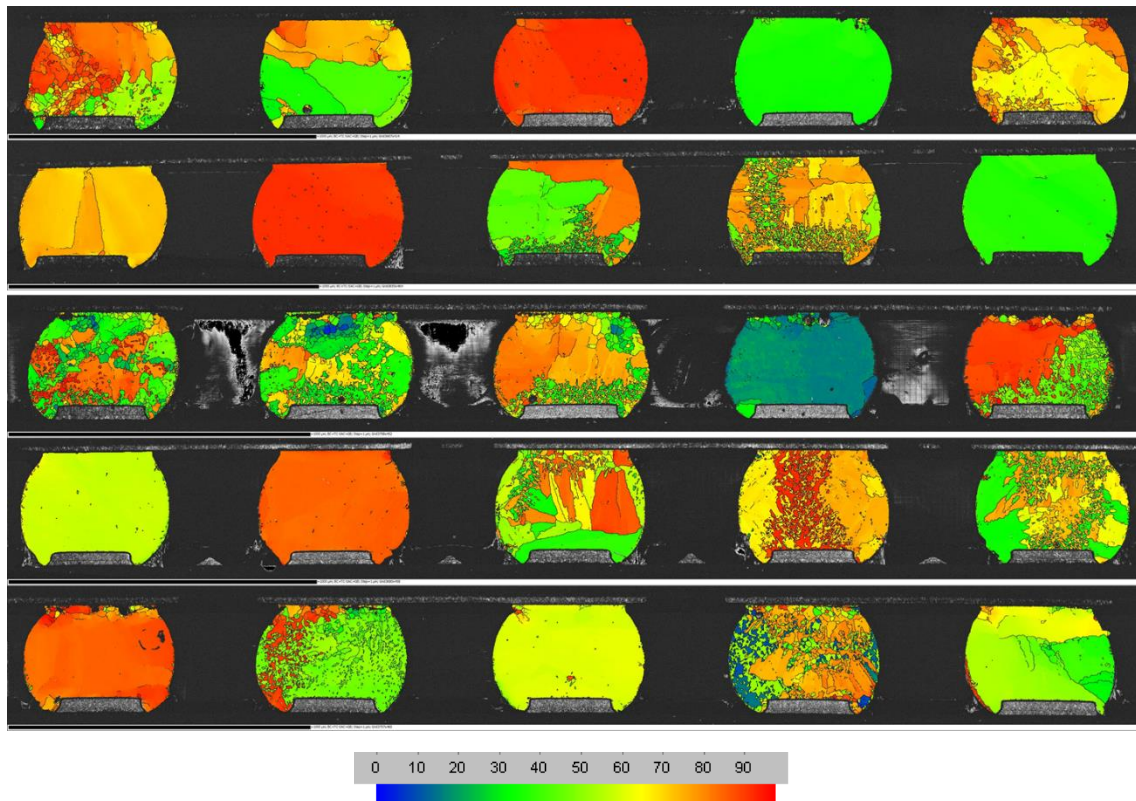


Figure V.4–6: C-axis orientation map of SAC solder taken at different numbers of thermal cycles

However, given the random aspect that characterizes the crystalline orientation and the morphology of the tin grains in the lead-free solder joints, the number of analyzed samples does not seem to be sufficient to be able to study the effect of the crystalline orientation on the SAC solder joints under thermal cycling. It would be interesting to analyze the degree of recrystallization and cracking of various joints with different grain orientation and DNP values to compare to the FEM results.

V.4.2 Tin grain structure influence

Since the initial microstructure has a significant role in the study of solder joints reliability, the fatigue life of an area array component can be also strongly affected by the tin morphology in the solder joints. The statistical study presented in chapter III showed that our interconnections are generally characterized either by a macro grained morphology or by the mixed structure.

(a) *Impact of the poly-grained structure*

The data from the experimental characterization of microstructure were also not sufficient to study the effect of the macro-grained structure on the thermomechanical behavior of SAC solder joints. Simplified Ball scale models were performed to understand the effect of having multiple orientations at the solder joint.

Simulations were performed on 1-crystal, 2-crystal and 3-crystal solder ball. The implemented crystalline orientations are those considered during the study of the effect of the crystalline orientation. The SAC alloy was modelled as anisotropic elastic by implementing its stiffness matrix. The elastic coefficient matrix are presented Table V.4–1.

The top plane was imposed to a shear load, which has a sense along positive Z-direction and imposed to a zero y-displacement in order to restrain rigid rotation. The bottom plane was imposed to fixed condition (Figure V.4–7(a)). C3D8R node was used in the simulations (Figure V.4–7(b)).

First simulations were generated in model with one crystalline orientations. Results validates one again that the crystalline orientation influences the Von Mises distribution in the SAC solder joints. For same loading condition, interconnections do not respond similarly if they have dissimilar orientation. However, the stress concentration zone is always near the neck of the solder joints regardless of the implemented crystalline orientation (Figure V.4–8 (a) and Figure V.4–8 (b)).

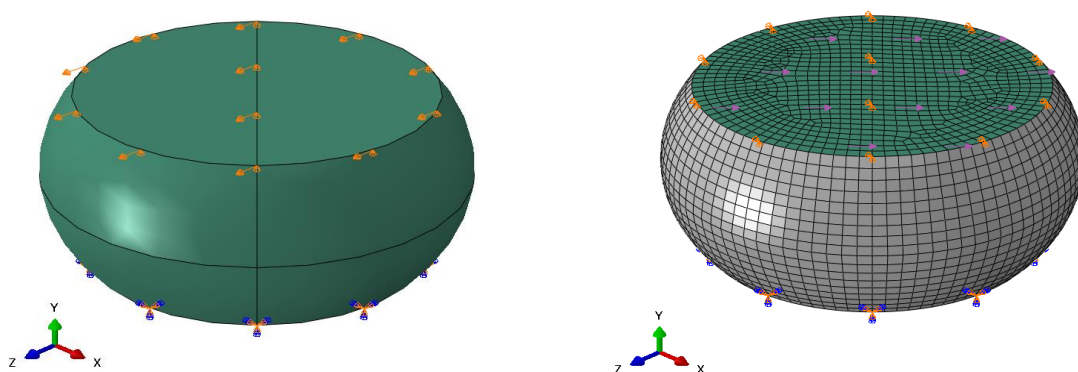


Figure V.4–7: Solder ball model, (a) Boundary and load conditions, (b) meshing

Poly-grained structure modelling by considering two or three crystalline orientations shows the appearance of a discontinuity in the Von Mises stress distribution at the grain boundaries level (discontinuous black lines shown in Figure V.4–8 (c) and Figure V.4–8 (d)). The solder neck remains the zone with the highest level stress. However, it seems to have a more strain area compared to the rest. We can clearly see in Figure V.4–8 (c) and Figure V.4–8 (d) that the stress concentration is always at the level of the grain having the blue orientation (black arrows). This means that the mutual relationship among the grains in terms of orientation and structure is influential to induce material deformation.

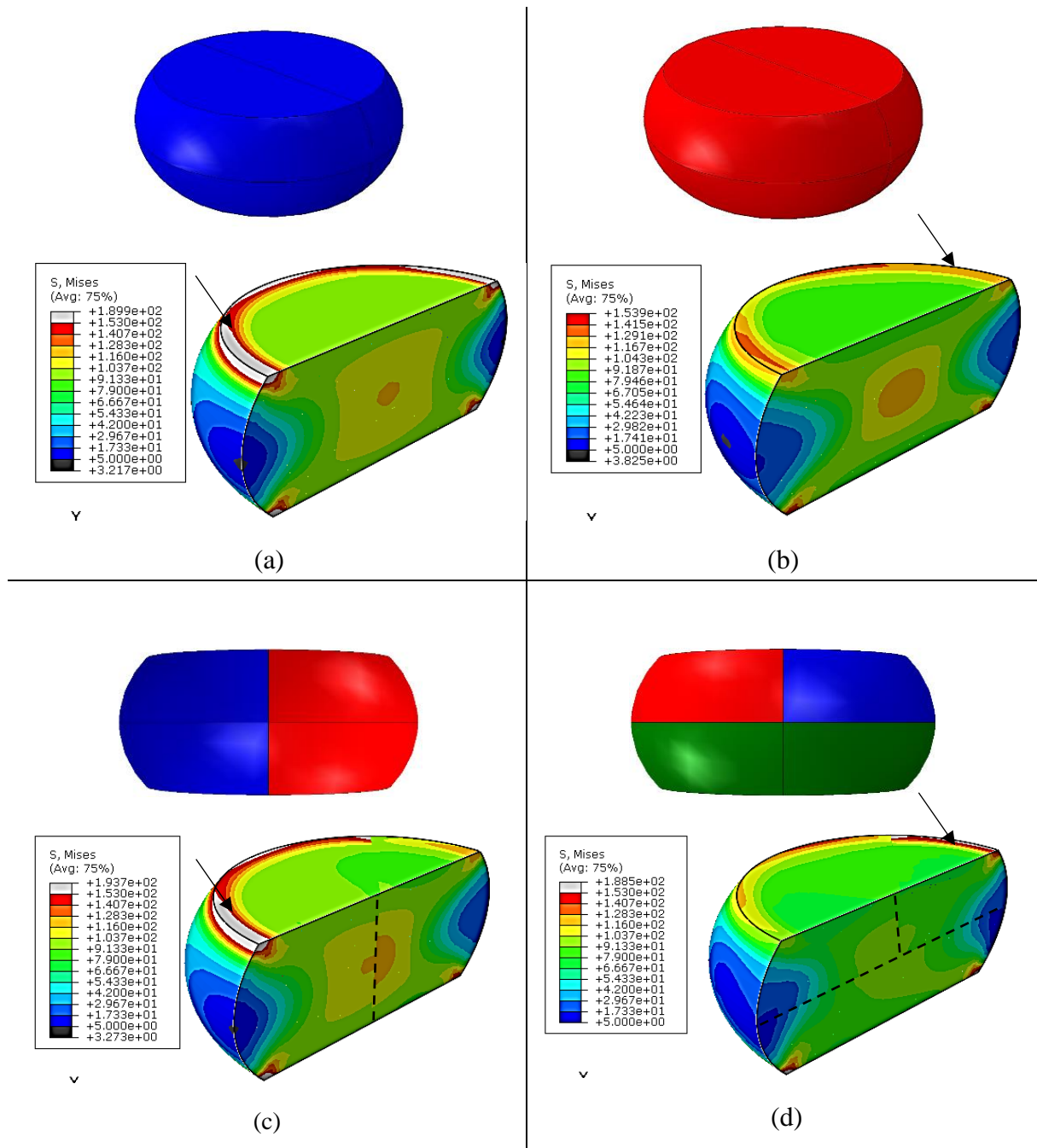


Figure V.4–8: Combination of the macro-grained structures used for simulation in ABAQUS (a,b) 1-crystal, (c) 2-crystal and (d) 3-crystal; the arrow points to the area where the Von Mises stress is maximum

(b) *Impact of the mixed morphology*

The impact of mixed morphology on the behavior of joints during thermal cycling is the purpose of this section.

i. Evolution of twinned interlaced structure on solder with mixed structure

The different steps of tin grains evolution under thermal cycling was easier to identify in the case of the macro-grain morphology. In the previous chapter, we provided an accurate description of these stages. The process begins with the recovery phenomenon. β -Sn sub-grains (misorientation $<5^\circ$) and low disorientated grains ($<15^\circ$) appear in the most stressed areas under the component. Then a global recrystallization begins. Grain boundaries with larger angles ($>15^\circ$) form and delimit new tin grains. This network of recrystallized grains spreads across the bulk of the solder joint under thermomechanical stress until total recrystallization of the most stressed area of the solder

The solder joints having mixed structure are characterized by the presence of both the cyclic and interlaced twinned morphologies. The interlaced structure is often localized near the interface between the solder and the copper pad on component or PCB side.

It is important to first characterize the evolution of this structure under thermal cycling. EBSD mapping was carried on solder joints presenting mixed structure and subject to different numbers of thermal cycles. The tin grain recrystallization and the Ag_3Sn particles coarsening are again the phenomena responsible for the cracking of SAC interconnections

The interlaced morphology seems to have no effect on the failure mechanism of SAC solder joint under thermal cycling.

Figure V.4–9 reveals each step of the formation of a network of new recrystallized grains in an interlaced region. All the steps identified during the characterization of the macrograin structure have been well found on the interlaced zone of the mixed morphology. The recovery phase was detected after 225 cycles. Then the tin grain recrystallization starts. Grain boundaries with angle superior to 15° emerge and progressively cross the crystal twin. New crystalline orientations were well observed on solder joints taken out at 1000 and 1700 cycles.

The continuous evolution of tin grain boundaries during thermal cycling can also be illustrated by the crystal disorientations diagram. It makes it possible to characterize the evolution of the angular distribution of all the tin grain boundaries detected during thermal cycling. Figure V.4–10 shows the distribution of disorientation angles for BGA joints corresponding to three levels of damage. These results show a significant reduction in grain boundaries exhibiting disorientation angles around 60° which means that the crystal twins tend to disappear as thermomechanical damage increases. We can also observe that the population of joints with angles greater than 15° increases.

A correlation between the tin grain recrystallization and the evolution of Ag_3Sn particles has validated the activation of the coarsening phenomenon by thermal cycling in solder joints with a mixed structure (Figure V.4–11).

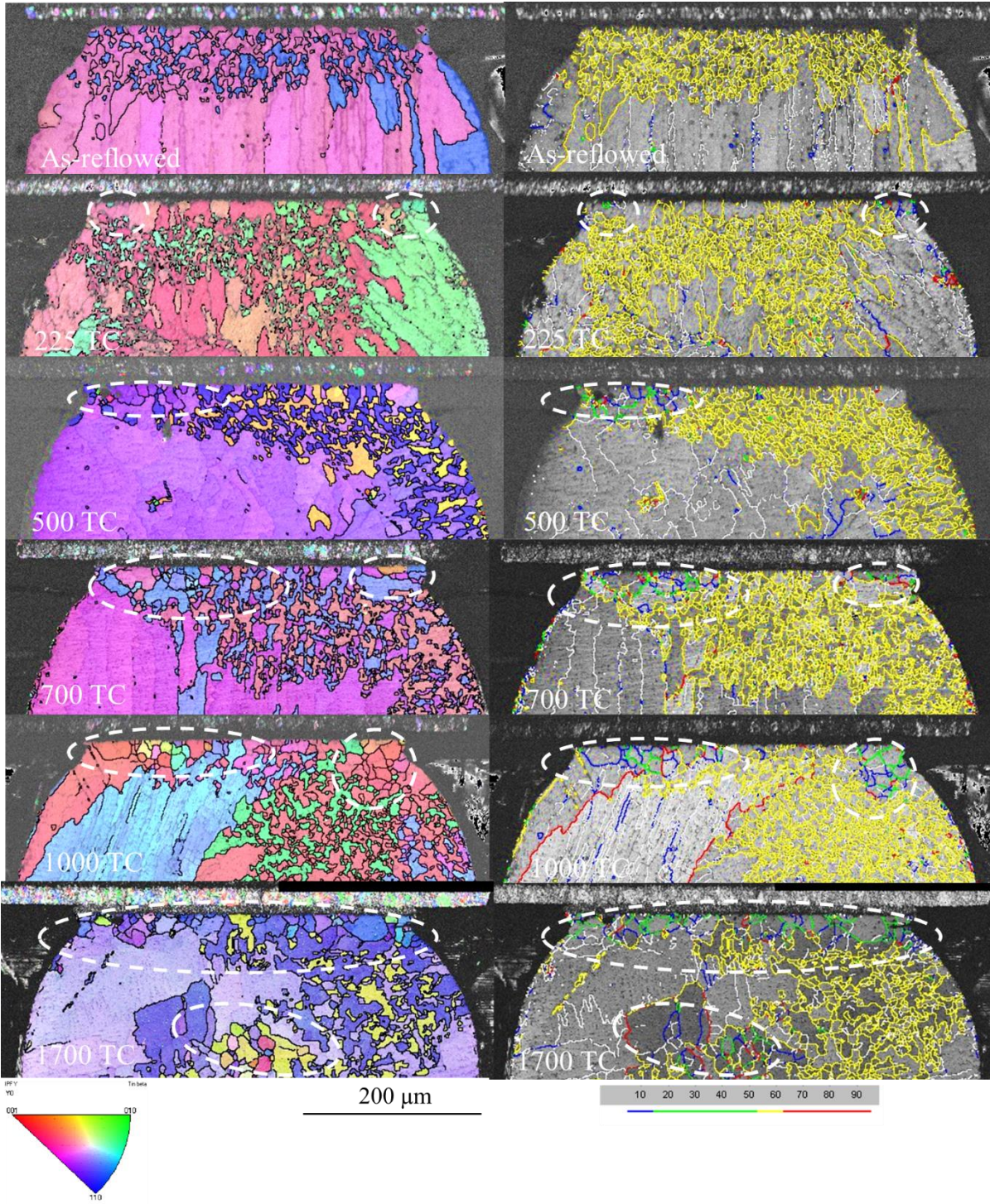


Figure V.4-9: Tin grain evolution on mixed solder joints subject to thermal cycling

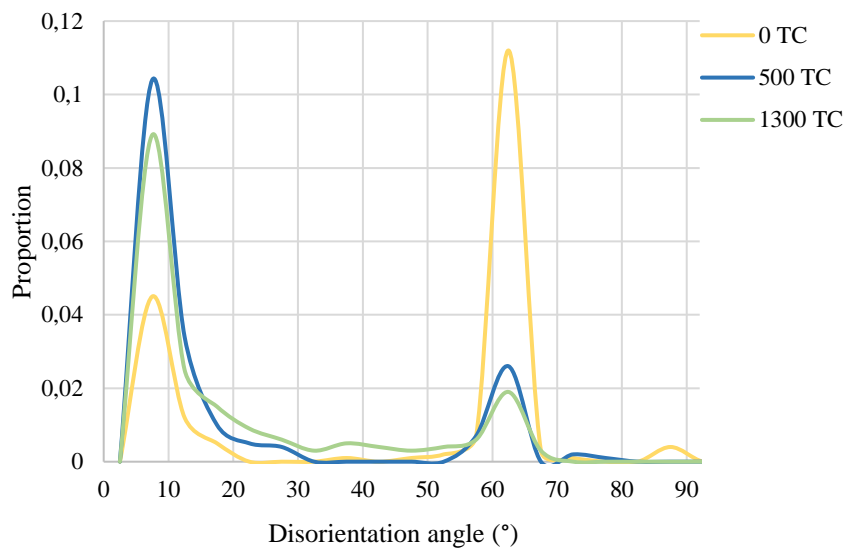


Figure V.4-10: Evolution of the crystal disorientations of the mixed structure under thermal cycles

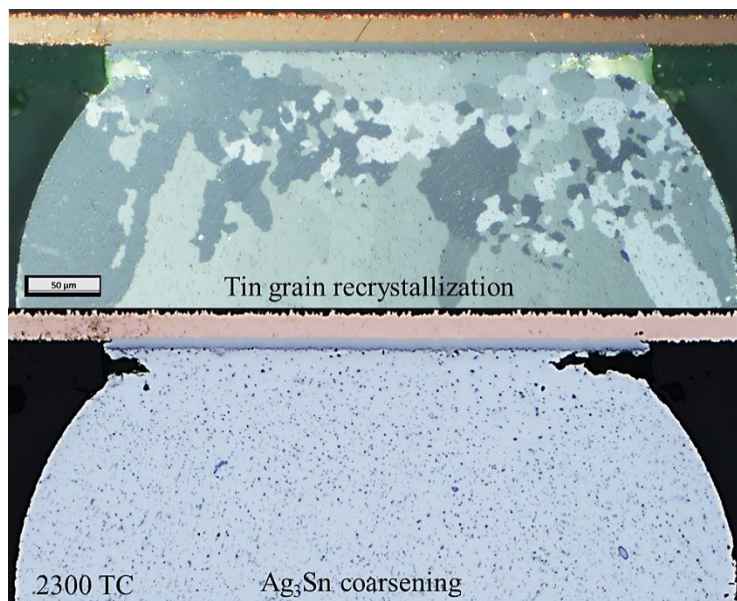


Figure V.4-11: Correlation between the recrystallization and Ag_3Sn coarsening on solder presenting mixed morphology

ii. Evolution of the recrystallization degree as function of the SAC solder joints morphology

The results of the previous section were used to plot the evolution of the degree of recrystallization as a function of the solder joints morphology. Figure V.4-12 presents the measured degree of recrystallization on interconnections presenting macro grained and mixed morphologies (blue and green bars respectively) and taken at different levels of the thermal cycling. Solder joints with mixed morphology are systematically the most recrystallized independently of the solder position in the matrix of the BGA.

The macro-grained morphology has a dendritic structure which gives them the ability to oppose to the movement of dislocations. This structure seems to be beneficial and delay the tin grains recrystallization. On the contrary, the morphology of interlaced twins presents several predispositions which make it a critical morphology in thermal cycling. Indeed, at the level of the interlaced zone, the dendritic structure of the SAC is missing, which weakens the reinforcing effect of the Ag₃Sn precipitates and accelerates the tin grain recrystallization. Moreover, it has been found in other studies that the mechanical properties of the interlaced zone are different from those with macro grained structure. Thus, the intrinsic property gradient of the joint generates additional stresses which materialize by the appearance of important recrystallization in solder joints with mixed structures.

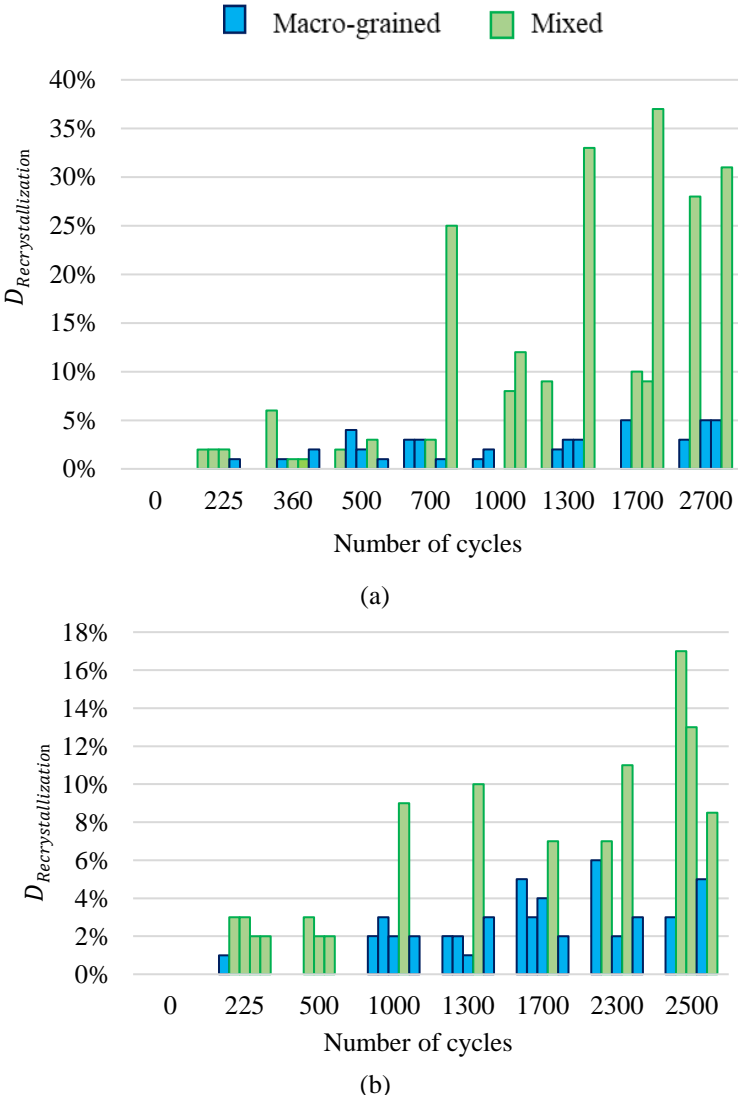


Figure V.4–12: Evolution of the recrystallization degree as function of the solder morphology (a) solder joints under the component edge (b) solder joints under the die edge

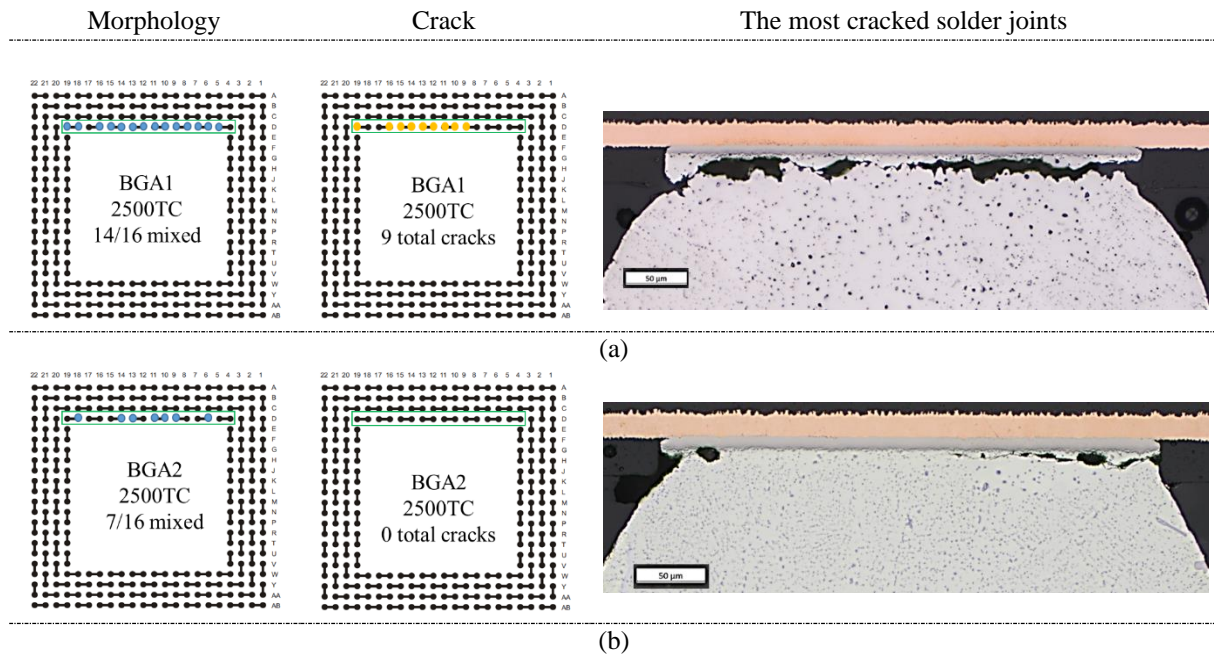


Figure V.4-13: Impact of the mixed morphology on the solder joints cracking

Observations of the cracking state of two components taken at the same time were carried out to validate the effect of the tin grains morphology on the behavior of the solder joint under thermomechanical loading. Analyzes were done only on the joints under the die edge since they have the first detected failures. The results show that total cracks are present on 56% of the joints of the component having 87.5% of its joints with the mixed morphology. These cracks are always located in the solder joint presenting the mixed structure (Figure V.4-13 (a)). However, no total crack was observed on the component with a low percentage of mixed structure (43%) ((Figure V.4-13 (b)).

V.4.3 Synthesis

The effect of the as-reflowed microstructure were investigated through finite element simulations and microstructural analysis. The behavior of the BGA solder joints as function their crystalline orientations and morphologies was studied. Results highlight that the response of each solder joint is impacted by its own crystalline orientation and those of its neighbors.

The solder joint morphology plays an important role in identifying the location of the critical joint. The mixed morphology seems to accelerate the evolution of recrystallization during thermal cycling and consequently the appearance of cracks. The observations showed that the first total cracks were observed on the solder joints under the die edge having a mixed structure independently of their position in this row.

V.5 Conclusion

Accelerated tests in a thermal chamber took place throughout the thesis. They have generated a significant amount of lifetime results and microstructural data for different types of SMD components. They also allowed the study of the influence of certain parameters like the microstructure of the SAC interconnections and their location on the thermomechanical fatigue of lead-free assemblies. The main goal of this chapter was to identify the mandatory parameters to be taken into account in the reliability study of SAC solder joints subjected to thermal cycles.

The impact of isothermal aging on the behavior of the SAC305 alloy in thermal cycling, both at the level of the microstructural behavior and on the characteristic lifetime of the different studied components, was evaluated for several aging conditions, dependent on time and temperature. The thermomechanical durability of SAC solder joint was slightly lowered by aging at 100°C and increased by aging at 150°C. This shows that constitutive laws of the SAC alloy must consider the isothermal storage effect for an accurate prediction of the reliability of electronic assemblies.

The study of the impact of the location of the joints in the BGA package has shown that the distance to the neutral point does not always make it possible to identify the position of the critical joint. The lifetime data shows that the solder joints under the die edge present the lowest durability. Interconnections under the component edge have the highest lifetime. In our case, we can consider that the die shadow effect is more weighting than the distance from the neutral point. It is interesting to note that the solder under the die edge and the component corner do not behave in the same way under thermal cycling. Different distributions of recrystallization have been observed depending on the position of the solder joint. Finite element simulations was used to better understand die shadow effect on the SAC solder behavior. Results show that the slightest change in the material properties can modify the location of the most strained joints which means that the good characterization of the material properties of the assembly is a crucial task for the accurate prediction of the critical joint position.

On the other hand, the failure analysis of all solder joints under the edges of the component and the die was carried out to localize the critical position on these rows. Observations highlight that the corner balls under the component edge are the first to fail with respect to its neighbors. However, the first failures at the die edge were not necessarily observed in the corner but on solder joints having mixed morphology.

The as-reflowed microstructure has been thus identified as influential factors on the SAC solder behavior and the kinetics of the failure mechanism under thermomechanical loading. The impact of the tin grain crystalline orientation and morphology was investigated through FE simulations and microstructural characterization. Numerical results emphasize the SAC solder stress distribution depend strongly on its orientations and affected by the response of its solder joints neighboring. The generation of a combination of solder joints having random crystalline orientation, which is the closet case to reality, underlined an increase of 37% in the Von Mises stress level compared to the configuration where all interconnections have the same orientation. From a morphological point of view, observation indicate that partially interlaced solder joints

could be detrimental for the characteristic fatigue life. Solder joints presenting the mixed morphology were more sensitive to recrystallization than macro-grained structure. They present the highest recrystallization degree whatever their location in the package which can accelerate the crack propagation under thermal cycling. This finding shows the need to take into account the microstructure in the identification of the thermomechanical fatigue model of the SAC305 alloy.

General conclusion

The majority of existing predictive models do not capture the effect of the as-reflowed microstructure and its evolution during thermal cycling tests. Lack of that information greatly influence the accuracy of predicted failure times of electronic packages. Significant efforts are needed to develop constitutive models that take into account the evolving microstructural effects, such as Ag_3Sn particles coarsening and formation of a network of tin grain boundaries in high-strain regions, which ultimately result in the intergranular cracking that is unique to Pb-free assemblies. A detailed understanding of these microstructural interactions is crucial to develop representative reliability models. This thesis presented a research work contributing to a better comprehension of the effect of the as-reflowed microstructure and its evolution on the thermomechanical fatigue behavior of lead-free solder joints. The work dealt with both the study of degradation physics and the development of methods for assessing the reliability of SAC solder joints. In-situ monitoring, failure analysis, microstructural investigation and multiscale finite element modelling are the used tools to identify factors that need to be considered to provide an accurate fatigue law.

A large accelerated thermal cycling campaign was therefore carried out in order to determine the link between each step of the failure mechanism and the life service of the solder joints. Isothermal aging followed by accelerated temperature cycles is the accelerated test type considered to study the thermomechanical reliability of SAC solder joints. For the isothermal pre-aging two temperatures (100°C , 150°C) and three durations (100h, 500h, and 1000h) were investigated. Some boards have not been stored and remained on their as-reflowed state (a condition called "pre-aging at 20°C "). Two thermal cycles were also considered according to the TC4 ($-55^\circ\text{C}/125^\circ\text{C}$) and TC5 ($-55^\circ\text{C}/100^\circ\text{C}$) test conditions of the IPC-9701. Three types of components, BGA, QFN and R1206 were studied in order to define a common microstructural damage criterion. The investigation of the evolution of the microstructure was based on subjecting the components to different state of aging test and analyzing the solder joints by optical imaging and EBSD analysis.

As-reflowed SAC305 solder joint microstructure

The observations of as-reflowed solder joints showed that the classic SAC microstructure characterized by the presence of β -Sn tin matrix with cellular structures of fine Ag_3Sn particles in the eutectic regions. The inter-dendritic spaces are characterized by the presence of $(\text{Cu},\text{Ni})_6\text{Sn}_5$ intermetallic compounds, which are larger than Ag_3Sn particles. The presence of nickel in these precipitates depends on the amount of dissolved nickel from the component and PCB finish. Nickel also participates in the formation of intermetallic layers at the component and PCB side interfaces. The layers are composed of $(\text{Cu}, \text{Ni})_6\text{Sn}_5$ and $(\text{Ni}, \text{Cu})_3\text{Sn}_4$ or a mixture of these IMCs depending on the quantity of nickel. This microstructure has a truly random distribution with very varied morphologies. Polarized light observation highlight that it consists of few large β -Sn grains and can be described as macro grained or mixed with presence of both cyclic twinned and interlaced structures.

As the initial microstructure is expected to have an impact on the solder thermomechanical behavior due to tin anisotropy, a quantitative analysis of tin grain morphologies distribution was made on several components. It highlights the significant presence of the macro-grained morphology in the BGA and R1206 components. QFN interconnections show a practically equal distribution between SAC solder with poly-grained and mixed structure.

However, a large number of parameters like the undercooling condition can affect tin grain structure during solidification and the interconnections geometry. A particular distorted macro-grained morphology was highlighted by EBSD analysis of QFN solder joints. We have qualified it with a noticeable gradient in crystalline orientation and a clear substructure in the form of long slats compared to the other types of solder. This specificity is probably linked to the cooling conditions of the solder in this geometric configuration.

Role of tin grain recrystallization and Ag₃Sn coarsening on the SAC solder cracking under thermomechanical fatigue

An in-depth microstructural investigation of the evolving SAC305 solder joint microstructure along thermomechanical fatigue is the global approach to understand the role of tin grain recrystallization and Ag₃Sn coarsening on the SAC solder cracking under thermomechanical fatigue. According to analyses performed on the BGA, QFN and R1206 interconnections at different levels of cycling, the main failure mechanism in lead-free solder under thermomechanical fatigue can be summarized in three steps.

First, a recovery process occurs in the high strain regions accompanied by a slight precipitate coarsening of Ag₃Sn IMC particles. Slow growing of crack initiation at the interface between tin and (Cu, Ni)₆Sn₅ intermetallic appears also at the same time. The crack initiation is associated with local recrystallization at the interface of IMCs.

In the second stage, recrystallization with a high Ag₃Sn coarsening will occur all the way through the highly stressed area until a well-defined recrystallization degree coupled with a threshold of Ag₃Sn particle density value providing favorable intergranular propagation paths. In the recrystallized region, a large number of highly disorientated tin grains will be generated. Ag₃Sn IMCs migration takes place and the large particles tends to move towards grain boundaries to facilitate intergranular crack growth.

Finally, the intergranular cracks will propagate in the recrystallized area with local recrystallization at the crack tip. This process repeats itself until complete cracking.

A second failure mechanism that does not require tin grain recrystallization and Ag₃Sn coarsening to occur was observed only on the QFN solder joints. Micro cracks appear at the interface between solder bulk and intermetallic layers and make this region brittle. Then, they propagate under thermal cycles into a total crack along the solder. This failure mode presents an interfacial brittle crack. It is generally generated due the high tensile stress located at the interface IMC-solder bulk. A competition between the intergranular and the interfacial cracking was also detected and may be the cause of appearance of a mixed failure mode. This mode is usually due to shear stresses that generates considerably higher solder bulk plastic deformation compared to the tensile stress located at the interface IMC-solder bulk.

Identification of SAC alloy microstructural damage criterion

An innovative microstructural approach allowing the identification of a SAC alloy microstructural damage criterion was developed. The link between measurement of the solder joints lifetimes by electrical monitoring, the study of crack development and the quantitative investigation of the microstructural evolution was established to determine the most important phases on the SAC solder joint life service.

Results of lifetime analyses validated the different behavior of the QFN solder joints compared to the BGA and the R1206 components. Putting life analysis data into perspective with measurement of crack evolution showed that the interfacial cracking is faster than the intergranular cracking which is the origin of early failures on QFN interconnections. It revealed also that the lifetime of solder joint under thermomechanical fatigue is controlled by the crack propagation phase and that the crack nucleation phase does not exceed 24% of SAC solder life service.

The intergranular crack propagation represents the most observed failure mode on BGA, QFN and R1206 solder joints under thermal cycling. The tin recrystallization and the Ag_3Sn coarsening are phenomena leading to this failure mode in the different solder geometries. A quantitative analysis of the microstructural evolution was done in order to define the microstructural state promoting the intergranular cracking. The size of recrystallized grains and the degree of recrystallization, the size of Ag_3Sn particles and their density have been defined as microstructural indicators allowing monitoring the microstructural evolution of the SAC solder alloy.

The study of the evolution of tin grain size during the thermal cycling highlighted that the equivalent diameter of recrystallized grains is between 1 and 30 μm for the BGA, QFN and chip resistor component. This range did not evolve under temperature cycles. The recrystallized grain size can be thus considered as a feature of the solder alloy. The correlation between the evolution of the recrystallization degree and the crack development showed that crack propagation does not need total recrystallization of the high strain region. A low degree of recrystallization seems to be sufficient to trigger crack propagation. This degree is of the same order for the BGA and R1206 geometries (8% and 10% respectively). A higher recrystallization degree is required for the crack propagation in QFN solder joints (27%). This can be explain by their different behavior characterized by the mixed cracking mode, which is a competition between the interfacial and intergranular cracks. It is assumed that this mode requires a high degree of recrystallization for crack propagation. Therefore, the degree of recrystallization can be used as a way of measuring the damage state of solder joint presenting the same failure mode.

The evolution of the size and the density of Ag_3Sn particles under thermomechanical loading was also studied in the BGA, QFN and R1206 components. Measurements highlighted that equivalent diameters of Ag_3Sn IMCs is between 0.4 and 4 μm whatever the solder geometries. The analysis of the Ag_3Sn density evolution under thermal cycles shows a similar behavior in the three studies geometries. However, the Ag_3Sn precipitates present too different behavior as function of their diameter range. A decrease of density was measured on the finest particles

having diameter between 0.4 and 1 μm . For larger precipitates ([1; 4] μm), the density increases during thermal cycling. On the other hand, particles with a diameter superior than 2 μm were identified as the most favorable for the tin grain recrystallization and crack development. Their appearance correlates with the time when the highest recrystallization degree was measured. Thus, the equivalent diameter ranges of the Ag_3Sn particles and their densities can be used to assess the damage state in solder joints under thermal cycles. Taking into account these two factors in the prediction models can advance the field of reliability of SAC joints.

Different factors affecting solder joint reliability under thermomechanical fatigue

Lifetime results, failure analyses as well as microstructural investigations have shown that QFN solder joint exhibit a different thermomechanical behavior compared to the BGA and the R1206 components. The unexpected highly complex microstructure observed on the as-reflowed QFN solder joints can have an impact on their response. The material properties and the assembly design represent factors influencing solder joint reliability under thermomechanical fatigue.

The effect of the properties materials/design of the assembly (die shadow effect and solder location) and of the initial microstructure (before cycling) have therefore been studied to determine those necessary to be implemented on reliability models.

The assessment of the properties materials/design of the assembly was carried out by studying the effect of solder joint position on the BGA package behavior. Results highlighted that the distance from the neutral point (from the center of the components to the corners) is not the only unfavorable factor in terms of position. In our case, solder joints under the die edge presented the lowest characteristic lifetimes and interconnections under the components edge were characterized by the highest durability. This can be explained by the die shadow effect. The identification of the most critical solder by failure analysis of each balls row of the package showed that the first failures often happen in the corner for solder located under the component edge. However, no particular position seems to be critical for interconnections under the die edge. The observations also revealed that the joints under the component corner and under the die have different recrystallization distributions. Finite element simulations validated that solder joints under the component edge do not behave like the balls under the die. The Coefficient of Thermal Expansion (CTE) of the die and the component are the reason of this behavior. The presence of the silicon die near of the inner row also generates significant shear stresses due to its low CTE, which can change the critical positions of the first BGA solder ball to fail. The study of the electronic assemblies' reliability should not be thus based only on geometric considerations (distance from the neutral point) but earlier by taking into account the good properties of each material present in the package.

To understand the effect of the initial state of the microstructure on the thermomechanical reliability of SAC solder joints, we started with the study of the isothermal pre-aging effect. Results showed that solder joints lifetimes may decrease or increase depending on storage temperature. The impact of changing the material properties of the assembly under the effect of isothermal storage must be thus considered in the prediction of failure times.

The presence of voids in the initial state can be considered as a critical factor for the thermomechanical performance of SAC solder joint. The analysis of the crack evolution shows that interconnections having voids presents faster crack propagation rate. It is then important to define proper rules of qualification regarding voids distribution in such packages.

The effect of the as-reflowed microstructure was also investigated by evaluating of the impact of the crystalline orientation and morphologies of tin grains on thermomechanical response of BGA components. Results revealed a clear dependence of the thermomechanical response of SAC solder joints on Sn grain orientation. Finite element simulations showed that SAC solder joints stress distribution is strongly impacted on its orientations and affected by the response of its neighboring interconnections. The generation of a combination of solder joints with different crystalline orientations increases of 37% the Von Mises stress level compared to the configuration where all solder joints have the same orientation. This analysis demonstrates that certain combinations of orientations applied stress that may result in anomalously early failures.

The tin grain morphology effect was also provided. The comparison of the evolution of recrystallization degree on solder joint having polygrained and mixed structures showed that mixed morphology could be critical for the characteristic fatigue life. Solder joints presenting partially interlaced structure often present the highest recrystallization degree whatever their location in the package which can accelerate the crack propagation under thermal cycling. It should be noted that the characterization of the stages of the evolution of tin grain identified in the interlaced zone are the same as that found during the study of the joints presenting the polygrained morphology. The mixed structure only accelerates the onset of recrystallization. The tin grain orientation and morphologies are thus primordial factors that need to be take into account in the development of the thermomechanical fatigue model of the SAC305.

Perspectives

The presented work opens up a relatively large number of perspectives, complements to certain parts or new axes of study. The thesis results well validated the need to take into account the SAC microstructure in the reliability study of lead-free assemblies under thermomechanical loading.

A design of a specimen allowing the mechanical characterization of the solder joints behavior by considering the effect of as-reflowed microstructure and its evolution was done, and is currently under validation in the process of validation. The objective is to carry out strain hardening and creep tests to refine the identification of the Anand model parameters for the description of the viscoplastic behavior of SAC interconnects. This step is necessary to provide representative prediction models.

With regard to the continuation of the work carried out on the effect of the crystalline orientation on SAC solder joint thermomechanical behavior, the identification of the most critical combination of tin crystalline orientation by experimental process requires an infinite number of samples. FEM should be used in future work to run an important number of simulations with different sets of joint orientations. A sensitivity analysis based on Monte Carlo method would allow us to define multiple distributions of orientations. The results compiled into a response surface would permit to define the most critical case. These response surfaces would also be useful for studying the distribution of predicted lifetime as a function of crystalline orientations and positions of solder joints. However, the experimental study of the distribution of the crystalline orientations of the grains in the components remains necessary to generate models close to reality.

The modeling of tin recrystallization and Ag_3Sn coarsening also seems important to refine reliability models of SAC solder joints. The identified microstructural indicators (size of recrystallized grains and the degree of recrystallization, the size of Ag_3Sn particles and their density) can be used to define a more representative fatigue criterion that depends on the microstructure features. These indicators can also be useful for evaluating the state of aging of SAC interconnections. Artificial intelligence is a good way to quickly post-process EBSD data from several samples and then compare their status.

The study of the thermomechanical response of QFN components by finite element models will make it possible to evaluate the nature of the constraints applied to this solder geometry and reveals the points of difference with the other studied components studied (BGA and R1206).

The multiscale modeling (boards, components, solder joints and tin grains) then became a primary approach to assess the thermomechanical lead-free solder joints reliability.

References

- [1] W. C. M. FILHO, "Methodologie d'essais accélérés de torsion et de detections de défaillance appliquée aux assemblages électroniques à billes," Thesis, University of Bordeaux 1, France, 2008.
- [2] JEDEC Association, "IPC / JEDEC J-STD-020C Moisture / Reflow Sensitivity Classification for Non-hermetic Solid State Surface Mount Devices Proposed Standard for Ballot," no. January, 2004,
- [3] N. C. Lee, "Getting Ready for Lead-Free Solders," *J. Solder. Surf. Mt. Technol.*, vol. 9, no. 2, pp. 65–69, 1997.
- [4] K. S. Kim, S. H. Huh, and K. Suganuma, "Effects of intermetallic compounds on properties of Sn-Ag-Cu lead-free soldered joints," *J. Alloys Compd.*, vol. 352, no. 1–2, pp. 226–236, 2003
- [5] J. W. Yoon, S. W. Kim, and S. B. Jung, "IMC morphology, interfacial reaction and joint reliability of Pb-free Sn-Ag-Cu solder on electrolytic Ni BGA substrate," *J. Alloys Compd.*, vol. 392, no. 1–2, pp. 247–252, 2005
- [6] D. Q. Yu and L. Wang, "The growth and roughness evolution of intermetallic compounds of Sn-Ag-Cu/Cu interface during soldering reaction," *J. Alloys Compd.*, vol. 458, no. 1–2, pp. 542–547, 2008
- [7] K. Moon, W. J. Boettinger, U. R. Kattner, F. S. Biancaniello, and C. A. Handwerker, "Experimental and Thermodynamic Assessment of Sn-Ag-Cu Solder Alloys," *J. Electronic Materials*, vol. 29, no. 10, pp. 1122–1136, 2000.
- [8] C. P. W. E. Suhir, Y.C. Lee, C. P. Wong "Micro- and Opto- Electronic Materials and Structures: Physics, Mechanics, Design, Reliability Packaging," Volume I Materials Physics, Book, Chapter 10, p356, 2007.
- [9] L. D. Brownlee, "Lattice constant of grey tin," *Nature*, vol. 166, no. 4220, p. 482, 1950.
- [10] R. Clark, G. B. Craig, and B. Chalmers, "Mechanical twinning in white tin," *J. Acta Crystallogr.*, vol. 3, no. 6, pp. 479–479, 1950.
- [11] W. J. Plumbridge, "Tin pest issues in lead-free electronic solders," *J. Mater. Sci. Mater. Electron.*, vol. 18, no. 1–3, pp. 307–318, 2007.
- [12] B. Dompierre, "Fiabilité mécanique des assemblages électroniques utilisant des alliages du type SnAgCu," Thesis, Ecole Centrale de Lille, France, 2011.
- [13] A. Lövberg, P. E. Tegehall, S. Akbari, and D. Andersson, "On the formation and propagation of laminate cracks and their influence on the fatigue lives of solder joints," 2018 19th Int. Conf. Therm. Mech. Multi-Physics Simul. Exp. Microelectron. Microsystems (EuroSimE), pp. 1–13, 2018.
- [14] L. P. Lehman, S. N. Athavale, T. Z. Fullem, A. C. Giamis, R. K. Kinyanjui, M. Lowenstein, K. Mather, R. Patel, D. Rae, J. Wang, Y. Xing, L. Zavalij, P. Borgesen and E. J. Cotts, "Growth of Sn and intermetallic compounds in Sn-Ag-Cu solder," *J. Electron. Mater.*, vol. 33, no. 12, pp. 1429–1439, 2004.
- [15] J. Hokka, T. T. Mattila, H. Xu, and M. Paulasto-Kröckel, "Thermal cycling reliability of Sn-Ag-Cu solder interconnections - PART 2: Failure mechanisms," *J. Electron. Mater.*, vol. 42, no. 6, pp. 963–972, 2013.

- [16] G. Cuddalorepatta, M. Williams, and A. Dasgupta, "Viscoplastic creep response and microstructure of as-fabricated microscale Sn-3.0Ag-0.5Cu solder interconnects," *J. Electron. Mater.*, vol. 39, no. 10, pp. 2292–2309, 2010.
- [17] V. V. S. J. Gong, C. Liu, P.P. Conway, "Micromechanical modelling of SnAgCu solder joint under cyclic loading: Effect of grain orientation," *J. Comput. Mater. Sci.*, vol. 39, no. 1, pp. 187-197, 2007
- [18] J-B. Libot, "Méthodologie d'évaluation de la durée de vie des assemblages électroniques sans plomb en environnements thermique et vibratoire," Thesis, University of Toulouse, 2017.
- [19] L. P. Lehman, Y. Xing, T. R. Bieler, and E. J. Cotts, "Cyclic twin nucleation in tin-based solder alloys," *J. Acta. Mater.*, vol. 58, no. 10, pp. 3546–3556, 2010.
- [20] B. Arfaei, N. Kim, and E. J. Cotts, "Dependence of Sn grain morphology of Sn-Ag-Cu solder on solidification temperature," *J. Electron. Mater.*, vol. 41, no. 2, pp. 362–374, 2012.
- [21] T. R. Bieler, H. Jiang, L. P. Lehman, T. Kirkpatrick, E. J. Cotts, and B. Nandagopal, "Influence of Sn Grain Size and Orientation on the Thermomechanical Response and Reliability of Pb-free Solder Joints," *IEEE Trans. On Comp. And Pack. Tech.*, vol. 31, no. 2, pp. 370–381, 2008.
- [22] A. Lalonde, D. Emelander, J. Jeannette, C. Larson, W. Rietz, D. Swenson and D. W. Henderson, "Quantitative metallography of β -Sn dendrites in Sn-3.8Ag-0.7Cu ball grid array solder balls via electron backscatter diffraction and polarized light microscopy," *J. Electron. Mater.*, vol. 33, no. 12, pp. 1545–1549, 2004.
- [23] T. K. Lee, T. R. Bieler, C. U. Kim, and H. Ma, "Fundamentals of lead-free solder interconnect technology: From microstructures to reliability," Book, Chaper 4, pp. 85–112, 2015.
- [24] T. R. Bieler, B. Zhou, L. Blair, A. Zamiri, P. Darbandi, F. Pourboghrat, T. Lee and K. Liu, "The role of elastic and plastic anisotropy of Sn in recrystallization and damage evolution during thermal cycling in SAC305 solder joints," *J. Electron. Mater.*, vol. 41, no. 2, pp. 283–301, 2012
- [25] P. Darbandi, T. R. Bieler, F. Pourboghrat, and T. K. Lee, "Crystal plasticity finite-element analysis of deformation behavior in multiple-grained lead-free solder joints," *J. Electron. Mater.*, vol. 42, no. 2, pp. 201–214, 2013
- [26] B. Arfaei, L. Wentlent, S. Joshi, A. Alazzam, T. Tashtoush, M. Halaweh, S. Chivukula, L. Yin, M. Meilunas, E. Cotts, and P. Borgesen, "Improving the thermomechanical behavior of lead free solder joints by controlling the microstructure," *Intersoc. Conf. Therm. Thermomechanical Phenom. Electron. Syst. IOTHERM*, pp. 392–398, 2012.
- [27] L. Yin, M. Meilunas, B. Arfaei, L. Wentlent, and P. Borgesen, "Effect of microstructure evolution on Pb-free solder joint reliability in thermomechanical fatigue," *xw IEEE 62nd Elec. Compo. and Techno. Conf (ECTC)*, pp. 493–499, 2012.
- [28] B. Arfaei, L. Wentlent, S. Joshi, M. Anselm, and P. Borgesen, "Controlling the superior reliability of lead free assemblies with short standoff height through design and materials selection," *ASME 2012 International Mechanical Engineering Congress and Exposition. Volume 9, Parts A and B*, pp. 467-473, 2012.
- [29] B. Arfaei, F. Mutuku, R. Coyle, E. Cotts, and J. Wilcox, "Failure mechanism and

- microstructural evolution of Pb-free solder alloys in thermal cycling tests: Effect of solder composition and Sn grain morphology,” IEEE 65th Elec. Compo. and Techno. Conf. (ECTC), pp. 118–126, 2015.
- [30] I. E. Anderson, “Development of Sn – Ag – Cu and Sn – Ag – Cu – X alloys for Pb-free electronic solder applications,” *J. Mater. Scien.*, vol. 18, pp. 55–76, 2006.
- [31] P. E. Tegehall, “Impact of solder pad finish and solder composition on the microstructure of solder joints to various types of components,” Technical Report, 2019.
- [32] M. Berthou, “Fiabilite des assemblages sans-plomb en environnement severe,” Thesis, University of Bordeaux 1, France, 2010.
- [33] KANG, “Microstructure and mechanical properties of lead-free solder joints,” *J. Acta Phys. Pol. A*, vol. 128, no. 4, pp. 750–753, 2005.
- [34] G. Parks, M. Lu, E. Perfecto, and E. Cotts, “Controlling the Sn grain morphology of SnAg C4 solder bumps,” IEEE 64th Elec. Comp. and Techno. Conf. (ECTC), pp. 690–696, 2014.
- [35] A. R. Zbrzezny, P. Snugovsky, and D. D. Perovic, “Impact of board and component metallizations on microstructure and reliability of lead-free solder joints,” *Microelectron. Reliab.*, vol. 47, no. 12, pp. 2205–2214, 2007.
- [36] K. S. Kim, S. H. Huh, and K. Suganuma, “Effects of cooling speed on microstructure and tensile properties of Sn-Ag-Cu alloys,” *Mater. Sci. Eng. A*, vol. 333, no. 1–2, pp. 106–114, 2002.
- [37] M. Grieu , “Etude de la fatigue des joints brases de composants electroniques soumis à des sollicitations thermomecaniques , vibratoires et combinées,” Thesis, École nationale supérieure des mines de Paris, France, 2011.
- [38] M. Berthou, P. Retailleau, H. Frémont, A. Guédon-Gracia, and C. Jéphos-Davennel, “Microstructure evolution observation for SAC solder joint: Comparison between thermal cycling and thermal storage,” *Microelectron. Reliab.*, vol. 49, no. 9–11, pp. 1267–1272, 2009.
- [39] T.-K. Lee, H. Ma, K.-C. Liu, and J. Xue, “Impact of Isothermal Aging on Long-Term Reliability of Fine-Pitch Ball Grid Array Packages with Sn-Ag-Cu Solder Interconnects: Surface Finish Effects,” *J. Electron. Mater.*, vol. 39, no. 12, pp. 2564–2573, 2010.
- [40] P. Chauhan, S. Mukherjee, M. Osterman, A. Dasgupta, and M. Pecht, "Effect of Isothermal Aging on Microstructure and Creep Properties of SAC305 Solder: A Micromechanics Approach," ASME 2013 Inter. Techni. Conf. and Exhibi. on Packa. and Integra. of Electro. and Photonic Microsystems, vol. 1, 2016.
- [41] H. Ma, Y. Zhang, Z. Cai, J. C. Suhling, P. Lall, and M. J. Bozack, “Aging induced evolution of free solder material behavior,” EuroSimE 2008 - Int. Conf. Therm. Mech. Multi-Physics Simul. Exp. Microelectron. Micro-Systems, pp. 1–12, 2008.
- [42] R. Ghosh, A. Kanjilal, and P. Kumar, “Effect of type of thermo-mechanical excursion on growth of interfacial intermetallic compounds in Cu/Sn-Ag-Cu solder joints,” *Microelectron. Reliab.*, vol. 74, pp. 44–51, 2017.
- [43] H. Ma, J. C. Suhling, P. Lall, and M. J. Bozack, “Reliability of the aging lead free solder joint,” IEEE 56th Electron. Components Technol. Conf. (ECTC), pp. 849–864, 2006.
- [44] M. Motalab, Z. Cai, J. C. Suhling, J. Zhang, J. L. Evans, M. J. Bozack and P. Lall,

- “Improved predictions of lead free solder joint reliability that include aging effects,” IEEE 62th Electron. Components Technol. Conf (ECTC), pp. 513–531, 2012.
- [45] U. Sahaym, B. Talebanpour, S. Seekins, I. Dutta, P. Kumar, and P. Borgesen, “Recrystallization and Ag_3Sn particle redistribution during thermomechanical treatment of bulk Sn-Ag-Cu solder alloys,” IEEE Trans. Components, Packag. Manuf. Technol., vol. 3, no. 11, pp. 1868–1875, 2013.
- [46] T. T. Mattila and J. K. Kivilahti, “The role of recrystallization in the failure of SnAgCu solder interconnections under thermomechanical loading,” IEEE Trans. Components Packag. Technol., vol. 33, no. 3, pp. 629–635, 2010.
- [47] B. Zhou, T. R. Bieler, T. K. Lee, and K. C. Liu, “Crack development in a low-stress PBGA package due to continuous recrystallization leading to formation of orientations with [001] parallel to the interface,” J. Electron. Mater., vol. 39, no. 12, pp. 2669–2679, 2010.
- [48] Q. Jiang, A. N. Deshpande, and A. Dasgupta, “Grain-Scale Anisotropic Analysis of Steady-State Creep in Oligocrystalline SAC Solder Joints,” Materials, vol. 14, no. 20, pp. 5973, 2021.
- [49] T. Gu, C. M. Gourlay, and T. Ben Britton, “The Role of Lengthscale in the Creep of Sn-3Ag-0.5Cu Solder Microstructures,” J. Electron. Mater., vol. 50, no. 3, pp. 926–938, 2021,.
- [50] I. Dutta, D. Pan, R. A. Marks, and S. G. Jadhav, “Effect of thermo-mechanically induced microstructural coarsening on the evolution of creep response of SnAg-based microelectronic solders,” Microelectron. Reliab., vol. 411, pp. 48–52, 2005.
- [51] S. Mukherjee, P. Chauhan, M. Osterman, and A. Dasgupta, “Mechanistic Prediction of the Effect of Microstructural Coarsening on Creep Response of SnAgCu Solder Joints,” J. Electron. Mater., vol. 45, no. 7, pp. 3712–3725, 2016.
- [52] L. Yin, L. Wentlent, L. Yang, B. Arfaei, A. Qasaimeh, and P. Borgesen, “Recrystallization and precipitate coarsening in Pb-Free solder joints during thermomechanical fatigue,” J. Electron. Mater., vol. 41, no. 2, pp. 241–252, 2012.
- [53] J. B. Libot, J. Alexis, O. Dalverny, L. Arnaud, P. Milesi, and F. Dulondel, “Microstructural evolutions of Sn-3.0Ag-0.5Cu solder joints during thermal cycling,” Microelectron. Reliab., vol. 83, pp. 64–76, 2018.
- [54] B. Arfaei, S. Mahin-Shirazi, S. Joshi, M. Anselm, P. Borgesen, E. Cotts, J. Wilcox and R. Covle, “Reliability and failure mechanism of solder joints in thermal cycling tests,” IEEE 63rd Electr. Compo. and Techn. Conf. (ECTC), pp. 976–985, 2013.
- [55] L.F.Coffin, “A study of the effects of cyclic thermal stresses on a ductile metal,” Trans. ASME, vol. 76, no. 6, pp. 931–949, 1954.
- [56] I. H. Lau, "Reliability Solder Joint Theory And Applications", Book, chapter 9, 1991.
- [57] J.D. Morrow, “Cyclic Plastic Strain Energy and the Fatigue of Metals, Internal Friction, Damping, and Cyclic Plasticity, ” ASTM STP 387, pp. 45–84, 1965.
- [58] R. Darveaux, “Effect of simulation methodology on solder joint crack growth correlation,” IEEE 50th Elec. Comp. and Techno. Conf. (ECTC), pp. 1048–1058, 2000.
- [59] A. Lovberg and P. E. Tegehall, “The Stress State of BGA Solder Joints Influenced by the Grain Orientations of Neighboring Joints,” IEEE 68th Elec. Compo. and Techno.

- Conf. (ECTC), pp. 882–889, 2018.
- [60] D. W. Henderson, J. J. Woods, T. A. Gosselin, J. Bartelo, and D. E. King, “The microstructure of Sn in near-eutectic Sn – Ag – Cu alloy solder joints and its role in thermomechanical fatigue,” *J. Materials Research*, vol. 9, no. 6, pp. 1608-1612 2004.
- [61] A. Gracia, A. Badetz, F. Arabi, B. Plano, and H. Frémont, “Statistical study of SAC solder joints in QFN and BGA assemblies,” *MiNaPaD 2019*.
- [62] A. Syed, “Accumulated Creep Strain and Energy Density Based Thermal Fatigue Life Prediction Models for SnAgCu Solder Joints,” *IEEE 54th Elec. Compo. and Techno. Conf. (ECTC)*, pp. 737–746, 2004.
- [63] L. P. Lehman, R. Kinyanjui, J. Wang, Y. Xing, L. Zavalij, P. Borgesen and E. Cotts, “Microstructure and damage evolution in Sn-Ag-Cu solder joints,” *IEEE 55th Elec. Compo. and Techno. Conf. (ECTC)*, pp. 674–681, 2005.
- [64] J. Smetana, R. Coyle, T. Sack, A. Syed and S. Kummerl, “Pb-free solder joint reliability in a mildly accelerated test condition,” *IPC APEX EXPO Tech. Conf. 2011*, vol. 4, pp. 2686–2735, 2011.
- [65] S. Mukherjee, B. Zhou, A. Dasgupta, and T. R. Bieler, “Multiscale modeling of the anisotropic transient creep response of heterogeneous single crystal SnAgCu solder,” *Int. J. Plast.*, vol. 78, pp. 1–25, 2016.
- [66] B. Arfaei, F. Mutuku, J. Wilcox, R. Coyle, E. Cotts, and M. Hill, “Failure Mechanism and Microstructural Evolution of Pb-free Solder Alloys in Thermal Cycling Tests : Effect of Solder Composition and Sn Grain,” *IEEE 65th Elec. Compo. and Techno. Conf. (ECTC)*, pp. 118–126, 2015.
- [67] P. E. Tegehall, “Impact of various combinations of PCB laminate , solder pad finish and solder joints to various types of components,” *Technical Repport*, 2020.
- [68] A. Lovberg, P. E. Tegehall, G. Wetter, K. Brinkfeldt, and D. Andersson, “Simulations of the impact of single-grained lead-free solder joints on the reliability of ball Grid Array components,” *18th Int. Conf. Therm. Mech. Multi-Physics Simul. Exp. Microelectron. Microsystems (EuroSimE)* , pp. 1–10, 2017.
- [69] A. Lövberg, P. E. Tegehall, S. Akbari, and D. Andersson, “On the formation and propagation of laminate cracks and their influence on the fatigue lives of solder joints,” *19th Int. Conf. Therm. Mech. Multi-Physics Simul. Exp. Microelectron. Microsystems, (EuroSimE)*, pp. 1–13, 2018.
- [70] T.-K. Lee, T. R. Bieler, C.-U. Kim, and H. Ma, “Challenges in Future-Generation Interconnects: Microstructure Again,” *Fundamentals of Lead-Free Solder Interconnect Technology: From Microstructures to Reliability*, Springer, pp. 231–249, 2015.
- [71] J. P. M. Clech, R. J. Coyle, and B. Arfaei, “Pb-Free Solder Joint Thermo-Mechanical Modeling: State of the Art and Challenges,” *JOM* 71, pp. 143–157, 2019.
- [72] P. Borgesen, “Microstructurally Adaptive Constitutive Relations and Reliability Assessment Protocols for Lead Free Solder,” *Technical Report*, 2015.
- [73] K. Moroka and Y. Kariya, “Fatigue Life Prediction of BGA Solder Joint with Consideration of Microstructural Coarsening,” *6th Int. Work. Low Temp. Bond. 3D Integr. LTB-3D*, p. 48, 2019.
- [74] J. Li, T. T. Mattila, and J. K. Kivilahti, “Multiscale Simulation of Microstructural

- Changes in Solder Interconnections During Thermal Cycling,” *J. Electron. Mater.*, vol. 39, no. 1, pp. 77–84, 2010.
- [75] J. Li, H. Xu, T. T. Mattila, J. K. Kivilahti, T. Laurila, and M. Paulasto-Kröckel, “Simulation of dynamic recrystallization in solder interconnections during thermal cycling,” *Comput. Mater. Sci.*, vol. 50, no. 2, pp. 690–697, 2010.
- [76] T. Mattila, “The failure mechanism of recrystallization-assisted cracking of solder interconnections,” 142nd Annu. Meet. Exhib. Annu. Meet., pp. 403–411, 2013.
- [77] J. H. L. Pang, “Lead free solder: Mechanics and reliability,” Book, Chapter 2, pp. 7–22, 2012.
- [78] M. Dusek, “The measurement of creep rates and stress relaxation for micro-sized lead-free solder joints,” *Solder. Surf. Mt. Technol.*, vol. 17, no. 4, 2005
- [79] S. Pin, A. Guédon-Gracia, J. Y. Delétage, and H. Frémont, “Creep measurement and choice of creep laws for BGA assemblies’ reliability simulation,” *Microelectron. Reliab.*, vol. 90, pp. 1172–1176, 2018.
- [80] J. Castellanos, S. National, O. A. Ruano, and S. National, “Analysis of Garofalo equation parameters for an ultrahigh carbon steel,” *J. Mater. Sci.*, vol. 45, pp. 5522–5527, 2010.
- [81] R. Darveaux and K. Banerji, “Constitutive Relations for Tin-Based Solder Joints,” *IEEE Trans. Components, Hybrids, Manuf. Technol.*, vol. 15, no. 6, pp. 1013–1024, 1992.
- [82] R. Darveaux and K. Banerji, “Fatigue analysis of flip chip assemblies using thermal stress simulations and a Coffin-Manson relation,” *IEEE 41th Elec. Compo. and Techno. Conf. (ECTC)*, pp. 797–805, 1991.
- [83] L. Anand, “Constitutive equations for hot-working of metals,” *Int. J. Plast.*, vol. 1, no. 3, pp. 213–231, 1985.
- [84] R. Hill, “Acceleration waves in solids,” *J. Mech. Phys. Solids*, vol. 10, no. 1, pp. 1–16, 1962.
- [85] R. J. Asaro and J. R. Rice, “Strain localization in ductile single crystals,” *J. Mech. Phys. Solids*, vol. 25, no. 5, pp. 309–338, 1977.
- [86] M. Reynell, “Advanced thermal analysis of packaged electronic systems using computational fluid dynamics techniques,” *Comput. Eng. Journa*, vol. 7, no. 4, p. 104_106, 1990.
- [87] IPC-9701, “Performance Test Methods and Qualification Requirements for Surface Mount Solder Attachments,” 2002.
- [88] A. Qasaimeh, S. Lu, and P. Borgesen, “Crack evolution and rapid life assessment for lead free solder joints,” *IEEE 61th Elec. Compo. and Techno. Conf. (ECTC)*, pp. 1283–1290, 2011.
- [89] Toray Research Center, INC, “<https://www.toray-research.co.jp/en/technicaldata/techniques/EBSD.html>,” 1978.
- [90] A. Guédon-Gracia, E. Woïrgard, and C. Zardini, “Reliability of lead-free BGA assembly: Correlation between accelerated ageing tests and FE simulations,” *IEEE Trans. Device Mater. Reliab.*, vol. 8, no. 3, pp. 449–454, 2008.
- [91] S. Mukherjee, “Multiscale Modeling of the Anisotropic Transient Creep Response of Heterogeneous SAC Single Crystal,” *Inter. J. of Plas.*, vol. 78, pp. 1–25, 2016.

- [92] A. Lovberg and P. E. Tegehall, "The Stress State of BGA Solder Joints Influenced by the Grain Orientations of Neighboring Joints," IEEE 68th Elec. Compo. and Techno. Conf. (ECTC), pp. 882–889, 2018.
- [93] B. Arfaei, M. Anselm, S. Joshi, S. Mahin-shirazi, P. Borgesen, E. Cotts, J. Wilcox and R. Coyle, "Effect of Sn Grain Morphology on Failure Mechanism and Reliability of Lead-Free Solder Joints in Thermal Cycling Tests," SMTA Int., pp. 539–550, 2013.
- [94] IPC-9701A, "Methods and Qualification Requirements for Surface Mount Solder Attachments," 2002.
- [95] A. Qasaimeh, Y. Jaradat, L. Wentlent, L. Yang, L. Yin, B. Arfaei and P. Borgesen, "Recrystallization behavior of lead free and lead containing solder in cycling," IEEE 61th Elec. Compo. and Techno. Conf. (ECTC), pp. 1775–1781, 2011.
- [96] S. Terashima, K. Takahama, M. Nozaki, and M. Tanaka, "Recrystallization of Sn grains due to thermal strain in Sn-1.2Ag-0.5Cu-0.05Ni solder," Mater. Trans., vol. 45, no. 4, pp. 1383–1390, 2004.
- [97] P. Roumanille, E. Ben Romdhane, S. Pin, P. Nguyen, J. Delétage, and A. Guédon-gracia, "Evaluation of thermomechanical fatigue lifetime of BGA lead-free solder joints and impact of isothermal aging," Microelec. Reliability, vol. 116, 114201, 2021.
- [98] T. K. Lee, B. Zhou, and T. R. Bieler, "Impact of isothermal aging and sn grain orientation on the long-term reliability of wafer-level chip-scale package Sn-Ag-Cu solder interconnects," IEEE Trans. Components, Packag. Manuf. Technol., vol. 2, no. 3, pp. 496–501, 2012.
- [99] E. Ben Romdhane, P. Roumanille, A. Guédon-gracia, S. Pin, P. Nguyen, and H. Frémont, "Early microstructural indicators of crack initiation in lead-free solder joints under thermal cycling," IEEE 71th Elec. Compo. and Techno. Conf. (ECTC), pp. 2293–2301, 2021.
- [100] P. Lall, S. Deshpande, N. Kothari, J. Suhling, and L. Nguyen, "Effect of Thermal Cycling on Reliability of QFN Packages," Proc. 17th Intersoc. Conf. Therm. Thermomechanical Phenom. Electron. Syst. ITherm 2018, pp. 1357–1365, 2018.
- [101] E. A. S. L.P. Troeger, "Particle-stimulated nucleation of recrystallization for grain-size control and superplasticity in an Al–Mg– Si–Cu alloy," Mater. Sci. Eng., vol. 293, no. 1–2, pp. 19–29, 2000.
- [102] E. Ben Romdhane, P. Roumanille, A. Guédon-Gracia, S. Pin, P. Nguyen, and H. Frémont, "From early microstructural evolution to intergranular crack propagation in SAC solders under thermomechanical fatigue," Microelectron. Reliab., vol. 126, 114228, 2021.
- [103] A. Deshpande, Q. Jiang, A. Dasgupta, and U. Becker, "Fatigue life of joint-scale SAC305 solder specimens in tensile and shear mode," Intersoc. Conf. Therm. Thermomechanical Phenom. Electron. Syst. ITherm, vol. 2019-May, pp. 1026–1029, 2019.
- [104] E. Ben Romdhane, P. Roumanille, A. Guedon-Gracia, S. Pin, P. Nguyen, and H. Fremont, "Evaluation of SAC solder joint thermomechanical fatigue in different types of components," 23rd Int. Conf. Therm. Mech. Multi-Physics Simul. Exp. Microelectron. Microsystems (EuroSimE), pp. 1–6, 2022.
- [105] I. Dutta, P. Kumar, and G. Subbarayan, "Microstructural coarsening in Sn-Ag-based

- solders and its effects on mechanical properties,” *Jom*, vol. 61, no. 6, pp. 29–38, 2009.
- [106] M. Hasnine, M. Mustafa, J. C. Suhling, B. C. Prorok, M. J. Bozack, and P. Lall, “Characterization of aging effects in lead free solder joints using nanoindentation,” *IEEE 63rd Elec. Compo. and Techno. Conf. (ECTC)*, pp. 166–178, 2013.
- [107] V. A. Raghavan, B. Roggeman, M. Meilunas, and P. Borgesen, “Effects of ‘Latent Damage’ on pad cratering: Reduction in life and a potential change in failure mode,” *Microelectron. Reliab.*, vol. 53, no. 2, pp. 303–313, 2013.
- [108] P. E. Tegehall and G. Wetter, “Impact of laminate cracks under solder pads on the fatigue lives of ball grid array solder joints,” *Microelectron. Reliab.*, vol. 55, no. 11, pp. 2354–2370, 2015.
- [109] A. Lövberg, P. E. Tegehall, S. Akbari, and D. Andersson, “On the formation and propagation of laminate cracks and their influence on the fatigue lives of solder joints,” *19th Int. Conf. Therm. Mech. Multi-Physics Simul. Exp. Microelectron. Microsystems, (EuroSimE)*, pp. 1–13, 2018.
- [110] S. Akbari, A. Lövberg, P. E. Tegehall, K. Brinkfeldt, and D. Andersson, “Effect of PCB cracks on thermal cycling reliability of passive microelectronic components with single-grained solder joints,” *Microelectron. Reliab.*, vol. 93, pp. 61–71, 2019.
- [111] E. Ben Romdhane, A. Guédon-Gracia, S. Pin, P. Roumanille, and H. Frémont, “Impact of crystalline orientation of lead-free solder joints on thermomechanical response and reliability of ball grid array components,” *Microelectron. Reliab.*, vol. 114, 113812, 2020.